Lab-On-Chip for *Ex-Vivo* Study of Bio-Mechanical-Chemical Behavior of Tip Growing Plant Cells

AMIR SANATI NEZHAD

A Thesis

in

the Department

of

Mechanical and Industrial Engineering

Presented in partial fulfillment of the requirements for the
Degree of Doctor of Philosophy (Mechanical Engineering) at
Concordia University
Montreal, Quebec, Canada

July 2013

CONCORDIA UNIVERSITY
SCHOOL OF GRADUATE STUDIES

This is to certify that the thesis prepared

By: **Amir Sanati Nezhad**

Entitled**: Lab-On-Chip for *Ex-Vivo* Study of Bio-Mechanical-Chemical Behavior of Tip Growing Plant Cells**

and submitted in partial fulfillment of the requirements for the degree of

DOCTOR OF PHILOSOPHY (Mechanical Engineering)

complies with the regulations of the University and meets the accepted standards with respect to originality and quality.

Signed by the final examining committee:

_____ Chair
Dr. Yousef R. Shayan

_____External Examiners
Dr. Meenakshinathan Parameswaran

_____ External Examiners
Dr. Anja Geitmann

_____ External to Program
Dr. Sheldon Williamson

_____ Examiner
Dr. Ali Dolatabadi

_____ Examiner
Dr. Javad Dargahi

_____ Thesis Supervisors
Dr. Muthukumaran Packirisamy

_____ Thesis Supervisors
Dr. Rama Bhat

Approved by _____
Chair of Department or Graduate Program Director
Dr. Ali Dolatabadi, Graduate Program Director

_____

Dean
Faculty of Engineering and Computer Science

ABSTRACT

Lab-On-Chip for *Ex-Vivo* study of bio-mechanical-chemical behavior of tip growing plant cells

Amir Sanati Nezhad, Ph.D.
Concordia University, 2013

This thesis presents design, modeling, fabrication, and testing of different Lab-on-chip (LOC) devices to study static and dynamic behavior of pollen tubes in bio-mechanical-chemical environments. The main components of microfluidic platform include microfluidic network for manipulation, trapping and growing of a series of pollen tubes in a controlled environment, actuating channels in order to introduce chemicals and drugs toward the pollen tube, microstructural elements such as microgaps and microcantilevers to provide *Ex-Vivo* environment for characterizing static and dynamic responses of pollen tubes.

A Lab-On-Chip (LOC), called, TipChip was developed as a flexible platform that can simplify sophisticated functions such as chemical reactions, drug development, by integrating them within a single micro-device. The configuration of the microfluidic network was developed in such a way that it allows observation under chemical or mechanical manipulation of multiple pollen tubes. The growth of pollen tubes under different flow rates and geometrical dimensions of microfluidic network has been studied and the challenges have been identified. The microfluidic platform design was enhanced to deal with the challenges by adapting the dimensions of the microfluidic network and the

inlet flow. It provides identical growth environments for growing pollen tubes along each microchannel and improves the performance of microfluidic device, through varying the dimensions and geometries of the microfluidic network.

The thesis identifies the static response of pollen tube to chemical stimulation which was used to determine the role of a few of the growth regulators such as sucrose and calcium ions as they regulate tube turgor pressure and cell wall mechanical properties of pollen tube. New experimental platforms were fabricated to treat locally the pollen tube at the tip in order to characterize its static response to local treatment in reorienting the growth direction. The device is also used to locally stimulate the cylindrical region of pollen tube. Using these LOC devices we attempted to answer some questions regarding the role of regulators in pollen tube growth.

The thesis explores in detail the dynamic growth of pollen tube in normal condition and also under chemical stimulation. Waveform analysis is employed in order to extract primary and secondary oscillation frequencies of pollen tube as significant indicators of dynamic growth of pollen tube. The dynamic response of pollen tubes is implemented as a whole-plant cell sensor for toxicity detection in order to detect toxic materials in concentration-based manner. Aluminum ions were tested as the toxic substance. The degree of toxicity was defined by measuring the reduction in growth rate as well as peak oscillation frequencies in the case of static and dynamic response of pollen tube, respectively.

The thesis addresses the quantification of mechanical properties of pollen tube cell wall using the Bending LOC (BLOC) platform. The flexural rigidity of the pollen tube and the Young's modulus of the cell wall are estimated through finite element modeling of the observed fluid-structure interaction.

The thesis also explores the feasibility of studying the pollen tube response to the mechanical stimulation. The microfluidic device also enables integrating mechanical force obstructing pollen tube growth in order to characterize the interaction of pollen tube and mechanical structures which are similar to the *in-vivo* interaction between a pollen tube and the growth matrix during the course of growth toward the ovule. The behavior of the pollen tube while passing through microgap was also explored in detail. The deflection of microgap under growth force and the changes in diameter of the pollen tube under reaction force from microgap were evaluated. This part explores the role of mechanical forces in bursting the pollen tube tip which could explain the contribution of mechanical signal in the bursting of tube near the vicinity of the ovule. In addition, the configuration of microgap enabled the estimation of the maximum invasive force exerted by pollen tube.

Thus, the proposed microfluidic platform is highly suitable for cellular analysis, pollen tube biology and detection of toxicity.

ACKNOWLEDGEMENTS

Here, I sincerely thank Dr. Muthukumaran Packirisamy for his supervision, invaluable guidance, practical ideas and encouragement, which have been inspirational in the successful completion of this thesis. I am very thankful to Dr. Rama Bhat for his supervision and suggestions during my Ph.D. I express my thanks to Dr. Anja Geitmann at plant cell biology Lab, University of Montreal for her outstanding support in developing the ideas related to the biological aspects of the thesis.

My very sincere thanks to Carlos Agudelo, Mahmood Ghanbari and Mahsa Naghavi for their outstanding collaboration in developing new techniques and ideas and for their tremendous discussion and supports. I would like to thank the financial support offered by Concordia University, in the form of different awards and fellowships during the PhD program. The project was funded by a grant from the Fond Quebeqois de Recherche - Nature et Technologies. I am thankful to all the support staff at Concordia University: Leslie Hosein, Maureen Thuringer, Arlene Zimmerman and Sophie Merineau of the MIE department for steering me through the logistics of my Ph.D program. I thank Danius Juras, Henri Sczhwinski and Gilles Houard for their technical support in handling the experiment setups and Dylan Lu, the manager of ConSiM for his tutoring and support for clean room operations.

It has been my pleasure to be a member of the Optical-Bio Microsystems laboratory, and I am sincerely thankful to the members of the lab for their help and assistance in handling the lab affairs during my Ph.D program. Many thanks to Simona

Badilescu, Hamid SadAbadi and Jayan Ozhikandathil for helping me at different stages of the thesis.

Above all, I would like to express my deep gratitude to my parents Mr. Ali Sanati Nezhad and Mrs. Zahra Iravani and my wife Mrs. Atefeh Rafiei for their encouragement and support during my PhD and my whole life.

Dedicated to my parents ...

TABLE OF CONTENTS

LIST OF FIGURES

LIST OF TABLES

NOMENCLATURE

3D	3 Dimensional
Al	Aluminum
$AlCl_3$. $6H_2O$	Aluminum Chloride Hexahydrate
AT	After Treatment
BioMEMS	Bio-Micro-Electro-Mechanical System
BLOC	Bending Lab-On-Chip
BT	Before Treatment
C50	Criterion of detecting growth rate reduction
Ca	Calcium
CCD	Charge-Coupled Device
CFM	Cellular Force Microscopy
Cr(III)	Chromium-3
Cr(VI)	Chromium-6
DFT	Discrete Fourier Transform
DWL	Direct Writing Laser
FFT	Fast Fourier Transform
FRAP	Fluorescence Recovery After Photobleaching
Gd^{+3}	Gadolinium
IP	Interface Point
H_3BO_3	Boric Acid
La^{+3}	Lanthanum
LOC	Lab-On-chip

MEMS	Micro-Electro-Mechanical Systems
$MgSO_4$	Magnesium Sulfate
PEB	Post-Exposure Bake
PDMS	Polydimethylsiloxane
PME	Pectin Methyl-Esterase
PMI	Pollen-Medium Inlet
PSD	Power Spectral Density
PTG	Pollen Tube Growth
SEM	Scanning Electron Micrograph
STFT	Short-Time Fourier Transform
SU8	Negative Photoresist
UV	UltraViolet
VSC	Vesicle Supply Centre

LIST OF SYMBOLS

A_p	Cross sectional area of particle
C_D	Drag coefficient
CA_{max}	Maximum contact zone
C	Concentration
D	Diffusivity of the reagent
E	Young's modulus of pollen tube cell wall
F_{FL}	Flow-induced bending force
F	Wedge force
F_D	Viscous drag force per unit area
X(f)	Frequency domain signal
K_T	Translational stiffness
K_R	Rotational stiffness
K	Inlet velocity ratio
P_f	Power of growth
P_f^t	Power after treatment
P_f^n	Power before treatment
Re_p	Reynolds number
S_w	Trap length
W_m	Main chamber width
W_{out}	Outlet drain width
W_{in}	Inlet width
W_μ	Microchannels width

d_p	Particle diameter
F	Frequency
f_c	Maximum desired frequency
f_m	Maximum frequency of signal
f_s	Sampling rate frequency
P	Fluid pressure
u	Fluid velocity
u_p	particle velocity
x(t)	Time series signal
A	Toxicity level
T	Degree of toxicity
δ_T	Deflection of pollen tube's tip
δ_θ	Rotational deflection
δ_T	Total tip deflection
δ_B	Pure bending deflection
σ_r	Circumferential tensile stresses
σ_x	Longitudinal tensile stresses
ρ_p	Particle density
μ	Fluid dynamic viscosity
τ	Trapping coefficient

Chapter 1

Introduction to Bio-Micromechanical System (BioMEMS)

1.1 Introduction to Bio-Micromechanical System (BioMEMS)

In recent years, there has been an increasing interest in applying micro-electro-mechanical systems (MEMS) technology for studying biological phenomena that led to the development of a new area called BioMEMS. MEMS is a technology that can be defined as miniaturized mechanical and electro-mechanical elements. BioMEMS basically deals with miniaturization of conventional chemical and mechanical biosensors to the micro level. Today, BioMEMS are extensively used in diagnostic, drug development, cellular biology, biosensors and lab-on-chip (LOC) systems (Cheung *et al.*, 2006b; Giouroudi *et al.*, 2008a; Nuxoll *et al.*, 2009b). Cost effective and portable microfluidic platforms have provided closed environment for *in-vitro* single cell analysis (Tatic-Lucic, 2007) and characterizing the cell response to the chemical cues in growth environment (Grossmann *et al.*, 2011b; Takayama *et al.*, 2001).

1.2 BioMEMS for cell studies

Application of BioMEMS in cell analysis has been developed in order to study biological systems, especially at the cellular level. BioMEMS is supporting cell biology research by providing miniaturized platforms to study the cell to cell interaction and to analyze the behavior of a cell in response to environmental reactions including mechanical or chemical interaction. Biological procedures including cell counting, cell sorting using electrophoresis and micromechanical structures have been used to develop our capability

for cell analysis. In addition, this application brings a new development in drug discovery, diagnosis of medicine and *toxicology*[1] due to its capability in handling of cells, local transferring of biological medium and integrating biosensors to detect the cell response to various *pharmacological*[2] effects on the cell. Real time diagnosis of infection, allergies or toxicity is the advantage of miniaturized bio-devices.

1.3 History of BioMEMS for cellular analysis

Developing a new technology with the main advantage of miniaturization comparable to the size of the cell has been always desirable in order to provide controlled experimental conditions in biology in order to answer fundamental questions involved in cell regulating mechanisms and its interaction with other cells or tissues. One starting point to use microenvironment for cellular analysis is the use of the patch clamp technique reported in 1980 by Neher and Sakmann (Sakmann *et al.*, 1980) [1] which later received a Nobel Prize in 1991. This technique was based on micropipette technology (Hamill *et al.*, 1981) and was used to study the cells at the single cell level to identify cell membrane ion channels. Afterwards, the microelectronic technology area emerged to provide 3D structured silicon chips. Gas chromatograph was carried out using integrated silicon-based microdevice including an injection valve, a capillary separation column and a detector (Terry *et al.*, 1979). Microfluidics based lab-on-chip technology was then developed to provide simple platforms to miniaturize the environment around the cells and to enable more detailed

[1] [Toxicology is a branch of biology, chemistry, and medicine concerned with the study of the adverse effects of chemicals on living organisms] (https://en.wikipedia.org/wiki/Toxicology)
[2] [Pharmacology is the branch of medicine and biology concerned with the study of drug action] (http://en.wikipedia.org/wiki/Pharmacology).

analysis of cellular biology. The controlled microenvironment enabled by microfluidic chips provides suitable condition for experiments with single cells (Wheeler *et al.*, 2003) or single molecules (Spetzler *et al.*, 2007). It should be noted that the key feature of lab-on-chip technology for cell biology is the capability of microfluidics environment to introduce precise spatial and temporal concentrations of compound around the cells (Haessler *et al.*, 2009) (Lin *et al.*, 2004). This unique feature has been employed to study the response of different cells to external signals such as cell response to chemotaxis of neutrophils in medium gradients (Lin *et al.*, 2005), bacteria in glycerol gradients (Diao *et al.*, 2006) and stem cells for next differentiation process (Flanagan *et al.*, 2005). Fig 1.1 shows the application of microfluidic device to apply diffusive gradient of chemoattractant to study the cancer cell migration along the microchannel and to characterize the nucleus deformation during the migration (Tong *et al.*, 2012). This study has an application for characterizing cancer cells and tumor diagnosis.

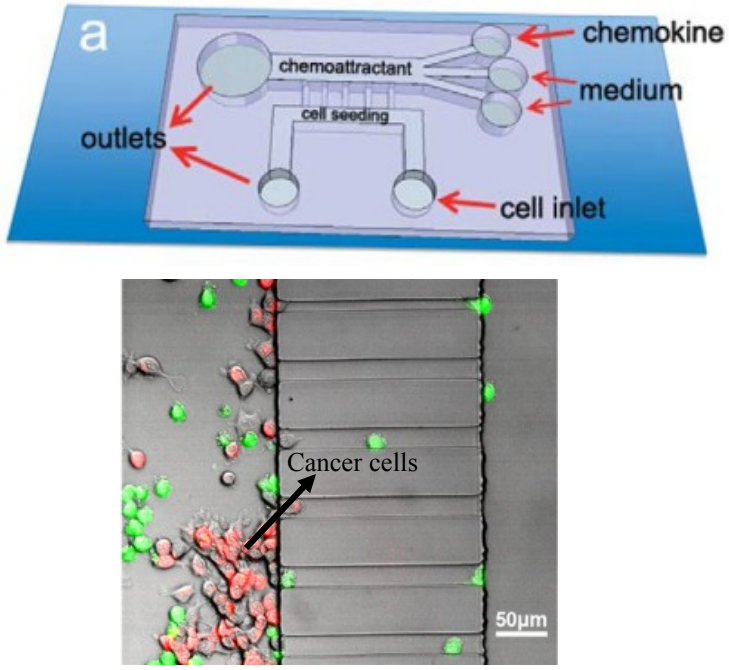

Figure 1.1: Microfluidic device for chemotaxis study of cancer cells (Tong *et al.*, 2012)

In addition to the application of lab-on-chip for single cell analysis, the microfluidics has the power to handle array based cellular response. This has the application potential in pharmaceutical development and drug screening (Dittrich *et al.*, 2006). For this purpose, the cells are captured at defined locations within the microfluidic environment using different techniques such as localized surface modifications (Falconnet *et al.*, 2006) and then the cells are exposed to the drugs or chemical agent to monitor the cells response. However, for employing LOC devices for cell assays, cell capturing at defined locations is required.

1.4 Pollen tube as the carrier of gamete cell

Among various cells, pollen tube as the main part of flowering plants are important for humanity because of *fertilization*[3], through which seeds are produced that are essential for food supply and raw materials. The pollen tube is an excellent candidate for the study of growth and *morphogenesis* of biological systems. It elongates dramatically up to few centimeters and is one of the most fast growing plant cells. As an example, the growth of pollen tube elongation reaches up to 1 cm/hr in maize species (Cheung & Wu, 2008). This pattern of tube growth can be employed for developing toxicology and pharmacology studies by analyzing the response of the cell growth to biological and pharmacological change of culture medium surrounding the pollen tube. Fig 1.2 shows different shapes of plant cells generated by heterotropic as well as the position of pollen tube growth. The

[3] Fertilization is the fusion of gametes to produce a new organism.

orange and red colors indicate the expanding areas on the cellular surface (Geitmann, 2010a).

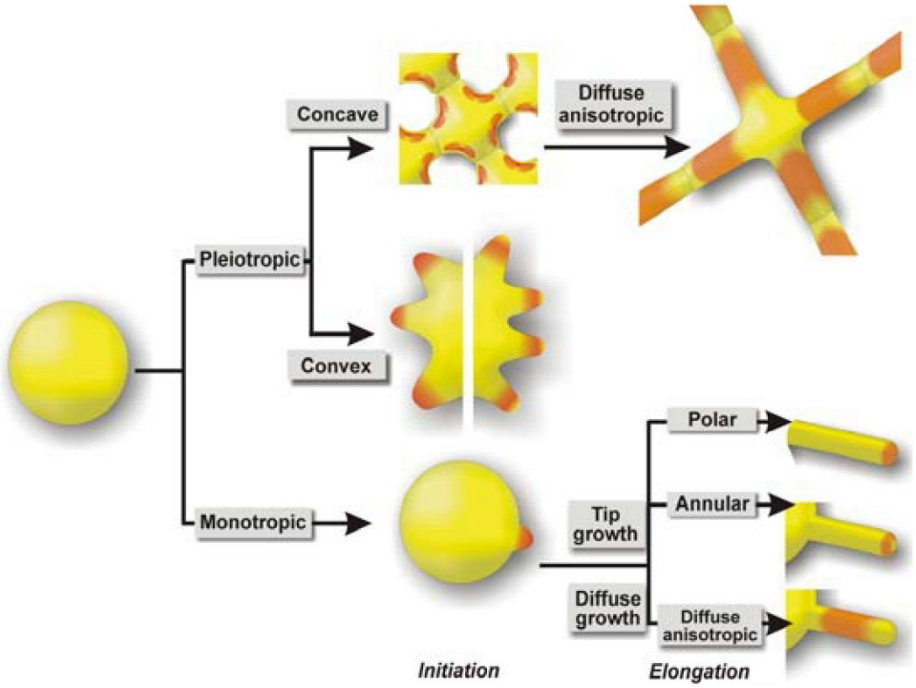

Figure 1.2: Different shapes of plant cells generated by heterotropic growth. Orange and red indicates expanding areas on the cellular surface (Geitmann, 2010a).

1.4.1 Pollen tube journey toward the ovule

Briefly, pollination starts by germinating the pollen grains on a receptive stigma followed by growth of pollen tubes formed by grain through the pistil tissue toward ovule. The function of the pollen tube is to decipher the guidance cues from the female tissue and to elongate toward the ovule (Fig 1.3a). A Scanning Electron Micrograph (SEM) of a *Camellia* pollen grain and germinated pollen tube are shown in Figure (1.3b) for lily pollen grain (Geitmann, 2010a). Once the pollen tube is near the ovule, a set of signal transduction events occur that guide the pollen tube towards its target, the femal gametophyte. Pollen tubes stop growing and burst to deliver the sperm cells at this stage (Franklin-Tong, 1999).

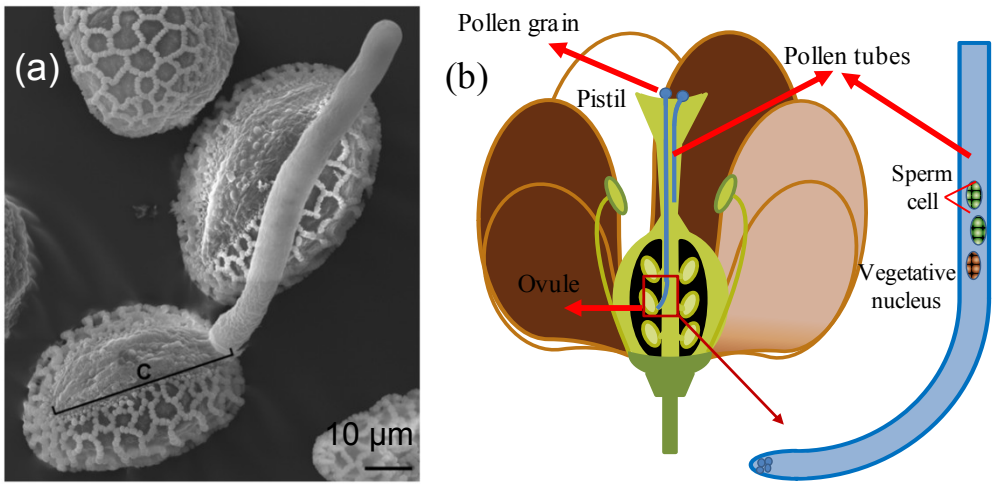

Figure 1.3: a) Scanning Electron Micrograph of germinated *Lilium* pollen grains (Geitmann, 2010a), b) The growth of pollen tube through the pistil tissue to deliver sperm cells to ovule.

1.4.2 Introduction to pollen tube growth

The pollen tube basically consists of semi-permeable membrane and cell wall surrounding the *cytoplasm*[4]. Three different cytoplasmic regions characterize cyto-architecture of a pollen tube (Fig 1.4). In the shank region, long *actin*[5] filaments transport the organelles to the subapical cytoplasm and recycle them back towards the rear of the pollen tube along the central region (Chebli *et al.*, 2013). The subapical region is identified by a collection of shorter actin filaments and is free of large organelles. In the apical cytoplasm, transmembrane trafficking (flow of proteins and other macromolecules with the aim of transport to destinations inside and outside of the cell) have been observed as the apex is

[4] The cytoplasm is a gel-like substance located within the cell membrane and contain all substances within the cell
[5] Actin is rod-shaped polymeric protein that in plant cells serves as intracellular transport system

the site of *endocytosis*[6] while *exocytosis*[7] delivers new synthetic materials required for cell elongation into the apical dome (Picton *et al.*, 1983b).

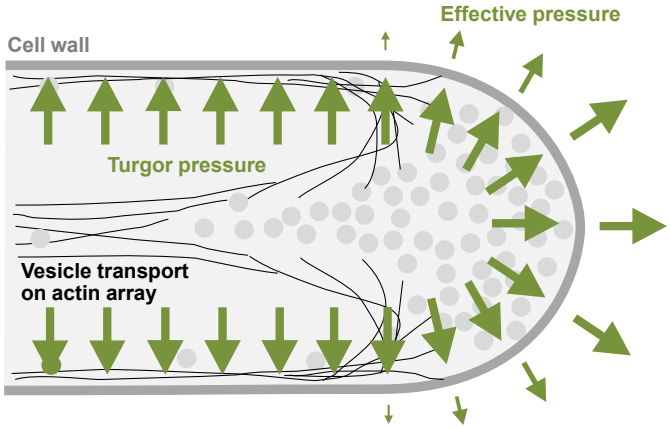

Figure 1.4: Schematic of pollen tube. Depending upon the species, the diameter of pollen tubes varies between 6-30 µm.

1.4.3 Characterizing polar growth of pollen tube

There were many attempts to characterize the tip growth of pollen tube. Although there are species that grow in steady manner, the growth rate of pollen tube is typically pulsative or oscillatory (Geitmann *et al.*, 1998) (Pierson *et al.*, 1995). Fig 1.5 shows the dynamic growth of a sample pollen tube in the form of growth length and growth rate over time (Geitmann and Cresti, 1998).

[6] [Endocytosis is a process by which cells absorb molecules (such as proteins) by engulfing them] (http://en.wikipedia.org/wiki/Endocytosis)
[7] [Exocytosis is the durable process by which a cell directs the contents of secretory vesicles out of the cell membrane]. (http://en.wikipedia.org/wiki/Exocytosis).

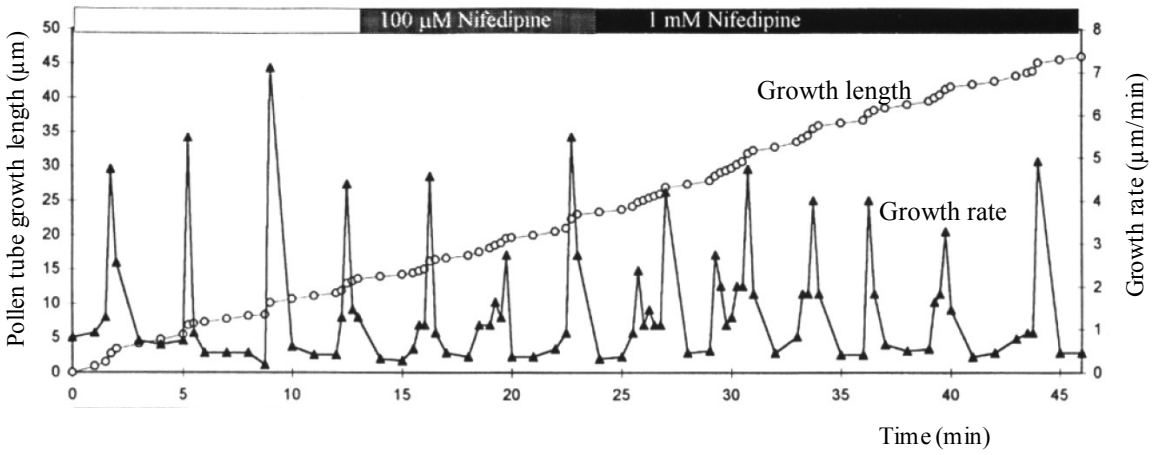

Figure 1.5: The dynamic pulsative or oscillatory growth behavior of pollen tube (Geitmann and Cresti, 1998)

Three different elongation patterns have been reported to occur sequentially during the growth. It can be informed that one cellular mechanism can generate different growth patterns due to the effect of regulators governing the dynamics of growth. The oscillatory growth rate is an important indicator for pollen tube to study the dynamic variation in effective regulators.

Various factors have been identified as regulators of the growth (Geitmann *et al.*, 2006a). However, it is mostly believed that turgor pressure and cell wall material properties are the main variables which control the cell growth. Hence, any other substance, ion or chemical material within the cell or the medium will affect either turgor pressure or cell wall mechanical properties.

Basically, in order to study the role of different growth regulators adjusting the turgor pressure or cell wall mechanical properties, the concentration of targeted ion or substance

is altered within the growth medium and the response of the pollen tube in the form of the change in 1) growth rate, 2) pattern of dynamic growth, 3) cell shape, 4) intracellular or extracellular ions gradient, 5) cellular biomechanics or 6) turgor pressure is detected. Any progress in detection techniques will help in understanding the growth regulators.

Turgor pressure as one of two main candidates of growth regulators is defined as the hydrostatic pressure within the cell. In steady state, it is equal to *osmotic pressure*[8] difference between inside and outside of the cell. A number of people have attempted to measure the turgor pressure and assess its role in plant cell growth through direct or indirect methods. The first direct measurement on turgor pressure was presented by (Green, 1968) using a pressure probe on *giant algal, Nitella*[9]. They used an air-water filled glass microcapillary to estimate turgor pressure. The compression of the air bubble allowed the measurement of intracellular pressure. (Hüsken *et al.*, 1978) developed the technique by replacing air bubble with oil filled capillary attached to a pressure sensor (Fig 1.6). They estimated turgor pressure for *Nitella* cell in the range of 0.1 to 0.6 MPa. Benkert et al. (Benkert *et al.*, 1997) used pressure probe apparatus to determine turgor pressure of lily pollen tube as 0.1 to 0.4 MPa. Lew et al. (Lew, 2005) employed a pressure-probe system for hyphal cell and the value of 0.4-0.5 MPa was estimated for turgor pressure. In all above experiments, a micropipette was filled with silicone oil with one end inserted into the cell and the other end connected to pressure sensor. Turgor pressure pushes the oil back into

[8] [Osmotic pressure is the pressure which needs to be applied to a solution to prevent the inward flow of water across a semipermeable membrane]. (https://en.wikipedia.org/wiki/Osmotic_pressure)
[9] [Algae is a large and diverse group of simple, typically autotrophic organisms, ranging from unicellular to multicellular forms]. (http://simple.wikipedia.org/wiki/Algae)

the pipette tip. By applying the pressure, the oil column is moved back to the tip position and turgor pressure is then estimated.

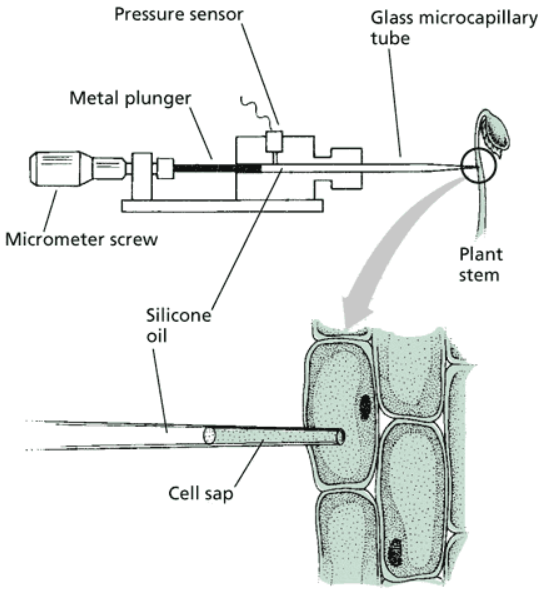

Figure 1.6: Schematic of pressure probe for measuring turgor pressure Zimmermann et al. (1978)

Although the pressure probe method is the only practical method of directly measuring the inside pressure, it requires a micropipette insertion into the cell which is considered as an invasive method. Indirect techniques were also applied to estimate the turgor pressure in which the cell is exposed to different known values of medium concentration. The method is based on determining at what concentration the cell collapses. This technique was used to measure the turgor pressure of about 0.8 MPa for fungal hyphae (Howard *et al.*, 1996).

Regardless of measuring techniques, two different arguments have been reported about the role of turgor pressure on the pollen tube growth. The primary approach proposed by a number of researchers (Plyushch *et al.*, 1995); (Messerli *et al.*, 2000a) introduced the local

change of turgor pressure as the cause of growth and specifically the cause of oscillatory pattern. Messerli et al. presented the evidence of increase on growth rate by sharp decrease on *osmolarity*[10] of the medium (Messerli *et al.*, 2000a). They introduced turgor pressure as the main regulator of growth. The same result was also reported showing that the change on turgor pressure through osmolarity variation affects the pollen tube growth rate (Winship *et al.*, 2010; Zerzour *et al.*, 2009a). Other group showed that the increase on the level of osmolarity in the culture medium inhibits pollen tube growth and it suggests that turgor pressure is essential for cell elongation (Pierson *et al.*, 1996). The change on turgor pressure was measured by the pressure probe, but could not find an obvious relation between turgor pressure and the growth rate oscillation in lily pollen tube (Benkert *et al.*, 1997). It was only argued that that turgor pressure is necessary for growth.

The effect of turgor pressure on the growth rate of the pollen tube was numerically modeled (Fayant *et al.*, 2010b). They attempted to model the cell wall deformation resulting from hydrostatic pressure. They modeled the tip apex by considering the gradient of Young's modulus changing from 4000 MPa for the shank down to 12 MPa for the pectin at the extreme apex. They showed that the change in turgor pressure results in the increase in tube length per load cycle.

The other argument about the role of turgor pressure on cell growth was presented by a number of researchers who claimed that turgor pressure is not the regulator for the growth

[10] [Osmolarity is the measure of solute concentration, defined as the number of osmoles (Osm) of solute per litre (L) of solution] (osmol/L or Osm/L). (http://en.wikipedia.org/wiki/Osmotic_concentration)

(Harold *et al.*, 1995); (Heath *et al.*, 1999). To verify their claim, they reported the observation of fungal hyphae growth without any measurable turgor pressure in some species of fungal hyphae. Some species of hyphae also grow faster with zero or at most very low value of turgor pressure (Davis *et al.*, 2000). In addition, the idea is enforced especially when growth rate of pollen tube growing in a gel type medium is comparable with the rate of growth in liquid medium (Tomos, 1988). This group of researchers argued that the growth is not because of increase in turgor pressure, but it is due to cell wall relaxation.

Cell wall relaxation is a phenomenon in which the material strength of the cell wall reduces either due to turgor pressure (Panovko *et al.*, 1973) or enzymatic reaction at the apex (Schopfer, 2006). In the latter case, relaxation seems to be the cause of temporal reduction on turgor pressure, increasing the water influxes and then leading to the cell growth. It means that any likely oscillation of the turgor pressure follows the cell wall relaxation at the apex. But in the case of turgor pressure, it causes cell wall deflection as well as cell wall relaxation due to opening for insertion of new materials through semi-permeable cell wall.

In order to understand the role of cell wall relaxation on cell growth, two main strategies are dominant. The first is the technique of manipulating the cell wall, named micro-indentation, which has been used for various tip growing cells. Micro-indentation has also been used to characterize the mechanical stiffness of the plant cell wall (Parre *et al.*, 2005c); (Zerzour *et al.*, 2009a). This method uses a glass stylus actuated by a horizontal

beam. By monitoring the cell wall deflection and measuring the reaction force applied to glass stylus, the mechanical strength of the wall is estimated. It was successfully implemented to estimate the stiffness of the cell wall at the distal and apical regions. It showed that stiffness at the apex of pollen tube is significantly lower than stiffness at the shank part of the cell (Parre and Geitmann, 2005c).

The second technique refers to the bio-chemistry side to identify the material components of cell apex. In the tip of the pollen tube, pectin appears to be the major component of the cell wall. *Pectin*[11] exists at the apex esterified and is required to resist against turgor pressure (Roggen & Stanley, 1969); (Holdaway-Clarke et al., 2003). Parre et al. (Parre and Geitmann, 2005c) argued that the amount of pectin and also the degree of its esterification are essential in determining the cell wall stiffness. To demonstrate the effect of amount of pectin, various concentrations of *Pectinase*[12] were added to the medium. Pectinase has the digesting enzyme activity on pectin and is considered as pectin inhibitor. They showed that by moderately increasing the pectinase, the pectin reduces at the apex, cell wall stiffness lowers and in consequence, the growth rate increases. They also observed cell bursting as a result of higher amount of pectinase. This observation indicates the digestion of pectins at the apex destabilizes the cell wall in such a way that it enables turgor pressure to expand the cell wall until it bursts.

---

[11] [Pectin is a structural heteropolysaccharide contained in the primary cell walls of terrestrial plants]. (https://en.wikipedia.org/wiki/Pectin)

[12] [Pectinase is a general term for enzymes, such as pectolyase, pectozyme and polygalacturonase, commonly referred in brewing as pectic enzymes. These break down pectin, a polysaccharide substrate that is found in the cell walls of plants]. (http://en.wikipedia.org/wiki/Pectinase)

In order to know the degree of esterification of pectin on material properties, the activity of the enzyme pectin methyl-esterase (PME) has been evaluated (Geitmann, 1999). This enzyme is supposed to de-esterify methyl-esterified pectin into acidic pectin. Ca^{2+} ion is then cross-linked to acidic pectin and forming a semi rigid gel (Carpita *et al.*, 1993). Parre et al. (Parre and Geitmann, 2005c) studied the effect of PME as growth inhibitor and observed that after specific concentration of PME, the growth rate starts reducing. They argued that the raise of de-esterification level of pectin increases the cell wall stiffness and reduces the growth rate.

Based on what is reported in the literature, it is believed that both cell wall relaxation and turgor pressure influence the growth and could be considered as the fundamental variables of the growth. The effect of other intracellular ions can be interpreted as the regulator processes on pollen tube growth likely mediated either by influencing turgor pressure or cell wall material properties (for example for alteration in the exocytosis rate). This is supported by the fact that many of the underlying events such as vesicle trafficking, actin microfilament polymerization, and apical ion flux oscillate with the same period of growth rate, but usually with different phases (Holdaway-Clarke *et al.*, 2003),(Chebli *et al.*, 2007b).

The effect of Ca^{+2} ion as the dominant ion at the apex has been already studied with specific required concentration limit (Picton *et al.*, 1983a). Increasing calcium concentration from 10^{-5} M to $2.5*10^{-5}$ M raises the growth rate by 20%, but further increase leads to reduction in growth. In addition, they used La^{+3} and Gd^{+3} as Ca ion

inhibitors for lily pollen tube to study the behavior of pollen growth due to change in conductance of Ca^{+2} channels. They suggested that Ca^{+2} signal probably leads to sudden liberation of vesicles to the wall and in consequence, the *local cell wall relaxation* occurs. Oscillation of Ca^{+2} magnitudes with the same period as that the growth rate was then detected (Messerli *et al.*, 2000a).

Modeling of tip growth has also been employed to understand the pollen tube growth. It is introduced as the process in which only a highly confined area of surface expands and new material is deposited at the tip. Many biological events such as vesicle transport, ion concentration, cell wall extensibility and internal pressure have been considered as effective elements on the cell growth, but presenting a comprehensive model covering the effect of all these variables is still a challenge in cell modeling. Few theoretical models have been developed to study the role of biological parameters such as vesicle supply centre (VSC) (Bartnicki-Garcia *et al.*, 2000) or Ca ion concentration (Kroeger *et al.*, 2008), but most of the models have focused on the turgor pressure and dynamic change of cell wall material deposition as the fundamental variables (Dumais *et al.*, 2006). In these models, motion of plant cells is considered as turgor pressure driven event pushing against a viscoelastic wall material. Although the recent biomechanical model predicts tip growth of pollen tube (Chebli and Geitmann, 2007b), still there is the lack of experimental results to verify the current models (Kroeger *et al.*, 2012b).

Recently, a kind of interplay between turgor pressure and cell wall material was assessed (Schopfer, 2006). The cell wall was presented as a viscoelastic composite with stress

relaxation property which is activated at a specific time depending on the amount of stretching. It was argued that both turgor pressure and cell wall relaxation have to be considered as the regulators of growth. Later, it was argued that to affect cell growth, all growth regulators within the cell ultimately have to take action on one of the two main regulators of the growth: cell wall softening or turgor pressure (Zerzour *et al.*, 2009b). It is believed that the study of the change of biological events influencing turgor pressure or cell wall relaxation will be valuable to better understand the polar growth phenomenon.

Mechanical sensing is an effective method that has recently been used to measure the growth force as one of detectable parameters for studying pollen tube behavior. Geitmann et al. (Geitmann, 2001) tried to formulate the force applied on the obstacle by considering the role of both turgor pressure and wall material properties. They argued that there is a difference between the value of turgor pressure and the pressure that pollen tube applies against the mechanical barrier and this is because of resistance of cell wall against the internal pressure. By controlling the material properties of the tube wall, the pollen tube has the capability to transfer the force between zero to a maximum value against the barrier.

Money et al. (Money *et al.*, 2004) practically estimated the growth force of hyphae cell by positioning strain gauge normal to the direction of growth at the apex of hyphal fungus to approximately 0.2-0.8 MPa. Electrical signal from the strain gauge was calibrated to measure the growth force (Fig 1.7). By knowing the cross section of the pollen tube and measured value of the growth force, turgor pressure of cell was estimated. They noticed

that there is indirect relation between the turgor pressure and the measured force, verifying the result of Benkert et al. (Benkert *et al.*, 1997).

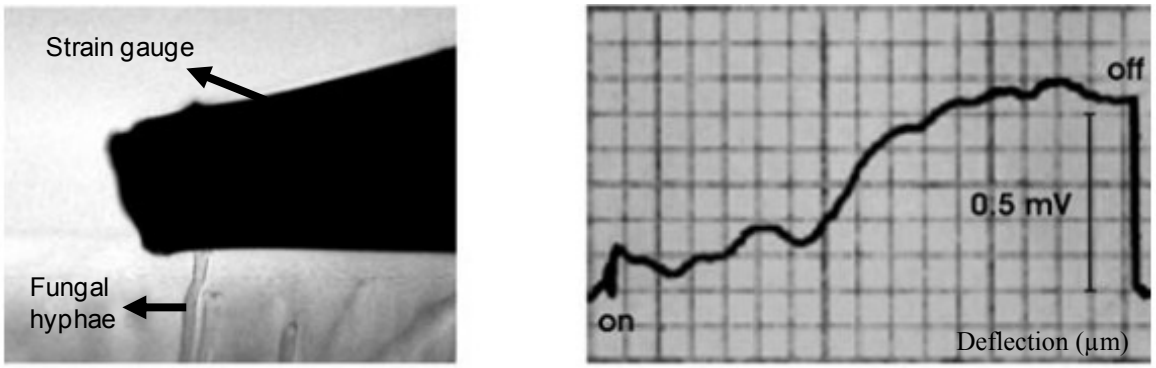

Figure 1.7: Mechanical sensing of hyphae growth force against silicon beam (Money *et al.*, 2004), a) Fungal hyphae senses the strain gauge, b) strain gauge response

Although mechanical sensing of hyphal cell (Money *et al.*, 2004) looks as a significant technique for detecting the biological events occuring within the cell and to see how the interaction of pollen tube and mechanical structure affects on either turgor pressure or cell wall mechanical properties, no other research has been reported to use the mechanical sensing for characterizing the behavior of small plant cells. This might be because the experiment with the strain gauge was difficult. There was no control on the direction of the growth, so the normal contact against the strain gauge occurred by chance and the interpretation of the data was not simple. They used a large silicon beam (100 μm thickness and 10 mm width) compared to the size of the cell (10 μm). The comparison between 10 μm diameter of hyphal cell and the large size of silicon beam depicts the complexity of detection. The silicon beam is not soft enough to be a good candidate for sensing force variation at the level of cell force.

1.4.4 Biological aspects about pollen tube

In spite of extensive research on pollen tube growth in order to detect various regulators of the growth, many questions are still unknown and should be addressed. It is not still clear what is the main regulator of the growth, or what extent the other regulators influence the growth, or how the pollen tube adapts both turgor pressure and cell wall mechanical properties in response to mechanical or chemical stimulation, or how it controls the growth passage through different matrices with different mechanical stiffnesses, or how the chemical or mechanical signals altogether cause pollen tube reorientation toward the ovule, or how pollen tube can grow within the air during the way towards the ovule, or how the pollen tube bursts once it approaches the ovule and passes the micropyle in order to deliver the gamete cell to the ovule, or what kind of mechanical or chemical signals prevent entering the second pollen tube into the ovule and reorient it away from the ovule.

Clearly, to answer these levels of biological questions, new external experimental platforms more similar to *in vivo* environment (*ex vivo* environment) with the possibility of local cell treatment and potential of applying more controllable mechanical and chemical stimulation is promising. It is believed that more effort is still required to have a better understanding of polar cell growth analysis.

1.4.5 Challenges in studying pollen tube in open assay

Up to now, there have been technical limitations to the manipulating of the pollen tube apex during the cell growth. In addition, a unique growth platform with reliable detection system has always been vital to make the experimental results comparable. So far, no

micro-device has been used to study the pollen tube growth at the apex. It is believed that micro-device will be an appropriate environment to characterize the pollen tube growth and to study different aspects of tube growth towards the ovule since its size is compatible with that of the pollen tube. It has the capability to locally apply biological and chemical change on growth environment around the pollen tube tip and also to induce mechanical signal during the cell growth. Application of micro-sensors inside the micro-device enables a more comprehensive local characterizing of the pollen tube during the growth. Hence, the purpose of the thesis is to present *ex-vivo lab-on-chip* [13] (LOCs) to provide microenvironment more similar to pollen tube pathways from stigma to the ovule. The platform helps to study the dynamics of pollen tube growth in response to mechanical and chemical signals. Using these LOC devices, the interplay of the turgor pressure and cell wall mechanical properties are studied in response to a mechanical signal and also the pollen tube adaptation growing in different growth environment is evaluated.

1.4.6 Application of BioMEMS for plant cell studies

It is believed that micro-systems have high potential to overcome the constraints of controlled mechanical or chemical stimulation of pollen tube. The first report on the application of a micro-device for analyzing the pollen tube behavior was presented on monitoring the pollen tube guidance in response to pistil tissues (Yetisen *et al.*, 2011b) (Fig 1.8). The design involves a main central groove with side chambers. A schematic layout of

[13] A lab-on-a-chip (LOC) is a device that integrates one or several laboratory functions on a single chip of only millimeters to a few square centimeters in size.

the micro-device and the experimental results of growing pollen tube in microenvironment is shown in Figure 1.7.

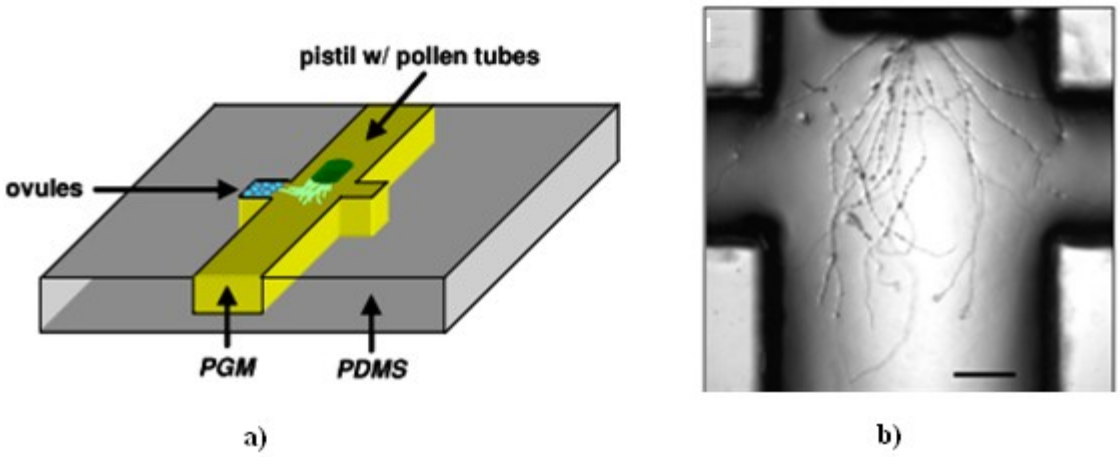

Figure 1.8: Schematic of microdevice for growing pollen tubes, a) schematic layout of microfluidic chip designed to support pollen tube growth, b) Experimental testing of pollen tubes growth within fabricated chip, scale bar: 200 µm (Yetisen *et al.*, 2011b)

It was reported that the growth rate and length of pollen tube in microdevice was comparable to those pollen tubes growing in plate assays. They fabricated microfluidic environment that mimics the in-vivo micro-environment of ovule fertilization.

Although the earlier studies have attempted to present appropriate interpretation of polar cell growth, the overall insight to the literature confirms that more research is required in this field.

1.5 Rationale and scope of the thesis

The development of measuring techniques to obtain more experimental data related to the growth behavior is obviously essential in order to approach comprehensive explanation of the polar cell growth. In addition, due to the lack of common experimental setups for

biological testing, the results are occasionally not comparable. Presenting a unique platform will serve to have more convergence on the results of similar tests and to make them more comparable.

In order to answer some unknown and fundamental aspects of pollen tube growth such as 1) Chemical attractor steering towards the ovule or 2) Growth behavior in air during the journey towards the ovule or 3) Bursting of pollen tube at the vicinity of ovule and 4) Understanding of its invasive life style, new experimental platforms identical *ex vivo* growth environment is required. The study of pollen tube in open assay cannot provide such a microenvironment for studying the pollen tube.

The dynamic growth in the form of pulsative or oscillatory growth is a unique property of tip growing pollen tube which can be exploited to study the role of other ions in regulating the tube growth. However, changing the growth environment in open assay is still challenging for uniform alteration of medium. Developing new platforms with simpler and stable control on growth environment is necessary to find the relation between the dynamics of ion gradients around the tip and the dynamic of pollen tube growth.

No comprehensive study has been done to experimentally investigate the interplay role of cell wall mechanics and turgor pressure on cell growth. Even though, the recent work on studying the interaction between cell and mechanical beam has employed a mechanical element to assess the response of the cell (Money, 2004), up to now, no study has been reported that deals with the invasive behavior of pollen tube. Recently, microsystem assay

has joined the biological area to provide a better platform for growing the pollen tube, but still lack the ability to characterize the pollen tube growth at the apex area of the cell.

The contribution of proposed LOCs is to benefit the biological area of plant cell analysis by providing a unique *ex-vivo* micro-environment compatible with the size of an individual pollen tube. This environment will help analyze the effect of local chemical and mechanical stimulation of pollen tube in order to characterize the static and dynamic response of pollen tube growth. Study of bio-micromechanical interaction will develop new methods of cell analysis to enhance our knowledge about fundamental biological elements which control the pollen tube growth at the apex area that would help to understand the interplay role between turgor pressure and cell wall mechanical properties. The outcome resulting from this thesis will help understand some aspects of pollen tube growth from stigma to the ovule and is used to estimate biological parameters such as cell wall mechanics and invasive growth force.

1.6 Objectives of the thesis

In this research, the emerging microsystem technology is affiliated to cell biology, especially morphogenesis area to study the behavior of pollen tube in a microenvironment compatible with the size of pollen tube. The objective of the thesis is to improve the understanding of plant cell growth during the growth from stigma to the ovule by studying static and dynamic cell response to local mechanical-chemical stimulations.

More specifically, the objectives of the thesis are the following:

1. Develop a LOC *platform* to characterize the behavior of individual pollen tubes in *ex vivo* environment through design, fabrication and testing.

2. Studying of *static* and *dynamic* behavior of pollen tube in response to *local chemical* and *toxic treatment* at the tip or distal region in order to find more accurately the role of growth regulators and to understand the pollen tube biology. The study will help realize the application of tip growing pollen tube for toxicity detection.

3. Characterizing the interaction of pollen tube with *micromechanical structures* or *fluid load*ing in order to answer biological questions regarding the role of mechanical signals on pollen tube bursting in the vicinity of ovule, the regulation of growth during different environment with different matrix stiffnesses and quantification of mechanical properties of cell wall as essential parameters required for biomechanical and mathematical modeling of plant developmental processes.

1.8 Layout of the thesis

This thesis has been organized as follows:

Chapter 1 introduces BioMEMS and its application for cellular biology, and the capability of microfluidics for handling effective *ex vivo* microenvironment for monitoring cell response to the chemical, biological influences. Pollen tube as the main part of plant cells

is introduced and its difference with other cells is explained. The presented review on pollen tube growth behavior, different technical methods for cell characterizations and the main challenges on studying pollen tube is detailed. The potential of microfluidic environment for studying cell response to chemical and mechanical signals is presented. The chapter also presents the rationale and the scope of the present thesis, layout and contributions.

Chapters 2 and 3 describe the design, fabrication, testing and enhancement of microfluidic platform for future cellular studies on pollen tube. The numerical and experimental methods are employed to provide a stable and proper platform by which a series of pollen tubes could grow within microfluidic chip under identical growth conditions which facilitate the comparison of results of different pollen tubes growing in different microchannels.

Chapter 2 introduces Micro-Electro-Mechanical Systems (MEMS)-based TipChip platform with applications to simplify sophisticated functions such as chemical reactions, drug development and bioassays by integrating them within a single micro-device, a Lab-on-chip (LOC). This chapter describes the basic configuration of the microfluidic network developed to allow for simultaneous observation of multiple pollen tubes. The fluid flow conditions that are conducive for pollen grain positioning and pollen tube growth within the microchannel network were determined experimentally. Several basic configurations that can be included in the modular setup are described and tested experimentally. The

potential of using pollen tube for characterizing cell response to local treatment is evaluated by a case study.

Chapter 3 presents the challenges faced in studying the pollen tube within TipChip microfluidic device including pollen grain accumulations and critical flow rate. This chapter presents how to facilitate and enhance the positioning of pollen grains at the entrances of the microchannels and to provide identical growth environments for growing pollen tubes along each microchannel. The dimensions of the microfluidic network and the inlet flow are properly calculated using theoretical analysis and experimental testing in order to improve the performance of the microdevice. The criteria for an enhanced design are established and used to compare the performance of various designs based on modeling and experimental results. The enhanced design is chosen for the experiment in the next chapters.

Chapters 4-7 present different LOC and microfluidic platforms to study the static and dynamic response of pollen tube to the chemical, biological and toxic substances. Chapter 4 focuses on innovative methods for locally stimulating the pollen tube at the tip and at the distal region using side injection testing and tip growth in air trap, respectively. The Chapter 4 also explores more accurately the role of sucrose as the agent controlling the turgor pressure and calcium ion as the candidate controlling the cell wall mechanical properties on regulating the pollen tube growth rate and growth direction. Chapters 6,7 present LOC devices for characterizing dynamic response of pollen tube growth to the change on growth regulators and also to toxic substances within growth medium. Since

pollen tube has oscillatory growth, the change in dynamic oscillation frequencies is defined as the dynamic response to the change of growth regulators or the presence of toxic materials.

Chapter 4 addresses the local treatment of pollen tube tip through development of a new LOC device with laminar flow based continuous administration of two different solutions with a movable interface that allows to dynamically target *Camellia japonica* pollen tube. Here, the calcium which is known as the agent affecting reorientation of pollen tube growth was used as a test substance. A discussion about the role of calcium in mechanical properties of cell wall and regulating the cell growth and direction is presented at the end of the chapter.

Chapter 5 presents a new microfluidic platform for local treatment of pollen tube at the distal region without any direct effect on the tip. In this chapter, the effect of different calcium and sucrose concentrations on the growth behavior of pollen tube were studied once the tip was growing in the air. At the end, the capability of this platform in presenting new clues about the hypothesis on the existence of internal ca^{2+} ion stores within the tube and the hypothesis of the whole-cell pressure increase inside the tube are discussed

Chapter 6 addresses the dynamic growth of pollen tube within microfluidic environment. This chapter explores the primary and secondary oscillation frequencies of pollen tube which was not simply detectable on pollen tubes growing in open assays. In addition, the

effect of growth regulators such as sucrose on dynamic growth of pollen tube through characterizing the alteration of oscillation frequencies is studied.

Chapter 7 discusses the application of pollen tube as whole-plant cell sensor for toxicity detection. It exploits the benefit of trapping pollen grain and growing pollen tubes along microchannel in a directed manner in order to detect the pollen tube response to the existence of environmental toxic substances within growth medium. Aluminum ion, as toxic substance for animals and humans, was detected in concentration-based manner for a wide range of concentration.

Chapters 8 and 9 present the potential of MEMS technology to study the response of pollen tube to the *mechanical* stimulations through characterizing the interaction of pollen tube with *micromechanical structures* and *fluid load*ing. These chapters help answer several biological questions regarding the quantification of the mechanical properties of cell wall, invasive life style of the pollen tube, the role of mechanical signals on pollen tube bursting and the regulation of growth during growth along different cellular matrix.

Chapter 8 explains the performance of a Bending Lab-on-chip (BLOC) approach to quantitatively determine the Young's modulus of the pollen tube cell wall as essential parameter required for biomechanical and mathematical modeling of plant developmental processes under fluid loading. Pollen grains are injected into the LOC and the pollen tube is guided through the narrow microchannel to be subsequently bent by fluid flow orientated perpendicular to the tube. Based on the observed flexural rigidity of the cell wall, the

Young's modulus of the cell wall was estimated using a finite element model of the experimented geometry. The validity of the measured value is discussed at the end of the chapter.

In Chapter 9 the mechanical interaction of pollen tube with microgaps is studied. The microgap structure provides a condition very similar to those cellular distances that pollen tube penetrates through. The change of pollen tube diameter and the deflection of microgap are presented as the result of coupled interaction in this chapter. This chapter addresses several biological questions such as the role of mechanical signaling on pollen tube bursting once the tube reaches the ovule and delivers the germ cell and the interplay role of turgor pressure and cell wall mechanical properties on regulating the growth through mechanical barriers. The growth force of pollen tube is estimated as the biological parameter explaining the invasive life style of pollen tube.

Chapter 10 presents the conclusions of the present work. The work from the present thesis has been published in several international journals, and also has been presented in national and international conferences as listed in Chapter 10.

Chapter 2

TipChip - A Modular, MEMS-Based Platform For Experimentation and Phenotyping of Tip Growing Cells

2.1 TipChip

The Primary microfluidic platform for evaluating the feasibility of growing pollen tube within microfludic environment and guidance along growth microchannel with the size of slightly bigger than the pollen tube diameter is explained in this chapter. This work has been published in two Journals papers of *Journal of Micromechanics and Microengineering, vol. 22, 115009, 2011,* with my contribution as the second author and *The Plant Journal, vol: 73, pp:1057-1068, 2013*, with my equal contribution as author. In the results section, only my contribution to this work is presented.

Abstract

Large scale phenotyping of tip growing cells such as pollen tubes has hitherto been limited to very crude parameters such as germination percentage and velocity of growth. To enable efficient execution of more sophisticated assays, an experimental platform was developed based on microfluidic and MEMS technology, the TipChip. The device allows positioning of pollen grains or fungal spores at the entrances of serially arranged microchannels. The tip growing cells, pollen tubes or fungal hyphae, can be exposed to chemical gradients, microstructural features, integrated biosensors or directional triggers within the modular microchannels. An optimization of fluid network geometry and an experimental proof of concept for various channel configurations are illustrated. The platform will allow both,

more efficient experimentation and large scale phenotyping under precisely controlled, reproducible conditions.

2.2 Introduction

Tip growing plant and fungal cells have been widely used as model systems for the cellular morphogenesis in walled cells (Geitmann *et al.*, 2001; Geitmann *et al.*, 2000). Growth in walled cells occurs through the turgor driven expansion of the cell wall and simultaneous assembly of new cell wall material. Tip growth is characterized by a spatial confinement of this cellular expansion process to the very end of the cell (Geitmann *et al.*, 2009b; Geitmann *et al.*, 2006b). The resulting structure is a perfectly cylindrical protuberance capped by a hemisphere- or oval-shaped apex. Among the hallmarks of tip growing cells are the speed of growth (up to 1 cm/h in pollen tubes and fungal hyphae) and the ability to control the direction of growth. This later function allows tip growing cells to follow external guidance cues, a crucial feature for the execution of their respective biological functions: Root hairs have to grow away from the root to efficiently absorb water and minerals, fungal and yeast hyphae have to invade hosts and find mating partners, and the pollen tube needs to reach a receptive ovule nestled deeply within the pistillar tissues. How tip growing cells focus their growth activity onto a single site on their cellular surface and how they control growth dynamics through exerting temporal and spatial regulation has been the subject of a substantial body of research (Feijó *et al.*, 2001; Geitmann *et al.*, 2007b; Malhó, 2006; Palanivelu *et al.*, 2011b). Intriguingly, numerous genes have been found to be expressed exclusively in tip growing cells (Honys *et al.*, 2003; Honys *et al.*, 2004; Pina *et al.*, 2005), but our understanding of the functions of many of the proteins

encoded by these genes warrants major efforts. These will require developing methods for more sophisticated experimentation and for large scale phenotyping. Here we describe a platform that has been developed to advance both experimentation and phenotyping in tip growth research. The platform has been optimized for use with pollen, but can be adapted easily to other tip growing cells produced from small cell bodies such as hyphae generated by fungal spores and rhizoids produced by algal zygotes.

Large scale assessment of pollen tube performance in the past has largely been limited to quantifying seed set (*in vivo* approach) and to determining the percentage of germination, the average growth rate, and the morphology of the cell (*in vitro* approach). These parameters can be determined microscopically in batch samples, and are based on simple *in vitro* cell culture techniques (Bou Daher *et al.*, 2008). However, tip growth is a complex process and many other parameters have been studied using highly sophisticated methods with the aim to investigate pollen tube biology. These include monitoring ion fluxes with a vibrating probe (Feijó *et al.*, 1995b; Feijó *et al.*, 1995c; Messerli *et al.*, 1997, 1998; Messerli *et al.*, 2003a), measuring the biomechanical properties with a micro-indenter (Geitmann *et al.*, 2004; Parre *et al.*, 2005a; Parre and Geitmann, 2005c; Zerzour *et al.*, 2009b), assessing invasive and tropic growth in experimental setups exposing pollen tubes to mechanical obstacles and directional triggers (Bou Daher *et al.*, 2011a; Gossot *et al.*, 2007; Malhó *et al.*, 1992b; Palanivelu *et al.*, 2000; Palanivelu and Tsukamoto, 2011b), as well as studying the dynamics of intracellular transport using FRAP (fluorescence recovery after photobleaching) and advanced image analysis (Bove *et al.*, 2008a; Malhó *et al.*, 2005; Parton *et al.*, 2003) and triggering internal signaling processes using laser-mediated release

of caged calcium (Malhó *et al.*, 1996). These experimental approaches have yielded important information on the functioning of the pollen tube and many of them would be extremely useful as assays to discriminate the characteristics of pollen tube phenotypes. However, these approaches are typically extremely time-consuming (since only one cell can be observed at any given time) and associated with high variability that makes them unsuitable for the investigation of large numbers of cells and phenotyping. We therefore designed an experimental platform that allows for the simultaneous investigation of multiple tip growing cells, in a highly reproducible manner, under precisely controlled conditions. Importantly, the platform enables the design of a panoply of different experimental approaches including exposing pollen tubes to a microstructural feature and/or chemical gradients, applying chemical and enzymatic agents locally and measuring forces, currents and turgor pressure. The modular nature of this platform makes it ideally suited both for phenotyping and for the development of new experimental approaches to study the biology of tip growing cells.

The TipChip platform is based on Micro-Electro-Mechanical Systems (MEMS) technology. This technology has been exploited in biological and medical applications to simplify sophisticated functions such as chemical reactions, drug development and bioassays by integrating them within a single micro-device, a Lab-on-chip (LOC) (Cheung *et al.*, 2006a; Giouroudi *et al.*, 2008b; Nuxoll *et al.*, 2009a). Here we describe the basic configuration of the microfluidic network developed to allow for simultaneous observation of multiple pollen tubes. The fluid flow conditions that are conducive for pollen grain positioning and pollen tube growth within the microchannel network were determined

experimentally. Biocompability testing was performed to determine which materials generally used in MEMS fabrication are compatible with pollen tube growth. Several basic configurations that can be included in the modular setup are described and tested experimentally.

2.3 Overall Lab-On-Chip (LOC) design

In order to be able to manipulate individual tip growing cells, these need to grow through narrow channels that are suitable for harboring the desired test geometry or experimental test device. Conventional and commercially available microfluidic perfusion systems (Lee *et al.*, 2008a) are not suitable since they typically collect the cells in a central flow chamber and would not force tip growing cells to grow in any particular direction. The TipChip is specifically designed to enable investigation of longitudinally elongating cells. In addition to being adapted to tip growing cells, the platform developed here was designed to respond to a number of criteria that were considered essential: The LOC has to allow high resolution brightfield and fluorescence imaging and should be possible to observe multiple cells simultaneously. The setup was conceived to be modular to allow incorporation of various structural, micro-mechanical and chemical testing methods.

Fabrication of the designs was done as explained in Materials and Methods (Section 2.7). Tests using two different methods for photomask (transparent sheets and glass chromium mask) production revealed that more expensive technology is required to fabricate microchannels with surfaces that are sufficiently smooth compared to the dimensions of the pollen tube (see Fig. 2.6 for examples for both techniques). In order to ensure the

simultaneous observation of multiple cells, the setup was designed to comprise a serial arrangement of microchannels through which the tip growing cells are supposed to elongate. Contrary to macroscopic channel setups such as those used for *Arabidopsis* seedlings (Grossmann *et al.*, 2011a), the manual positioning of individual cells such as pollen grains or fungal spores in front of microchannels would be highly unpractical if not unfeasible because of their small size. We therefore designed the microfluidic network to allow for fluid flow driven positioning of cells at the entrances of a series of microchannels. The overall microfluidic network consists of an inlet, a distribution chamber giving access to the entrances of numerous microchannels, and two types of outlets (Fig. 2.1,a). One outlet allows for the evacuation of excess pollen from the distribution chamber, the second type of outlet drains liquid from the ends of the microchannels and thus allows for continuous liquid flow through the microchannels. The configuration encloses the cells from all sides thus preventing the evaporation of the growth medium, a phenomenon which has proved difficult to control in open assays (Yetisen *et al.*, 2011a).

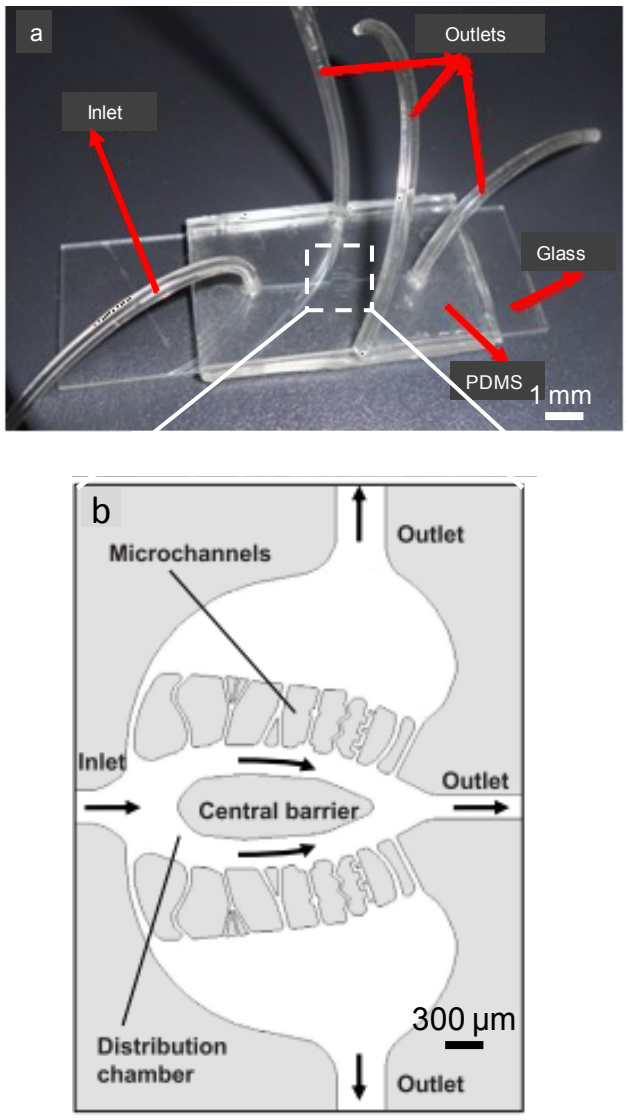

Figure 2.1: Overall design of the TipChip, (a) Image of the TipChip showing the PDMS layer attached to a cover slip and the attached inlet and outlets, (b) General schematic design principle of the microfluidic network in the TipChip. The pollen suspension is injected through the inlet and the pollen grains move through the distribution chamber and either get trapped at the entrances of the microchannels or evacuated through the distribution chamber outlet. There is a central barrier to guide the pollens toward the microchannels.

The whole platform was conceived to be planar with a limited thickness in order to avoid the accumulation of cells into stacks that would represent a mechanical impediment to fluid flow and a visual obtrusion preventing microscopical observation. The height of the

distribution chamber was therefore set to be between 1.2 and 1.5 times the diameter of the cells to be distributed. Here and in the following, optimized dimensions for pollen grains of the species *Camellia* are provided. The pollen tube of this species grows extremely straight and rapidly thus making it an ideal model system for cytomechanical studies (Bou Daher and Geitmann, 2011a) and suitable for a proof of concept experiments in the present context. For pollen grains from other species or fungal spores, the dimensions can be adjusted easily. *Camellia* pollen grains typically have a diameter of 60 μm, therefore the height of the microfluidic network was set to 80 μm, thus allowing the grains to move freely within the distribution chamber but preventing accumulation in z-direction.

The principle of the setup is to inject a suspension of pollen or spores into the distribution chamber through the inlet and to trap individual cells at the entrances of each microchannel, similar to other setups developed in the past (Kobel *et al.*, 2010; Tan *et al.*, 2007), but with the difference that the adjacent microchannels would have to be of substantial length. One of the main challenges was to design the distribution chamber such that most or ideally all entrances of the microchannels would be occupied by a single or very few cells after simple injection of the cell suspension. Large accumulations of cells were to be avoided, since preliminary experiments suggested that these hamper fluid flow through the microchannels thus affecting the experimental conditions and reproducibility. Two geometries for the distribution chamber were tested, by an oval shape with a central barrier (Fig. 2.1,b). A combination of fluid flow simulation and iterative experimentation is required in order to find the ideal dimension to prevent accumulation and increase the number of trapped channels. We will do this comprehensive analysis in Chapter 4 to

estimate the ideal dimensions. Briefly, the experimental testing showed that exactly one pollen grain per microchannel entrance can be trapped in the setup with rectangular distribution chamber (Sanati Nezhad *et al.*, submitted-b). Trapping is achieved by pollen grains moving along the streamlines created by the laminar flow imposed by slow injection of the pollen suspension (Fig. 2.2a). To accomplish optimal trapping, the entrances were designed as a curved notch, the narrow end of which is smaller in the x-y plane (30 µm) than the size of the pollen grain (2.2b,c). The microchannels proper are narrow conduits through which pollen tubes are expected to grow. In modular manner, these microchannels can be equipped with the desired experimental setups such as mechanical obstacles, microstructural features, chemical gradients, electric fields and biosensors.

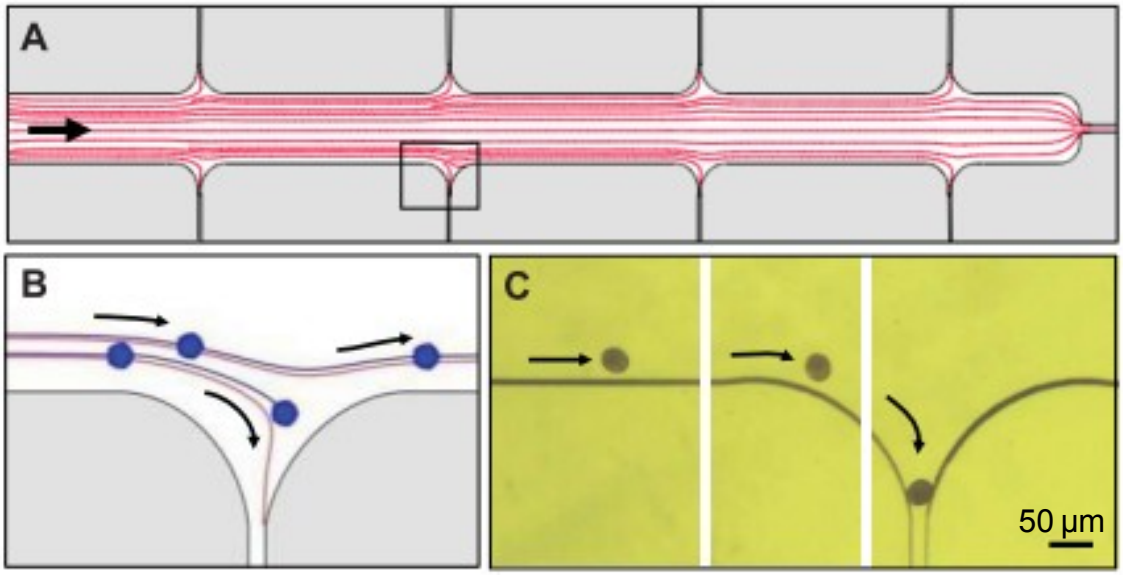

Figure 2.2: Geometry and fluid flow in the rectangular distribution chamber of the TipChip (a) Fluid flow simulation showing the streamlines within the distribution chamber. (b) Detail of the simulated streamlines (red) and experimentally observed pollen grain movement (blue) through the distribution chamber. (c) Micrographs of a pollen grain driven by fluid flow and trapped at the entrance of a microchannel. The stitched images show the same pollen grain at three different times. Bar = 100 µm

2.4 General design features of microchannel modules

For most of the envisaged applications, the microchannels would have to be only slightly bigger than the diameter of the tip growing cell. In the case of *Camellia*, a typical microchannel would measure 30 µm in plane (80 µm high), whereas the tube is 15 to 20 µm large. This is very different from conventional *in vitro* setups used for pollen tube culture, in which the elongating pollen tubes are surrounded by relatively large volumes of medium. This includes micro-structured devices such as (Yetisen *et al.*, 2011a), since the pollen tube in that assay were surrounded by an amount of medium that was orders of magnitude bigger than the volume of the cell.

2.5 Sensitivity of pollen tube to the fluid flow rate

For certain experimental approaches, continuous medium flow through the microchannel may be desired (e.g. laminar flow gradient and toxicity testing), whereas for others, the absence of any flow movement is a prerequisite (e.g. static gradient). The amount of flow can be regulated by injecting medium via a motor-controlled syringe, and by strategically blocking outlets. The parameter that can be modified by the experimenter is the inlet velocity, whereas the fluid velocity experienced locally by individual pollen grains and tubes depends on the geometry of the microfluidic network. This variation is much more pronounced when the distribution chamber outlet is blocked and all fluid is evacuated through the microchannels. When the distribution chamber outlet is open, fluid flow through microchannels with different dimensions is less variable (Fig 2.3a,b).

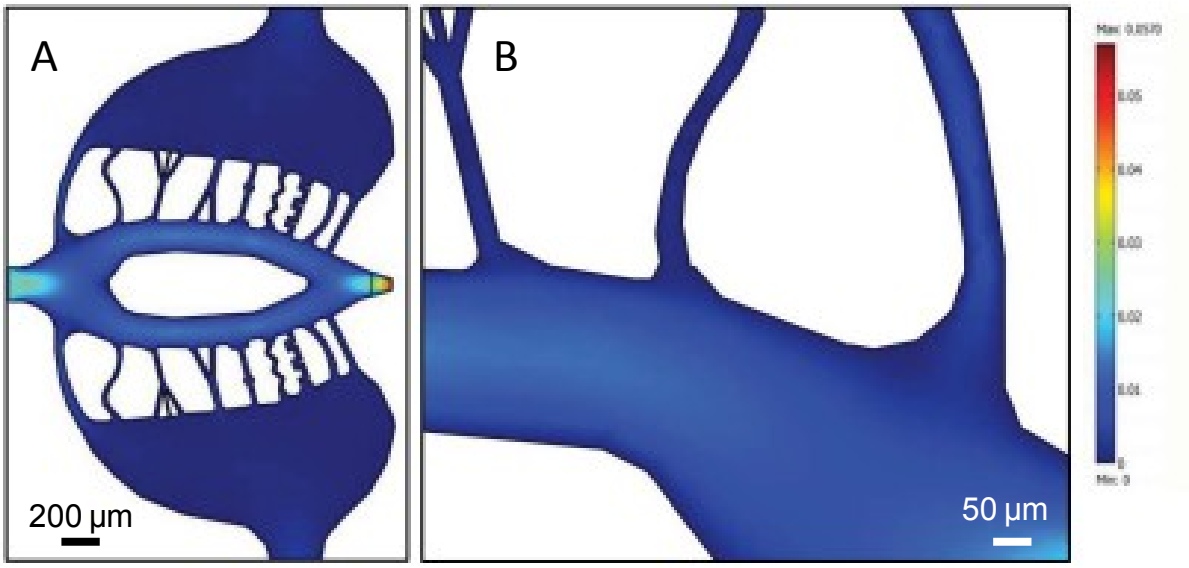

Figure 2.3: Fluid flow simulation within microchannel network, (a) Fluid velocity in the oval shaped distribution chamber with distribution chamber outlet open, (b) Detail of A showing that microchannels with different diameters have similar fluid velocities when the distribution chamber outlet is open.

To test how pollen tubes respond to the absence and presence of fluid flow, different flow velocities were applied. The absence of medium flow was conducive for pollen tube growth for the duration of a typical experiment (1-2 hours). However, the presence of slow fluid flow enhanced pollen tube growth, likely because the flow increased the supply of oxygen and nutrients which were consumed by the elongating tube. On the other hand, excessive flow rates were found to be damaging, likely due to shear forces. At inlet velocities above 100 mm/sec, more than 50% of pollen tubes were observed to burst (Fig 2.4). The optimal inlet flow rate for the present configuration was therefore determined to be between 10 to 30 mm/sec. A minimum inlet medium velocity of 10 mm/s during injection of the pollen suspension was found necessary to ensure that most of the pollen grains actually enter the distribution channel and do not remain at the bottom or top

surfaces near the inlet, a phenomenon that occurred at very slow inlet velocity. From both the experimental tests and fluid flow simulations it was clear that the geometry of the overall design of the microfluidic network and the inlet velocity need to be tested on a case-by-case basis to ensure that flow rates within the microchannels remain below the critical value of approximately 30 mm/sec, but are sufficiently high to carry the grains toward the microchannel entrances (Fig 2.4,c).

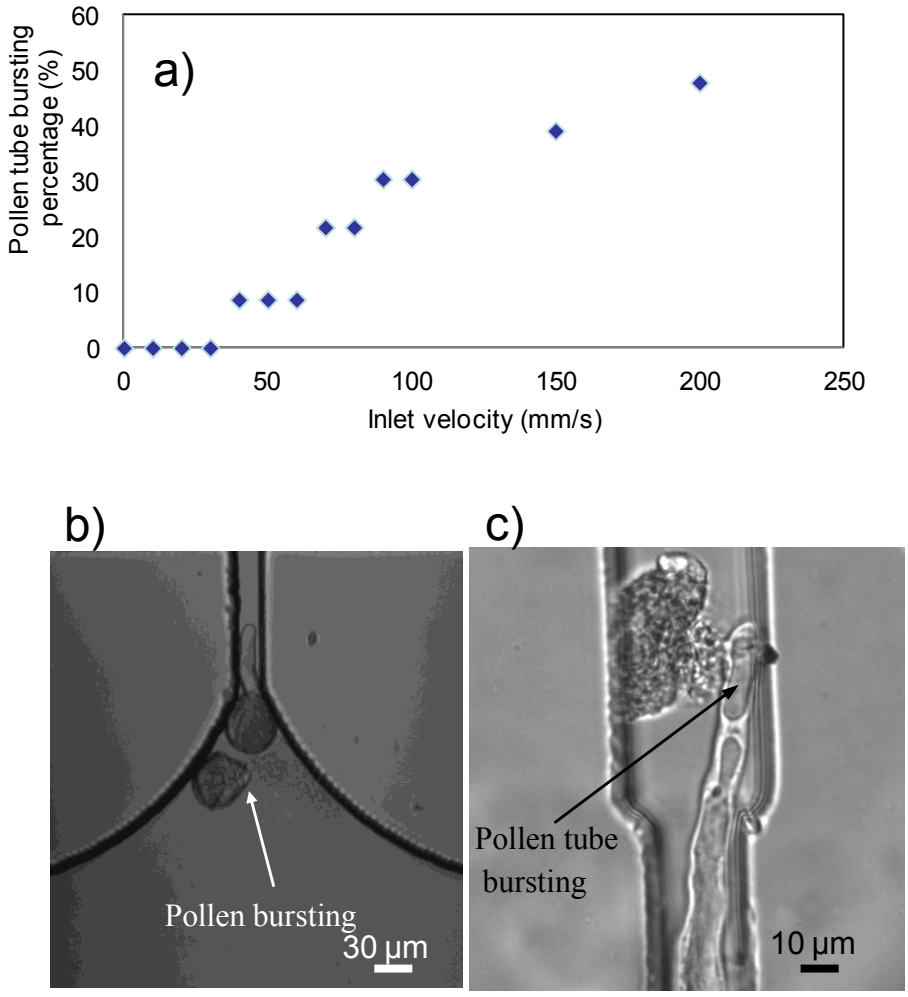

Figure 2.4: a) The dependence of pollen tube bursting to the inlet velocity, The optimal inlet flow rate for was determined to be between 10 to 30 mm/sec. b) pollen bursting under higher flow rate, c) Pollen tube bursting under high flow rate

The pollen grains are transported to the microchannel entrances by fluid flow and in experimental setups that allow for continuous flow, the fluid force keeps the grain at the entrance. However, in experiments that require absence of flow or a reverse direction of flow, or in experiments that expose elongating tubes to mechanical obstacles, the grain is not held in place but can either drift away or be pushed backwards by the force generated by the growing tube hitting an obstacle. Therefore we conceived an additional feature to the microchannel design that prevents backward displacement. For this purpose a kink consisting of three consecutive 90° angles was incorporated into the microchannel shape (Fig. 2.5). Tests showed that this configuration was successful in preventing pushback of the grain and that it allowed for experiments in which the elongating tube was forced to negotiate mechanical obstacles.

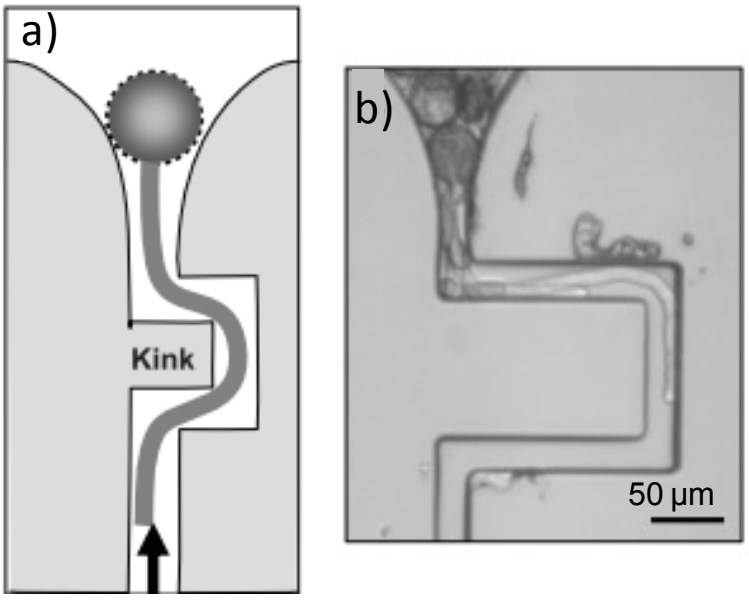

Figure 2.5: Microchannel feature preventing pushback . Incorporation of a kink in the microchannel architecture enables fixing the pollen tube in place. Mechanical obstacles encountered after passing this kink therefore do not cause a displacement of the grain and allow the tube to exert a pushing force.

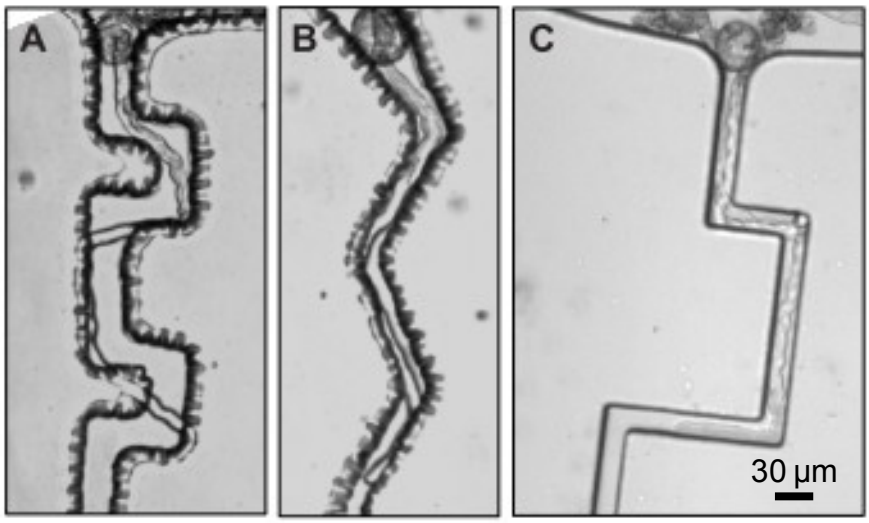

Figure 2.6: Pollen tubes growing through a serpentine like microchannel grow straight until they encounter an obstacle and deviate. A and B are microchannels fabricated using a transparency film photomask prepared by high resolution digital printing (3600 dpi), whereas C was produced using a high resolusion glass mask made by direct write lithography. The smoother surfaces of the PDMS in A and B illustrates the need for this higher resolution technique for the present application.

2.6 Examples for specific microchannel designs

We developed a series of LOC for very specific applications in pollen tube research. These will be described elsewhere. Here we tested features that will be of general importance and are common to most present and future applications of the TipChip.

2.6.1 Air-liquid interface

During the initial phase of pollen germination on the stigma surface, pollen tubes are able to grow extended distances surrounded mostly by air. In the microfluidic setup, pollen tubes were occasionally observed to enter air bubbles trapped in the microfluidic network,

but more typically they avoided these bubbles. To be able to more systematically assess the ability of pollen tubes to elongate in air, we devised a setup that would force pollen tubes to grow into an air chamber (Fig. 2.7). The extremely narrow entrance of the air chamber consists of two horizontal PDMS posts/rods that allow the pollen tube to penetrate into the chamber, but prevent liquid to enter or gas to exit. In this configuration, the grain and distal region of the tube are exposed to liquid medium, and the setup could also be used to test nutrient and water uptake by the distal region of the tube which has been hypothesized to be rather impermeable due to the presence of a callosic cell wall layer. *Camellia* pollen tubes were found to be able to enter the air chamber and to grow for up to 1 mm, thus demonstrating that water and nutrient uptake through the grain or distal region of the tube was sufficient to sustain pollen tube growth. Alternatively, this setup can be used to expose only the distal region of the pollen tube to an inhibitor or other growth affecting agent. We will discuss in Chapter 5 about the potential of this LOC for answering some biological questions.

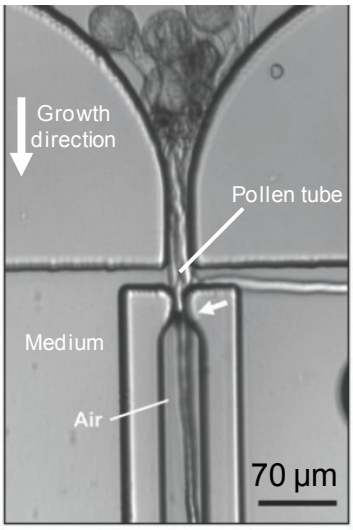

Figure 2.7: Pollen tube growth in air, An air chamber device consisting of two opposing PDMS posts allows pollen tubes to penetrate into the chamber without gas exiting. This setup can also be used to expose exclusively the distal portion of the tube to selected nutrients or inhibitors.

2.6.2 Exposure to chemical gradient

Pollen tubes are known to grow towards certain chemical attractants (Geitmann and Palanivelu, 2007b), and recently, proteic factors have been identified to be involved in pollen tube guidance (Palanivelu and Tsukamoto, 2011b). To fully understand the roles of chemical and proteic signals in pollen tube guidance, *in vitro* exposure to various combinations and concentrations of these agents will be indispensable. Two different configurations were devised to allow pollen tubes to be exposed to reproducible and quantifiable chemical gradients:

2.6.2.1 Diffusion based, static gradient*:*

Pollen tubes grow through a microchannel that enters into a larger, transverse channel fed by two inlets. Administration of two different solutions through the two inlets is used to

establish a diffusion generated gradient over the distance of the transverse channel (Fig. 2.8). This configuration allows for shallow gradients to be established over extended spatial distances. Its principal application would be the investigation of pollen tube guidance.

2.6.2.2 Laminar flow based, steep gradient*:*

The microchannel is fed laterally through an additional inlet through which growth medium complemented with the desired agent is administered (Fig. 2.8c). Flow experiments with ink-stained solutions showed that laminar flow in the microchannel creates a gradient across the channel that is sufficiently steep to expose the two sides of the elongating tube to significantly different concentrations of the agent in question (Fig. 2.8d). This gradient is maintained over the remainder of the microchannel. In proof of concept experiments, *Camellia* pollen tubes exposed to growth medium containing 8% and 12% displayed a clear directional growth response towards the medium with the higher sucrose concentration (Fig. 2.8e). When faced with a choice between 2.5 and 5.1 mM calcium, the *Camellia* pollen tubes opted for the lower concentration, consistent with batch tests performed to optimize the growth medium for this species (Bou Daher and Geitmann, 2011a). In addition to assessing the pollen tube's response to a directional trigger, the laminar flow based configuration can also be used to administer inhibitors or enzymes specifically to one side of the pollen tube (Sanati Nezhad *et al.*, submitted-c).

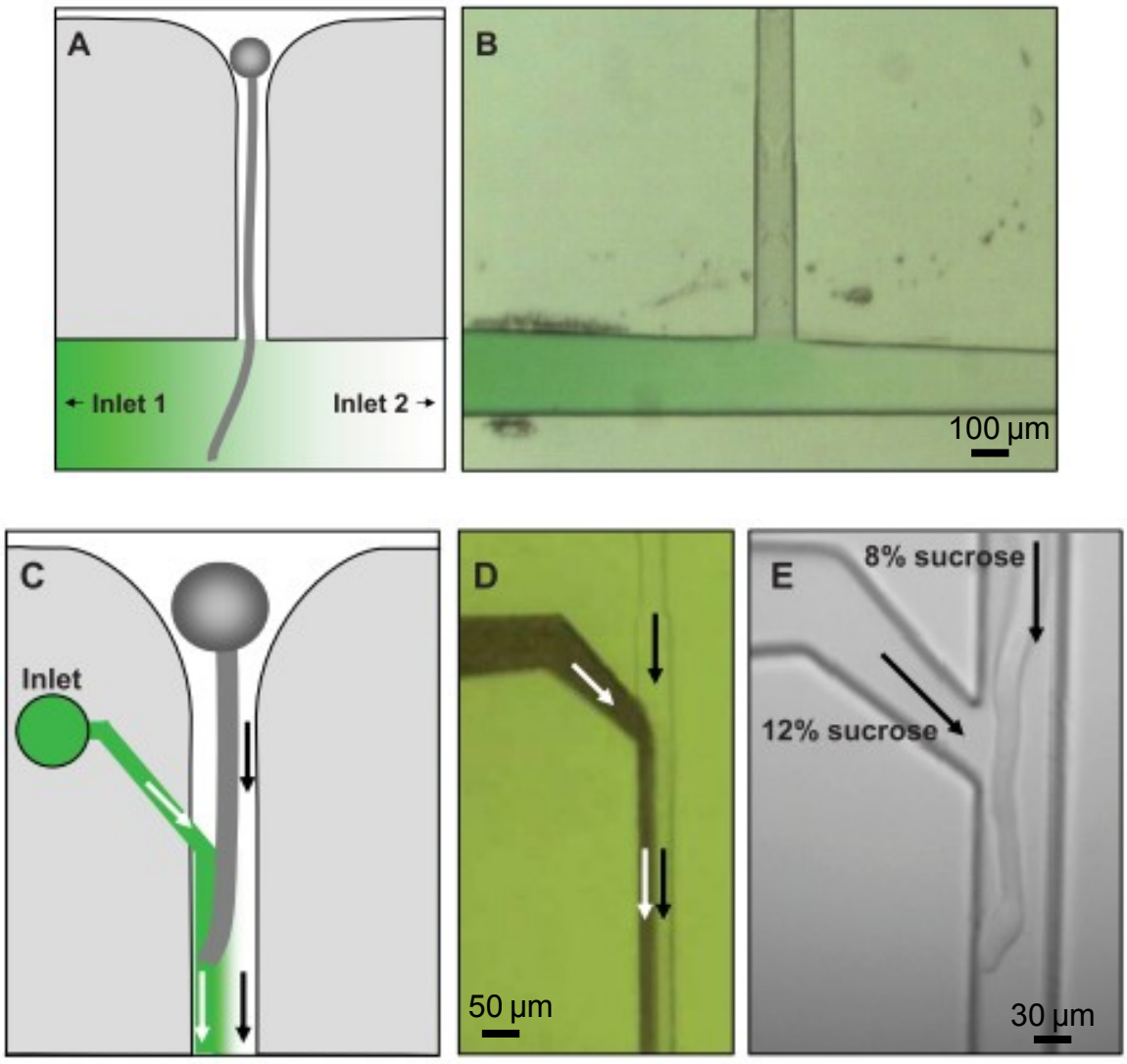

Figure 2.8: Exposure to chemical gradient, (A,B) Static, shallow gradient. A pollen tube guided by a microchannel enters a larger transverse channel in which a chemical gradient is established through two inlets. This configuration is ideal for the investigation of pollen tube guidance. Tests with food color (B) confirm that the gradient can be established by injecting two different media through the two inlets. (C,D) Laminar flow based, steep gradient. Side injection from an additional inlet establishes a steep gradient within the microchannel that exposes the elongating pollen tube to two different solutions. This setup can be used for the investigation of pollen tube guidance or to administer inhibitors or enzymes to one side of the pollen tube. Ink was used to demonstrate that the gradient is stable along the channel (D). (E) In a proof of concept experimental test, pollen tubes were exposed to a gradient between 8 and 12% sucrose in growth medium and turned towards the higher concentration.

2.7 Materials and methods

2.7.1 Fabrication of LOC devices

The LOC was designed with Autocad 2011 software and reproduced onto a glass mask using a DWL 66 machine to achieve high resolution. Molds were fabricated onto 10 cm silicon wafers as described in detail in (Agudelo *et al.*, submitted; Sanati Nezhad *et al.*, submitted-b). Briefly, using a photolithographic technique a SU8 mold is fabricated as negative photoresist (MicroChem Corp.) by employing the glass mask. To reach the thickness of 80 μm, SU-8 2035 is spin coated on a silicon wafer. The SU-8 is baked for 5 min at 65ºC and for 10 min at 95ºC in a hotplate. After soft-baking, the resist is cooled down at room temperature and exposed to UV light using a photo mask for 30 s. The post-exposure bake step is then carried out by baking the resist for 5 min at 65ºC and for 10 min at 95ºC in order to cross-link the SU-8. The SU-8 layer is then developed to obtain the SU8 mold. The microfluidic device is next fabricated by curing PDMS on the SU8 mold. This PDMS layer is peeled off from the mold and bonded to a cover slip to seal the fluidic network.

2.7.2 Pollen culture and germination

Pollen of *Camellia japonica* was collected from a plant in the Montreal Botanical Garden, dehydrated and stored on silica gel at -20ºC until use. Prior to experimentation, a few micrograms of the pollen were thawed and rehydrated in humid atmosphere for 1 hour and subsequently immersed in 1 mL liquid growth medium optimized for this species (Bou Daher and Geitmann, 2011a).

2.7.3 Imaging

Brightfield imaging was done on an Olympus BX60M Brightfield microscope equipped with a Nikon Coolpix 4500 camera and with a Nikon Eclipse 80i digital imaging microscope system.

2.8 Summary and conclusions

The presented MEMS-based platform for tip growth research represents a novel and extremely powerful tool for multiple applications in research on pollen tubes, fungal hyphae and other polarly elongating cells. Its modular design allows for the incorporation of various features and future models will be equipped with flow sensors (Sanati Nezhad *et al.*, submitted-a), force sensors (Felekis *et al.*, 2011), electric fields (Zou *et al.*, 2006) and other devices. Here we provided experimental evidence for a proof of concept and we demonstrated the solutions to numerous technical problems associated with the microfluidic setup at micrometer resolution. The design of the TipChip allows high resolution and fluorescence imaging and it is conceived to allow parallel observation of multiple cells making is suitable for large scale approaches such as phenotyping.

Chapter 3

Flow Assisted Entrapment of Pollen Grains in a Microfluidic Platform for *In-Vitro* Study of Plant Cell Growth

3.1 Enhancing microfluidic platform for chemical treatment of pollen tube

Although the TipChip platform explained in Chapter 2 was able to depict the potential of microfludiic platform to simplify some complicated testing, the chip is not for applying drug or chemical agent. Furthermore, the accumulation of pollen grains at the entrance of microchannels or the outlet drain prevents simple flow passage toward the pollen tube, increases the pressure inside the chip and causes pollen tube bursting. In addition, due to sensitivity of pollen tube growth to medium flow, the results of different microchannels are not comparable. To integrate some biosensors such as cantilever-based force sensors along the growth channels, multilayer fluidic chips are required which cannot be simply handled with the TipChip design due to difficulty in alignment of layers. Hence, more modifications and fluidic enhancement is essential to provide a stable platform. This chapter presents the enhancement of microfluidic platform by employing numerical simulation and experimental testing. This work has been submitted to *Journal of Biomedical Microdevices* (2012) with my contribution as the first author (Sanati Nezhad *et al.*, 2012a).

Abstract

A biocompatible polydimethylsiloxane (PDMS) biomicrofluidic platform is designed, fabricated and tested to study protuberance growth of single plant cells in a micro-vitro

environment. The design consists of one inlet to introduce suspension into the chip, three outlets to conduct the medium or cells out of the chip, a main distribution chamber and eight microchannels connected to the main chamber to guide the growth of tip growing plant cells. The test cells used here were *pollen grains* which produce cylindrical protrusions called *pollen tubes*. The goal is to facilitate and enhance the positioning of pollen grains at the entrances of the microchannels and to provide identical growth environments for growing pollen tubes along each microchannel. The dimensions of the microchannels and the inlet flow rate are selected in order to improve the performance of the microdevice. Computational fluid analysis is carried out to estimate the *trapping coefficient* of pollen grain at the entrance of each microchannel. The criteria for an enhanced design are established and used to compare the performance of various designs based on modeling and experimental results.

3.2 Introduction

In recent years, there has been an increasing interest in applying micro-electro-mechanical systems (MEMS) technology for studying biological phenomena that led to the development of new area called BioMEMS. Today, BioMEMS are extensively used in diagnostic, drug development, biosensors and lab-on-chip (LOC) systems (Cheung and Renaud, 2006b; Giouroudi *et al.*, 2008a; Nuxoll and Siegel, 2009b). Cost effective and portable microfluidic platforms have provided closed environment for in-vitro single cell analysis (Tatic-Lucic, 2007) and characterizing the cell response to the chemical cues in growth environment (Grossmann *et al.*, 2011b; Takayama *et al.*, 2001).

An important challenge for the application of BioMEMS devices for cell analysis is the immobilization of single cells that is required to maintain them at a desired position while continuous fluid flow is applied to provide nutrients or to administer drugs and other agents influencing cell behavior. Cell immobilization has been achieved by growing cells on a solid substrate or hydrogel (Braschler *et al.*, 2005) or through trapping the cells suspended in growth medium (Lee *et al.*, 2008b). In order to immobilize the cells on a solid surface, chemical surface modification has been employed using different techniques such as microcontact printing (Kanea *et al.*, 2007) and micromolding (Mrksich *et al.*, 1996). Alternatively, cell immobilization on hydrogel networks is achieved by preparing cell-hydrogel scaffolds through injecting the cell and matrix into microfluidic device and incubating the mixture for gelation (Tan *et al.*, 2003).

To enable single cell analysis on cells suspended in a liquid medium, the cells typically have to be handled, manipulated and trapped within the microfluidic device. Ultrasound handling, optical tweezers and dielectrophoresis (DEP) have successfully been integrated within the microdevice (Burgarella *et al.*, 2010; Kendrick *et al.*, 2009; Yasuda, 2000) for handling and manipulation of microscopic particles or single cells in microfluidic devices. Trapping of red blood cell has been achieved by laser trapping (Bragheri *et al.*, 2010), dielectrophoretic trapping (Hughes *et al.*, 1998) and flow assisted techniques (Wheeler *et al.*, 2003). The later is particularly promising as it does not require any high technological approach and can be applied to multiple specimens simultaneously. In the case of microflow assisted trapping, the microfluidic design needs to address the specific needs of respective experimental setup. Flow assisted hydrodynamic based traps operate by trapping

a particle or cell in a gap with a size smaller than the object to prevent it from passing through while allowing the liquid to flow by. For the purpose of trapping single cells, Wheeler et al (Wheeler *et al.*, 2003) presented a microfluidic chip that allows separating single cells from a bulk cell suspension using the fluid dynamics of a T junction. The cell is trapped at the point of stagnation at the center of T junction at which a small drain channel is added. However, the success of devices designed for single cell analysis is largely based on trial and error. In order to capture high number of cells within a single microfluidic device, flow assisted hydrodynamic based cell trapping has been developed based on various geometries such as perpendicular and parallel dam structures (Yang *et al.*, 2002), or patch-clamp arrays (Seo *et al.*, 2004) that use lateral cell trapping junctions. Tan et al. (Tan and Takeuchi, 2007) presented a self-regulating technique in which one portion of medium flow enters the gap and the rest is reconnected to the gap exit through a main channel to produce a pressure gradient along the gap. The performance of this hydrodynamic single cell trapping mechanism was optimized by Kobel et al (Kobel *et al.*, 2010) revealing that the trapping efficiency depends largely on the ratio of flows through the trap and the main channel.

Recently, we designed a microfluidic device for the purpose of analyzing tip growing cells (Agudelo, 2012). The portion of the cell to be exposed to experimental testing is a cellular protuberance that is germinated from a spherical cell body, such as a hypha or a pollen tube emerging from a fungal spore or a pollen grain, respectively. These protuberances can become hundreds of μm long and the microfluidic device has to be designed to guide the individual protuberances through narrow microchannels into which experimental assay can

be incorporated. However, to get the protuberances into the microchannels in the first place, the spherical cell bodies have to be placed at their entrances, which in turn have to function as traps. To make this setup suitable for large scale experiments, it must be optimized to ensure that desired numbers of cells are trapped at each microchannel entrance, and that all microchannels provide identical conditions for tube growth in terms of flow nutrients. This second condition is critical since experimental tests have shown that growth of pollen tube is sensitive to fluid velocities and that excess flow velocity can cause growth arrest or cell bursting (Agudelo *et al.*, 2012d). In terms of cell numbers to be trapped, in the present application, acceptable device performance is defined as the capacity of all traps in the chip to capture between one and three pollen grains.

Unoccupied traps in the device would reduce the usage capacity of the experiment, whereas accumulations of more than three grains would block and affect fluid flow at the individual trap, hence altering fluid velocity and nutrient conditions through the microchannel. The aggregation of the cells in the perpendicular dam structure (Yang *et al.*, 2002), lack of identical growth conditions in patch clamp array design (Seo *et al.*, 2004) and the self regulating technique (Tan and Takeuchi, 2007) make these designs unsuitable for the present application. In the present chapter, we address both challenges by designing a serial trap arrangement that ensures the trapping of an optimal number of cells and identical flow rates in all microchannels.

The proposed microfluidic device is developed for and tested with pollen grains from the species *Camellia japonica*. The pollen grain is the male gametophyte in the flowering

plants and it has the function of delivering the sperm cells from one flower to the other to ensure successful reproduction. The pollen grain is typically spherical or oval shaped and its species dependent size is typically between 20 and 100 μm.

The extremely fast growth and the easy in-vitro culture have made the pollen tube one of the best investigated plant cells (Chebli and Geitmann, 2007b). There are many areas that have to be addressed, such as mechanical principles governing the polar growth mechanism (Fayant *et al.*, 2010b; Geitmann *et al.*, 2004; Zerzour *et al.*, 2009a), temporal regulation of the elongation process (Kroeger *et al.*, 2011a; Kroeger *et al.*, 2008), logistics of intracellular transport processes (Bove *et al.*, 2008b; Kroeger *et al.*, 2009), and the ability of the tube to follow directional cues (Bou Daher *et al.*, 2011d). Even though numerous modeling approaches have been developed based on experimental data (Kroeger *et al.*, 2011c), the technical challenges have limited many attempts to determine quantitatively the mechanical properties of the cell. In this regard, microdevices will make an important contribution to various research avenues addressing the biology of pollen tube.

In this chapter, a simple flow assisted polydimethylsiloxane (PDMS) microfluidic platform is designed, fabricated and tested for the study of individual pollen tubes in in-vitro microfluidic environment. The design consists of the following, (i) one inlet to introduce pollen grains suspended in the growth medium into the chip, (ii) three outlets to evacuate medium or pollen grains from the chip, (iii) a main fluidic chamber and (iv) eight microchannels connected to the main chamber through which pollen tube elongation is

guided. The number of traps is chosen so as to overcome the constraints of the multi-layer fabrication process on fabricating the maximum number of microchannels. In this study, the dimensions of the main chamber and outlet drain as well as the inlet flow rate are selected such as to ensure 1) positioning a single pollen grain at each microchannel entrance, 2) providing identical nutrient flow conditions in all microchannels. Computational fluid analysis and experimental testing were carried out in order to estimate the performance of the device in terms of the desired number of pollen grains trapped at the entrance of each microchannel. Upon understanding the parameters that influence the trapping coefficient of individual microchannels, criteria for selecting an efficient design are identified. The performance of the enhanced design is compared experimentally with other proposed designs.

3.3 Materials and methods

3.3.1 Pollen germination

Camellia japonica pollen was dehydrated on anhydrous silica gel in gelatin capsules overnight and stored at -20°C. Prior to use, pollen was rehydrated in humid atmosphere at room temperature for at least 1 hr. Pollen was suspended in a growth medium made of 2.54 mM of $Ca(NO_3)_2 \cdot 4H_2O$, 1.62 mM of H_3BO_3, 1 mM of KNO_3, 0.8 of mM $MgSO_4 \cdot 7H_2O$ and 8% sucrose (w/v) (Bou Daher and Geitmann, 2011d). Pollen germination was monitored microscopically and upon initiation of germination, the pollen suspension was introduced into the microdevice.

3.3.2 Determination of the density of *camellia* pollen grains

The average density of individual, hydrated *Camellia* pollen grains was determined based on the mass and the particle size. 5.3 mg of dry pollen grains were hydrated for 1 hr resulting in an increase of 0.9 mg to 6.2 mg due to hydration. The pollen grains were suspended in 10 ml liquid and the number of pollen grains in an aliquot of 20 µl was determined microscopically to be 208. This allowed us to calculate the average mass of a single pollen grain to be 56.9 ng. Hydrated *Camellia* pollen grains are spherical and have an average diameter of 60 µm with a density of 492.6 kg/m^3. This value is used in modeling the flow of the pollen suspension (Section 3.5).

3.4. Design and fabrication

The microfluidic network is based on a main distribution chamber with inlet, eight microchannels (CH1 through CH8), a main outlet for distribution chamber and outlets evacuating fluid from the microchannels (Fig. 3.1). The pollen grains are to be positioned at the entrances of the microchannels CH1 to CH8 (Fig 3.1a) as schematically shown in Fig 2b, so that a single pollen tube grows in each microchannel where it can be subjected to experimental analysis such as local application of inhibitors or enzymes, or mechanical testing. Insertion of the pollen grains occurs by injection of a pollen suspension and any positioning has therefore to be controlled by fluid flow.

The *outlet drain* serves to evacuate excess pollen grains from the main chamber and to prevent their accumulation at the far end of the main chamber or at the entrances of the microchannels. The other two *medium outlets* evacuate culture medium through the

microchannels and serve to position the pollen grains at the entrances of the microchannels as well as to allow continuous flow of growth medium along the microchannels harboring the elongating pollen tubes as shown in Fig 3.1d.

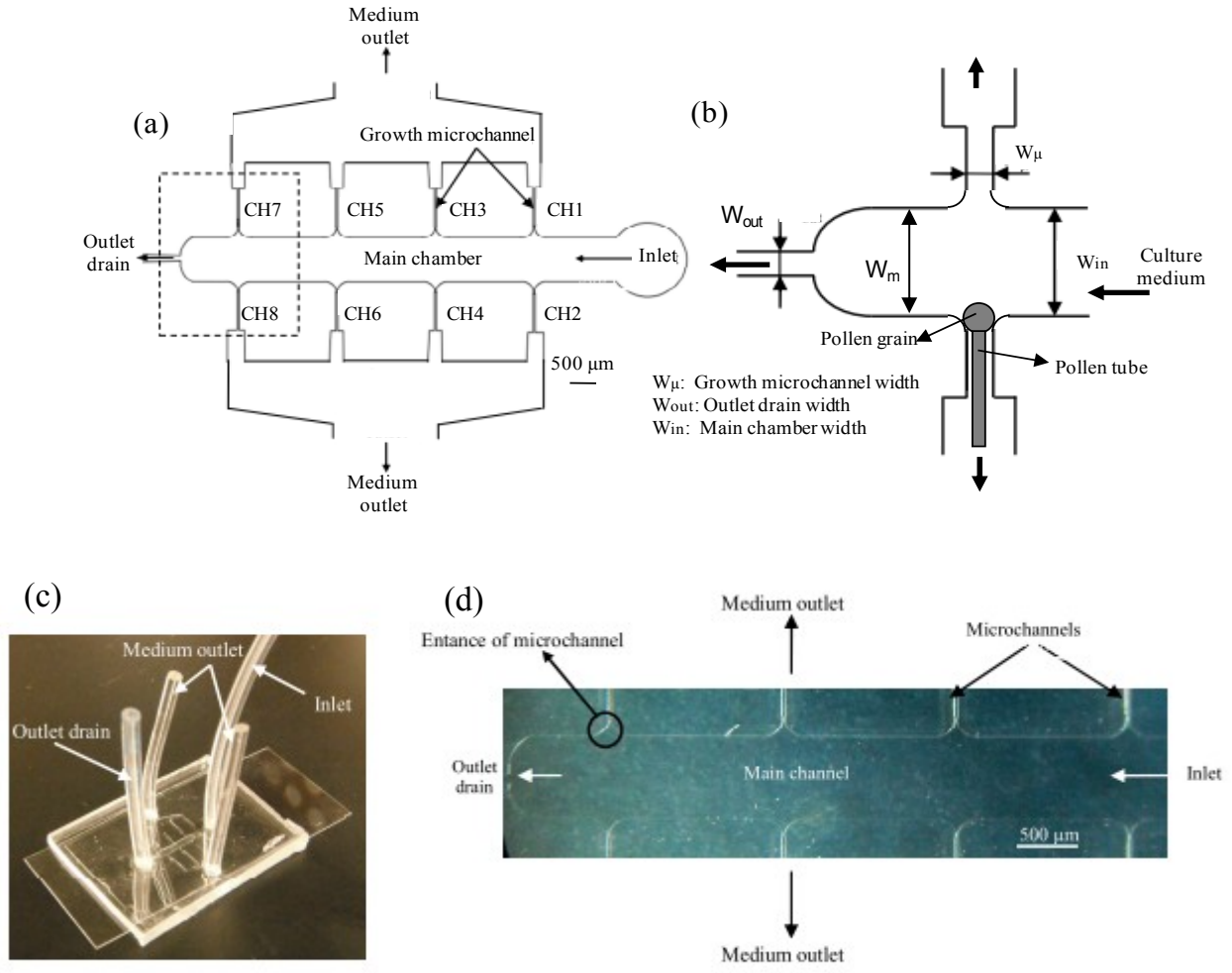

Figure 3.1: Initial design and fabricated microfluidic platform for pollen tube studies: a) design of microfluidic network, b) close up of the network dimensions near the outlet drain, c) fabricated chip, d) micrograph of the microfluidic network

The following geometrical constraints were considered in selecting the dimensions of the device. Inlet, main chamber and outlet drain have to be sufficiently large to permit the passing of the pollen grains. The hydrated grains of *Camellia* are spherical and have a

diameter of approximately 50-60 μm. The size of the main chamber (W_m) has to be large enough to allow excess pollen grains to be evacuated through the outlet drain after the microchannel entrances are occupied. While the size of the outlet drain (W_{out}) should be larger than the diameter of the pollen grains to permit their evacuation, excessive draining through a large drain may result in the evacuation of all pollen grains and hence the chamber may fail to retain pollen grains at the entrances of the microchannels. On the other hand, accumulation of the pollen grains at the outlet drain would be expected to reduce the medium flow through this drain which in turn would cause a pressure change within the microchannels harboring the pollen tubes. In order to provide stable growth conditions, the pressure inside the chip has to be maintained stable as continuous flow of medium is required to ensure oxygen and nutrient supply for pollen tube growth. Consequently, the size of outlet drain is a crucial parameter.

The width of the microchannels (W_μ) has to be smaller than the diameter of the pollen grain to prevent it from entering into the microchannel and bigger than the diameter of the pollen tube which is typically 13-19 μm. Hence, a width of 20-40 μm has to be used. The depth of the microfluidic network was selected larger than the diameter of the pollen grains, but smaller than twice the diameter to allow the grains to move easily, but to prevent them from stacking in vertical direction (Fig 3.1b).

The present microdevice shown in Fig 3.1c is fabricated using two layer fabrication technique. It is also possible to extend this technology for developing multilayer PDMS configurations. In this situation, the device will have another thin PDMS layer sandwiched

between other covering PDMS layers. Complexity associated with peeling of the PDMS layers (Mengying Zhang, 2010) imposes constraints on the maximum number of microchannels that can be fabricated. Earlier experiments in fabricating thin PDMS layers have demonstrated that a thin PDMS layer with eight integrated microchannels can successfully be peeled off from the mold (Sanati Nezhad *et al.*, 2013a). Based on the geometrical constraints, the dimensions of the initial design are selected as seen in Table 3.1.

Table 3.1 Dimensions of initial design

Initial design	Inlet width (W_{in})	Outlet drain width (W_{out})	Main chamber width (W_m)	Microchannels width (W_μ)	Channels depth
Size (µm)	1200	200	1200	30	80

The initial design was fabricated using standard photolithography and soft lithography methods for fabricating PDMS microfluidic devices (Ziaie *et al.*, 2004). The device is tested by injecting the pollen suspension using a syringe pump. Various inlet velocities were used to inject the pollen suspension. For each inlet velocity, a new PDMS microdevice was tested to ensure that no residual grains from previous experiments blocked the microfluidic network. When using inlet velocities below 10 mm/s, most of the pollen grains stuck to the top or bottom surface of the main fluidic chamber near the inlet and did not enter the main portion of the chamber. This suggests that pollen grains tend to stick to the PDMS material forming the channel and slightly higher inlet velocities need to be applied to overcome this effect. Higher inlet velocities also improved the positioning of pollen grains at the microchannel entrances. However, higher inlet flow rates also resulted in the accumulation of several pollen grains at the microchannel entrances even when diluted pollen suspensions were used. In addition, elongating pollen tubes were

occasionally observed to burst at high flow rate (Agudelo *et al.*, 2012d). The optimal range of inlet velocity that ensured correct and stable positioning while preventing the accumulation of excess numbers of pollen grains and bursting was found to be approximately 10 mm/s.

The ultimate goal of the present optimization procedure is to 1) optimize the geometry of the microfluidic network in order to be able to position exactly one pollen grain at the entrance of each microchannel and 2) to provide identical growth conditions and fluid flow velocity within each microchannel. The performance of the initial design was assessed in terms of the number of pollen grains trapped at the entrances. For an inlet velocity of 10 mm/s, the pollen grains were trapped at the entrances of microchannels located near the outlet drain (CH5-CH8) while the four entrances near the inlet could not capture any pollen grains as shown in Fig 3.2a. At an increased inlet velocity of 100 mm/s the number of microchannels occupied by pollen grains increased. However, several pollen grains accumulated at each entrance thus potentially reducing the flow rate through the microchannels (Fig 3.2b).

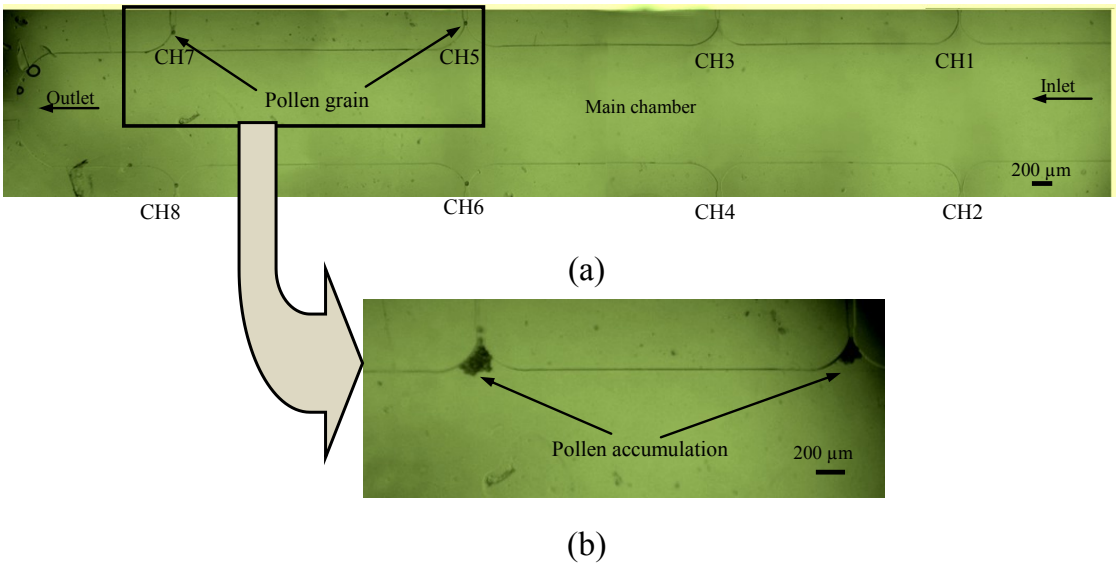

Figure 3.2: Experimental testing of initial design, a) At inlet velocity of 10 mm/s several microchannel entrances are unoccupied, b) At inlet velocity of 100 mm/s pollen grains accumulate at the microchannel entrances

Since optimal performance could not be achieved with the initial design, modifications were implemented. In addition to the previously stated objectives the new designs are also supposed to ensure 1) long-term stability of pollen positioning even for experimental designs that require absence of flow after the injection of the pollen suspension, 2) prevention of accumulation of the pollen grains at the outlet drain that would result in a blockage to the medium flow.

3.5 Design improvement

Since all of the design parameters such as W_{in}, W_m, W_{out}, W_μ and the depth of microchannels influence the fluid flow pattern, they potentially have great influence on the probability of the individual microchannels to trap pollen grains (Fig 3.1b). In order to improve the performance of the initial design, the effects of the dimensions of W_m and W_{out}

were assessed through finite element analysis of fluid flow using COMSOL software. The width of the microchannel (W_μ) was chosen to be 30 μm. The depth of microfluidic network was chosen to be 80 μm to allow pollen grains to move freely without stacking vertically. The width of the inlet (W_{in}) was selected equal to the width of main chamber (W_m) to prevent any accumulation of pollens at the inlet before entering the main chamber. The width of the main chamber (W_m) and the width of outlet drain (W_{out}) were varied as indicated in Table 3.2 and the resulting inlet velocities at the entrances of the four sets of microchannels were calculated. The inlet velocity into the main chamber was kept constant at 10 mm/sec. Three criteria were assessed: 1) The absolute values of inlet velocity at the entrances of the microchannels had to be below 30 mm/sec to avoid exposing pollen grains to excessive flow rates that might cause bursting (Agudelo *et al.*, 2012d). 2) The differences in velocities through the four sets of microchannels located at the near and far ends of the chamber have to be minimal to ensure identical conditions in all microchannels, 3) The *pollen trapping coefficient* of microchannel entrances has to be sufficiently high to ensure that one or a few pollen grains are trapped at each entrance. The trapping coefficients were calculated based on fluid flow analysis and tracing the trajectory of a pollen grain along the main channel toward the microchannels.

3.5.1 Modeling of the flow behavior

Finite element analysis was carried out to estimate the fluid velocity and pressure gradient within the microfluidic network. The fluid flow was modeled by incompressible Navier-Stokes equations and continuity equations as given by the following Equations (3-1), (3-2):

$$\rho_f \frac{\partial \mathbf{u}}{\partial t} - \nabla.[-p\mathbf{I} + \eta(\nabla\mathbf{u} + (\nabla\mathbf{u})^T)] + \rho\,(\mathbf{u}.\nabla).\mathbf{u} = \mathbf{F} \quad (3\text{-}1)$$

$$\nabla.\mathbf{u} = 0 \quad (3\text{-}2)$$

Where **I** is the unit diagonal matrix, **u**= (u,v) is the velocity field within the microfluidic network, p is the fluid static pressure, ρ_f is fluid density and **F** is the volume force affecting the fluid. The volume force and also the effect of pollen grain movement on the fluid flow are considered negligible. In modeling, the constant velocity of 10 mm/s was considered as the inlet fluid velocity and atmospheric pressure was imposed at all the outlets. No-slip boundary condition was applied for the channel walls. COMSOL Multiphysics 3.5 software was employed to solve the governing equations. The velocities that were predicted at the entrance of each microchannel and the outlet drain are presented in Table 3.2. % variation of velocity in Table 3.2 is defined respect to the minimum value.

Table 3.2 Predicted velocity at the entrance of microchannels and outlet drain for various proposed designs. Channel numbers correspond to those indicated in Fig. 3.1

Design number	Main chamber width(W_m=W_{in}) µm	Outlet drain width (W_{out}) µm	Velocity (mm/s)					% Variation of velocity in microchannel
			CH1, CH2	CH3, CH4	CH5, CH6	CH7, CH8	Outlet drain	
1	**1200**	**200**	6.8	6.1	5.5	5.2	78	30.7
2	**1200**	**100**	17	16.8	16.2	16	134	6.25
3	**700**	**200**	10.3	6	3.2	2.5	48	312
4	**700**	**100**	12	11	10.5	9.8	86	22.4
5	**300**	**200**	10	8	5.6	3.5	16	185.7
6	**300**	**150**	8.2	5.8	4.1	2.3	22	256.5
7	**300**	**100**	9.5	6.8	5.5	4	30	137.5
8	**300**	**80**	12	10	8.5	7.5	24	60

Table 3.2 clearly shows the effect of inlet width on the variation of velocities at the entrances of the microchannels located near the inlet and outlet. The variation in velocity for Design 1 was very low between 5.2-6.8 mm/s (30.7% variation of velocity) when compared to the variation in velocities for Design 5 between 3.5-10 mm/s (185.7 % variation of velocity). The corresponding simulated flow velocity is shown in Fig 3.3. a,b.

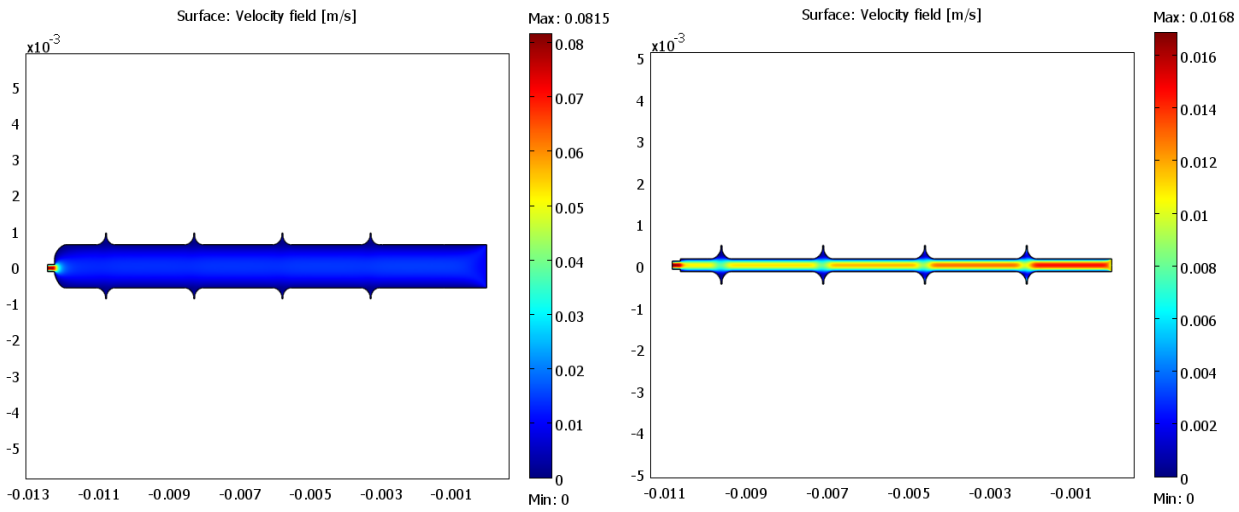

a) b)

Figure 3.3: Comparison of flow velocity field a) Design 1, b) Design 5. The velocity gradient at the entrance of microchannels in Design 5 is much steeper than the gradient in Design 1

Among the designs proposed in Table 3.2, the least variation in fluid velocity at the four sets of microchannel entrances was obtained for Design 2 (6.25%) and Design 4 (22.4%). However, the microchannel velocities in Design 4 were also close to the inlet velocity of 10 mm/s ($V_{\mu} = V_{in}$). Designs 3, 5 and 6 performed less well, since they display high variation in microchannel velocities depending on the distance of the microchannels from the inlet.

3.5.2 Simulation of pollen trajectories under fluid flow

In order to estimate the trapping behavior of the chip to trap at least one pollen grain at each microchannel, finite element analysis is carried out to trace the trajectories of pollen grains entering the main chamber. In this model, the pollen passes through a specific point at the inlet, enters the main channel and is carried toward either the outlet drain or the entrance of one of microchannels by fluid interaction. The concentration of pollen grains is assumed to be low enough to neglect the interaction between them. If external gravitational force is considered negligible, the motion of suspended particles is influenced only by the particle diameter (d_p), particle density (ρ_p), fluid dynamic viscosity (μ) and fluid density ($\rho_{f,}$). The average mass and spherical radius of the particle are considered as 5.69e-9 ng and 30 μm, respectively, based on the weight determined for *Camellia* pollens. The medium is assumed to have properties similar to water with a density of 1000 kg/m^3 and dynamic viscosity of 0.001 Pa.s. The Lagrangian equation governing the in-plane motion of particles is derived by the Equation (3-3) (Ma *et al.*, 2009):

$$m\frac{d\mathbf{u}_p}{dt} = \mathbf{F}_D - \frac{m}{\rho_p}\nabla p \tag{3-3}$$

where $\mathbf{u}_p$ is the particle velocity vector, F_D is the viscous drag force, ρ_p is particle density and p is fluid pressure. The drag force F_D is estimated by

$$\mathbf{F}_D = \frac{1}{2}C_D\rho_f A_p(\mathbf{u} - \mathbf{u}_p)^2 \tag{3-4}$$

where A_p is cross sectional area of particle, **u** is fluid velocity obtained by solving Navier-Stokes and continuity equations and C_D is drag coefficient which is a function of particle Reynolds number (Dinesh, 2009) defined as:

$$Re_p = \frac{\rho_f(|\mathbf{u} - \mathbf{u}_p|)d_p}{\mu} \tag{3-5}$$

According to Stokes's drag law, when the particle Reynolds number is less than unity, the particle follows the streamline with acceptable accuracy (Melling, 1997). Considering the maximum velocity of a pollen grain when entering the nudge shaped microchannel entrance in the proposed designs (Table 3.2), the particle Reynolds number for pollen grains moving toward the microchannels is less than 0.6. This confirms that for an inlet velocity of 10 mm/s, the pollen grains follow the flow streamline with acceptable accuracy in all the designs analyzed. The finite element analysis of microflow with pollen grains is carried out using the commercial software COMSOL 3.5. The trajectories of pollen grains are estimated for various entrance points located at the inlet. Since the pollen grain has the radius of 30 μm, its center has to be located at least 30 μm away from the sidewalls of the main channel. Therefore, the possible locations of entry points are confined to a narrower region across the inlet called *trap length* indicated by the region A in Fig 3.4a. Fig 3.4b,c show the predicted streamlines and trajectories of pollen grains for Designs 1 and 4, given an inlet velocity of 10 mm/s and initiating at various start points located at distances of 50, 100, 150, 200 μm from the sidewall. The simulations predict that pollen grains follow the streamlines to get trapped into the microchannels. One could note that a pollen grain located at the distance of 50 μm from the sidewall will be trapped at CH1 for Design 4 and

not for Design 1. Hence, each channel can have unique trap length (S_w) along the region "A". A pollen grain entering the input through the trap length (S_w) of each channel will get trapped at the corresponding channel. The trap CH1 has no trap length in Design 1.

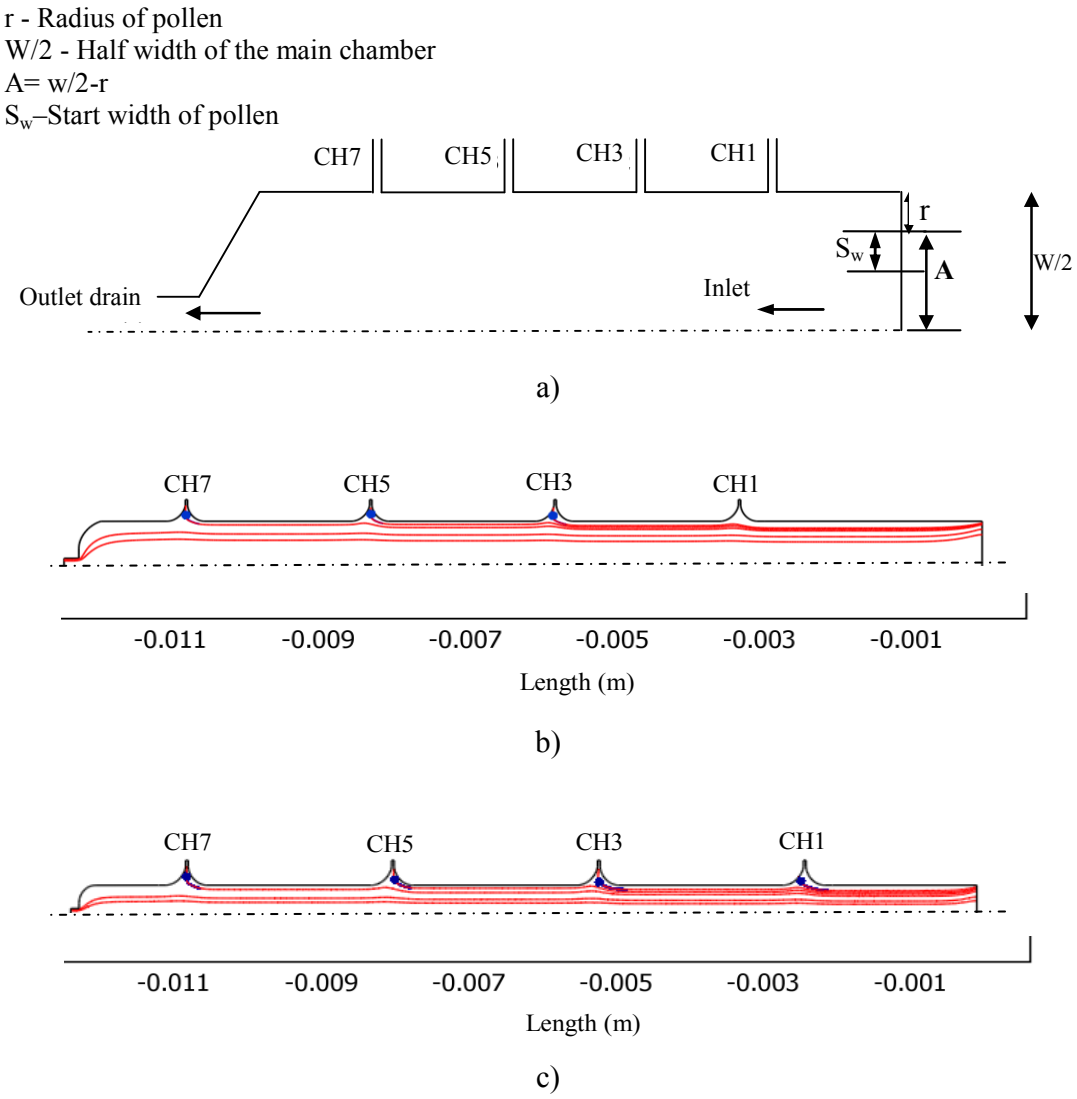

Figure 3.4: Model used for simulating pollen trajectories, a) geometry, b) predicted trajectories of pollen grains for Design 1 for the start points of 50, 100, 150, 200 µm away from the sidewall, c) predicted trajectories of pollen grains for Design 4 for the start points of 50, 100, 150, 200 µm away from the sidewall.

3.5.3 Prediction of trapping coefficient for each microchannel

Because of the laminar flow behavior in the main chamber, each microchannel receives pollen grains from a precisely defined starting region located in the inlet cross section. Assuming arbitrary positioning of pollen grains in the inlet, the trapping coefficient of a pollen grain at the entrance of each microchannel (τ) is therefore defined as ratio of the trap length of a channel at the inlet to the total trap length of the trap zone, A, (Fig 3.4a):

$$\tau = \frac{\text{Trap length of a channel, } S_w}{\text{Total length of trap zone, A}} \times 100 \tag{3-6}$$

An efficient design with 8 microchannels would ensure an equal trapping coefficient of 25% for each of the four microchannels located on one side. However, this calculation neglects the presence of the outlet drain which also captures pollen grains and hence significantly reduces the trapping coefficient of the microchannels. The objective is to select a design with the highest possible but approximately equal trapping coefficients for all four sets of microchannels so that a pollen grain is trapped at each microchannel.

In order to determine the trap length and trapping coefficient for each microchannel, the particle trajectory analysis described in Section 3.5.3 is employed. The simulations are used to identify the inlet trap length for each microchannel and the trapping coefficient is then calculated as the ratio between trap length and total trap zone (A) (Table 3.3).

Table 3.3 Numerical analysis to predict the channel trapping coefficient (τ) for all the four sets of microchannels

Design number	Main chamber width (W_m=W_{in}) µm	Outlet drain width (W_{out}) µm	τ , %				
			CH1, CH2	CH3, CH4	CH5, CH6	CH7, CH8	Outlet drain
1	**1200**	**200**	0	0.52	2.45	2.1	94.9
2	**1200**	**100**	2.1	6.1	5.8	5.2	79.8
3	**700**	**200**	0	0	0.31	0.93	98.7
4	**700**	**100**	0.6	5.6	6.25	6.25	81.2
5	**300**	**200**	0	1.66	6.66	2.5	89.1
6	**300**	**150**	0	5	7.5	5.8	81
7	**300**	**100**	0	6.66	9.16	8.33	78.3
8	**300**	**80**	1.6	15	12.5	10.8	59.1

The results in Table 3.3 show that microchannels CH1 and CH2 have low trapping coefficient irrespective of the dimensions of the main chamber and the outlet drain. By contrast, microchannels CH5-CH8 are predicted to have relatively higher trapping coefficient. In all designs, the highest trapping coefficient is that of the outlet drain. This is consistent with the purpose of this outlet to evacuate excess pollen grains.

The trapping coefficient in Table 3.3 indicates a chance of trapping a pollen at a microchannel. The value of trapping coefficient also indicates the degree of trapping effectiveness for a random distribution of pollen at the entry. The high value of trapping coefficient indicates high degree of trapping resulting in less time taken to trap a pollen at the microchannel when the pollens are distributed randomly at the inlet. Hence, the time for trapping of a microchannel called, *trap time,* would be a measure of quantity for trapping coefficient or trapping effectiveness.

Comparison of the different designs shows that Designs 1, 3, 5, 6 and 7 are not efficient as trapping coefficient for at least one set of microchannels is zero. In Designs 2, 4 and 8 all four sets of microchannels have a trapping coefficient above zero. Among these, the best performance was considered to be the one that shows the least variation among the four sets of microchannels, both in terms of flow velocity (Table 3.2) and microchannel trapping coefficient (Table 3.3). Considering above criteria, the Design 4 was chosen for further experimental validation.

3.6 Experimental testing of the enhanced design

To validate the performance of Design 4 on cell trapping, it was fabricated and tested with an inlet velocity of 10 mm/s and its performance was compared with the performance of Design 1 which serves as reference. The trajectories of injected pollen grains were monitored microscopically and trapping coefficients of individual microchannels were evaluated by determining the time between injection and trapping of the first pollen grain. Optical microscopy (Nikon 80i equipped with an Infinity 1 camera with a frame rate 10 Hz) was used for this purpose. Fig 3.5 shows the experimentally determined trajectories of three pollen grains and superimposes the predictions made by the numerical analysis of velocity field streamlines. The experimental results confirm the validity of the numerical analysis and demonstrate that the particles follow the streamline with a high accuracy.

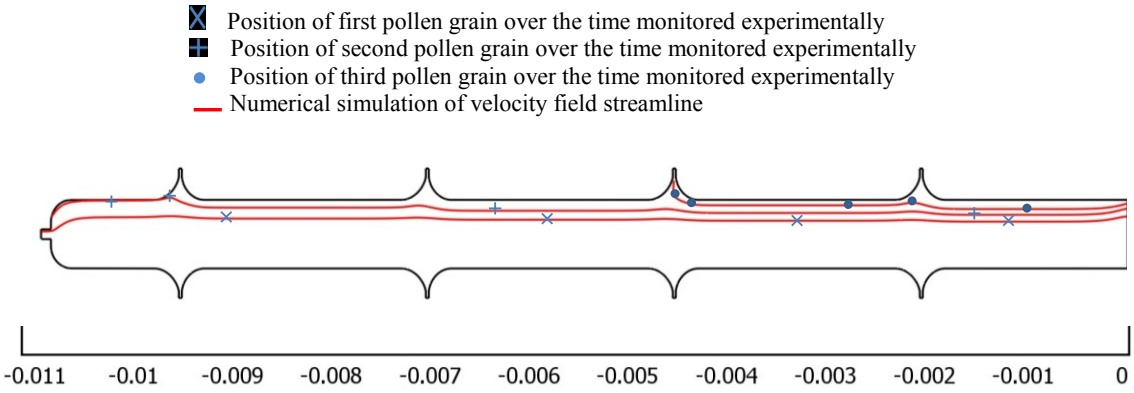

Figure 3.5: Comparison of numerical simulation of velocity field streamline and experimental testing on the trajectory of pollen for the Design 4

A close-up view of the pollen grain getting trapped at the entrance of a microchannel is shown in Fig 3.6. In this case, the pollen grain is guided along the main chamber's sidewall. While it approaches the entrance, it detaches from the sidewall and is then trapped at the entrance. The trajectory is very similar to the simulation results shown in Fig 3.4.

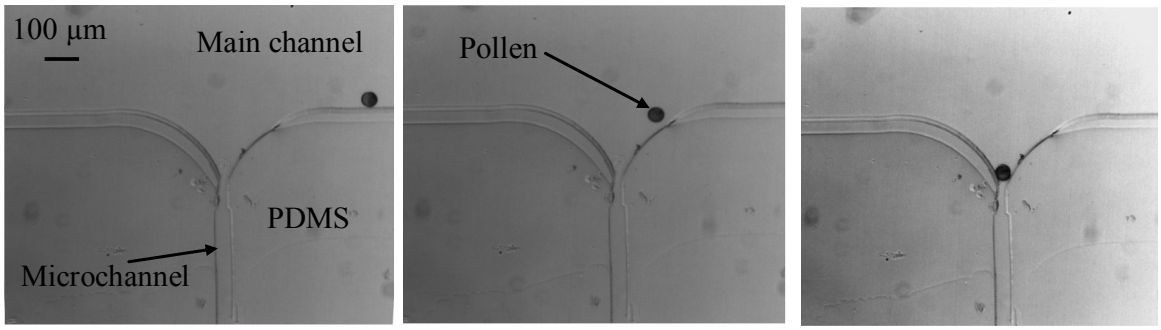

Figure 3.6: Close-up view of pollen grain entrapment at the entrance of the microchannel. The pollen grain is guided tangent to the chamber's sidewall toward the microchannel entrance

To evaluate the effectiveness of trapping of each microchannel, the time between injection of pollen suspension and trapping of the first pollen grain at the entrance of each

microchannel in Designs 1 and 4 was measured through observation under microscope as shown in Table 3.4. In Design 4, at least one pollen grain was positioned at the entrances of all eight microchannels within a few seconds, whereas in Design 1, several microchannels remained unoccupied even after introducing a total of 2 ml pollen suspension. The results also show that in Design 4, microchannels 5 and 7 capture pollen grains quicker than microchannels 1 and 3, which is consistent with the predictions of trapping coefficients given in Table 3.3.

Table 3.4 Experimental evaluation of the trapping coefficients quantified by trap time of individual microchannels. The time indicates the duration until a channel entrance is occupied by at least one pollen grain. Two runs were carried out for both Designs 1 and 4.

Trap time (s)					
Design	Test number	CH1	CH3	CH5	CH7
Design 1	Test 1	-	-	1	5
	Test 2	-	-	4	3
	Test 3	-	7	2	5
	Test 4	-	5	3	4
	Average	-	-	2.5	4.25
Design 4	Test 1	4	8	2	1
	Test 2	5	4	3	2
	Test 3	7	5	2	2
	Test 4	5	6	4	1
	Average	5.25	5.5	2.75	1.5

Fig 3.7 illustrates the performance of the Design 4. After injecting 2 ml of diluted pollen suspension, exactly one pollen grain was trapped in each microchannel entrance. The device was tested twice and in each test, no accumulation of pollen grains at the outlet drain or any of the microchannels was observed. The pollen grains remained stably trapped

at the entrances even after the fluid flow was stopped and bursting was not observed either before or after the arrest of fluid flow.

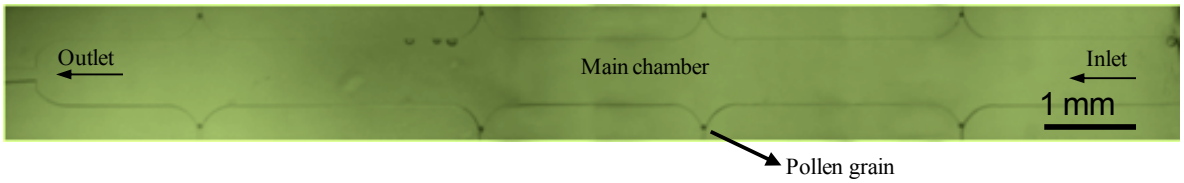

Figure 3.7: Brightfield micrograph of main chamber of Design 4 after injection of 2 ml of pollen suspension. One pollen is seen trapped at each entrance of microchannel.

Therefore, the proposed enhanced design provides a unique platform including a series of microchannels for single plant cell studies within a microfluidic environment. It satisfies the main goals of the proposed design on 1) presenting similar growth environment along the microchannels, 2) trapping only one pollen grain at the entrance of each microchannel. In order to verify whether the presented designs are conducive for pollen germination and growth, the trapped pollen grains were left to germinate as shown in Fig. 3.8. *Camellia* pollen tubes grew at an average growth rate of 8.5 µm/min through the microchannels, consistent with results obtained in conventional in vitro culture (Agudelo, 2012).

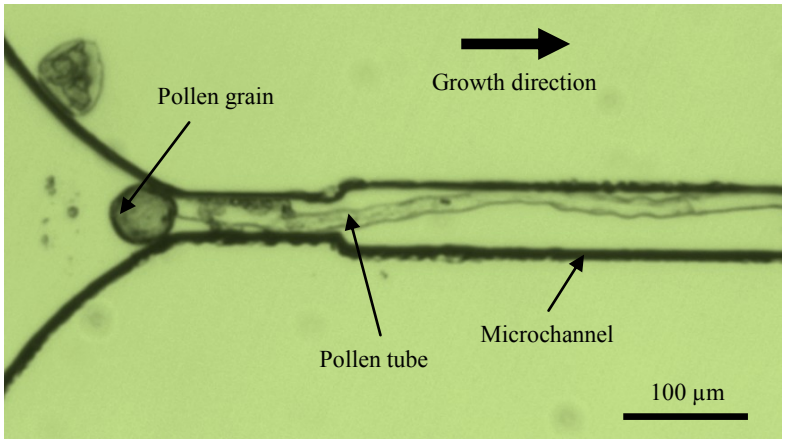

Figure 3.8: Growth of an individual pollen tube along a microchannel after 1 hr from germination with the average growth rate of 8.5 µm/min

Preliminary experiments demonstrate that pollen tubes are able to grow for more than 1 mm along the microchannels. This is a largely sufficient length for integrating various biosensors along the microchannel that will allow characterizing mechanical, electrical or biological aspects of an individual pollen tube within the microfluidic environment.

3.7 Summary and conclusions

An enhanced flow assisted microfluidic platform is designed and implemented for studying individual cells positioned in sequentially arranged traps. The performance of the design in terms of single cell entrapment is tested using pollen grains and improvements based both on simulations and experimental testing was incorporated to augment the trapping coefficient. The design is simple and has the potential for integration of various biosensors along the microchannels to allow investigation of polarly elongating cells such as pollen tubes, fungal hyphae and filamentous yeast. The design is also compatible with multilayer PDMS fabrication technique which would be required for integrating electrodes or microcantilevers for biosensors. The design positions single cells with high reliability in the presence and absence of continuous fluid flow which is essential for facilitating easy and rapid exchange of growth medium for various types of experimentation. It also provides identical growth environment for growing pollen tubes along each microchannel as growing pollen tubes are sensitive to fluid velocities.

Chapter 4

Aiming at a Moving Target - Using Microfluidics to Locally Administer Drugs to the Growing End of a Pollen Tube

4.1 Chemical treatment of pollen tube within microfluidic environment

There are basically two methods to expose the pollen tube to a drug, enzyme, molecular target, chemical agent or toxic material: 1) Global treatment and, 2) local treatment. In global treatment, the whole medium around the pollen tube is altered in order to observe the cell response to the change of target agent in the culture medium. But in local treatment, only one portion of the cell is exposed to the target agent and then its influence to the other portion of the cell and also on the whole cell response is studied. Any of these global or local treatments have their own benefits detailed in the next chapters. The enhanced design presented in Chapter 3 is ready to be used for chemical treatment of pollen tube in microfluidic environment. Although this design can be used for local and global treatment, but in this chapter, a modified version of enhanced design is used to apply local treatment to the growing tip. In Chapters 5-7 and 9, the enhanced design presented in Chapter 3 is directly used to characterize pollen tube behavior in response to mechanical-chemical signals. This work is to be submitted to *Journal of Nature Communications* with my contribution as the first author.

Abstract

Local administration of pharmacological or other agents has become an important tool to study cellular functioning such as the intracellular propagation of signals or control of the

cell growth and morphogenesis. Local drug administration has successfully been carried out using laminar flow in microfluidic devices, but in past typical applications of the technique, the target was statically positioned in the device. The situation becomes much more challenging when the target region constantly moves, even more so when the movement occurs with two degrees of freedom (anywhere in the x-y plane). To address this problem, we developed a laminar flow based microfluidic device that allows for continuous administration of two different solutions with a movable interface that allows to dynamically target a moving object. The device was tested on a growing plant cell, the pollen tube of *Camellia japonica*. This polarized cell elongates rapidly and the expanding tip region of the cell behaves in chemotropic manner providing an excellent test system with immediate response. Calcium is known to orient pollen tube growth and was used as a test substance. Although the geometry of the microfluidic prototype was adapted to the cellular test system and chemical agent used here, the device can easily be adapted to other growing or moving cells and other substances to be administrated locally.

4.2 Introduction

The administration of agents manipulating selected cellular processes is one of the fundamental experimental tools to understand cellular functioning. This experimental strategy includes the application of specific drugs interfering with cellular processes, enzymes, ions and proteins. Typically, an agent is added to the medium surrounding the cells (Andersson *et al.*, 2003; Breslauer *et al.*, 2006), but such a global administration alters the functioning of the entire cell. Much can be learned from administering agents to a spatially confined region of the cell, since the unexposed cellular region serves as an

internal control. Also, local administration allows targeting a particular region of polarly arranged cells or it allows studying the propagation of local effects to other cellular regions. Various methods have been developed to administer agents at subcellular resolution, most of which rely on the use of micromanipulation of micropipettes. Typically, the agent of interest is injected to the medium close to the targeted cellular surface (Bradke *et al.*, 1999). However, micromanipulation requires precise handling of a manipulator and even if the location of agent administration can be controlled exactly, the eventual local concentration of the agent is difficult to regulate because of local diffusion and convection.

A much higher degree of precision in terms of the applied local concentration can be achieved using microfluidics. Using the principle of laminar flow, different solutions can be administered to different regions of a cell placed within the microfluidic network. As the low flow rate within a microchannel has a small Reynolds number (Re) (Re<1), fluid streams injected through different inlets and meeting in a common channel continue flowing strictly in parallel. At the interface between the two streams no mixing takes place except diffusion (Knight *et al.*, 1998). The sharpness of the concentration gradient at the interface depends on the diffusion coefficient of the agent of interest and the stability of the width of the interface. The width of each stream, and the relative position of the interface between adjacent streams (one containing and one lacking an agent) can be controlled by adjusting the relative amounts of fluid flowing. This principle has been exploited to locally disrupt cytoskeletal filaments (Takayama *et al.*, 2001, 2003), to differentially label subpopulations of mitochondria (Lucchetta *et al.*, 2005), and to locally stimulate epidermal growth factor signaling (Sawano *et al.*, 2002).

In these experiments, the target cell was immobilized within a microfluidic network and the area of the cell to be targeted by the agent delivered by parallel laminar flow remained at a constant position. The situation becomes much more challenging when the target region constantly moves, even more so when the movement occurs with two degrees of freedom (anywhere in the x-y plane). To successfully and continuously aim at such a moving target requires a novel design of the microfluidic network.

At least two cellular processes can be responsible for making a cellular region a moving target: the displacement of the entire cell by crawling or migration, and the displacement of a cellular region by growth or cellular shape change. In our cellular model system, the pollen tube, cellular growth is the principal challenge. The pollen tube is a tubular protrusion emitted from the male gametophyte in higher plants, the pollen grain. It grows by tip growth, similar to fungal and yeast hyphae, root hairs, and neurons. The pollen tube attains growth rates of up to 1cm/h and it is able to change its growth direction either spontaneously or as a result of a directional trigger (Cheung *et al.*, 2008). Its function is the delivery of the sperm cells - a prerequisite for fertilization, seed set and fruit formation in higher plants (Franklin-Tong, 1999). The pollen tube has an axially symmetric, cylindrical shape, capped by an approximately hemispherical dome. All growth activity is spatially confined to this apical dome, which is why this cellular region has been the focus of a large body of research on the spatial and temporal regulation of polar growth in walled cells (Chebli and Geitmann, 2007b; Feijó *et al.*, 1995a; Geitmann *et al.*, 2009a; Hepler *et al.*, 2001) and on the intracellular transport and signaling mechanism that are responsible for

maintaining polarity (Bove *et al.*, 2008b). The axial symmetry of the growth process can be broken by exposing pollen tubes to asymmetric triggers such as electrical fields (Bou Daher and Geitmann, 2011d), chemical gradients (Geitmann *et al.*, 2007a). However, how the tube is able to actually redirect growth, and what composes the pathway of intracellular signaling and response, is poorly understood. It would therefore be of immense importance to be able to administer various agents, including cell wall modifying enzymes and cytoskeletal inhibitors, as well as ions and ion channel blockers at precisely defined concentrations and with exact timing to a portion of the apical dome only. Depending on the species, the diameter of the pollen tube apex measures between 6 and 20 μm. The interface of a laminar flow based gradient must therefore be sufficiently sharp to expose the two halves of the apex to significantly different concentrations of the chosen agent. This can be achieved by applying a laminar flow based gradient in parallel to the growth direction of the tube. The challenge arises through the rapid growth activity of the pollen tube. Since the tip elongates continuously at rates of approximately 4 to 8 μm/min, an interface between the laminar flow streams that is oriented in parallel to the growth direction needs to be sufficiently steep over an extended distance to ensure that the elongating tube at the location of moving tip is continuously exposed to the two fluids. More importantly, the position of the center point of the pollen tube apex can change on the axis perpendicular to the growth direction, either spontaneously or triggered by the administered agent. To follow this displacement in real time, the position of the interface needs to be easily adjustable in space.

To address this challenge, we developed a laminar flow based microfluidic device that allows for continuous administration of two different solutions with the interface dynamically targeted at the pole of the pollen tube, even if this cellular region moves in xy plane. Numerical diffusion analysis and experimental testing of parallel laminar flows with adjustable interface were performed to prove the capability of the device to target the motile tip both with growth induced increasing distance from the point of origin and varying position in perpendicular direction. As a proof of concept, the device was tested using *Camellia japonica*, whose pollen tubes grow extremely straight and have a large diameter. The testing agent chosen is calcium, a main regulator of polarized growth in pollen tubes. Ca^{2+} ions play an important role in the signaling pathway controlling both growth rate and growth direction (Geitmann and Palanivelu, 2007a; Malho *et al.*, 1996; Takeuchi *et al.*, 2011). Ca^{2+} ions enter the apex of the pollen tube from the extracellular medium (Kühtreiber *et al.*, 1990) resulting in a tip-focused gradient of the ion in the cytosol (Feijó *et al.*, 1995a; Pierson *et al.*, 1994).Dissipation of the calcium gradient causes the arrest of growth (Pierson *et al.*, 1994) and the ion is supposed to be involved in regulating the direction of growth likely by affecting actin polymerization and/or exocytosis (Bou Daher and Geitmann, 2011d; Malhó *et al.*, 1992a). Although a specific cell type and agent are tested here, the device can easily be adapted to other growing or moving cells and other substances to be administrated locally.

4.3 Microfluidic design and fabrication

The design consists of a main chamber to trap the pollen grains, two microchannels into which the pollen tubes elongate and side inlets for introducing different media. The main

chamber has an inlet for the injection of the pollen suspension and an outlet to evacuate excess pollen in order to prevent their accumulation at the microchannel entrance or at the exit of the main chamber (Fig. 4.1a). Although only one microchannel will be used at any given time, two are provided for redundancy offering the possibility to select the better or faster growing between two cells or to perform two subsequent experiments. Once the selected pollen tube has grown to the desired length, the pollen-medium inlet, the outlet drain and the medium outlet of the unused microchannel are blocked to configure the microfluidic network for laminar flow (Fig. 4.1b).

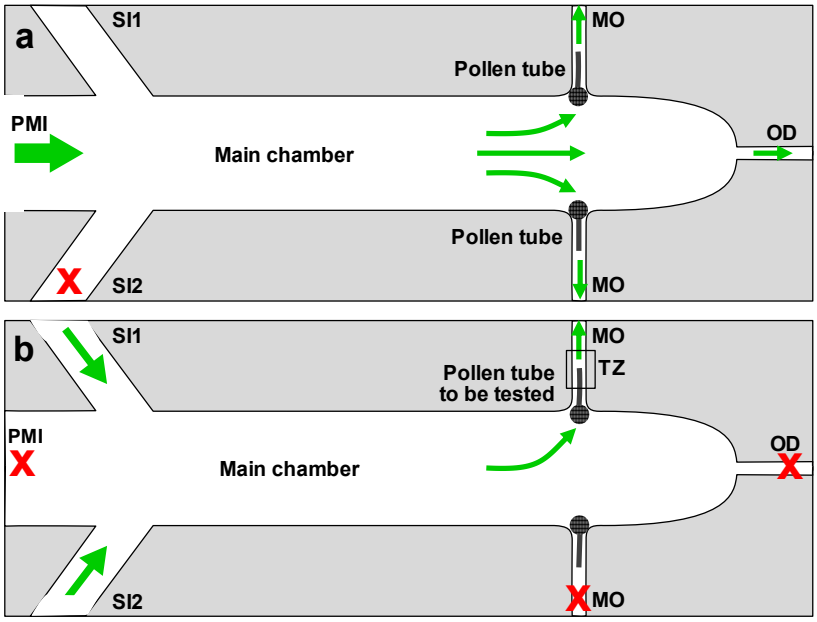

Figure 4.1: (a) Schematic diagram of microfluidic device designed for testing local calcium treatment of pollen tube. The pollen suspension is introduced to trap the pollen grains at the entrance of microchannels and to grow the pollen tube along the growth microchannels. (b) The configuration of proposed microdevice after blockage of outlet drain, the pollen-medium inlet and the non-objective microchannel at the time of local treatment testing.

Two different media are then injected through side inlets using controlled flow of a micropump to generate parallel laminar flow along the growing pollen tube, along its

growth direction (Fig. 4.2). Overall flow rates are kept below a threshold of 50 mm/sec to prevent tube bursting (Agudelo *et al.*, 2012d) and the relative flow rates are adjusted to position the interface between the two media at the desired position (Section 4.4).

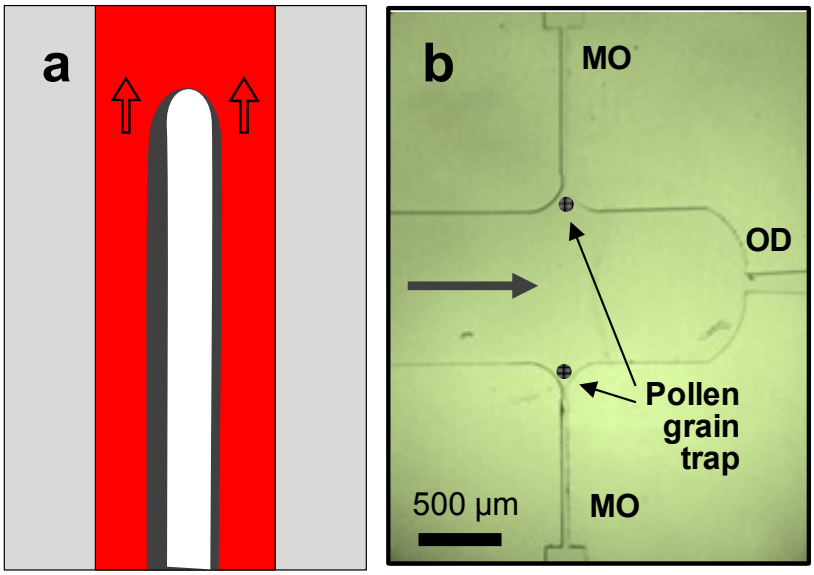

Figure 4.2: (a) Two parallel streams carrying medium with different Ca^{+2} ion concentration toward the growing pollen tube tip (b) The close up of fabricated design at the location of pollen entrapment and growth microchannels. Bar, 500 µm

The dimensions of the components of the microfluidic network are based on a previously developed platform for pollen tubes, the TipChip (Agudelo *et al.*, 2012d). Briefly, the inlet size has to be wide enough to provide enough space for entering few pollen grains. The growth microchannel has the width of 30 µm, slightly smaller than the diameter of 50-60 µm of the *Camellia* pollen grain and bigger than the typical diameter of 12-19 µm of the pollen tube. This traps the pollen grains at the microchannel entrance and allows the pollen tube to grow into the microchannel. The depth of the microfluidic network is set to 80 µm, slightly larger than the diameter of the pollen grains to let them freely pass along the distribution chamber and reach the entrance of microchannels, but to prevent vertical

stacking. Conventional methods are used to fabricate the microfluidic device as detailed in Agudelo et al. (Agudelo *et al.*, 2012d) and Agudelo et al (Agudelo, 2012) (Fig. 4.3).

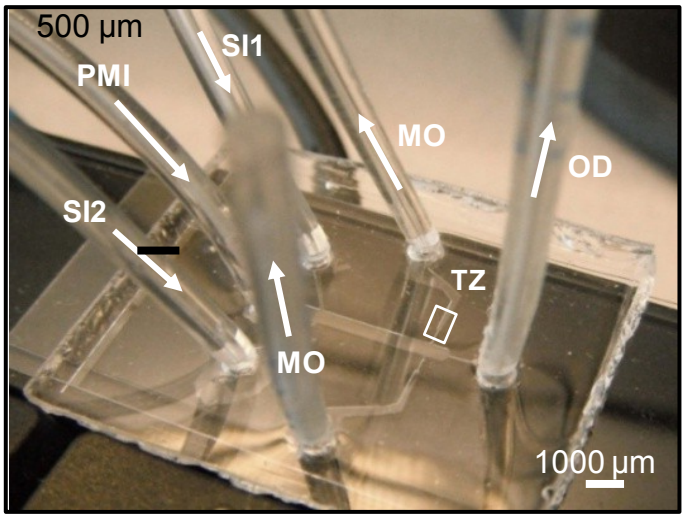

Figure 4.3: Fabricated microfluidic device for local treatment testing on tube. Bar, 1000 µm

The pollen-medium inlet (PMI) and two side medium inlets (1) and (2) are connected to syringe pumps. Pollen tube growth is monitored using optical microscopy and quantified by image analysis (Fig. 4.4).

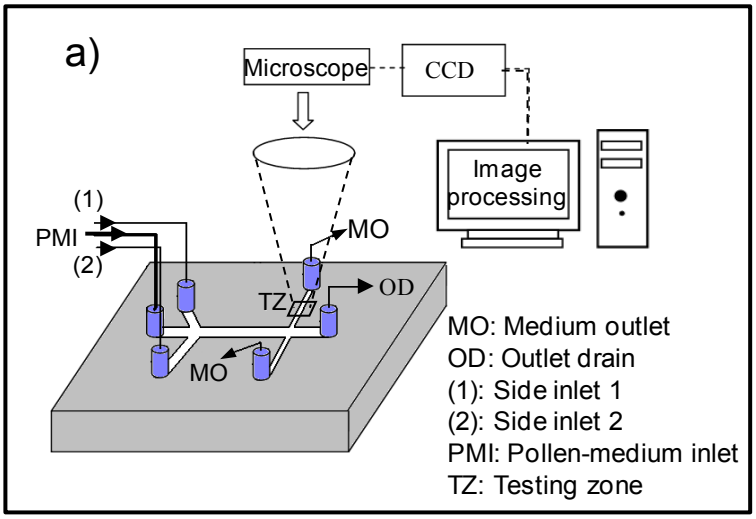

Figure 4.4: Overall design for drug administration at subcellular resolution on a moving target (a) The schematic of experimental setup.

4.4 Modeling parallel laminar flows and molecular diffusion

In order to determine how the interface between the two different media is controlled through adjusting the inlet flows, three-dimensional simulation of steady state fluid flow and molecular diffusion within the microfluidic device is performed. A 3D model is employed with the same dimensions as the fabricated microdevice. The model consists of two side inlets for the two different media, one main chamber, the growth microchannel and one medium outlet. The second microchannel is neglected as it is blocked during experimentats. The flow within the microfluidic network is governed by Navier-Stokes and the continuity equations (Wang *et al.*, 2008) given in equations (4-1) and (4-2).

$$-\nabla p + \nabla(\mu \nabla \mathbf{u}) = 0 \qquad (4\text{-}1)$$

$$\nabla . \mathbf{u} = 0 \qquad (4\text{-}2)$$

where $\mathbf{u}$ is the velocity vector, p is the fluid pressure and μ is the dynamic viscosity of the medium. Both media are assumed to behave like water with the density of 1000 kg/m^3 and dynamic viscosity of 0.001 Pa.s. The inlet velocity is defined as the boundary condition for the medium inlets. The pressure at the main chamber outlet is set to atmospheric pressure. At all other boundaries, no-slip condition is defined. COMSOL Multiphysics 3.5 software is used to solve the governing equation of fluid flow. The result of spatial distribution of fluid velocity for identical 1 mm/s inlet velocities for both side medium inlets is shown in Fig. 4.5. Comparison of the streamline flows in presence and absence of a pollen grain at

the microchannel entrance revealed slight differences in the first micrometers of the microchannel since the grain represents an obstacle, but no significant effect was noticeable in the remainder of the channel. Since pollen tubes burst when exposed to excessive flow, the numerical fluid analysis also enables us to determine the inlet flow rates necessary to remain within the critical limit of 50 mm/sec within the microchannel.

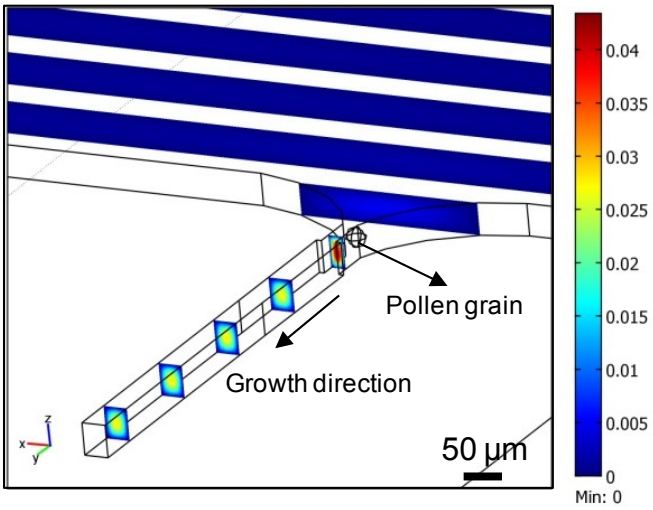

Figure 4.5: 3D simulation of fluid flow and molecular diffusion within fluidic network, The fluid velocity at a few sections of growth microchannel away from trapping point in presence of pollen grain.

To ensure that the tip of the elongating pollen tube is indeed exposed to two significantly different concentrations of the administered agent despite diffusion occurring at the interface, the effect of diffusion was assessed based on the governing convection–diffusion transport equation (Wang *et al.*, 2008) as seen in equation (4-3).

$$\frac{\partial C}{\partial t} + (\mathbf{u}.\nabla).C = D\nabla^2 C \tag{4-3}$$

where C and D are the concentration and diffusivity of the reagent within the medium. The system is assumed to be steady state as $\frac{\partial c}{\partial t}$=0. As the boundary condition for convection–diffusion transport equation, the unit concentration is set for side inlet 1 and zero concentration for side inlet 2. No-flux conditions are imposed at all channel walls, $(\frac{\partial c}{\partial n})$ =0. The outlet of growth microchannel has the boundary condition of convective flux as there is flow outward. The diffusion analysis is carried out for sample diffusion coefficient of D=1×10^{-10} $m^2 s^{-1}$ for a calcium ion (Donahue *et al.*, 1987; Kamholz *et al.*, 2001). Finite element analysis is employed to solve the convection-diffusion transport equation using COMSOL software 3.5. The element type of Lagrange Quadratic was chosen to mesh the geometry. The results of concentration gradient at several cross sections of growth microchannel away from the trapping point and in the presence of grain are depicted in Fig. 4.6 in the case of identical 1 mm/s inlet velocities imposed at both side inlets. The number of mesh elements are 23880. The steepness of the gradient that is maintained over the extended length of the microchannel proves the feasibility of generating two significantly different calcium ion concentrations along the two sides of the apical pollen tube surface. The sensitivity of the results to the number of mesh elements was evaluated considering 5% criterion error.

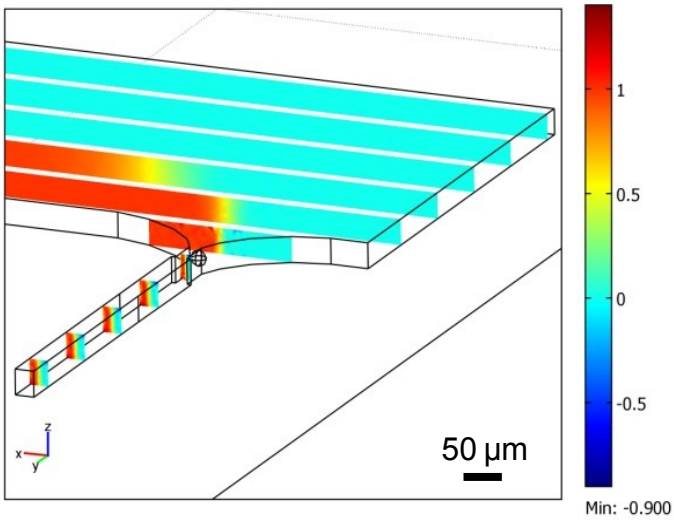

Figure 4.6: 3D simulation of fluid flow and molecular diffusion within the fluidic network, The concentration gradient at few cross sections of growth microchannel in the presence of pollen grain.

At the flow velocities used here, the steepness of this gradient does not change significantly between the beginning and the end of the 1000 µm long microchannel (Fig. 4.7). Higher flow velocities would be expected to generate even sharper concentration gradients, because of the reduced time interval between the initial contact between the two media in the main chamber and the arrival of the interface at the target. However, excessive velocities cause shear stress and lead to pollen tube bursting (Agudelo *et al.*, 2012d) and, therefore, flow speeds have to remain below a threshold. At the flow velocities used here, the calcium ion gradient across the microchannel is sufficiently steep to expose the advancing apex to different concentrations of the ion even at a distance of 150 µm (Fig 4.7a) and 500 µm (Fig 4.7b) from the trapped grain.

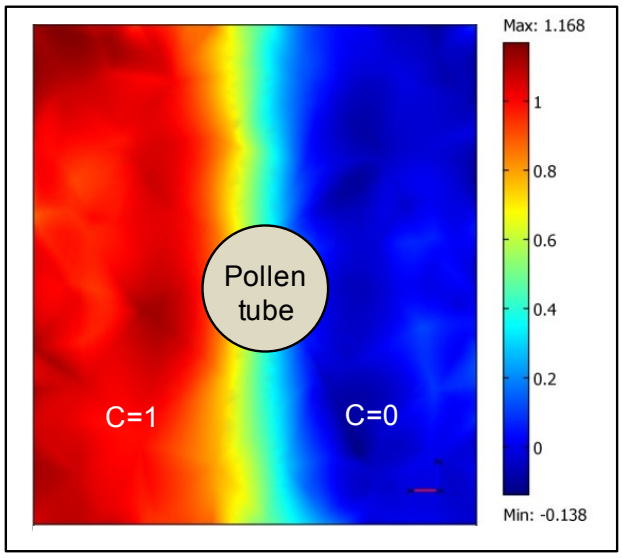

(a)

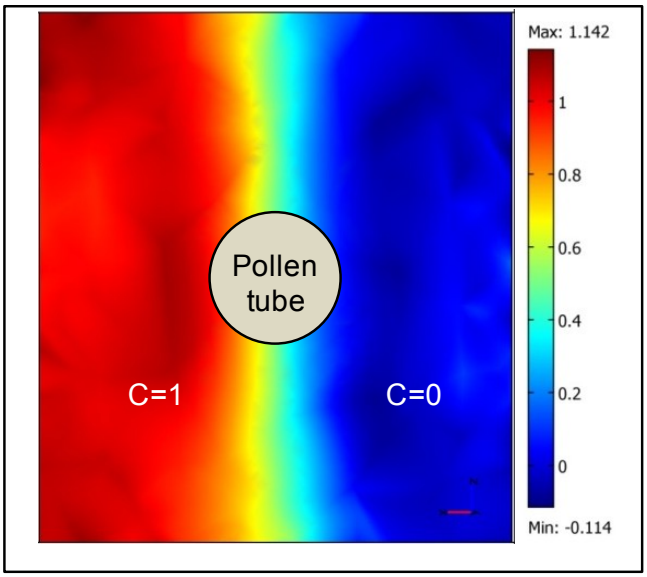

(b)

Figure 4.7: The concentration distribution of calcium ion across the microchannel at a)150 µm and b) 500 µm away from the trapping point of pollen tube. The distribution is steep enough for local treatment testing.

The exact position of the growing pollen tube tip relative to the side walls of the microchannel is essentially arbitrary and can change either spontaneously (rare in *Camellia*

tubes) or as a response to an asymmetric application of a growth influencing agent. To continuously maintain the interface between the two parallel streams aligned with the pole of the cell, the relative inlet velocities of the two side inlets are manipulated to adjust the position of the interface. The velocity ratio K of the inlet velocities is calculated from equation (4-4):

$$K = \frac{V_{\text{Side inlet 2}}}{V_{\text{Side inlet 1}}} \tag{4-4}$$

On the right-side of the microchannel's centerline, the effect of the manipulation of ratio K on the location of the interface respect to the centerline (D) is estimated by finite element analysis. Once the inlet 1 and inlet 2 are switched in Fig. 4.8, similar relation between D and K is obtained on the left side of the microchannel's centerline. Using the data in Fig. 4.8, the position of the interface between the two media can be continuously adjusted to be aligned with the microscopically determined position of the pollen tube apex inside the microchannel. Since most pharmacological agents are colorless and the two media can therefore not be distinguished optically, this calibration is an essential tool.

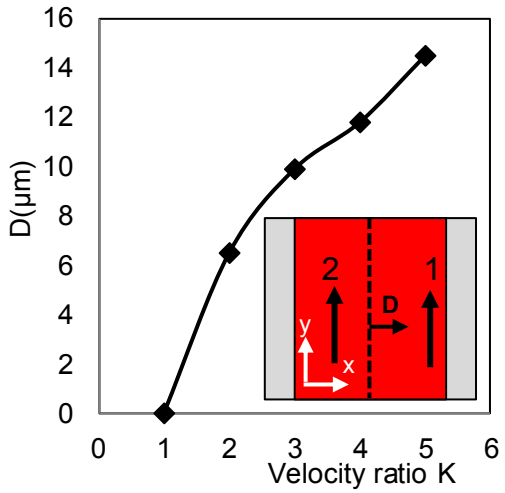

Figure 4.8: The effect of inlet velocity ratio (K) on the distance of the boundary line from the center line of microchannel (D) obtained from FEM analysis of fluid dynamic and molecular diffusion

4.4 Experimental testing of laminar flow pattern

To confirm the stability of the parallel laminar flow pattern and the effect of diffusion, the device was tested using media complemented with a dye. When the outlet drain was open, the flow carried medium 1 (containing dye) to microchannel 1 and towards the outlet drain. Medium 2 (transparent) filled the other half of the distribution chamber, towards microchannel 2 and to the other half of the outlet drain (Fig. 4.9a). Blocking the outlet drain and one of the microchannels resulted in both media to be conducted to the open microchannel (Fig. 4.9b). When imposing flow rates of 6 µl/min, the sharpness of the dye gradient was maintained over the entire length of the microchannel and was stable over extended periods of time. The effect of different media flow velocities on the position of interface between two parallel streams relative to the center line was tested in absence of pollen grains at the entrance (Fig. 4.9c). Positioning of a pollen grain at the microchannel entrance using K=1 only affected the laminar flow near the entrance of the microchannel

without lasting effect on the remained of the microchannel (Fig. 4.9d) as predicted by the simulation (Fig 4.5).

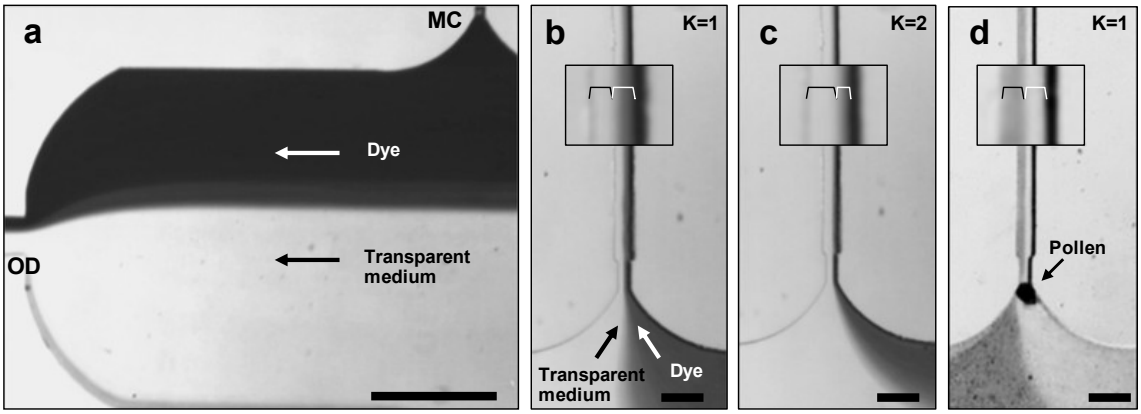

Figure 4.9: Flow visualizing the parallel laminar flows along the microchannel in the presence and the absence of pollen grain (**a**) The flow is distributed between the outlet drain and the growth microchannel when the outlet drain is open. (**b**) The parallel flows along microchannel in the absence of pollen grain when the outlet drain is closed and K=1. (**c**) The parallel flows along the microchannel in the absence of pollen grain when the outlet drain is closed and K=2. (**d**) Parallel flows in the presence of pollen grain when the outlet drain is closed and K=1. Scale: 100 μm

4.5 The response of pollen tube to asymmetric administration of calcium

To assess the functionality of the device, we first conducted a control experiment to assess the effect of different flow velocities on pollen tube growth. The design of Agudelo et al. (Agudelo *et al.*, 2012d) was exploited to expose pollen tubes growing along simple microchannels to different flow velocities. No gradient was within the width of the microchannel as the medium was applied in the entire microchannel. The experimental results demonstrate that for about 65% of pollen tubes exposed to the fluid velocities less than 20 mm/sec along the growth microchannel, increase of 20% fluid velocity led to up to 15% raise on the growth rate without any arbitrary change on growth direction. Above this

range of fluid velocity and up to critical limit, the growth rate does not change considerably or in a few cases the growth was arrested. This proves that below the fluid velocity threshold, the growth direction of pollen tubes is independent of the amount of fluid flow.

We then tested the effect of two media with different calcium concentrations. The optimal calcium concentration for *Camellia* pollen tubes growing in bulk conditions is 2.54 mM (Bou Daher and Geitmann, 2011d). Reducing this concentration to half (1.27 mM) or doubling it (5.08 mM) causes a moderate reduction in average pollen tube length by 14% and 19%, respectively (Bou Daher and Geitmann, 2011d). Outside of this concentration range, growth rate is affected much more dramatically. To confirm that in the microfluidic setup the pollen tube behaved similarly, we exposed elongating *Camellia* pollen tubes first to a continuous, slow flow of medium containing the optimal calcium concentration of 2.54 mM calcium (no gradient within the width of the microchannel) and then changed the medium with 5.08 mM or 1.27 mM calcium (applied in the entire microchannel). In both cases, the growth rates of individual pollen tubes dropped by approximately 15%. Neither globally applied concentration change caused the tube to change direction. As expected, this confirms that *Camellia* pollen tubes do not change growth direction when exposed to a global change in calcium concentration which is a non-direction trigger. (Figure 4.10)

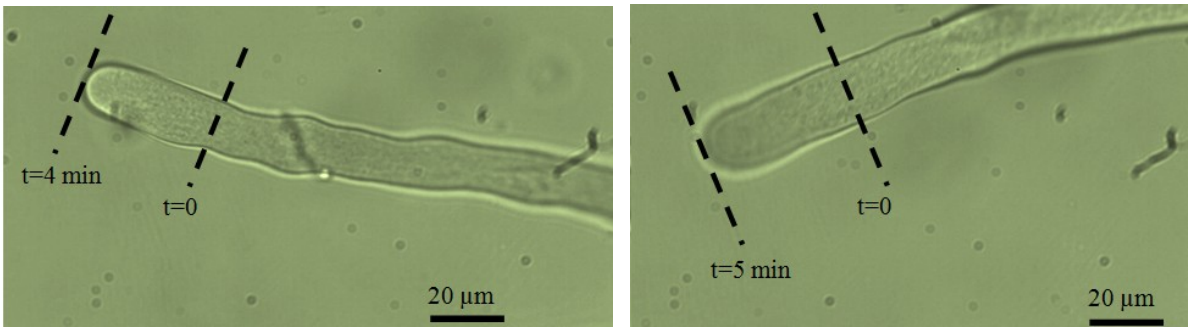

Figure 4.10: The response of pollen tube to the medium change containing twice optimal calcium concentration (5.08 mM), no arbitrary change of direction or growth arrest occurs. The growth rate reduced by 20%, time=0 corresponds to 2.5 min before the moment of injecting the different calcium ion concentration. Bar, 20 µm

Next, we let a *Camellia* pollen tube grow surrounded by optimal medium (2.54 mM calcium) supplied through both side inlets and then switched side inlet 2 to 5.08 mM calcium. After 35 sec residence time, the growth rate slowed down from 4.8 µm/min to 1.3 µm/min, likely because the higher calcium concentration reached the apex of the tube at this time (Fig. 4.11).

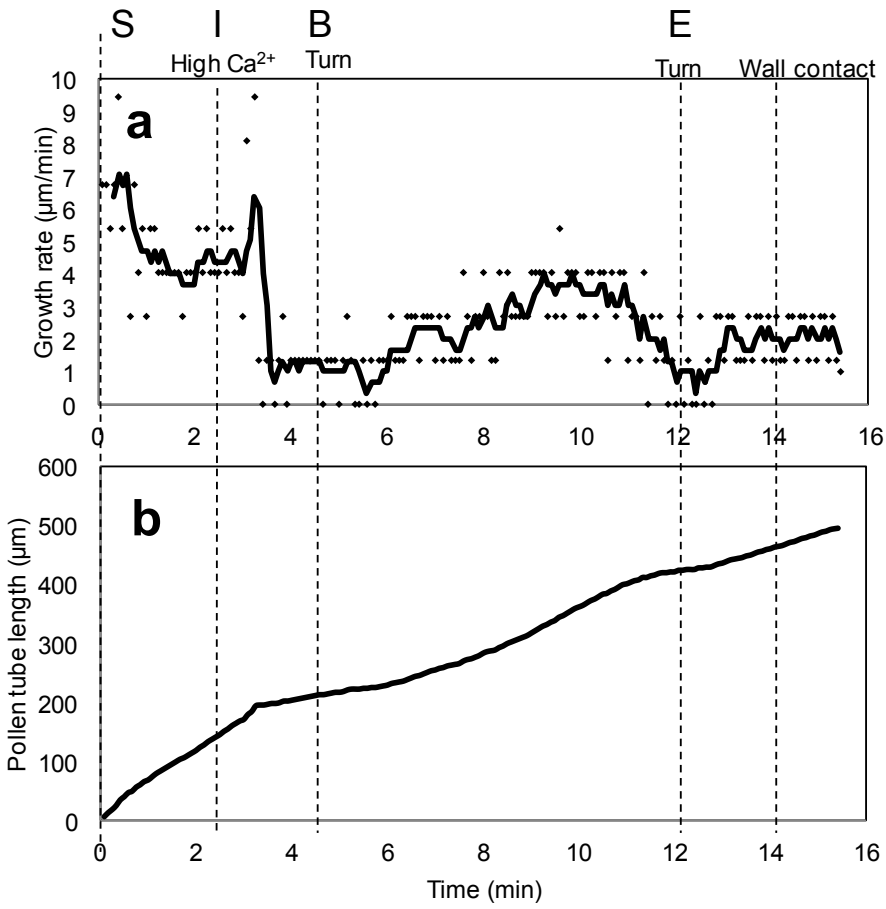

Figure 4.11: The alteration of (a) growth rate and (b) growth length before and after the time point (I) when gradient reaches the tube tip (Before and after treatment). Point S is the time a few moments before applying the local treatment testing. Point I is dedicated to the time when we introduce medium into the chip. Point B is the time point when the pollen tube responds to the local treatment. The time in which the tube sense two different media a point between point I and point B. Point E seems a point in which the pollen tube responds to the calcium concentration gradient for the second time.

90 sec later, the tube showed a clear reorientation away from the higher calcium concentration followed by an increase in growth rate (Fig. 4.12). Interestingly, 380 sec following the first turn, the tube slowed down a second time and turned again. The angles of both turns were similar with 16 º and 21º, respectively, and correspond to turning angles observed when *Camellia* pollen tubes are exposed to an electrical field (Bou Daher and

Geitmann, 2011d). This biphasic behavior suggests that the size of an individual chemotropic response event (i.e. the turning angle) is constant. If the directional trigger persists, then the response is repeated after a lag period. In the present case, the tube did not turn a third time but continued growing straight in its new growth direction until it hit the side wall. This can be explained with the fact, that following the second turn the apex was completely surrounded by the medium stream with lower calcium concentration.

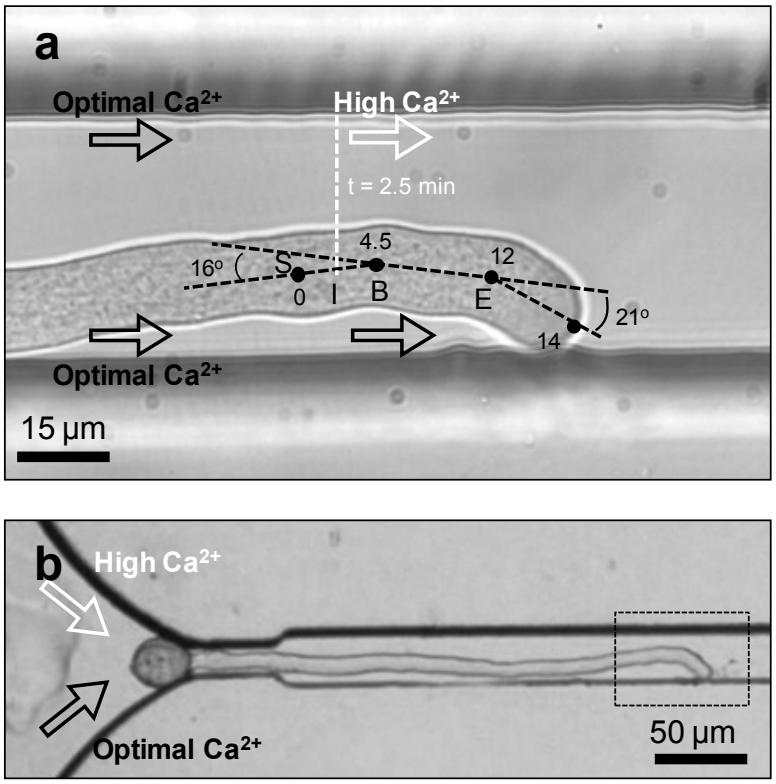

Figure 4.12: (a) The experimental results of pollen tube reorientation in response to local treatment of tip with two different calcium concentrations, The medium 1 has 2.54 mM calcium concentration and the medium 2 has 5.08 mM. Two times reorientation occurs at points B and E with reorientation angles of 16° and 21° respectively. The comparison of pollen tube tip and calcium ion gradient across channel proves that the pollen tube sense different calcium ion concentration on either sides of tip. (b) The pollen tube position after 17 min of local treatment testing. No redirection occurred after pollen tube hit the sidewall.

To test the capacity of aiming at a moving target at xy plane, the K ratio was manipulated depending upon the position of the pollen tube tip. (Fig. 4.13a). The position of the apical pole of a *Camellia* pollen tube growing surrounded from all sides by optimal medium (2.54 mM calcium) was about 8 μm away from the centerline of microchannel.

To target the apex with an interface between two different calcium concentrations, the medium at inlet 1 was changed to 5.08 mM calcium, whereas inlet 2 was maintained at 2.54 mM calcium, applying a K ratio of 3. After 95 sec, the tube showed a redirection of the growth toward the lower calcium (Fig 4.13b). The pollen tube continued the growth straight in its new growth direction, hit the sidewall and, forced by this mechanical constraint, continued elongating along the wall. To induce a second directional trigger, the media of the two inlets were switched and applied at ratio K=5 to target the pole of the cell now situated at 16 μm from the centerline of microchannel. After 1 min, the tube responded by reorienting away from the higher calcium concentration (Fig 4.13c). Following the turn, the pollen tube continued straight in the new growth direction until it hit the opposite sidewall.

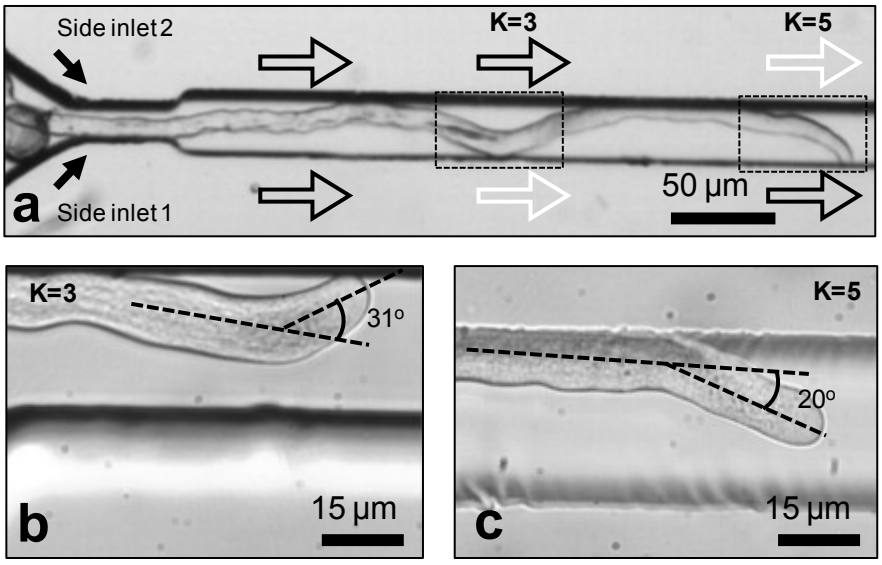

Figure 4.13: (**a**) The experimental results for aiming growing pollen tube in xy plane by local treatment of moving tip with two different calcium concentrations. The local treatment is carried out at two different position of pollen tube. In position 1, the treatment is done with K=3 where the tube centerline is at the distance of 8 µm away from the centerline of the microchannel. In position 2, the tube tip is about 250 µm after the first position treatment and the tube centerline is at the distance of 16 µm away from the centerline of the microchannel. In this case, K=5 was selected for local treatment experiment. selected as K=5, Bar, 500 µm, (**b**) The response of pollen tube reorientation to the medium change containing twice optimal calcium concentration (5.08 mM) at side inlet 1 and optimal calcium concentration (2.54 mM) at side inlet 2. The treatment is carried out under the condition of K=3 as the tube centerline is at the distance of 8 µm away from the centerline of the microchannel. The angle turn of 31^{o} was detected. Bar, 15 µm, (**c**) The response of pollen tube reorientation to the medium change containing optimal calcium concentration (2.54 mM) at side inlet 1 and twice optimal calcium concentration (5.08 mM) at side inlet 2. The treatment is carried out under the condition of K=5 as the tube centerline is at the distance of 16 µm away from the centerline of the microchannel. The angle turn of 20^{o} was detected. Bar, 15 µm.

4.6 Methods

4.6.1 Chip fabrication

The fabrication starts with the formation of a SU8 mold as negative photoresist (MicroChem Corp.) using a photolithographic technique. SU-8 2035 is spin coated on silicon wafer to reach the thickness of 80 µm. The SU-8 is baked for 3 min at 65 ºC and for

7 min at 95ºC in a hotplate. After soft-baking, the resist is cooled down at room temperature and is exposed to UV light using a photo mask for 30 s. Post-exposure bake step (PEB) is then carried out, baking the resist for 3 min at 65 ºC and for 6 min at 95 ºC in order to cross-link the SU-8. The SU-8 layer is then developed to obtain the SU8 mold. The microfluidic device is then fabricated pouring a layer (4 mm) of PDMS prepolymer mixture with curing agent with a mass ratio of 10:1 on SU8 mold. This PDMS layer is cured at 80 ^{0}C for 30 min in an oven, peeled off from the master mold and bonded to a glass layer to seal the fluidic network. The inlet and outlet holes are then maded for injection purposes. The PDMS layer is sealed with a glass layer to accomplish the microfluidic device.

4.6.2 Pollen culture and germination

Camellia japonica pollen collected from a plant grown in the Montreal Botanical Garden was dehydrated on anhydrous silica gel overnight and stored in gelatin capsules at -20°C. Prior to experimentation, pollen was rehydrated in humid chamber at room temperature for at least 30 min. *Camellia* pollen growth medium contains 2.54 mM $Ca(NO_3)_2 \cdot 4H_2O$, 1.62 mM H_3BO_3, 1 mM KNO_3, 0.8 mM $MgSO_4 \cdot 7H_2O$ and 8% sucrose (w/v) (Bou Daher and Geitmann, 2011d). After hydration, the pollen grains were suspended in the growth medium and upon beginning of germination the suspension was inserted into the microdevice.

4.6.3 Imaging

Brightfield imaging was done on an Olympus BX60M Brightfield microscope equipped with a Nikon Coolpix 357 4500 camera and with a Nikon Eclipse 80i digital imaging microscope system. Scanning electron microscopy 358 was done on gold-palladium coated samples with a FEI Quanta 200 3D operated at 15 kV.

4.7 Summary and conclusions

Administration of drugs or other agents influencing cellular behavior at subcellular level is an important tool for cell biological strategies. To enable the use of this local drug administration for moving targets, a dynamically adjustable application system was developed based on LOC technology. The device was tested using the rapidly growing pollen tube. The position of the target region of this cell moves constantly as the tube grows, and a localized administration of a growth influencing agent requires a steep concentration gradient over few micrometers. The present device was able to generate such a gradient that remained stable in the general growth direction of the tube and that could be repositioned to follow the position changes of the target region, the growing tip, on the perpendicular axis. The present version of the proposed LOC is suitable and will be extremely useful for testing attractants for pollen tube growth or agents causing repulsion (Geitmann and Palanivelu, 2007a; Takeuchi and Higashiyama, 2011) (Palanivelu *et al.*, 2011a). Moreover, it can be used to apply specific agents interfering with cellular functioning such as ion channel blockers, inhibitors of cytoskeletal polymerization or enzymes modulating the mechanical properties of the cell wall (Holdaway-Clarke and

Hepler, 2003). It can easily be adapted to be used for other cell types displaying target regions that move due to growth or crawling.

Chapter 5

Lab-On-Chip for Local Treatment of Pollen Tube in Distal Region

5.1 LOC for local treatment at distal region of pollen tube

In this chapter, the enhanced design presented in Chapter 3 is employed to manipulate a series of pollen grains at the entrance of growth microchannels and to force the pollen tube grow into the air trap. Once the tip is growing within the air without any contact with the medium, the distal region of pollen tube is treated with different growth regulators. The results will benefit in understanding some cues on pollen tube biology. The content of this work is about to be submitted to the *Nature Communication* with my contribution as the first author.

Abstract

The effect of tip-based water and ion fluxes on regulating the tip growing cells has been widely studied through introducing growth inhibitors or change of biological reagents in the growth medium. Due to the lack of local control of the medium change at either the distal or the apex, any change on the medium influences on both the tip and the distal region and makes it complex to distinguish the contribution of the tip or distal region on the growth. To distinguish the role of nutrient uptake through the distal region, a novel method of local treatment setup is presented in such a way that liquid medium is only surrounds the distal region of pollen tube without any effect on the tip. The effect of different calcium and sucrose concentrations on the growth behavior of *Camellia* pollen tube were studied once the tip was growing in the air. The results proved that the water and

nutrient uptake through the grain or distal region of the tube was sufficient to sustain pollen tube growth. It also presented new clues on the existence of internal ca^{+2} ion stores within the tube and also about the hypothesis of the whole-cell pressure increase inside the tube. The proposed design can be used to study the effect of other inhibitors of the growth, affecting on the ion influxes at the tip and has applications on drug discovery and pharmacology.

5.2 Introduction

For a few decades of studying tip growing cells such as pollen tube and hyphae, the question has been always to know to what extent the water influx-based turgor pressure and the ion fluxes at the tip are important for regulating the polar growth. Two different arguments have been reported in the literature about the role of turgor pressure on regulating the pollen tube growth. A number of researchers (Messerli *et al.*, 2000a; Pierson *et al.*, 1996) believe that the localized change of turgor pressure at the tip is the cause of growth. They presented the evidences on the dependence of the growth rate to the osmolarity of the medium. Benkert et al. (Benkert *et al.*, 1997) detected the change on turgor pressure of lilium pollen tube, though they could not find an obvious relation between turgor pressure and the growth rate oscillation. Recently Zonia et al. (Zonia, 2010; Zonia *et al.*, 2011) proposed hydrodynamic model confirming that the hydrodynamic fluxes regulate the growth rate and the oscillation frequencies. They punctuated on the prediction of localized pressure gradients by presenting the cues on localized electro-osmotic water flux at the tip and argued that the rapid and localized water influx is the cause of localized pressure change at the tip reasoning tube bursting within seconds.

Meanwhile, another group of researchers denied not only the prediction of localized turgor pressure gradients at the tip (Winship *et al.*, 2010), but also the effect of turgor pressure on regulating the tube growth (Harold *et al.*, 1995). In support of their claim, they observed that some species of hyphae grow faster with zero or at least very low value of turgor pressure (Davis *et al.*, 2000). In addition, the growth rate of pollen tube growing in a gel type medium is comparable with the rate of growth in liquid medium (Tomos, 1988). This group of researchers argued that the growth is not because of increase in turgor pressure, but it is due to cell wall relaxation. It is a phenomenon in which the material strength of the cell wall reduces due to enzymatic reaction at the apex leading to cell growth (Parre and Geitmann, 2005c). Winship et al. (Winship *et al.*, 2010) recently focused on cell wall model based on the experiment measuring turgor pressure at different distances from the apex grown in different osmotic conditions and interpreted the results as the evidence against the prediction of localized turgor pressure gradients at the tip. They proposed that any likely changes in turgor pressure would be in fact the effect of whole-cell pressure changes. Therefore, the regulatory effect of turgor pressure will remain a challenge until developing new techniques and presenting new experimental data assisting to prove one hypothesis.

The challenge also exists for ion fluxes at the tip especially in the case of calcium ion (Ca^{2+}) as the main ion for cell wall generation. It is clear that Ca^{2+} ion gradient at the tip is required to cross-link the pectin chains resulting in the raise of the cell wall rigidity. Both intracellular Ca^{2+} gradient (Pierson *et al.*, 1996) and extracellular tip-based Ca^{2+} influx

(Messerli *et al.*, 1999) were detected in growing pollen tubes (Holdaway-Clarke and Hepler, 2003). The effect of inhibitors such as lanthanides, La^{3+} and Gd^{3+} on blocking Ca^{2+} channels and attesting the tube growth verifies the effect of Ca^{2+} ion influx on regulating the growth (Malho *et al.*, 1994). Although the intracellular ion gradient appears to be resulting from the extracellular tip-based ion influx, the role of plausible internal Ca^{2+} sources cannot be easily excluded. Simple calculations on the amount of Ca^{2+} ion influx and the observed intracellular gradient displays that the magnitude of the tip-based Ca^{2+} influx is not sufficient to produce the observed Ca^{2+} ion gradient at the tip (Holdaway-Clarke and Hepler, 2003). In addition, the observation of Ca^{2+} ion at the tip in absence of tube growth (Messerli *et al.*, 2003b) and the delay of maximum extracellular Ca^{2+} influx respect to Ca^{2+} ion peak at the tip intensify the hypothesis of existence of an internal Ca^{2+} store as one source of tip-focused calcium ion gradient. A few potential candidates such as elements of the ER in the apical domain (Malhó, 1998), the secretory vesicles and the cell wall itself (Holdaway-Clarke and Hepler, 2003) have been proposed as the internal Ca^{2+} stores. However, new experimental methods are deserved to be employed to identify the role of these Ca^{2+} stored on generating Ca^{2+} tip gradient even in the lack of Ca^{2+} tip influx.

Local treatment of either the distal or the tip region of pollen tube is believed to be a new detection method to answer some of the unknown questions about tip growing cells. The local treatment of living cells within microfluidic environment has been reported for different mammalian cells to change a portion of the cell and to characterize the cell response to local change of medium (Lin *et al.*, 2001; Lucchetta *et al.*, 2005; Sawano *et al.*,

2002; Takayama *et al.*, 2001, 2003; Thiébaud *et al.*, 2002). However, the difficulty of performing local treatment on the cells clarifies the importance of developing new techniques such as micro-electromechanical system (MEMS) enabling to perturb local domains of single cell by applying different solutions to specific regions of cell. In the case of tip growing cells, it should assist to identify the role of water or ion fluxes at the tip as the main proposed regulators of the tube growth. The MEMS technology was formerly used for characterizing the pollen tube behavior such as studying the tube attraction to the in-chip positioned ovule by Yetisen et al (Yetisen *et al.*, 2011b), individual pollen tube growth characterization by Carlos et al (Agudelo, 2012) and growth force measurement by Sanati et al (Agudelo *et al.*, 2012d). The capability of microfluidic device was also employed to carry out local treatment on growing pollen tube by applying parallel laminar flows along either the sides of growing pollen tube to characterize the effect of calcium ion on tube reorientation (Sanati Nezhad A, 2012). Two different mediums with different calcium ion concentration were introduced into the either sides of pollen tube tip. However, in that design, the mediums surround a whole the pollen tube body.

In this chapter, to distinguish the role of nutrient uptake through either tip or the distal region, a new type of local treatment setup is presented in such a way that liquid medium is only changed around the distal region of pollen tube without any effect on the medium around the tip as the tip is growing along the air trap without any contact with the growth medium. This behavior of pollen tube has been observed in *in-vivo* growth of pollen tube in a part of journey toward the ovule. As it is shown in Fig 5.1, the pollen tube can leave

the funiculus and grows a portion of journey in the air and then enters the micropyles (Johnson *et al.*, 2002).

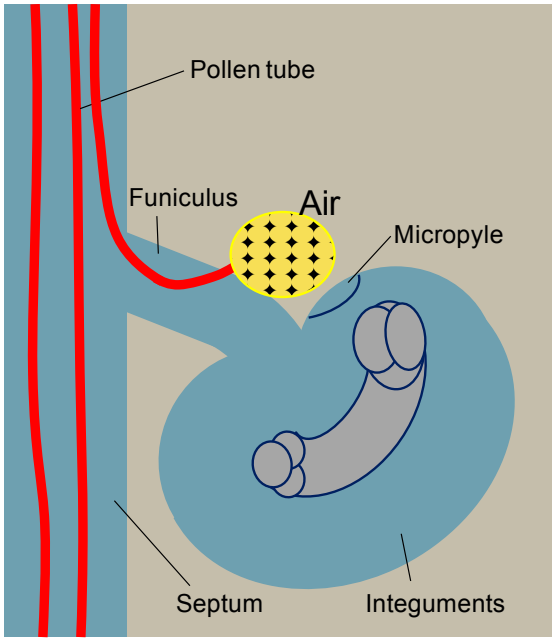

Figure 5.1: The growth of pollen tube in the air in a portion of its journey toward the ovule. The pollen tube leave the funiculus, enters the air and growth toward the micrpyle .

To more systematically assess the ability of pollen tubes to elongate in air, a high aspect ratio air trap consists of two horizontal PDMS posts/rods with the extremely narrow entrance is devised so as to allow the pollen tube to penetrate into the trap, but prevent liquid to enter or gas to exit. *Camellia* pollen tubes were found to be able to enter the air trap and to grow for up to 1 mm, thus proving that water and nutrient uptake through the grain or distal region of the tube was sufficient to sustain pollen tube growth. It is identical to the initial phase of pollen germination on the stigma surface where pollen tubes are able to grow distances surrounded mostly by air. This length of growth within air trap intensify the hypothesis of presence of internal Ca^{2+} ion store within the pollen tube generating the

ca^{+2} tip gradient required for cell wall generation. The effect of change of calcium concentration around the distal region even in zero calcium concentration showed no considerable effect of the growth rate. The setup also was used to test the effect of changing osmotic pressure on the tip growth behaviour. The results demonstrated that the fast rise of turgor pressure due to water uptake through the distal region causing cell bursting within a minute without any change on properties of cell wall at the apex. It verifies the hypothesis of the whole-cell pressure increase inside the tube with respect to the localized pressure gradient hypothesis at the tip. The proposed design can present experimental data to answer some unknown questions about the growth regulation, to study the effect of other inhibitors of the growth affecting the ion influxes at the tip. It also has applications on drug discovery and pharmacology.

5.3 Microfluidic device operation

The schematic of the air-trap design proposed to locally change the medium around the distal region of pollen tube is shown in Fig 5.2a. The design consists of 1) fluidic network to trap the pollen grain at the entrance of growth microchannel, 2) the PDMS rods/post to provide an enclosed air trap that allow the pollen tube penetrating into the trap, 3) the air trap enabling the growth of pollen tube tip within the air and applying local treatment exclusive on the distal region. The air trap has the length of 1 mm and the width of 50 μm about twice the diameter of pollen tube. The extremely narrow entrance is devised so as to allow the pollen tube to penetrate into the trap, but prevent liquid to enter or gas to exit. The air trap is located at the end of growth microchannel about 100-200 μm away from the trapping point of pollen grain. It is considered as the primary length required to ensure

stabilized growth before entering the tube into the air trap and to provide enough length of distal region for local treatment of pollen tube. The SEM image of the design is shown in Fig 5.2b. To increase the chance to grow pollen tube along the growth microchannel, the enhanced design presented in chapter 3 is exploited to provide a few air-trap designs within the microfluidic device. The architecture of microfluidic network and the geometrical constraints have been chosen similar to that of the enhanced design proposed by Sanati et al (Sanati Nezhad *et al.*, 2012a). It consists of 1) medium-pollen inlet for introducing pollen suspension into the device, 2) Outlets to conduct the extra pollen grains to the exit or help to guide the pollens to the entrances of microchannels, 3) main distribution trap to transfer to and trap the pollen grains at the entrance of growth microchannels, 4) growth microchannels and extremely narrow entranced-air traps. The microfluidic device was fabricated using conventional soft lithography technique detailed in Agudelo et al. (Agudelo *et al.*, 2012a).

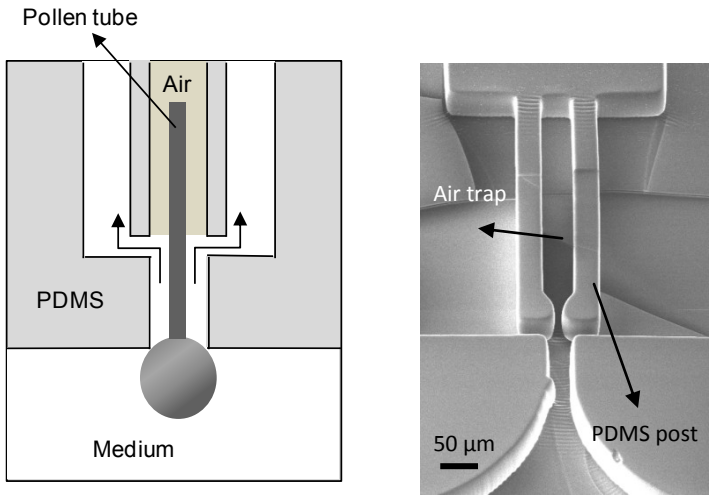

a) b)

Figure 5.2: a) Schematic view of the design for local treatment of the distal region of pollen tube. The pollen tube germinates from the trapping point, grows along the fluidic microchannel and enters the air trap, b) The SEM image of the air trap design,

The pollens suspension is introduced into the distribution chamber and the pollen grains are trapped at the entrances of the growth microchannels. The proper flow rates are chosen according to the practical range of flow rates required to prevent tube bursting (Agudelo *et al.*, 2012b). The extra pollens are transferred out to the outlet drain. The pollen tube starts growing from pollen grain, grows along the growth microchannel towards the air trap, enters the air environment and continues the growth until hitting the end wall of the air trap. The air trap testing provides a suitable microstructure to enable the growth of pollen tube tip into the air environment and to apply local treatment to the distal region of pollen tube.

5.4 Air trap performance

The air cavities and air pockets embedded perpendicular or angled to a fluidic microchannel have formerly been reported for acoustic micro-mixing and micro-pumping applications (Ahmed *et al.*, 2009; Tovar *et al.*, 2011). The injection of fluid into the microchannel resulted in trapped air bubbles in the sidewall cavities and the potential of air cavity as the energy absorbance is activated by acoustic excitation generating acoustic streaming for fluid pumping (Ahmed *et al.*, 2009). In previous air cavity designs (Ahmed *et al.*, 2009; Tovar *et al.*, 2011), a fully formed air bubble have been assumed inside the air trap, though the interface of bubble-liquid depends on the surface tension and viscosity of the liquid and determines the surface angle (Tovar *et al.*, 2011). However, the experiments on air bubble showed if the medium flow exists beneath or top surface of the air bubble, the colored ink or colored dye, is clearly observed under the bubble (Sung *et al.*, 2009).

Once the fluidic network is filled with the growth medium, the medium passes around the air trap structure toward two exit channels and induces a bubble in the air trap due to the surface tension (Ahmed *et al.*, 2009). In order to characterize the air blocked in the air trap, the colored liquid is introduced into the chip to ensure that the trap is only filled with the air without any liquid underneath the trapped air bubble. The experiment proves that no medium entering the air trap as no medium is observed underneath of air bubble (Fig 5.3a). One of the exit channels is also blocked to compare the region A in which the air is trapped within the exit chamber and region B with the air blocked in the air trap. Fig 5.3a clearly shows the feasibility of local treatment on distal region of pollen tube.

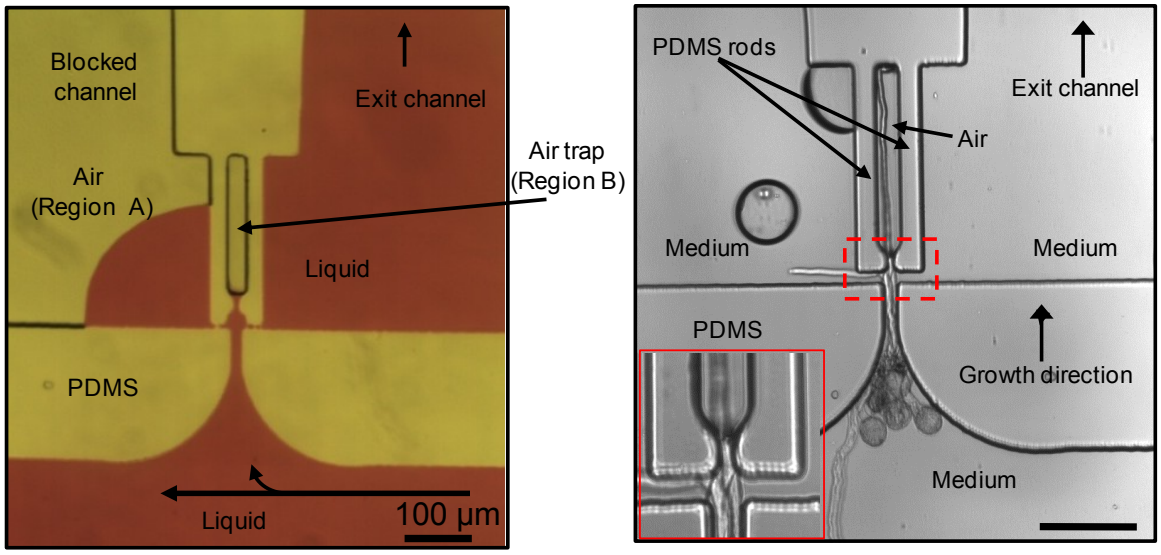

a) b)

Figure 5.3: a) Testing the air trap performance under colored fluid flow. The trap is filled only with the air without any liquid underneath the trapped air bubble. One of exit channels is blocked to compare the region of the picture in which the air is trapped in the exit channel (region A) and the region of the air blocked in the air trap (region B), b) The successful growth of pollen tube along the growth microchannel and within the air trap. The air-medium interface is clearly seen at the narrow entrance of the air trap. Bar, 100 µm

Once ensuring successful air blockage within the air trap, the growth of the pollen tube within the air trap is studied. The experimental testing consist of 1) characterizing the growth rate of pollen tube within air trap, 2) monitoring the pollen tube response to the local change of sucrose at the medium around the distal region and 3) assessing the pollen tube response exposed to the local calcium treatment at the distal region of tube.

The devised microfluidic device was tested in the presence of pollen grains. The pollen tube germinates from the trapped pollen grain, grows along the growth microchannel, passes the air-medium interface and continues the growth along the air trap to reach the end wall. Once the pollen tube tip enters the air chamber, only the portion of the pollen tube from the germinated point at the trapped pollen grain to the air-liquid interface is surrounded by the medium. The part of tube from the interface point to the tip is only in contact with the air (Fig 5.3b). The stable location of the air-liquid interface depends on the strength of layer bonding and the pressure within the device. As the PDMS is permeable to the air, under high pressure resulted from high inlet velocity, the blocked air gradually vanishes through either the PDMS or the leakage at the bonding boundaries. The experiments verify that under inlet velocity of 10 mm/s, the air-liquid interface remains stable.

5.4 The growth behavior of pollen tube within air trap

The optical microscopy (Nikon 80i, 60X objective) was used to capture the pollen tube growth with time intervals of 5s before and after entering the air trap. The sample

measured growth rate at the vicinity of air-medium interface starting from point S at few microns before interface to point E at a few microns after interface is shown in Fig 5.4. Once pollen tube passes the air-liquid interface toward the air trap, the average growth rate clearly rises from the average of 7 µm/min to the average of 11.5 µm/min. The pollen tube keeps the oscillatory growth behavior within the air trap.

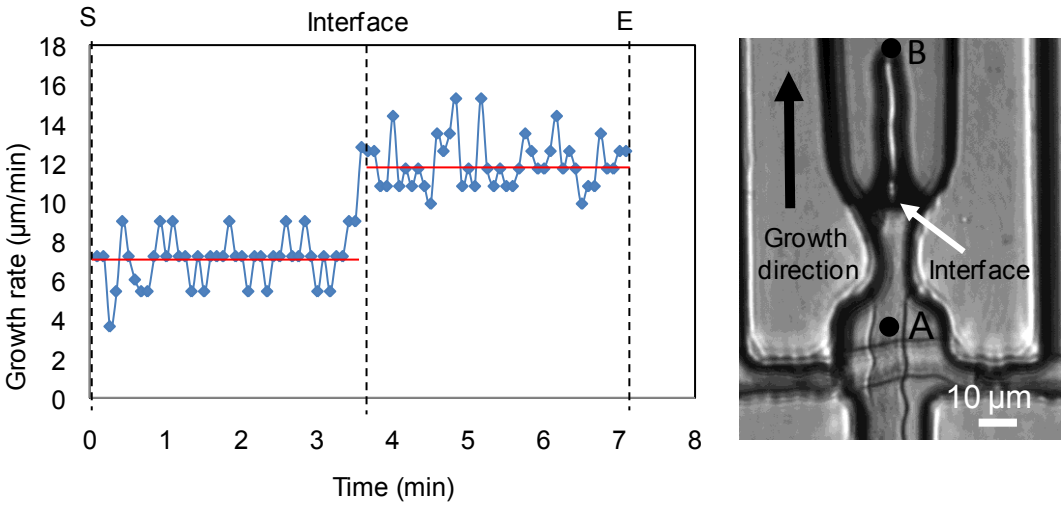

Figure 5.4. The growth rate of pollen tube before and after the air-liquid interface. The growth rate raises from an average of 7 µm/min to the average of 11.5 µm/min. The growth remain oscillatory. Bar, 10 µm

The results of the growth rate for few pollen tubes growing along the air trap are shown in Fig 5.5a. The dashed line starts from the measuring start point S and extends through the interface point (IP). The slope of the dashed line for each case shows the average growth rate before the pollen tube enters the air trap. The deviation of the growth rate from the dashed line after point IP shows the raise of growth rate of pollen tube when it grows along the air trap. It is concluded that in all cases, growth rate of the tip within the air is higher than that of the tube growing in the medium. In some cases, not only the growth rate increases, but the amplitude of oscillation increases inside the air trap (green line in Fig

5.5a). The results of average growth rate before and after the air-liquid interface is seen in Fig 5.5b for six different pollen tubes.

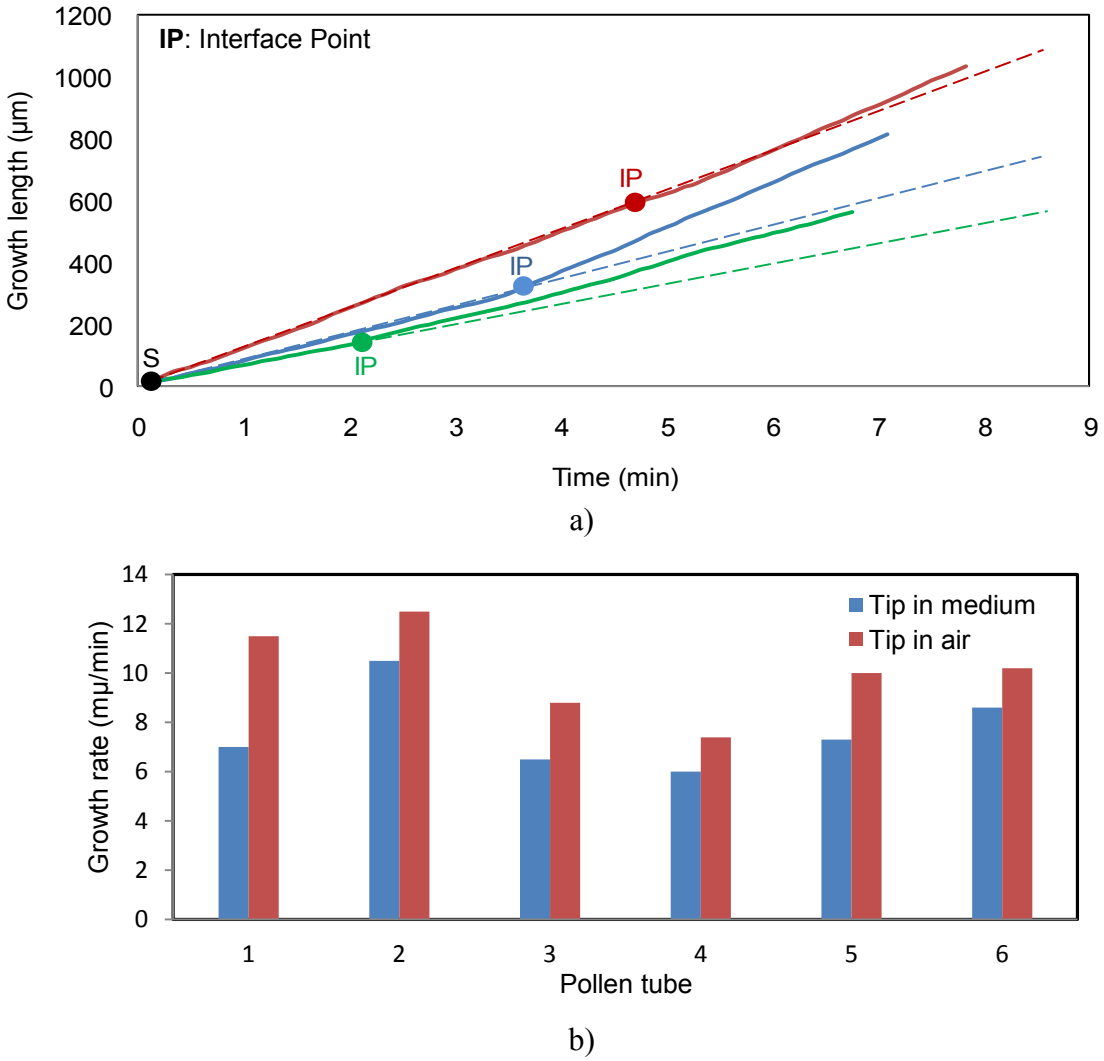

Figure 5.5: a) The experimental results of pollen tube growth length before and after the air-liquid interface for three different pollen tubes. The solid lines are the growth length of the pollen tube. The dashed line starts from the measuring start point S to the air-liquid interface point IP. The slope of the dashed line shows the average growth rate before the pollen tube enters the air trap. Point S is the measuring start point before the air-liquid interface. b) The average growth rate before (blue) and after (Red) the air-liquid interface for different pollen tubes

The results of Fig 5.5 show that in spite of reduction in the amount of nutrient around the tube especially at the tip, the escalation of the growth rate was observed once the pollen

tube passes the air-medium interface and enters the air trap. The plausible reason for the raise of growth rate is the removal of the fluid resistance against the growth as the air resistance is much less than the liquid resistance due to lower viscosity. The results present some cues for biological principles governing the regulation of pollen tube by the ion or water fluxes. The growth rate does not lessen along the trap even after the tube reaches the far end wall of the air trap. It proves that the nutrients supplied by the medium around distal region are sufficient even for the growth up to 1 mm along the air environment which is identical to in-vivo growth of pollen tube in the air in a portion of tube journey toward the ovule (Fig 5.1). The independence of the growth to the nutrient and ion fluxes at the tip and sub-apical regions raises a big question about the contribution of the ion influxes at the tip on the growth regulation.

The lack of intracellular ion influxes especially Ca^{2+} ion influx at the tip proves the existence of internal Ca^{2+} ion stores either in the tube or the cell wall as the source of Ca^{2+} ion assumed essential for generating the Ca^{2+} ion gradient at the tip for producing new cell wall (Holdaway-Clarke and Hepler, 2003). The lack of water uptake through the tip region proves that cell wall at the distal region is permeable enough for water uptake and it is against the former hypothesis of exclusive tip-based water influx (Zonia and Munnik, 2011), though the current results is not against the presence of water uptake at the tip. Nevertheless, it seems the portion of the distal region surrounded by the medium also seems large enough (150 μm) to provide sufficient water uptake. In some cases, the pollen tube hit the far end wall of the air trap, turns back toward the entrance of air trap and passes the interface for the second time (Fig 5.6a). In this case, the measurement of growth

rate before and after the interface shows 25% drop on the growth rate when the pollen tube tip penetrates from the air the medium (Fig 5.6b).

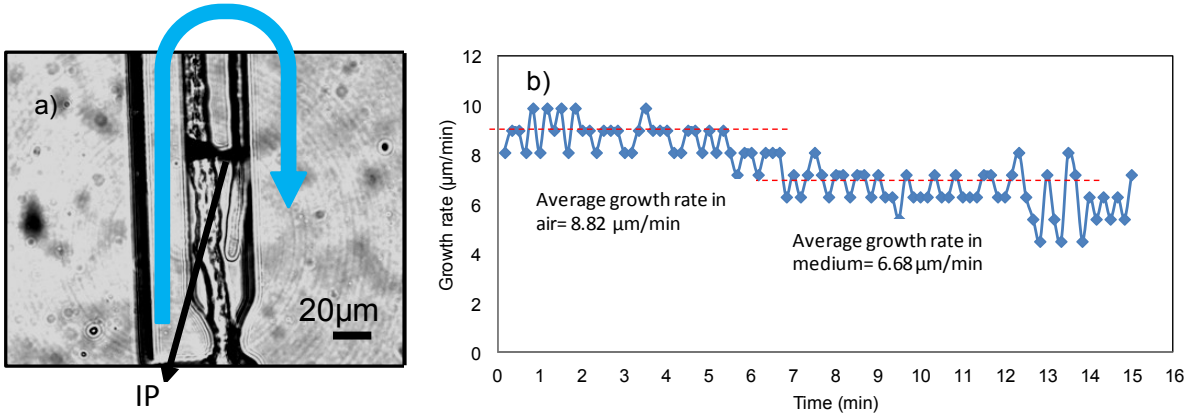

Figure 5.6: a) The pollen tube enters the medium from the air, b) the growth rate drops by 30% once enters air environment to the medium.

5.5 Local sucrose treatment on distal region of pollen tube

To investigate how the pollen tubes growing in the air trap respond to the change of sucrose concentration, the growth rate of each pollen tube in the air trap is measured before and after sucrose treatment and the change of growth rate is defined as the pollen tube response (Fig 5.7). The results show that for the sucrose concentrations more than the optimal value of 8% , the growth rate reduces. In this case, the osmotic pressure between the outside and inside of the cell reduces and in consequence, the water uptake drops, causes reduction in whole cell turgor pressure which lessens the growth rate. For the pollen tubes exposed to the sucrose concentrations less than the normal 8%, the growth rate slightly increases or under very low concentration, the pollen tube bursts. It seems the water uptake through distal region in this case increases, resulting the rise of turgor pressure and growth rate.

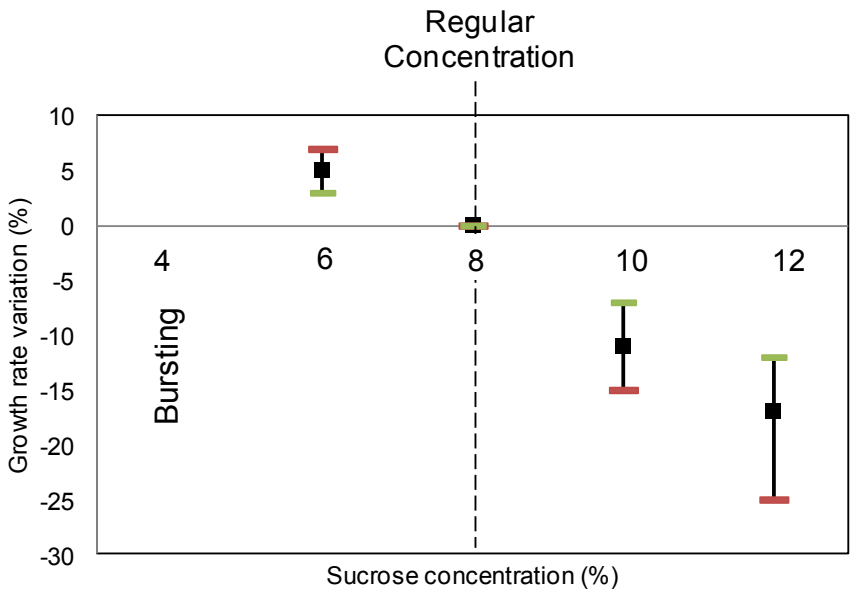

Figure 5.7: The change of growth rate (%) respect to the normal growth in 8% concentration in response to sucrose treatment though distal region.

The bursting under 4% sucrose concentration occurs seconds after the distal region is treated. It strengthens the hypothesis of whole cell turgor pressure increase. As there is no water uptake around the tip, the pressure should have been increased in whole the cell. This is against the hypothesis of local increase of turgor pressure at the tip as the cause of pollen tube bursting. We cannot simply expect the cell wall relaxation as the cause of bursting as the pollen tube tip is not surrounded by any medium. However, more effort is required to identify the ion concentration at the tip once the distal region is exposed to the medium change and the tip is growing within the air.

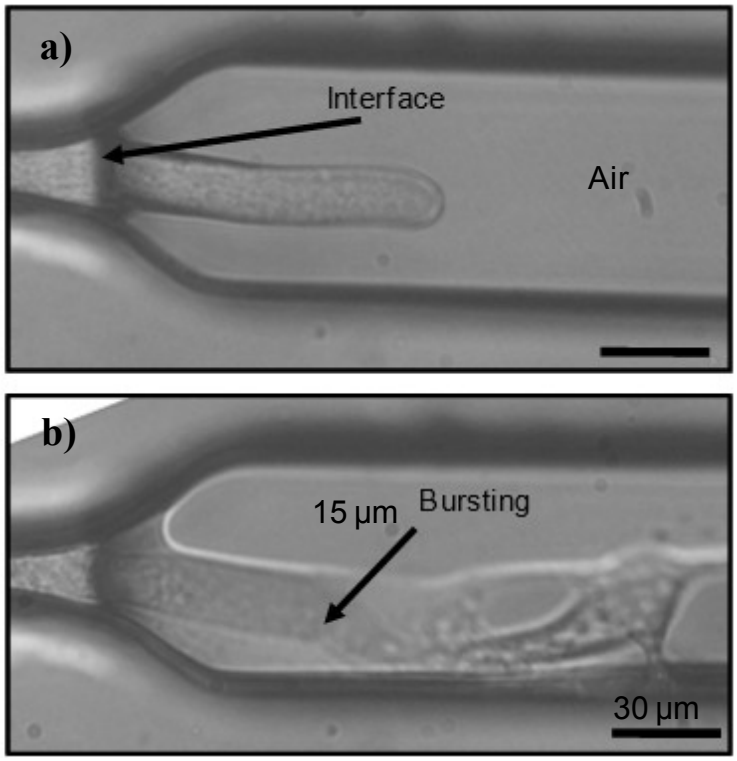

Figure 5.8: The pollen tube bursting in treatment of distal region to 4% sucrose concentration. The bursting occurs within a minute after treatment, Scale: 30 µm.

5.6 Calcium treatment on distal region of the pollen tube

Bou Daher and Geitmann (Bou Daher and Geitmann, 2011d) reported optimal calcium concentration of 2.54 mM for *Camellia* pollen tube growing in open assays. For the pollen tubes growing in the range of 1-5 mM calcium concentration, gentle reduction of 15% was observed for the growth rate of pollen tube. Out of this range, dramatic change of growth length was detected. The identical response was detected for the *Camellia* pollen tubes growing along microchannels (Sanati Nezhad *et al.*, 2012b). However, in these two kinds of experiments, the medium surrounds both the tip and distal region, and the change of growth rate is assumed due to the effect of the extracellular calcium ion at the tip. To explore the contribution of the tip-focused calcium influx on generating the calcium ion

gradient at the tip, the response of pollen tube to the calcium treatment around the distal region is studied. Once the tip enters the air trap the pollen tube is exposed to different calcium concentrations varied in sequence among 0 mM, 1.27mM, 2.54 mM, 5.08. The results show no significant change on growth rate even for zero calcium concentration of the medium. It intensifies the hypothesis of existing internal calcium store as the source of calcium ion gradient at the tip. It is also a clue for the hypothesis that the change of calcium influx at the tip disturbs the optimal tip-focused calcium gradient generated by the internal calcium stores and in consequence resulting the drop or arrest of the growth. As under treatment of distal region, no sudden disturbance at the calcium ion gradient at the tip and in consequence no change of cell wall mechanical properties is expected. This is what has been observed with air trap experiment for treatment of distal region of pollen tube to different calcium concentrations.

5.7 Summary and Conclusions

A lab-on-chip was designed, fabricated and successfully tested to study local treatment of pollen tube at the distal region. The growth rate of pollen tube increased once the tip entered the air trap and reduced once the tube penetrated from the air trap to the medium environment. The response of pollen tube to local sucrose change at the distal region showed that the whole-cell change of internal turgor pressure, in case of low sucrose concentration of 4%, led to tube bursting. No detectable change of growth rate was detected in response to the change of calcium concentration at the distal region even in case of zero calcium concentration of the medium. The proposed microfluidic device provided new clues to the influence of the whole cell turgor pressure with respect to the

localized tip-focused turgor pressure and to the role of internal calcium stores on generating tip-focused calcium gradient.

Chapter 6

In Vitro Characterization of Oscillatory Growth Dynamics of *Camellia* Pollen Tube Using a Microfluidic Platform

6.1 Microfludic platform to study oscillatory dynamic growth of pollen tube

In this chapter, the oscillatory dynamic growth of pollen tube is characterized by capturing the cell growth with high resolution image microscopy and waveform analysis. The change of oscillation frequencies in response to growth regulators is detected. The enhanced design presented in chapter 3 is exploited here to expose the pollen tube to different concentrations of sucrose as growth regulator. The content of this chapter is accepted for publication in the journal of *IEEE Ttransaction of Biomedical Engineering*.

Abstract

A hallmark of tip growing cells such as pollen tubes and fungal hyphae is their oscillatory growth dynamics. Multiple aspects of this behavior have been studied to identify the regulatory mechanisms driving growth in walled cells. However, the limited temporal and spatial resolution of data acquisition has hitherto prevented more detailed analysis of this growth behavior. To meet this challenge, we employed a microfluidic device that is able to trap pollen grains and to direct the growth of pollen tubes along microchannels filled with liquid growth medium. This enabled us to observe the growth behavior of *Camellia* pollen tubes without the use of the stabilizer agarose and without risking displacement of the cell during time lapse imaging. Using an acquisition interval of 0.5s we demonstrate the existence of primary and secondary peak frequencies in the growth dynamics. The effect of

sucrose concentration on the growth dynamics was studied through the shift in these peak frequencies indicating the pollen tube's ability to modulate its growth activity.

6.2 Introduction

The pollen tube is the carrier of sperm cells in the flowering plants. It is a cellular protuberance formed by the pollen grain and elongates through the pistil of the receptive flower to reach an ovule located deeply within the flower tissues (Krichevsky *et al.*, 2007). To reach the ovule the pollen tube elongates by expanding at its tip which is able to sense the guidance signals emitted from the female tissues and orient its growth direction accordingly.

Both growth velocity and growth direction in the pollen tube are tightly regulated by complex internal controlling mechanisms. The shape of the cell is cylindrical with a hemisphere shaped tip (Fig 6.1,a) and a typical diameter of 5 to 20 μm. The driving force for the cellular growth process is provided by the internal turgor pressure that results in cell wall stretching at the tip since the material properties of the wall in this region are much softer than in the cylindrical shank (Fayant *et al.*, 2010b) (Zerzour *et al.*, 2009a) (Fig 6.1,b). The growth process is sustained by a continuous supply of new cell wall and membrane material delivered to the apical cellular envelope through exocytosis (vesicle fusion to the apical plasma membrane).

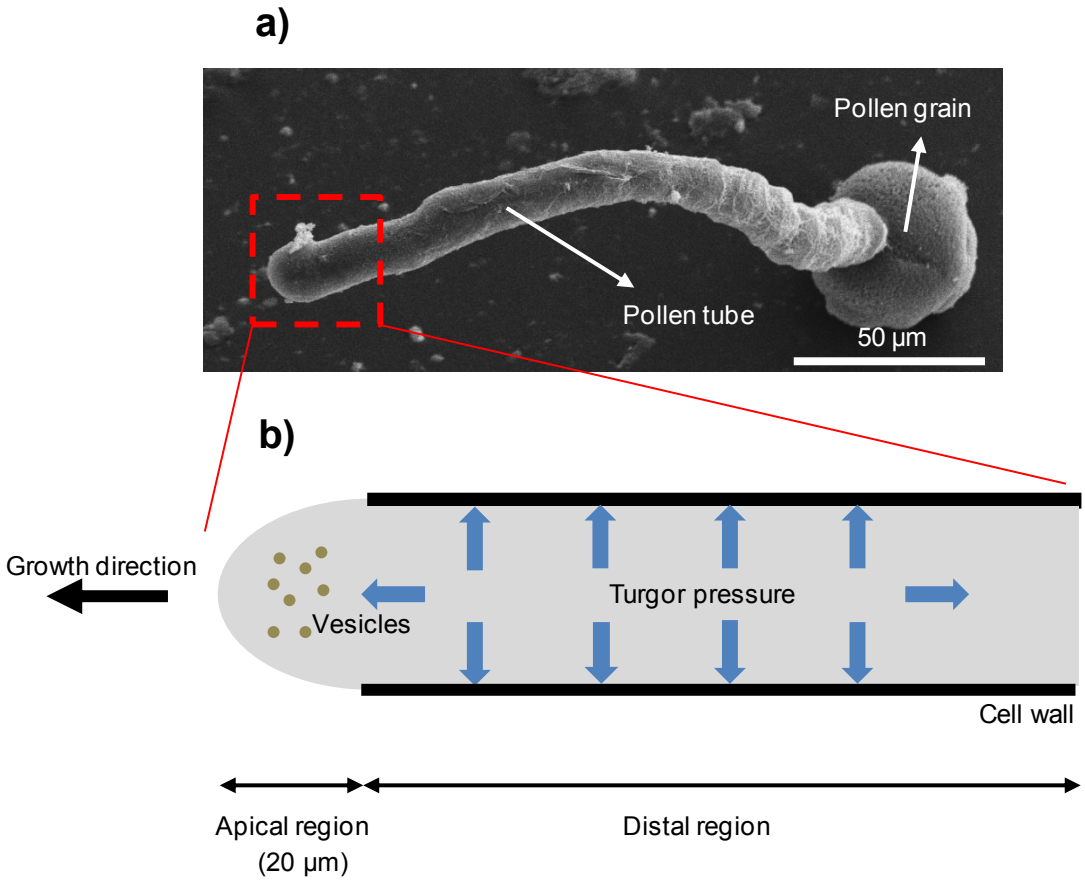

Figure 6.1: a) Scanning electron micrograph of pollen tube germinated from a pollen grain of *Camellia japonica*, b) Schematic representation of the tip growth process illustrating the gradient in material properties of the cell wall (soft at the apex) resulting in the formation of a cylinder under the effect of the internal turgor pressure.

Similar to other tip growing cells such as fungal hyphae (Lopez-Franco *et al.*, 1994) and neurons (Betz *et al.*, 2006), pollen tubes do not elongate in steady manner but display a complex growth dynamics that is subject to modulation in response to extracellular conditions. The dynamics varies between plant species and has been categorized as 1) sinusoidal oscillations in pollen tubes of *Lilium longiflorum* (Pierson *et al.*, 1996), 2) pulsatory oscillations in pollen tubes of *Petunia hybrida* and *Nicotiana tabacum* (Pierson *et al.*, 1995) (Geitmann and Cresti, 1998) (Geitmann *et al.*, 1996) or 3) steady growth with random small fluctuations around a trend line such as *Hemerocallis* (Feijo *et al.*, 2001).

The presence of some type of oscillatory change in the elongation rate is therefore considered as the common feature of the extension of the pollen tube (Messerli and Robinson, 2003b). The type of the growth dynamics is dependent on the plant species, but it also varies with the age of tubes and the growth environment (Zerzour *et al.*, 2009a). The effect of growth regulators on the growth mechanism of the pollen tube has been widely studied (Chebli *et al.*, 2007a; Messerli and Robinson, 2003b; Wilsen *et al.*, 2007). A change in the ion concentration of the extracellular growth medium affects the complex mechanism regulating the growth as evident from an altered pattern of the growth dynamics, typically in form of an altered amplitude and/or frequency (Kroeger and Geitmann, 2012b). Many physiological processes seem to be affected by or involved in regulating the velocity of pollen tube growth. Cellular parameters such as intracellular ion gradients, transmembrane ion fluxes, and the positioning of polarity markers display oscillatory patterns whose period is identical to that of the growth rate but whose phase is shifted relative to the maximum growth rate (Holdaway-Clarke and Hepler, 2003) (McKenna *et al.*, 2009).

To characterize the oscillatory behavior of pollen tubes, past studies have mostly focused on the following parameters: average growth rate, oscillation period and oscillation amplitude (Holdaway-Clarke and Hepler, 2003; McKenna *et al.*, 2009; Pierson *et al.*, 1996). The time domain data show that the period of growth rate oscillation varies between 15-50s for lily pollen tubes (Holdaway-Clarke and Hepler, 2003) (Holdaway-Clarke *et al.*, 1997), and several minutes for *Nicotiana tabacum* and *Petunia hybrida* (Geitmann *et al.*, 1996) (Geitmann and Cresti, 1998) (McKenna *et al.*, 2009; Pierson *et al.*, 1996). The frame

rate at which time lapse imaging was carried out in these studied depended on the species used, on the spatial resolution of the microscope, and on the temporal resolution of the camera, with typical rates being between one image per 1 sec (McKenna *et al.*, 2009) and one image per 5 sec (Michard *et al.*, 2008). Oscillation periods in the tens of seconds are easily detected in this manner, but the direct measurement of the time response may not reveal all the details of the oscillatory behavior. Especially in pollen tube species that change their behavior with the age of the cell (e.g. *Lilium* (Feijo *et al.*, 2001)), important characteristics of the different growth stages might be missed. Furthermore, while dramatic changes in the growth conditions induce visible changes in oscillation frequency, more subtle changes might be overlooked when using simple quantification of the time response. One of the best investigated pollen tube systems is that of *Lilium longiflorum*, which has tubes of a width of approximately 17 μm. In the majority of studies on this species, a relatively long oscillation period with the time period of 30-50s *(primary oscillation)* has been detected (Holdaway-Clarke and Hepler, 2003). However, no shorter periods were reported for the growth rate lily pollen tubes even when image acquisition was carried out at frame rates of 1/sec (McKenna *et al.*, 2009). These examples show that time domain analysis is not sufficient to comprehensively analyse the dynamic pattern of pollen tube growth.

To provide a more detailed characterization of the oscillatory behavior of pollen tubes, advanced wave function analysis including Fourier transforms, power spectra, wavelet analysis and correlation analysis have been employed (Holdaway-Clarke *et al.*, 1997; Messerli *et al.*, 1999; Michard *et al.*, 2008). These methods were not only used to detect

the variation in oscillatory frequency due to a change in growth environment (Crutchfield *et al.*, 1980; Feijo *et al.*, 2001), but also to establish the phase shift between cellular events and the growth rate (Pierson *et al.*, 1996). Any kind of medium change has the potential to influence the spectral profile by inducing a shift in oscillation frequency. Minor changes in the environmental conditions are likely to cause small frequency shifts, while major changes cause the emergence of new peak frequencies. Reducing the sucrose concentration of the medium was found to decrease the primary peak frequency and average growth rate (Messerli and Robinson, 2003b). Reductions in frequency were also noticed as a consequence of a change in medium pH (Messerli and Robinson, 2003b), increased concentrations of boric acid (Holdaway-Clarke and Hepler, 2003) and inhibition of calcium channels (Geitmann and Cresti, 1998). How these extracellular changes translate into a biological response has been modeled theoretically (Kroeger *et al.*, 2008). A secondary oscillation frequency has been detected for transmembrane H^+ fluxes using wavelet time-frequency spectrum, but only for few pollen tubes within the sample set based on the tobacco species (Michard *et al.*, 2008). Importantly, for the growth rate no secondary peak frequency has been detected due to lack of sufficient resolution imaging. Higher resolution images and the higher effective sample rates are essential to achieve this. Therefore, developing the techniques for capturing spatial imaging with high resolution and employing software with the capability of tracking the pollen tube tip will be necessary to assess putative secondary peak frequencies in the growth rate and hence characterize the dynamics of pollen tube growth.

In this study, the dynamic growth behavior of the *Camellia japonica* pollen tube is characterized using an enhanced microfluidic device (Sanati Nezhad *et al.*, 2013b). Pollen grains are trapped at the entrances of microchannels and the pollen tube growth direction is guided along the microchannel in a controlled micro-environment to capture high resolution images. A frame rate of 2/sec was used to detect both primary and secondary frequencies in the growth rate using FFT and PSD analysis. In order to assess the significance of these peaks, the influence of a change of growth conditions was tested and the frequency shift analyzed.

6.3 Materials and methods

6.3.1 Design and fabrication of microfluidic device

In order to capture images of the growing apex of the pollen tube in focus over extended periods of time, the pollen grain should be fixed such that pollen tube elongates in a controlled direction with minimum change in z-position during the growth. The enhanced microfluidic platform previously developed for pollen tube studies satisfies the above requirements (Sanati Nezhad *et al.*, 2012a). The pollen grains are independently trapped at the entrances of a series of microchannels and the design geometry was optimized to provide 1) trapping of only a few pollen grains at each microchannel entrance to prevent accumulation of pollen grains and 2) identical growth condition for all the growth microchannels. The dimensions of microfluidic network were chosen similar to the enhanced platform (Sanati Nezhad *et al.*, 2012a). Conventional photolithography and standard PDMS microfluidic techniques were used to fabricate the SU8 mold and the microfluidic device (Sanati Nezhad *et al.*, 2013b). Since the pollen grain is physically trapped, applying medium flow or exchanging one medium for another does not displace

the pollen grain or relocate the pollen tube. The PDMS layer forming the microfluidic network is sealed with a glass cover slip with a thickness of 100 µm, thus enabling us to capture the growth using an 80X objective lens. Fig 6.2 shows the schematic design of the enhanced design and the fabricated microfluidic device.

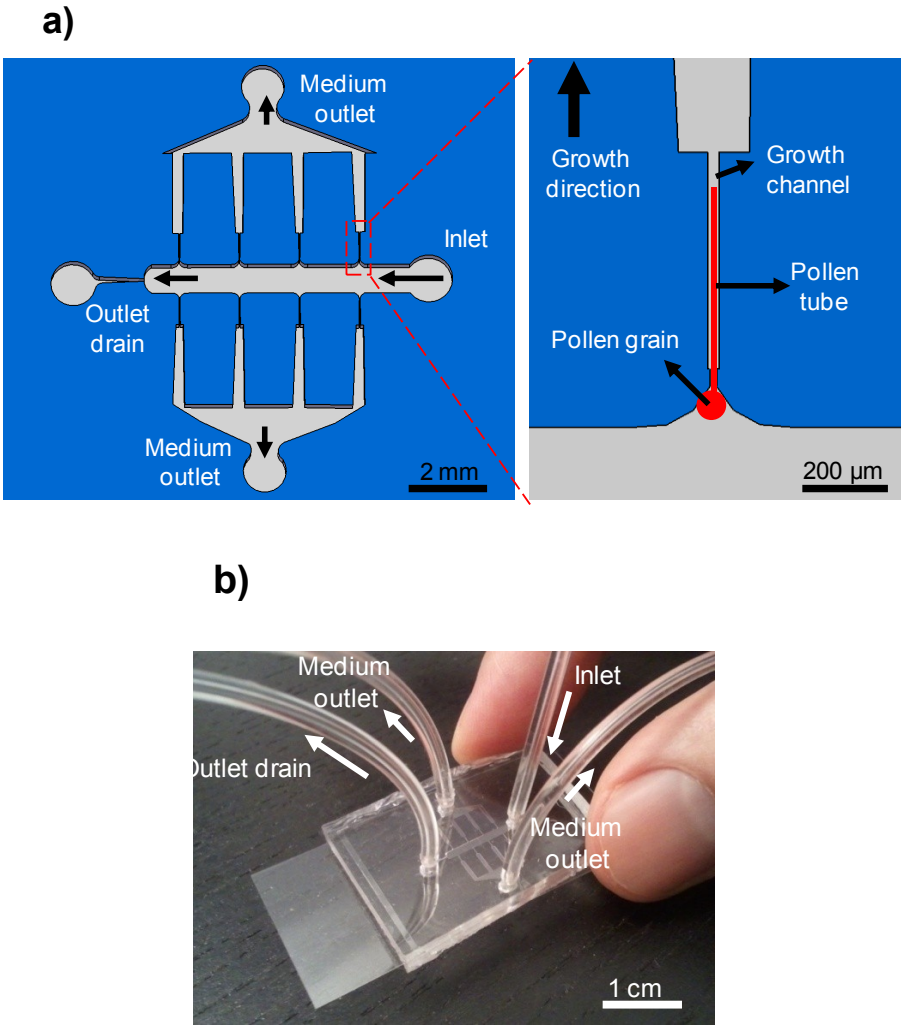

Figure 6.2: a) The fabricated microfluidic design optimized for pollen tube growth, b) The fabricated microdevice

6.3.2 Pollen collection and germination

Pollen grains of *Camellia japonica* were collected from a plant in the Montreal Botanical Garden. Pollen grains were dehydrated and stored in gelatin capsules at -20°C. Prior to use, the pollen was rehydrated in a humid chamber for at least 30 min at room temperature. A few milligrams of pollen were suspended in growth medium containing 2.54 mM $Ca(NO_3)_2 \cdot 4H_2O$, 1.62 mM H_3BO_3, 1 mM KNO_3, 0.8 mM $MgSO_4 \cdot 7H_2O$ and 8% sucrose (w/v). When the grains started germinating, the pollen suspension was introduced into the microdevice.

6.3.3 Microscopy

Brightfield imaging of microfluidic chip and pollen tube was done on Nikon Eclipse 80i digital imaging microscope system equipped with Infinity 1 digital CCD Camera and Capture Analyze software. The pollen tubes growth was observed with 80X objective (0.65 NA). The time- intervals between successive images were 0.5s to 1s. The growth of pollen tube at the tip is traced by MTrack2 tracking programs in NIH ImageJ software which sequentially tracks the pollen tube tip among captured images sequence.

6.4 Results

6.4.1 Measurement of the growth rate

In order to study the dynamics of pollen tube growth, images were captured with a bright field microscope using a 80X objective and incorporating Capture Analyze software. The growing apex of the pollen tube was tracked at intervals of 1s or 0.5s using Automatic

Tracking in NIH ImageJ software. Refocusing was rarely necessary since the pollen tube usually stayed at the bottom of the channel.

In order to confirm whether the chosen frame rate was sufficient for monitoring the primary and putative secondary peak frequencies, movies taken from several normally growing pollen tubes were analyzed in detail and it was found that *Camellia* pollen tubes typically display a primary oscillation frequency with a long time period in the range of 20-40s as well as secondary oscillation frequency with shorter time period in the range of 3-5s, corresponding to frequencies of 0.01-0.05 Hz and 0.2-0.3 Hz, respectively. Following the Nyquist–Shannon sampling theorem for choosing proper sample rate, for the maximum real oscillation frequency of pollen tube of about 0.4 Hz, the sampling rate must be set to be higher than 0.8 Hz. Hence, the primary sample rates of 1 Hz corresponding to the sampling intervals of 1s would be sufficient for capturing the secondary frequency. However, due to the limitations of the tracking software in tracing the tip and the resulting noise on the time-series of growth rate, the maximum possible peak frequency obtained from the time-series of growth rate signal can be higher than maximum expected secondary frequency. In this case, by increasing the sample rate to 2 Hz and employing filtering techniques, the effect of unwanted higher frequencies and the forced noise is eliminated. It must be noted that there is a limit on selecting higher sample rate due to the spatial resolution of the micrographs. Due to this limitation, the results of measuring the time-series growth rate with a sample rate of 4 Hz deteriorate the detection of secondary frequency due to emerging new peak frequencies beside the secondary peak frequency. The time variation in the growth rate of a *Camellia* pollen tube growing along

microchannel captured with 80X objective with sampling frequency of 2 Hz is shown in Fig 6.3,c. The oscillations with both primary and secondary frequencies are clearly observed.

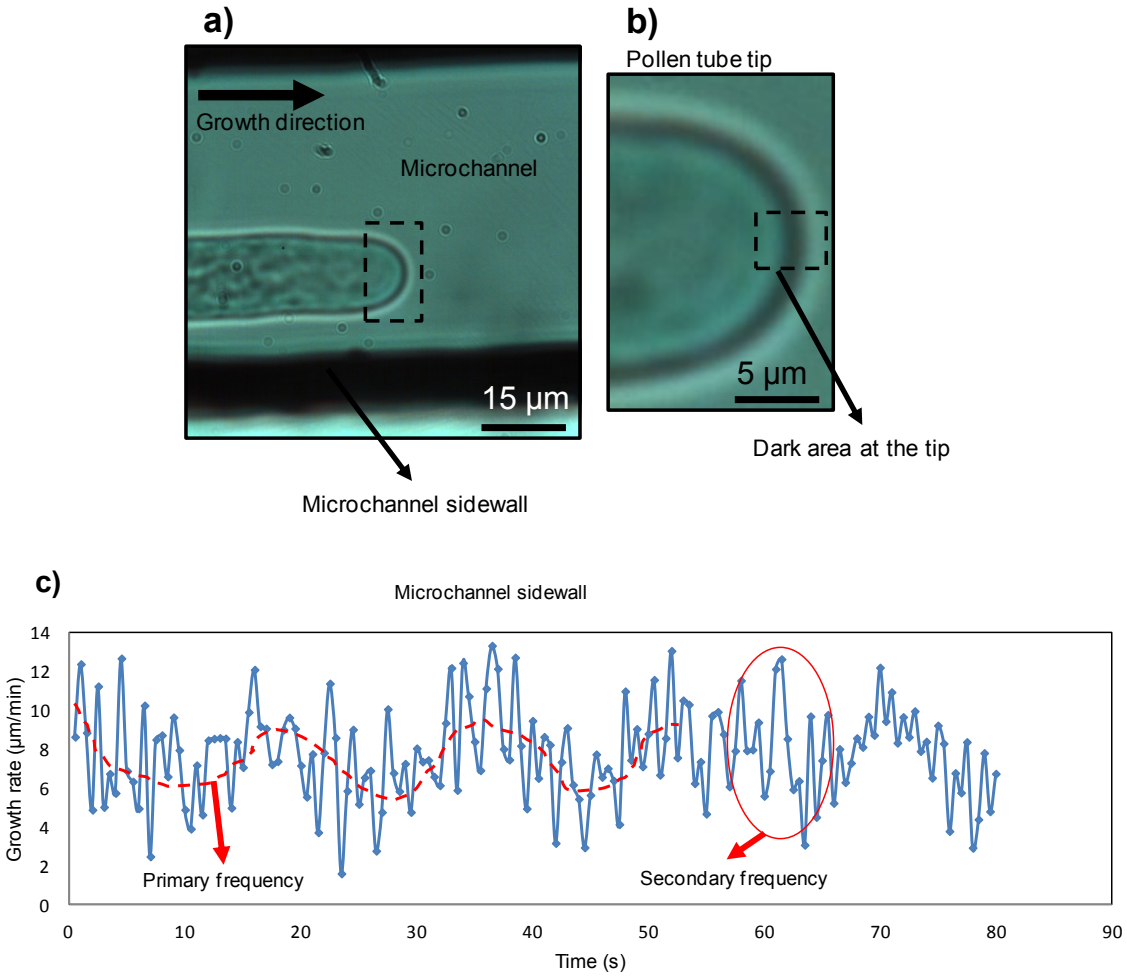

Figure 6.3: a) Brightfield micrograph of *Camellia* pollen tube growing along microchannel captured with 80X objective, b) The dark area representing the apical cell wall is the moving region of interest, c) Time-series of growth rate for a *Camellia* pollen tube captured with acquisition interval of 0.5s. Marked regions shows that a sampling frequency of 2 Hz is able to detect both primary and secondary peak frequencies

6.4.2 Measurement of peak oscillation frequencies

Initially, the stationary nature of oscillatory growth rate signal was verified. A stationary process is one in which statistical properties including the mean value and standard deviations of the signal's amplitude do not change over time. In order to assess these variations for each pollen tube, the statistical properties of several samples of identical duration were calculated. The results of mean and standard deviations for different samples of 60s duration are shown in Fig 6.4 for several pollen tubes captured with a sampling rate of 2 Hz and with a total sampling length of 240s. For each pollen tube, the variation of statistical properties between different windows was small indicating the stationary pattern of pollen tube growth growing under microfluidic conditions.

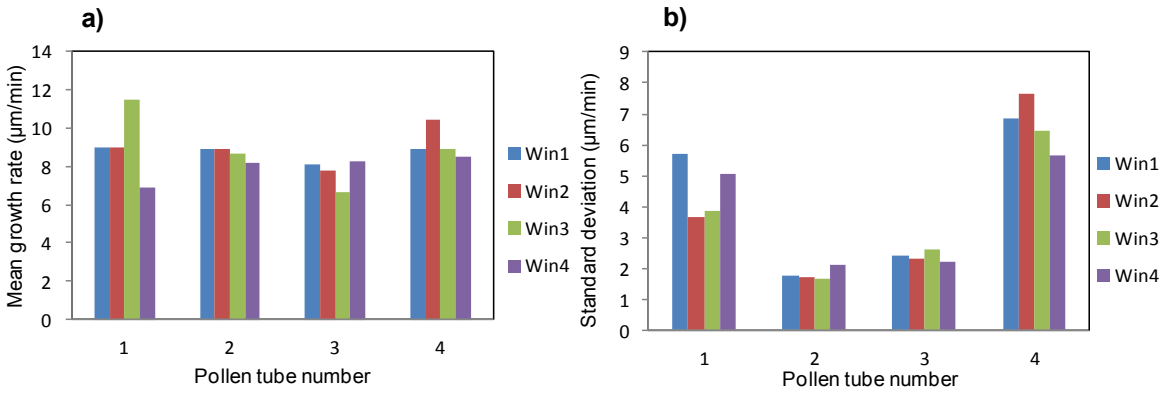

Figure 6.4: The results of mean values and standard deviation values of growth rate for different windowed samples of a several pollen tubes. The variation is confined in a limited range reflecting the stationary pattern of pollen tube growth. The windows were equally spaced to cover the 240s total period without overlap.

It is difficult to identify the frequency components only by evaluating the original signal. Therefore, to obtain discrete data, the time domain signal was converted to the frequency domain using Discrete Fourier Transform (DFT) in order to detect the peak frequencies of

oscillation. DFT of the signal is calculated using Fast Fourier Transform (FFT) algorithm (Zerzour *et al.*, 2009a). Prior to the transform, the average growth rate data were subtracted from the time series in order to remove the non-oscillating component of the time series. Power spectral density (PSD) was then used to obtain waveform analysis reflecting the power of each frequency components associated with the oscillatory growth.

Assuming stationary growth, FFT and PSD were obtained for the growth rate signal. As stated, if the sampling rate frequency (f_s) is chosen at least twice the maximum frequency of the signal (f_m), no aliasing effect in the FFT analysis would be detected. However, due to the limitation of the tracking software, the noise influenced the time-series growth rate signal which led to the maximum frequency of interest in signal (f_m) to be significantly higher than our maximum desired frequency (f_c) (secondary frequency in the range of 0.2-0.3 Hz). In this case, setting the sampling frequency to more than $2f_m$ might be impractical to prevent aliasing. Hence, it is preferred to use low-pass filter (*antialiasing filter*) which attenuates the amplitude of the frequencies above f_c (Wheeler *et al.*, 1996). The maximum frequency of the filtered signal (f_m) is now still higher than f_c, but lower than the value before filtering. In our analysis, we applied a low-pass Butterworth filter with a cut off frequency in the range of 0.35-0.5 Hz and a filter order between 1 to 5 was applied to eliminate the effect of aliasing frequencies generated by the noise in the time domain data. For the chosen sampling time of 0.5s, the first order Butterworth filter with the cut off frequency of 0.4 Hz was generally sufficient to detect both primary and secondary frequencies. The FFT and PSD analysis of a sample pollen tube growth rate is shown in Fig 6.5,a. Two dominant peak frequencies around f=20 mHz and f=220 mHz are shown

corresponding to the primary and secondary peak frequencies of the growth rate oscillations. The windowed PSD analysis also shows similar peak frequencies (Fig 6.5b) where all three PSD graphs with three windowing functions, namely Hamming, Kaiser and Chebyshev identified the peak frequencies at 20 mHz and 220 mHz.

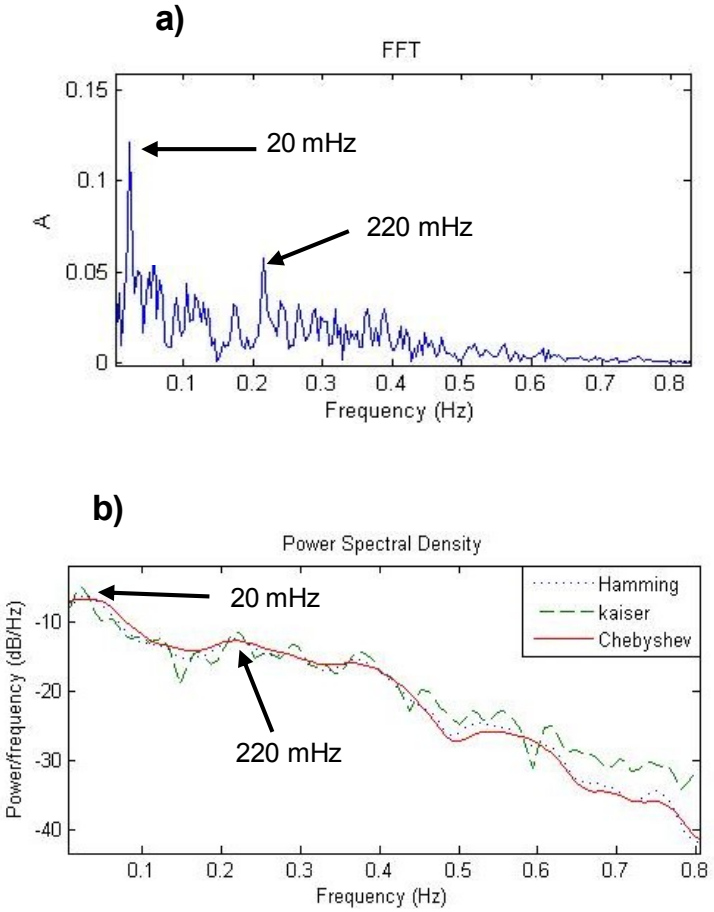

Figure 6.5: a) FFT analysis on the time-series data of a sample *Camellia* pollen tube growth rate. Two peak frequencies are seen around f=20 mHz and f=220 mHz, b) Windowed PSD analysis of sampled *Camellia* pollen tube.

For most pollen tubes within the sample set (n=15), FFT and PSD detected both primary and secondary frequencies. However, in two of these specimens only weak or no primary oscillation frequency was detected, but the secondary frequency was clearly present (Fig. 6a). In addition, in several specimens, FFT analysis revealed unexpected peaks (around the

frequency of 280 mHz, Fig 6.6,b). This is likely the result of a phenomenon called *leakage*, caused by the fact that the sampled value of the particular frequency at the start of the sampling interval was different from the value at the end of sampling (Wheeler and Ganji, 1996).

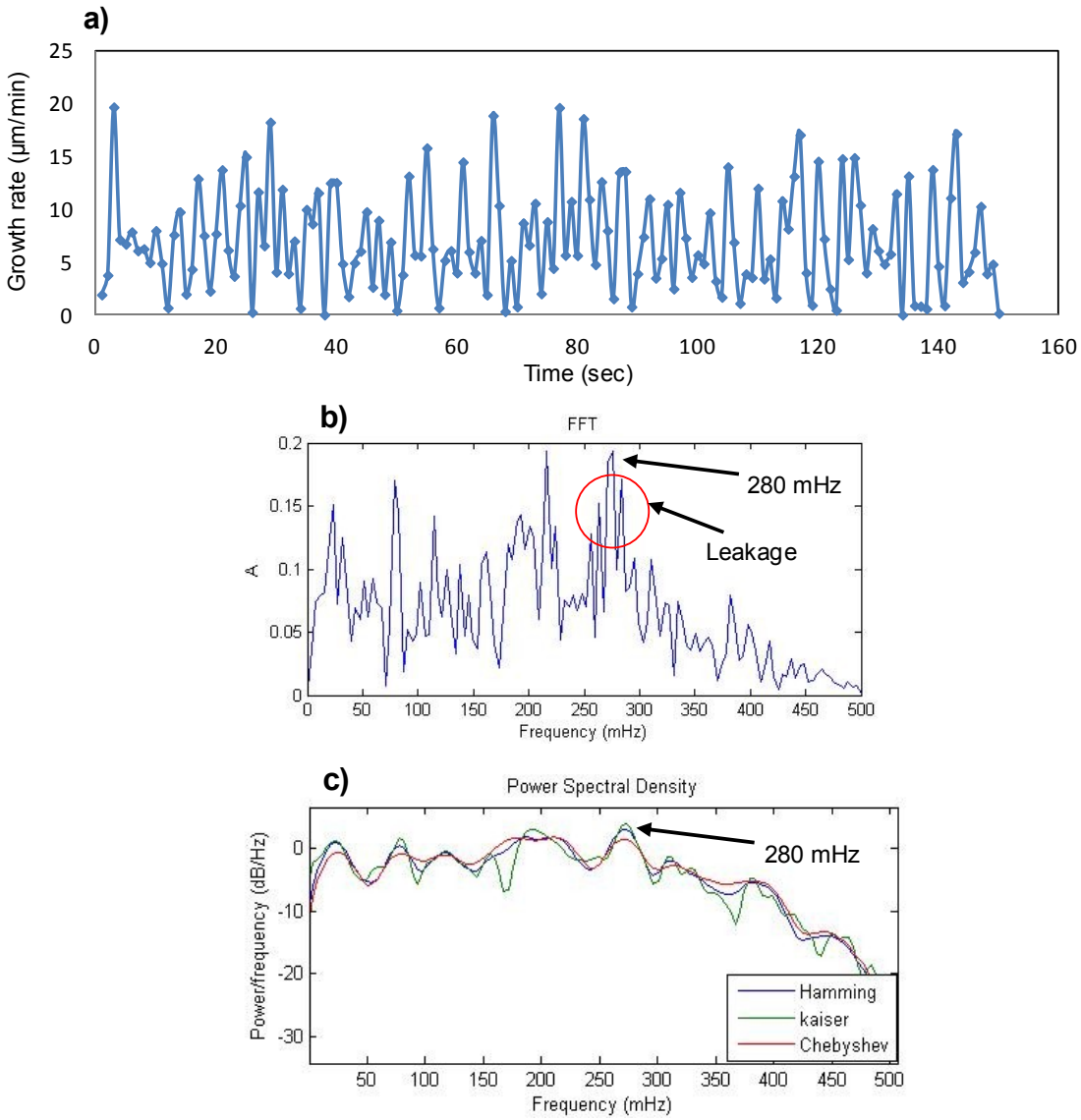

Figure 6.6: a) Time series of pollen tube without strong primary frequency, b,c) FFT analysis of pollen tube growth rate (sample rate = 1s). No strong primary peak frequency was detected. The secondary frequency was detected at 280 mHz. Due to a leakage effect, three peaks are seen around the frequency of 280 mHz, c) Windowed PSD analysis clearly detect the secondary frequency at 280 mHz.

The common method to deal with this problem is the use of proper *windowing function* to attenuate the signal at the beginning and the end of sampled range. Different types of windowing functions were tested and all successfully removed the leakage effect (Fig 6.6,c corresponding to the same data shown in Fig 6.6,b. This treatment confirms that there are no two truly independent frequencies adjacent to each other around f=280 mHz. Clearly, the selection of proper windowing function is important to determine the true peak frequencies of oscillation.

6.4.3 Stability of peak frequencies over time for pollen tube growing in normal condition

The dynamic growth characterization shows that most of *Camellia* pollen tubes growing under normal conditions oscillate with a primary frequency in the range of 20-50 mHz and a secondary frequency in the range of 200-300 mHz (n=15). Next, we used Short-time Fourier Transform (STFT) in order to be able to determine the variation trend of peak frequencies of local sections of growth rate signal over time with respect to the peak frequencies of the overall signal. To assess the baseline variations during undisturbed growth, we analyzed four of the previously analysed samples. The results show that in the absence of any change in growth conditions, the primary frequency shows up to 13% variation, while the secondary frequency varies up to 10% between the windows of a single sample (Fig 6.7). The peak frequencies did not vary significantly for different window spans. Hence, FFT analysis over a long window covering all sub-windows can define the overall peak frequencies of pollen tube growing under normal conditions.

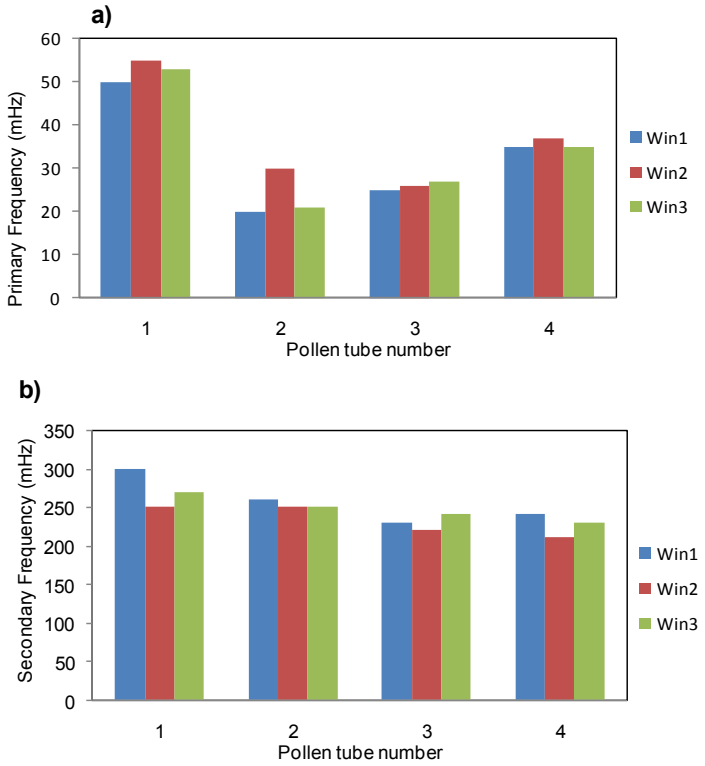

Figure 6.7: STFT analysis of different pollen tube to detect the variation of primary and secondary peaks in different time interval of normally growing pollen tube (n=4), Window size is 50 seconds. The average variation of peak frequencies among the three windows is 13% for primary frequency and 10 % for secondary frequency

6.4.4 Effect of sucrose concentration on growth oscillation frequencies

In order to assess how the primary and secondary oscillation frequencies in the pollen tube growth rate are affected by a change in growth conditions, the sucrose concentration in the growth medium was modified. Sucrose is both taken up and metabolized, and it alters the turgor pressure of the cell. The latter effect is caused by an osmotic shock and is transient. The cell usually compensates for the change in osmotic conditions within few minutes. Here we observed that changing the concentration of sucrose from 8% in normal medium to 10% caused the pollen tubes to interrupt the normal growth in a transient manner followed by an adjustment to a new stable condition. In order to identify the transient and

stationary regions of the growth, the variation in the mean growth rate within 50s time spans before change of the growth medium (BT) and after change (AT) was analyzed (Fig 6.8,a). The variations within the sub-regions at the moment of change of sucrose concentration (from region BT2 to region AT2) are depicted in Fig 6.8,b. Region BT1 identifies normal growth of the pollen tube before treatment, region AT1 is the transient period during which the growth is disrupted, region AT2 is the time period when the pollen tube resumes growth under the new environmental condition and AT3 identifies the stationary growth of pollen tube once it has adapted to the new condition.

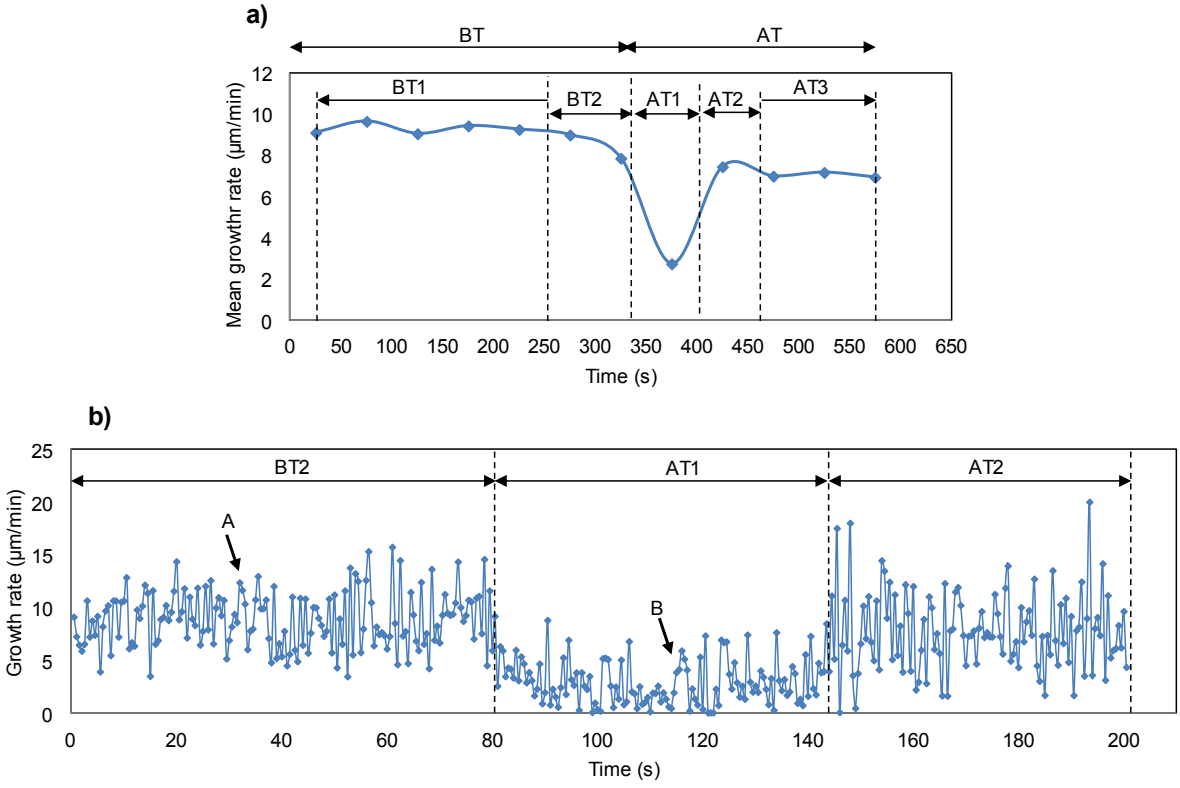

Figure 6.8: a) Mean pollen tube growth rate , each over 100 data points before treatment (BT region) and after administration (AT) of higher concentration of sucrose, sampling rate= 2Hz. b) Time course of pollen tube growth rate before and after treatment. Pollen tube growth was interrupted for about 1 min in region AT1 and resumed with a lower mean growth rate from region AT2. Points A and B clearly show the oscillation with secondary frequency in stationary growth region before medium change and in transient region after the change respectively.

In the case of a change from 8 to 10% sucrose concentration, the duration of the transient interruption of pollen tube growth varied between 1-3 min (n=3). Once the pollen tube had recovered from the osmotic shock it established a new stationary grow pattern (regions AT2 and AT3). FFT analysis was applied to the stationary signal in region AT3 to identify the new peak frequencies of the growth rate (Fig 6.9). In the pollen tube shown here, a shift of 8 mHz for the primary frequency towards longer oscillation periods was detected. The secondary peak frequency on the other hand was reduced by 30 mHz.

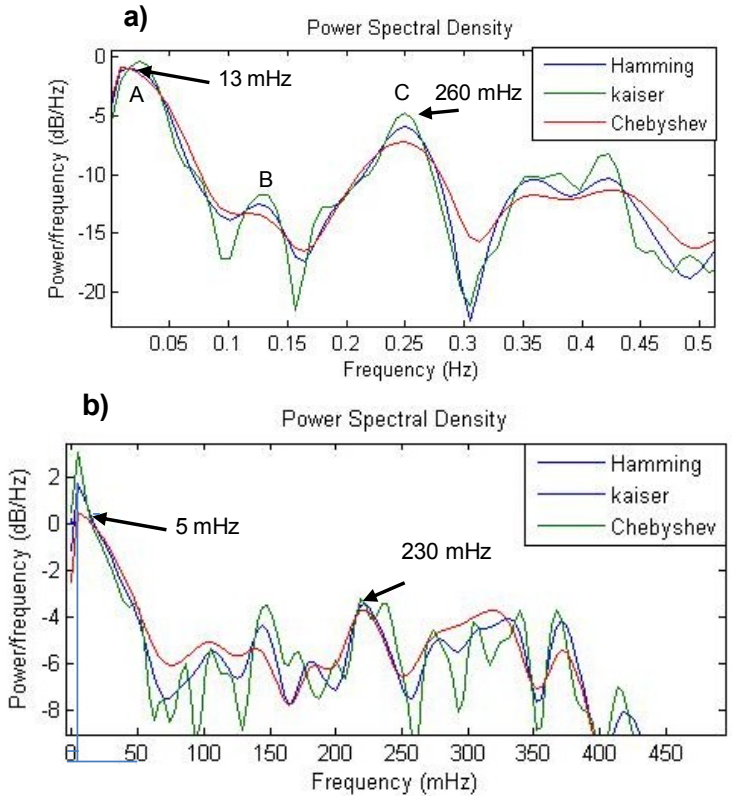

Figure 6.9: a) FFT analysis of pollen tube growing in 8% sucrose within the stationary regions of growth (region BT1). The pollen tube displays oscillations with a primary frequency of 13 mHz and secondary frequency of 260 mHz. b) FFT analysis of the same pollen tube within the stationary regions of growth after change of sucrose concentration (region AT3). The primary frequency has shifted to 5 mHz and and the secondary frequency to 230 mHz, corresponding to a shift of 8 mHz and 30 mHz, respectively.

Moreover, the mean growth rate was reduced by 25% compared to the value observed before the increase in sucrose concentration (Fig 6.10). On average, for the three tested *Camellia* pollen tubes the primary frequency was reduced by 68% and for the secondary frequencies the frequency was reduced by 12%.

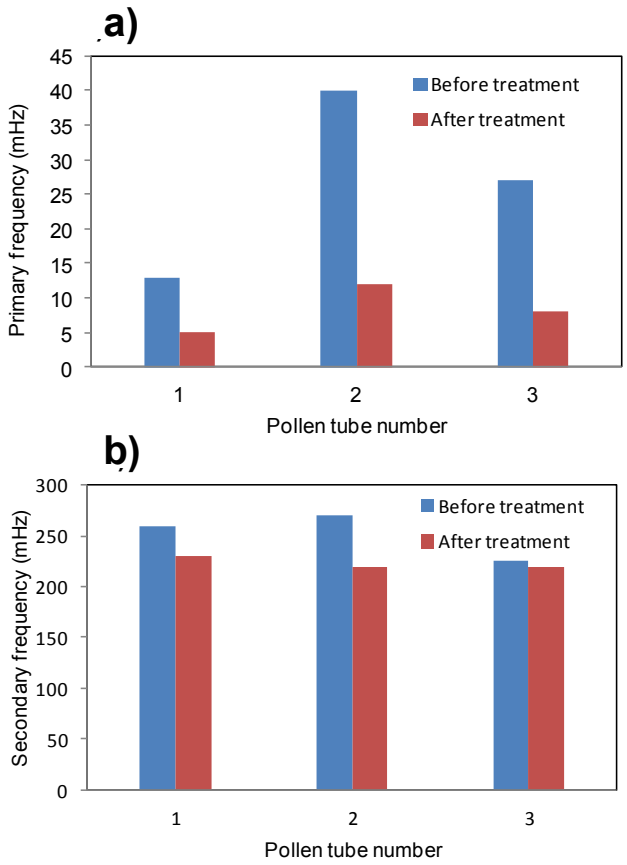

Figure 6.10: a) Primary peak frequencies before treatment (BT) and after treatment (AT) for the analysed pollen tubes, b) Secondary peak frequencies before treatment (BT) and after treatment (AT) for the same pollen tubes.

The windowing function was used not only to remove the leakage phenomenon, but also to detect more precise peak frequencies as seen in Fig. 6.9,a. In points A and C, all three windows act similarly to detect a significant peak frequency. In the case of point B, the Chebyshev windowing function did not clearly detect a peak at this point.

6.5 Discussion

The oscillatory growth behavior in pollen tubes offers an extraordinary phenomenon that can be used to understand the mechanisms that regulate cellular growth in plants both in space and time. Our detailed analyses have shown that the pollen tube displays at least two superimposed frequencies which are maintained constant over extended periods of time in stable growth conditions. Hence, any stable shift in the peak frequencies that is larger than the normal variations encountered during normal growth is a sign for a disturbance. Frequency analysis thus provides us with a tool to detect and quantitatively assess the effect of disturbances on cellular growth behavior. We demonstrated the use of this tool by comparing pollen tube growth rate in stationary regions before and after the change of growth medium revealing a clear shift in peak oscillation frequencies. During the transition period the pollen tube lost its primary frequency peak and only displayed a secondary peak frequency. After adapting to the new growth condition, the pollen tube recovered and displayed again a primary and secondary oscillation frequency, but both were significantly shifted compared to the original growth conditions. Analysis of the growth dynamics therefore provides us with several independent parameters that can be measured to quantitatively assess the effect of a pharmacological or other external agent on cellular functioning: the duration of the transition period, and the shift in both primary and secondary frequencies in the growth rate.

These quantitative parameters will not only enable the analysis of the pollen tube growth rate upon external triggers, but they also provide a tool to understand the cellular feedback mechanisms that regulate normal growth. The extracellular and intracellular concentrations

and fluxes of various ions such as calcium (Pierson *et al.*, 1994) and protons, as well as the dynamics of cellular features such as vesicles and the cytoskeleton are known to oscillate with the same frequency as the growth rate (primary frequency) (Holdaway-Clarke and Hepler, 2003; McKenna *et al.*, 2009; Parton *et al.*, 2001), but with a phase delay (Messerli *et al.*, 2000b). In the present study, we successfully detected a secondary oscillation peak frequency in the growth rate and we should therefore expect to observe the corresponding secondary peak frequencies in the dynamics of these cellular processes. Detecting these will pose a challenge to the measuring techniques required such as the vibrating probe (for ion flux) and the sensitivity of fluorescent markers (for ion concentrations and motion of cytoplasmic structures such as vesicles and organelles), but future implementations of our microfluidic device will be used to meet these challenges. A detailed analysis of secondary oscillation frequencies may contribute to solving outstanding questions in this field such as the controversy around the fundamental underpinnings of the change in growth rate (Winship *et al.*, 2010) (Winship *et al.*, 2011b). Oscillations in turgor pressure were suggested as the cause of the oscillatory changes in growth rate (Zonia *et al.*, 2003) (Messerli and Robinson, 2003b), but these were not confirmed experimentally either by pressure probe (Benkert *et al.*, 1997) or micro-indentation (Geitmann and Parre, 2004). However, there might be oscillations in turgor pressure with an amplitude below the resolution of measuring technique and more detailed analyses are warranted. On the other hand, the presence of a complicated oscillation pattern with primary and secondary frequencies is probably easier to explain with variations in the material properties of the cell wall as postulated earlier (Geitmann, 1999; Holdaway-Clarke and Hepler, 2003). The material properties are influenced by subtle changes in the ion flux pattern and exocytosis

rate (Kroeger *et al.*, 2008), but more research is warranted to clarify this issue. The analyses of secondary frequencies offer a promising avenue to do so.

The frequency shifts can be considered as the dynamic response of pollen tube to the change of growth conditions whereas the change of mean growth rate can considered as the static response of the pollen tube. By incorporating static and dynamic response of pollen tube to the change of growth environment, the proposed microfluidic platform reported in this paper has application to be used as a point-of-care microdevices for detecting the existence of biological or toxic agents in the growth medium.

6.6 Summary and conclusions

The present study demonstrates how the use of a microfluidic device combined with high resolution imaging increases the precision of the analyses of cellular behavior. Unlike earlier dynamic analyses of pollen tube growth, we were able to detect secondary oscillation frequencies with higher frequency values superimposed on the previously reported primary frequency. Our findings illustrate that even in the apparent absence of low frequency oscillations - a phenomenon that is typical for young pollen tubes - there always are secondary peak frequencies indicating that pollen tube growth is constantly under dynamic control. Our finding that slight changes in the growth environment change both frequencies offers a promising avenue for the investigation of the feedback mechanisms governing cellular growth.

Chapter 7

ToxChip: Whole cell microfluidic platform for toxicity detection through dynamics of growth

7.1 LOC for toxicity detection using pollen tube as cell sensor

In this chapter, the application of pollen tube as whole-plant cell sensor for toxicity detection is realized. The benefit of trapping pollen grain and growing pollen tubes along microchannel in a directed manner presented by the enhanced design in chapter 3 helps to detect more accurately the dynamic oscillatory growth of pollen tube in response to the existence of environmental toxic substances within growth medium. The content of this chapter is about to submitted to the journal of *Lab on Chip*.

Abstract

Since toxicity detection using real testing on human or animal is no longer an appropriate technique, development of new technical methods for detecting toxic materials is highly demanded. Fast response of living cells to the chemical signals makes them a useful and reliable method for detecting toxic materials. This paper presents a novel microfluidic-based whole cell lab-on-chip (LOC), called ToxChip, to enable detection of environmental toxic substance through dynamics of oscillatory growth as well as non-oscillatory growth behaviors of a whole cell. Pollen tube is used in this paper as an example of whole cell for demonstration. The oscillatory dynamic growth includes both fundamental and higher modes of oscillation frequencies associated with growth. The non-oscillatory parameters include growth rate, growth length and cell life time. ToxChip has many advantages over previous platforms such as high throughput,

low sample volume, less expensive due to mass production, disposability and portability. The proposed microfluidic-based sensor can represent rapid and reliable results for detecting the existence of biological or toxic agents in the growth medium and to distinguish friendly and non-friendly substances. The aluminum (Al) ion was used as test substance for demonstration in order to evaluate the feasibility of using pollen tube as whole-cell sensor system for toxicity detection.

7.2 Introduction

Toxicity detection using real testing on humans is no longer an appropriate technique. Hence, new models of animal cells are widely used to detect the toxic materials. Nevertheless, millions of animals are annually killed to test the toxic behavior of ions and this rises the interest for non-animal based methods to detect toxicity (Bhanushali *et al.*, 2011). A variety of non-animal methods which are available for toxicity detection consist of in-vitro analysis of living cells and tissue cultures (Magrez *et al.*, 2006) (Jin *et al.*, 2007), microarray technology (Waring *et al.*, 2001) and computerized modeling (Greene, 2002). These methods can provide more reliable, faster and cheaper results (Bhanushali *et al.*, 2011). Fast response of living cells to the environmental signals makes them an ideal, useful and reliable method for detecting toxic materials. Various cells such as bacterial, mammalian and plant cells have been used as biosensor for the application in pharmacology, toxicology and environmental measurements (Catroux *et al.*, 1993) (Qureshi *et al.*, 1998) (Stammati *et al.*, 1981) (Bhogal *et al.*, 2005) (Bentley *et al.*, 2001).

The cell is expected to respond differently to friendly and unfriendly substances. Under treatment with friendly substance, continues and gradual change of cell behavior is expected while due to presence of toxic material, discrete and sudden change in cell behavior is predicted. In order to use a whole cell as sensor to identify the toxic substance (non-friendly agent), it is necessary to characterize various aspects of the cell response to both friendly and unfriendly substances and then discover appropriate aspect of cell response which can effectively distinguish toxic and friendly agents and represent the cell behavior for toxicity detection. The more ability of the cell behavior to distinguish the friendly and unfriendly agents, the better is the suitability of the cell type for efficient toxicity detection.

Among different cell types, pollen tube is extremely sensitive to the external signals which and makes them suitable cellular models for characterizing cell response to the influence of various chemicals involved in cellular metabolism as well as environmental chemicals (KRISTEN *et al.*, 2002; Kristen *et al.*, 1995). Pollen tube is the fastest tip growing plant cell that plays essential role in the life cycle of flowering plants. It germinates from the pollen grain on stigma, senses multiple extracellular mechanical and chemical signals from its floral environment and elongates in polarized shape toward the ovule in the interior of the flower. It has the function to deliver the migrating sperm cells to the eggs for fertilization purpose. Pollen tube grows through distinctive cellular matrix as tip growing cells follow properly the guidance cues. Fig. 7.1a shows the scanning electron micrograph of *Camellia* pollen grain and the pollen tube germinated from its grain.

The pollen tube is an appropriate snesor for toxicity detection as it is inexpensive and easily accessible. In addition, the results from the study of pollen tube have been verified with the response of animals to toxic materials (Barile *et al.*, 1994). This indicates that the study of pollen tube behavior will have the potential of assessing the effect of toxicity even on human. The effect of toxic substance on the cell growth was investigated by measuring various parameters, such as, percentage of pollen grain germination, the change of growth length and alteration of pollen tube morphology (Sawidis *et al.*, 1995). Using these criteria, the pollen tube-based assay has been first reported as a toxic indicator of environmental herbicides (Strube *et al.*, 1991). It was then developed as an effective nominee to detect the presence of various detergents (Paoletti, 1992) and pollutants (Xiong *et al.*, 2001) (Rezanejad, 2009) effective on plant reproduction and food health. Moreover, the pollen tube was used to detect heavy metals consisting of aluminum ion as toxic metallic ion (Blamey, 2001); chromium Cr(III) and Cr(VI) as dangerous environmental pollutant (Shanker *et al.*, 2005; Speranza *et al.*, 2007), cadmium as toxic substance with relatively high mobility into the plant system (Sawidis, 2008) and also other toxic chemicals such as mercury and mouthwash irritating ingredients (Sawidis and Reiss, 1995) (Kristen *et al.*, 2006). Recently, the toxicity effect of lead on *Picea wilsonii* pollen tube development was studied in a concentration-dependent manner (Sheng *et al.*, 2012).

As stated, in all above experiments, the effect of different substance on the pollen tube living cell was investigated by measuring the percentage of pollen grain germination, change of growth length, growth rate or alteration of pollen tube morphology (Sawidis and

Reiss, 1995). In order to provide common understanding for the degree of cytotoxic potential of test substances, the Pollen Tube Growth (PTG) protocol introduced the C50 criterion (Zhang *et al.*, 1999). This criterion is the concentration of the toxic substance in which the growth length of pollen tube under toxicity testing reduces to half of the normal growth length. Since measuring the growth length of large number of pollen tubes was time consuming, photometric quantification method was developed to determine the mass of pollen tube growth during the testing period. In this study, the concentration of test substance that reduces the growth mass to 50% of the control test was used (Nye, 2006). In addition to the PTG protocol, the alteration of the average growth rate of individual pollen tubes was also used to study the toxicity degree of test substance where the alteration of average growth rate against different concentrations of the test substance was defined as typical way of illustrating the degree of toxicity (Sawidis, 2008).

Although the pollen tube was useful to detect the presence of various toxic substances as unfriendly substances, the similar change in growth rate and cell death (tube bursting or growth arrest) was detected when the cell was exposed to different concentrations of friendly substances such as sucrose and calcium (Bou Daher *et al.*, 2011c). In addition, the results also show that, despite possibility of reduction in the growth rate of pollen tube under chemical treatment, the change in the oscillatory growth pattern to higher peaked spike type growth may keep the average growth rate unaltered (Messerli and Robinson, 2003b). Hence, the growth rate criterion cannot reliably distinguish between friendly and unfriendly (toxic) substances because in both cases, the growth rate may reduce. The static cellular response to friendly and unfriendly materials through quantifying the change in

average growth rate, growth length or the cell life may not solely define the influence of toxins on the behavior of cells as the cell is expected to undergo stressful behavior which is fundamentally dynamic in nature.

Despite use of diverse criteria in cellular systems for toxicity sensing, the question still at large is to know which biological feature of a living cell would better represent its higher level organism, the plant or animal. On this regard, application of scaling relationship between the activity of the cells and the behavior of animals or plants will be an essential help. It has been shown that the ratio metabolic rate of an organism to its body mass are correlated based on the equation of allometric scaling on a logarithmic scale as "criteria of similarity" (Lindstedt *et al.*, 1981; West *et al.*, 2002). It means that the scaling of metabolism is extended down through all levels of organization from the intact organism to the cell, mitochondrion, and eventually to its individual molecules. This theory which is based on fractal-like distribution networks can explain variations in metabolic rate over an amazing 27 orders of magnitude and present insights into the structure of metabolic pathways within cells and organelles as well as within the higher level organism which is an integration of these fundamental units. On the other hand, once an organism is subdivided into hierarchical levels reflecting flow of energy, the overall system terminates in a fundamental unit down to the cells and further down to the molecules which are the final terminal units of the entire metabolic system. Thus, the entire animal or plant can be viewed as a hierarchy of linked networks which proves that there should be a link between the activity of the living organism and its fundamental units. For instance, self similarity as a fundamental concept in nature can explain natural phenomena (West *et al.*, 2002) and

have been identified in material structures, biology and medicine (Lindstedt and Calder III, 1981).

Both structural and dynamical factors have been introduced as the origin of the self similarity. Hence, dynamical nature of the system is one main nature of self similarity (Desprat *et al.*, 2005; Galdberger *et al.*, 1990; Waliszewski *et al.*, 2001a). This oscillation generated from the metabolism is scaled up to higher level which assures survival and stability of plant and animal during their life span. We do not expect to see identical oscillation behavior among molecular level, cellular level and a higher level of organisms because the system of each organism and its underlying network of fundamental unit is a complex dynamics network. For instance, the results of screening molecular and cellular activity have indicated a relationship between genotype in nano scale and phenotype of cell in larger micro scale (Waliszewski and Konarski, 2001a). The similar phenomenon has been reported for both space and time in microscale for a system of interacting cells, for instance in tumor cells, so that every single cell of the tumor can restore the hierarchical organization and dynamic features of the entire tumor (Waliszewski *et al.*, 2001b). In this case, there is relationship between dynamics of gene expression in small size and dynamic of a population of cell. Despite the existence of dynamic activity, the behavior at different spatial scales varies. However, one would expect to see independent dynamic activity among different organisms constrained in different environments. For instance, one does not expect to see identical dynamic of gene expression in cancer cells existing in a malignant tumor with the cells cultured in the monolayer system (Waliszewski *et al.*, 2001b).

Knowing this, it is believed that the disease and aging that arise from stress relate to body's periodic rhythm meaning that decrease in periodicity is associated with disease. Similarly, one can expect to see the effect of any stress to the cellular system can be expressed by oscillatory and dynamic behavior of either cell growth or its underlying intracellular ionic activities. Knowing the importance of dynamic activity of the cells as an indicator of the organism property, any technique that assists to measure the dynamic oscillation of cell growth or intracellular ionic activities is promising to characterize the influence of environment on the health of the cell and to evaluate the potential of dynamic oscillatory growth in distinguishing friendly and unfriendly (toxic) substances.

In this paper, the previously enhanced microfluidic device (Sanati Nezhad *et al.*, 2013d) is employed to integrate tip growing plant cell, pollen tube, as a whole cell sensor for detecting the toxicity of aluminum with the potential of poisoning for human, animal, plant and microorganisms (Sawidis and Reiss, 1995) and was shown effective on cellular malfunction (Zhang *et al.*, 1999) (Piñeros *et al.*, 1997). The device is used to distinguish the cell response to friendly and unfriendly agents through both dynamics of oscillatory growth as well as non-oscillatory growth behaviors. The *Camellia* species were chosen for toxicity testing as it has large diameter, thus easier to be handled in micro-environment (Agudelo *et al.*, 2012c), has oscillatory growth in a long growth length where its elongation within microfluidic has been earlier proved. The enhanced design optimizes the growth condition of the pollen tube by providing stable environment for changing the growth condition, trapping and confinement of pollen

grains, conducting growth direction along growth microchannels. Using this enhanced device, both fundamental and higher modes of dynamic oscillation of tip growth as a biological feature representing the living organism has been detected (Sanati Nezhad *et al.*, 2013d). Here, the effect of stress from toxic substance on variation of the fundamental and higher modes of dynamic oscillation of growth rate was detected and compared with the dynamic response to the friendly sucrose concentration. Addition to dynamic oscillation of growth rate, the change of growth rate and cell life (Holdaway-Clarke *et al.*, 1997; Messerli *et al.*, 1999; Michard *et al.*, 2008) was exploited to enable detecting a wide range of toxic concentrations under the stress of toxic substance. This microdevice reduced the time period of sensing to few orders less than the previous assays through incorporating the dynamic response of the cell which make our design as a low cost, rapid and reliable device for detecting toxicity of various chemical, biological and environmental agents. The dynamic oscillatory response was able to distinguish friendly agents by maintaining, but shifting the oscillation frequencies while non-friendly substances by the disruption in oscillation frequencies.

7.3 Materials and methods

7.3.1 Preparation of pollen grains and germination

Pollen grains of *Camellia japonica* were collected from the newly opened flower in the Montreal Botanical Garden. The pollen grains were dehydrated and stored in gelatin capsules at -20°C in the dark. Prior to use, the pollen was rehydrated in a humid environment for 1 hr at room temperature. Few micrograms of pollen were suspended in culture medium containing 2.54 mM $Ca(NO_3)_2 \cdot 4H_2O$, 1.62 mM H_3BO_3, 1 mM KNO_3, 0.8 mM $MgSO_4 \cdot 7H_2O$ and 8% sucrose (w/v). A pollen grain was considered germinated once

the pollen tube length was more than twice the pollen diameter. When the grains start germinating, the pollen suspension was introduced into the microdevice. To study toxicity effect of Al, Aluminum Chloride Hexahydrate (AlCl3. 6H2O) with Molecular Weight of 241.43 g/mol (Baker Analyzed Reagent, from J.T. Baker company) was added to the culture medium to provide specified concentration of aluminum toxic solution. During toxicity testing, the regular medium was replaced with the toxic solution using the injection of toxic solution with the flow rate of 5 µl/min by syringe pumping.

7.3.2 Microscopy

Nikon Eclipse 80i digital imaging microscope equipped with Infinity 1 digital CCD Camera and Capture Analyzer software were used for bright-field imaging of microfluidic network and pollen tubes. The pollen tubes were observed with a 80X objective (0.65 NA). To measure pollen tubes growth rate, the time-series intervals between successive images of pollen tubes was 0.5s which was sufficient to detect both primary and secondary peak frequencies (Sanati Nezhad *et al.*, 2013d). Tracing program of MTrack2 in NIH ImageJ software was used to track the pollen tube's tip during the growth.

7.3.3 Design and fabrication of microfluidic device

The microfluidic platform was designed from the previously enhanced microfluidic device devised for chemical treatment of tip growing cells (Sanati Nezhad *et al.*, 2013d). Briefly, the design consists of main distribution chamber to introduce the pollen suspension into the

main chamber through the pollen suspension inlet, a series of growth microchannels linked to the distribution chamber along which the pollen tubes grow and three outlets to conduct the pollen grains or medium out of the chip (Fig. 7.1b,c). The pollen grains were injected into the chip, conducted through the main chamber toward the growth microchannels and trapped at the entrance of microchannels. The individual pollen tubes grow along the microchannels and were subjected to chemical treatment (Fig. 7.1d). The geometry and dimensions of microfluidic network was chosen from the previously optimized device to provide single pollen trapping at the entrance of growth channels and identical growth environment for the growing pollen tube along the channel (Sanati Nezhad *et al.*, 2013d). The microfluidic device was fabricated using PDMS replica molding on SU8 molds where the details are explained in Agudelo et al. (Agudelo *et al.*, 2012c) and Sanati et al. (Sanati Nezhad *et al.*, 2013c; Sanati Nezhad *et al.*, 2013e). Fig. 7.1e shows the microfluidic device fabricated for toxicity testing using pollen tube as whole cell sensor.

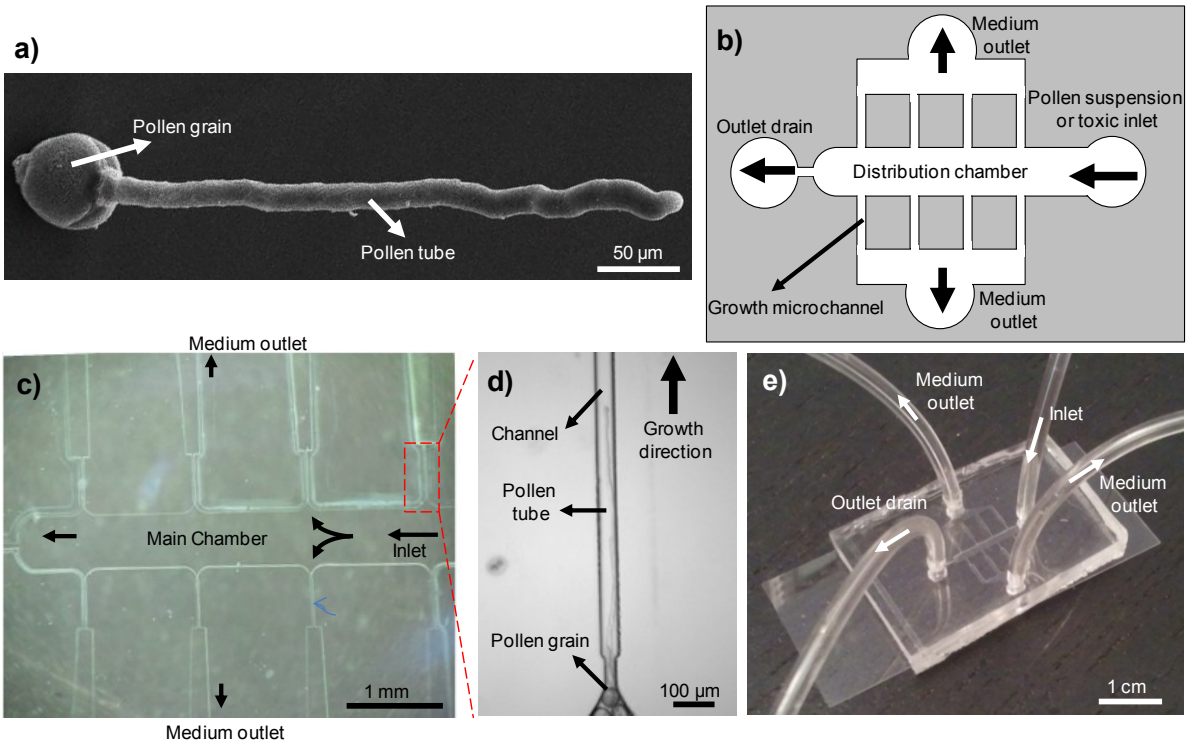

Figure 7.1: a) The scanning electron micrograph of *Camellia* pollen tube germinated from pollen tube, b) Schematic of design, c) The fabricated microfluidic design optimized for the purpose of toxicity testing using pollen tube growth, d) The growth of individual pollen tube along microchannel, e) The fabricated microdevice.

7.4 Results

7.4.1 Static response of pollen tube to friendly and unfriendly substances

It is important to identify the difference in behavior of cells under friendly and hostile environments before applying this principle for toxicity detection. Typical responses of cells under both friendly and unfriendly environments are schematically represented in Fig. 7.2. In this figure, the responses to friendly environment are represented in Fig.7.2(a,c,e) and to hostile environment are shown in Fig. 7.2(b,d,f).

The growth rate/length and the cell life (time before bursting or growth arrest) are the main parameters of cellular growth used to study cell response to the presence of chemical agent in the growth medium. One can note from Fig. 7.2(a,c,e) is that there exists an optimum range (active growth range) of concentration for friendly substances such as sucrose and calcium (Bou Daher and Geitmann, 2011c). Outside of the active growth range, the cells suffer in terms of reduced growth rate, increased death rate and reduced cell life. In contrary, there is no optimum range of concentration for unfriendly or toxic environments. Optimum condition corresponds to the minimum concentration of toxic substance. Toxic environment would results in monotonic deterioration of performance measured in terms of growth rate, death rate and cell life as seen in Fig. 7.2(b,d,f).

As seen in Fig. 7.2a, for a friendly environment such as sucrose or calcium, the growth rate is high in the optimum range of concentration and acceptable in the active growth range. When the concentration of friendly agent falls below a minimum value, the cell undergoes sudden burst. This region is indicated as the region of burst in Fig. 7.2(a,b,c). In the case of concentrations above the active growth range, called “growth arrest”, cells stop the growth and the growth rate is negligible. Under toxic treatment, the growth rate decreases monotonically with increase in concentration of toxic substance in environment. The best growth condition corresponds to the absence of toxins.

If the cell life is considered, it is normal during the active growth region of friendly environment and cell life decreases dramatically outside the active growth rate region as shown in Fig. 7.2c. When the concentration reduces below the minimum concentration,

cell undergoes death by bursting as indicated by the burst region. Finally, as seen in Fig. 7.2c when the concentration is above the maximum concentration of active growth region, the cell drops growing and the time to stop the growth decreases with increase in concentration beyond the maximum concentration. Thus, the life time of the cell decreases rapidly when the concentration of friendly substance varies away from the growth region. But, as shown in Fig. 7.2d, the cell life reduces when the concentration of toxic substance increases in environment.

In the case of percentage of cells in a population that undergoes death or stop growth, it is minimum in active growth region for friendly environment as seen in Fig. 7.2e. The percentage of death/stopped growth increases when the concentration of friendly substance is varied away from active growth region as shown in Fig. 7.2e. In the case of environment with toxic substance, percentage of cell death increases monotonically with concentration of toxic substance while all the cells undergoes death at a high concentration of toxic substance as shown in Fig. 7.2f.

In summary, cells require definite amount of friendly substance as defined by active growth region and the performance of the cell deteriorates when the concentration of friendly substance deviates from the active growth region. In contrary, there exist no active growth zone, for toxic environment and the presence of toxic substance deteriorates the performance of the cell detected by the monotonic decrease of cell performance with the concentration of toxic substance. These distinct behavior of cells under friendly and

unfriendly environments will be used to identify the toxic substance and degree of toxicity from the degree of performance deterioration.

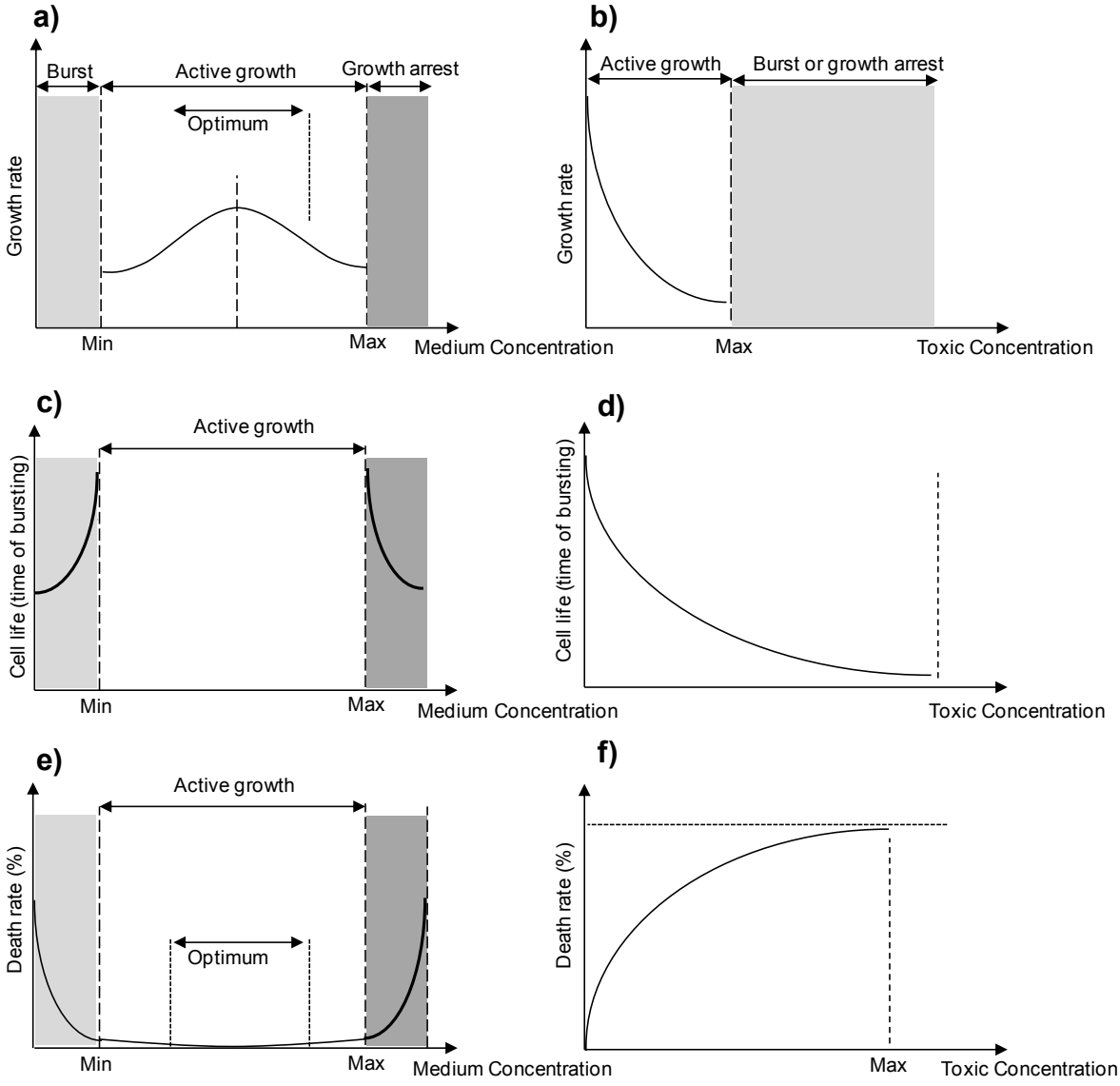

Figure 7.2: Schematic variation of a) growth rate/length in presence of different concentrations of friendly substances, b) growth rate/length in the presence of unfriendly (toxic) substances, c) cell life in presence of different concentrations of friendly substances, d) cell life in the presence of unfriendly (toxic) substances, e) Death rate (%) in presence of different concentrations of friendly substances, f) Death rate (%) in the presence of unfriendly (toxic) substances.

7.4.2 ToxChip for studying the static response of pollen tube to toxic Al substances

Prior to toxicity testing on pollen tube, the microfluidic chip was tested as control experiment in order to find the effect of medium flow and fluid stress on the cell growth or bursting. Once the pollen tubes growth along microchannels were established, the medium was continually injected into the chip for 45 min. Since no bursting were observed during this 45 min, it confirms that the any cell bursting or stop of growth under toxicity testing is due to the Al content of the medium not due to the effect of medium flow velocity.

Once the pollen tube growth along microchannels was established, the medium is then continually injected into the chip for 45 min. Since no bursting were observed during this 45 min, it confirms that the tube bursting under toxicity testing is due to the Al content of the medium not due to the effect of medium flow velocity.

In order to demonstrate ToxChip for toxicity detection, Aluminum was selected. The fabricated ToxChip shown in Fig. 7.1d was used to study the pollen tube response to aluminum (Al) toxicity. Once the growth of pollen tubes along growth microchannels were established to a length of at least 300 μm, a medium with particular concentration of Al was passed through the ToxChip using syringe pump with the flow rate of 5 ml/min. Based on the volume of microfluidic network and the flow rate of injection, it takes about 3 minutes to replace the regular medium with the toxic medium. After refreshing the medium in microfluidic network, the flow is stopped. The growth of pollen tube were observed under microscope before and after introducing the toxic medium. Growth rate, percentage of cell death and time to burst or stop growth were calculated for each concentration of Al.

The time of bursting which can represent the cell life has highest value in absence of toxic Al as shown in Fig. 7.3a. This time, called residence time, corresponds to the period of time starts with the time that the cell senses the toxic substance and finishes when the cell burst. When Al concentration increases, the time of bursting reduces representing the reduction in cell life. At 400 μM concentration and above, the pollen tube bursts immediately within 2-3 minutes of residence time. Similarly, the percentage of bursted pollen tubes against different Al concentrations can also represent the cell life parameter as shown in Fig. 7.3b. The bursting was not observed for pollen tubes exposed to Al concentration of 20 μM (Region A), while for the concentration of 200 μM and above, all the cells were bursted in less than 8 min after sensing Al toxic (Region C). The concentration of more than 400 μM was not tested, but based on the results of region C, all the tubes is expected to burst. Two sample pollen tubes growing along microchannel and busted under Al exposure are shown in Fig. 7.3c. However, the time of bursting under 200 μM was more than the time of bursting for pollen tubes treated with 400 μM Al concentration. The range of AL concentrations in which entire or several pollen tubes still have the growth is 20 μM-200 μM which is very small compare to the same for friendly sucrose and calcium concentrations in the order of a few mM (Bou Daher and Geitmann, 2011c). This limited Al concentration range indicated as region B in Fig. 7.3 shows the toxicity range of Al substance respect to friendly sucrose and calcium agents (Bou Daher and Geitmann, 2011c).

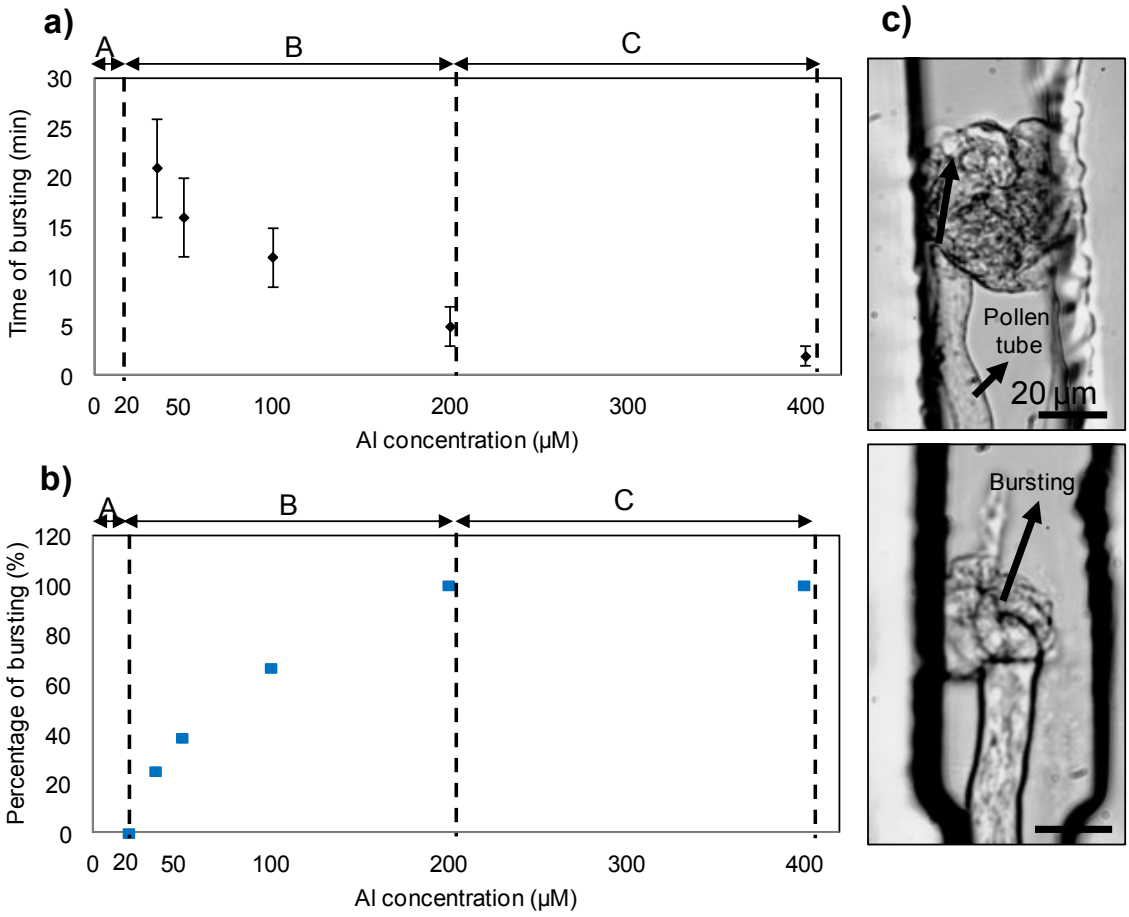

Figure 7.3: a) The effect of Al concentration on the time of bursting representing the cell life, b) The percentage of cell bursting under toxic treatment, c) The busting within microchannel for the cell exposed to 100 µM Al concentration. Scale Bar: 25 µm

Those cells that did not burst under Al treatment in region B of Fig. 7.3, were used to estimate the growth rate under Al influence. Fig. 7.4 shows the reduction of growth rate against the Al concentration ranging from 20 µM to 50 µM. In 20 µM Al concentration and below (region A), the drop of growth rate was not simply detected, though the variation or disruption of higher mode oscillation frequency in 20 µM was simply detectable. In the range of Al concentration between 20-50 µM (region B), the growth rate decreased monolithically with increase in Al concentration.

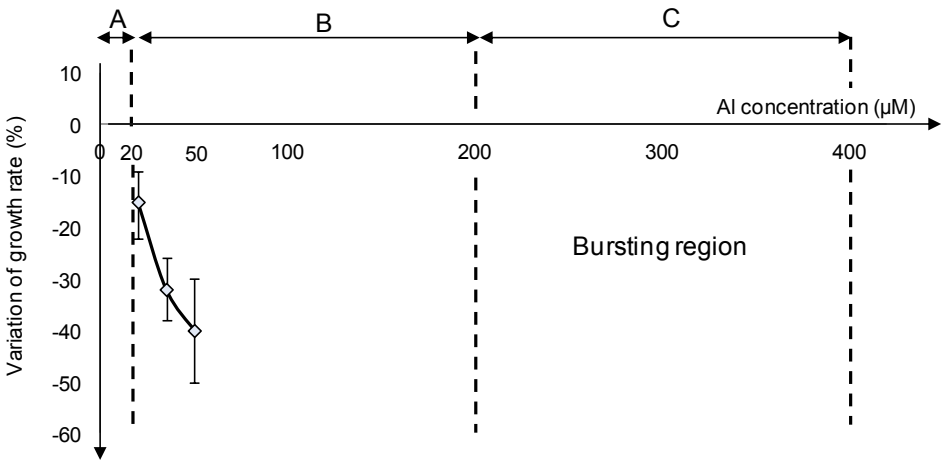

Figure 7.4: The reduction in cell growth rate against different Al concentrations. Region A: no bursting region, Region B: bursting region, Region C: full bursting region. The reduction in growth rate was not easily detectable before 20 μM. After 200 μM Al concentrations, all the pollen tubes burst (Region C). In region B, for non-bursted pollen tubes, the growth rate reduced. For 100 μM Al concentration, the pollen tube neither bursted nor reduced the growth rate, but the growth was arrested.

The percentage of bursting, time of bursting and change in growth rate are related to average properties or static response of the pollen tube to Al treatment and can be used to detect a wide range of Al concentrations. For Al concentrations below 20 μM, no pollen tube bursting was observed and the growth rate was only slightly reduced and hence, the detection of influence of Al concentration was challenging. Hence, 20 μM is considered as the sensitivity of this ToxChip for Al detection using static behavior.

7.4.3 Disruption of dynamic oscillation frequencies under toxic Al treatment

Because of the limitation with static response such as limit of sensitivity, slow sensing using PTG protocol (Few hours) and plausible reliability issue when average growth rate is used as the detection criterion, it is important to find alternative methods to detect the

effect of toxicity on cells. Since the pollen tube has dynamic nature of growth, implementing dynamic study of pollen tube may provide a faster and more reliable criterion for toxicity sensing. We previously characterized both fundamental mode and higher mode oscillation frequencies of pollen tubes in response to friendly sucrose agent as dynamic cell response (Sanati Nezhad *et al.*, 2013d). Fig. 7.5a shows the experimental setup used to characterize the variation of oscillation frequencies as the dynamic response of pollen tube.

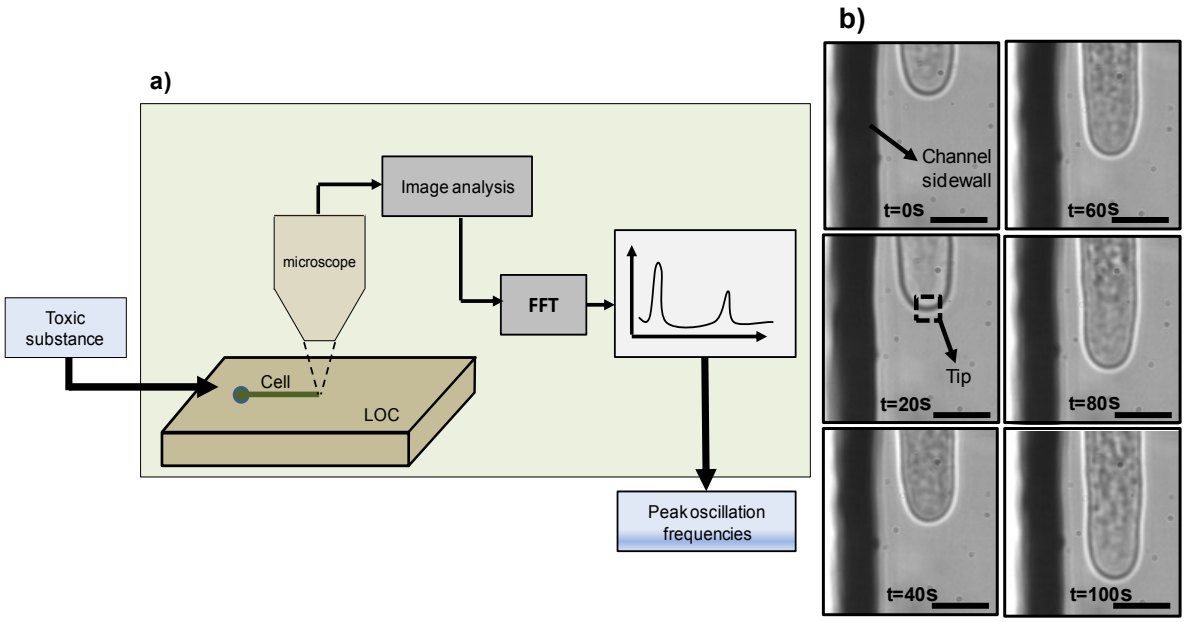

Figure 7.5: a) Experimental setup for toxicity detection by measuring the variation of higher and lower mode oscillation frequencies of the cell growth, b) Six different images of pollen tube growth with the time interval of 20s, Scale bar: 15 µm.

Briefly, the pollen tube growth was observed with bright-field microscope using 80X objectives. The straight growth of pollen tube along growth microchannels with time interval of 20s is shown in Fig. 7.5b for several frames of growth. The images of pollen tube growth were traced using NIH ImageJ software and the growth rate was measured from the relative distance of pollen tube tip in successive images. The statistical analysis of

pollen tube growth have shown that the growth of *Camellia* pollen tube in normal medium has steady growth pattern as the variation of properties of mean and standard deviation values of the growth rate were bounded within defined limits (Sanati Nezhad *et al.*, 2013d). The advanced waveform techniques of Fast Fourier transform (FFT) and Power Spectral Density (PSD) as well as window filtering techniques were used to identify the primary and secondary peak oscillation frequencies. In order to measure these two first oscillation frequencies of the growth rate, the sample rate of 2 frame per second was required. The normal *Camellia* pollen tubes growing in 8% sucrose concentration displayed oscillation with primary frequency of 0.01-0.05 Hz and a secondary frequency of 0.2-0.3 Hz. The pollen tube responded dynamically to the change of sucrose concentration from 8% to 10% through the shift of both primary and secondary peak frequencies (Sanati Nezhad *et al.*, 2013d).

Here in this paper, for toxicity detection of unfriendly agent on growth behavior of pollen tube, various concentrations of Al ranging from 20 μM to 400 μM were tested. Similar to static testing, after establishment of the pollen tube growth along microchannels to at least 300 μm, the medium including toxic Al was introduced into the chip with the flow rate of 5 μl/min using syringe pumping. Once the medium was replaced, the medium flow is stopped. For each concentration of Al toxic, one or few chips have been tested to find statistical variation of growth rate.

A large number of pollen tubes burst under high Al concentrations (Fig. 7.3), and hence, the toxicity detection using the dynamic of cell growth are carried out only under low Al concentrations where limited or no cell bursting occurs. Under 20 μM Al concentration, no

cell bursting was detected. Fast Fourier Transform (FFT) was used to extract the two first fundamental oscillation frequencies of the growth rate signal before and after inducing toxic agent. Because of difficulty of detecting peak frequencies from FFT analysis for some pollen tubes and knowing the effective range of secondary frequency of 20-30 mHz from statistical analysis (Sanati Nezhad *et al.*, 2013d), the waveform analysis of low pass filter with cutting frequency of 40 mHz, PSD analysis and Hamming and Chebychev window filters were applied to the signal in order to better distinguish the value of peak oscillation frequencies (Sanati Nezhad *et al.*, 2013d). For a sample pollen tube tested under 20 μM Al concentration, the results of FFT analysis and filtered PSD graph are seen in Fig. 7.6. The results of Fig. 7.6a,b show that the pollen tube oscillates with primary and secondary peak frequencies of 10 mHz and 270 mHz, respectively. The treatment with 20 μM Al solution did not alter the primary oscillation frequency while the secondary frequency was disrupted showing the high sensitivity of higher mode dynamic oscillation to the low concentration of toxic substance as shown in Fig. 7.6c,d.

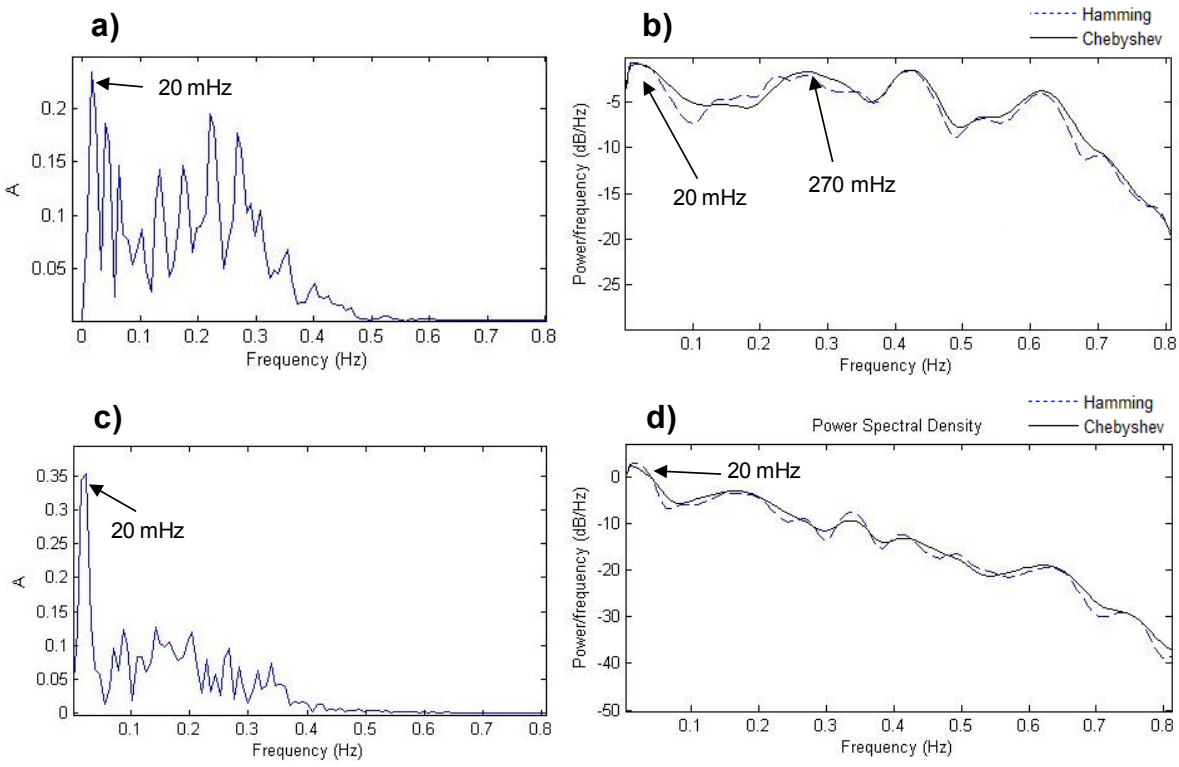

Figure 7.6: a,b) The FFT and filtered PSD analysis of cell growth rate for the pollen tube growing in a) normal medium, c,d) under 20 µM Al concentration. The primary peak frequency was not changed, while the secondary peak frequency was disrupted.

Despite the rise of the percentage of the bursted pollen tubes treated with 50 µM Al concentration, the effect of Al on the change of oscillation frequencies was studied using non-bursted pollen tubes. For a pollen tube oscillating with the primary and secondary peak frequencies of 43 mHz and 230 mHz, respectively before treatment, both primary and secondary peak frequencies were disrupted after exposure to 50 µM Al concentration. The primary peak frequency was disrupted as the new peak frequency was emerged at 110 mHz in presence of primary peak of 43 mHz as shown in Fig. 7.7. The secondary peak frequency (higher mode) was not detected with a strong peak after exposure which clearly shows a degree of disruption. The peak frequencies after treatment were measured when the pollen tube was subjected to the new growth environment. The results show that the

toxicity of Al is detectable using the observation of disruption of higher mode oscillation frequency under toxic stress. In several cases, the shift alteration of primary peak frequency can support the existence of toxic material in the growth medium detected by higher frequency modes.

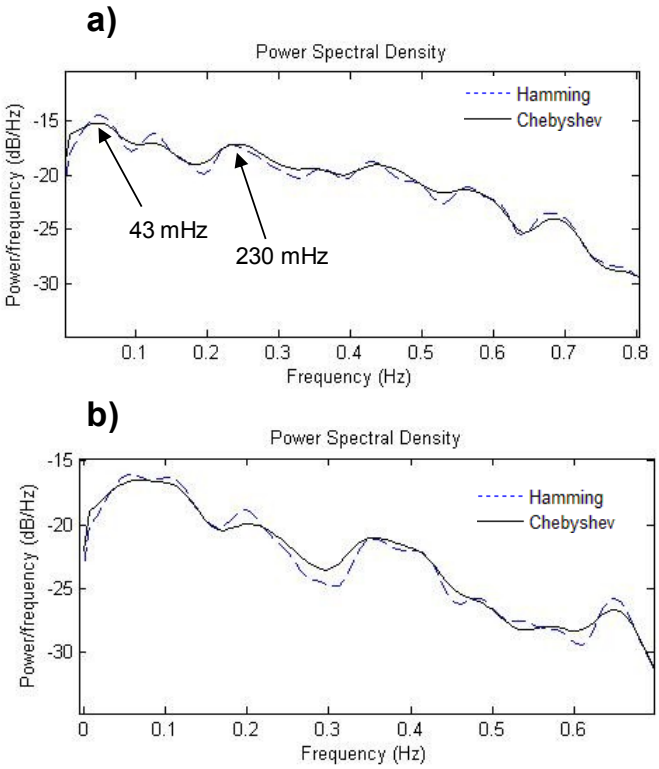

Figure 7.7: The power spectral density (PSD) analysis on growth rate of pollen tube growing in a) normal medium and b) under environment with 50 μM of Al concentration.

The results of Figures 6,7 show that the effect of toxic Al on dynamic oscillation frequencies cannot be simply detected in a concentration-based manner because the peak frequencies for different Al concentrations were disrupted. When the cell is subjected to toxic environment, the behavior of the pollen tube was altered at entire range of dynamic growth and thus it important to study the response of the cell over entire range of dynamic motion of the cell instead of studying only at discrete frequencies. The power associated

with cell growth rate (spectral power) is used as a criterion of dynamic response in order to quantify the cell behavior under different concentration of toxic Al. According to Parseval's theorem, the power of a time series signal x(t) integrated across all of time t is equal to the total power of its corresponding Fourier Transform X(f) integrated across all of its frequency components (f) defined by Eqn (7.1):

$$P_f = \lim_{t\to\infty}\left(\frac{1}{2t}\int_{t=-\infty}^{t=+\infty}|x(t)|^2\,dt\right) == \lim_{t\to\infty}\left(\frac{1}{2t}\int_{f=-\infty}^{f=+\infty}|X(f)|^2\,df\right) \quad (7.1)$$

Where f is the frequency, x(t) is the response at time t, X(f) is the amplitude of the frequency response of growth rate signal and P_f is spectral power. The integral of Fourier Transform over entire frequency range can be used to quantify the power associated with dynamic growth of the cell. Before using P_f as new parameter to detect the effect of toxic substance, the normal variations of P_f over long period of growth (300s) were tested for several pollen tubes growing in regular medium. For each pollen tube, the P_f was calculated for three subsequent time periods of growth, each period has the time span of 100s as shown in Fig. 8. The average variation of P_f for these three pollen tubes is below 13%.

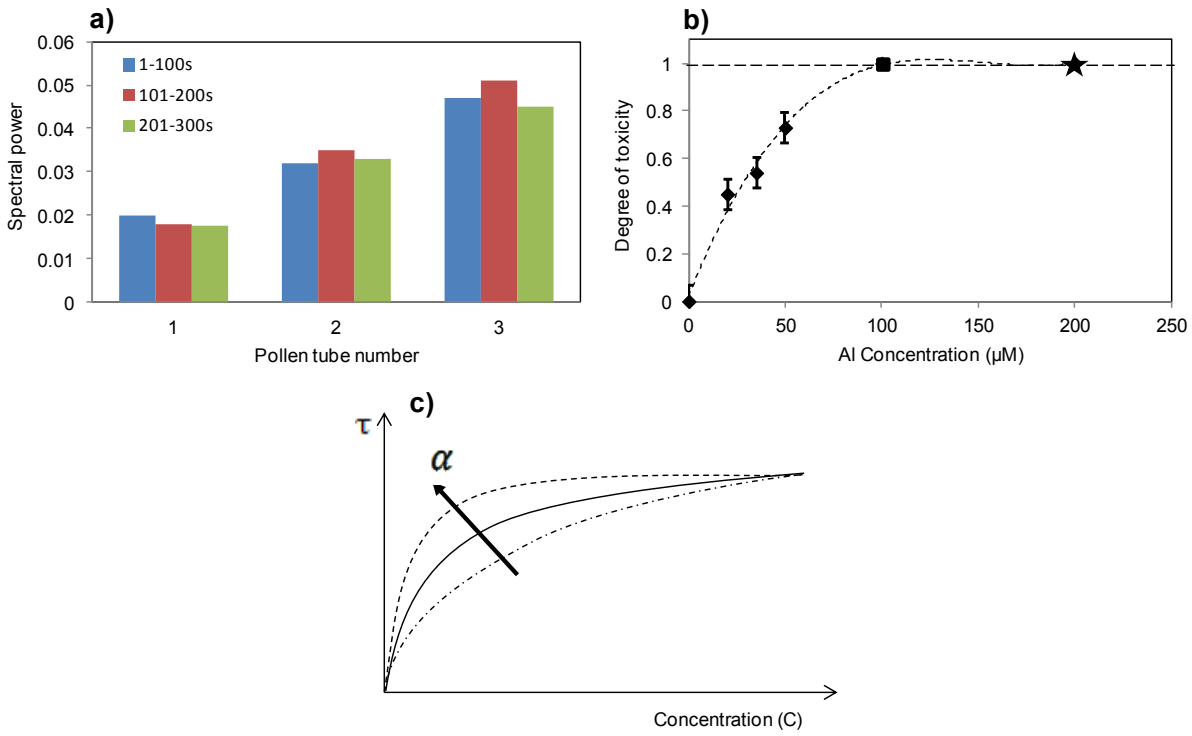

Figure 7.8: a) The normal variation of P_f for three different pollen tubes. For each pollen tube, P_f was obtained for three subsequent time periods of 100s for pollen tubes growing in normal medium, b) The change in P_f in presence of absence of toxic Al for three different pollen tubes treated with concentrations of 20 μM, 35 μM and 50 μM, respectively.

Although under toxic Al treatment, the peak oscillation frequencies were disrupted (Fig. 7.6,7.7) in compare to the shift of peak oscillation frequencies under friendly agents (Sanati Nezhad *et al.*, 2013d), P_f as a parameter associated with dynamic growth can represent how pollen tube responds to the chemical change of growth environment. Knowing the normal variation of P_f for pollen tubes growing in regular medium, any significant deviation of P_f from the normal variation reflects the effect of toxic agent on cell behavior. For different pollen tubes treated with Al concentration of 20 μM, 35 μM and 50 μM concentrations, P_f was calculated for before and after treatment of pollen tube with Al toxic, each, in time series of 100s (Fig. 8b). The degree of toxicity (τ) is defined based

on the spectral power of normal growth (P_f^n) of pollen tube and spectral power of tube after treatment with Al toxic (P_f^t) such that:

$$\tau = \frac{P_f^n - P_f^t}{P_f^n} \tag{7.2}$$

Since maximum normal spectral power variation of 13% is expected for pollen tubes, the same deviation is expected for the τ value for each concentration (Fig. 7.8b). The comparison of τ value calculated for each pollen tube treated with Al toxic in Fig. 8b with the normal variation of spectral power for regular pollen tubes (13% variation) proves that τ value can effectively be used for detection of toxicity in a concentration-based manner. For Al concentrations of 100 μM and 200 μM, the pollen tubes stop the growth or busted, respectively which means P_f^t=0 and corresponding $\tau = 1$. The variation trend of degree of toxicity over Al concentrations was estimated by a polynomial of degree 3 as shown in Fig. 7.8b. Similar trend of variation is expected for other toxic agents on pollen tube behavior. The degree of toxicity (τ) can be defined as a function of concentration (C) and the toxicity level of agent (α) as $\tau = f(C, \alpha)$. In the case of a more toxic substance with higher toxicity level of α, the trend varies sharper, but it will have slower trend for less toxic agents as schematically shown in Fig. 7.8c.

7.5 Discussion

Comparing the response of *Camellia* pollen tubes exposed to the change of friendly sucrose concentration (Sanati Nezhad *et al.*, 2013d) or toxic Al reveals that although in both cases, the average growth rate/length reduces under treatment, but the dynamic

response of pollen tube behaves in different ways. In treatment with friendly sucrose concentrations, the pollen tubes were able to adapt with the new growth environment. Hence both primary and secondary peak frequencies were shifted to new condition without any disruption of oscillation or emerging new peaks (Sanati Nezhad *et al.*, 2013d) even against 2 mM variation on sucrose concentration. But in the case of Al treatment, even under very low concentrations, the peak frequencies were either disappeared or weakened through emerging new peaks which indicates the presence of stress in cell induced by toxicity. This difference of dynamic behavior in response to friendly sucrose and toxic Al shows the potential of pollen tube to distinguish friendly and non-friendly substances and to detect the combinatory effect of different substances.

Compared to agarose-based assays for pollen tube studies and regular assays in toxicity detection, the chemical treatment of pollen tube within microfluidic platform simplify the change of growth environment and provide reproducible and identical growth conditions. In addition, since the pollen grain is fixed at the entrance of microchannel and the growth direction is confined along the channel with slight height change, the growth rate can be measured with a high sample rate of 2 frames per seconds sufficient enough to easily detect higher mode oscillation frequency. Moreover, toxicity diagnosis using characterization of static and dynamic response of pollen tube within microfluidic environment is simpler in handling and measurement, more accurate and also is carried out in 2-3 hr considerably shorter than the previous techniques (Sheng *et al.*, 2012).

From cellular mechanism point of view, in normal plant cell wall, pectin reacting with calcium ions causes the gelation of the pectins and generates relatively soft cell wall at apical region. Under large concentrations of Al treatment, the Al effectively interferes the binding of pectin-calcium and reduces the cell wall elasticity resulted in inhibition of normal growth and eventually busting. Under low Al concentration, this interference is limited and only interrupts the feedback loops responsible for controlling the oscillatory growth (Sawidis and Reiss, 1995) (Sheng *et al.*, 2012) (Zonia, 2010; Zonia *et al.*, 2006).

The effect of toxic Al substance on pollen tube growth or its oscillation pattern was concentration-dependent so that the time of bursting and degree of oscillation disruption could be related to the substance concentration. Similarly, the toxicity testing of other toxic materials such as various heavy metals and mercury using current technique within microfluidic platform can be carried with the same ToxChip.

7.6 Conclusions

The parameters of time of bursting, percentage of bursting and change of growth rate were used as complementary criteria to detect wide range of Al concentrations using pollen tube as whole cell sensor. The variation of both lower and higher mode dynamic oscillation of cell growth rate under different toxic Al concentrations was complementarily detected as dynamic cell response. This work presents an application of pollen tube as single cell sensor for toxicity testing and can be extended to detect other toxic substances and eco-friendly ions. Replacing the microscopy detection with integration of optical detection or

pressure sensors within microchannels would be beneficial to change the proposed device to a point-of-care (POC) microdevice for toxicity detection.

Chapter 8

Quantification of the Young's Modulus of the Pollen Tube Cell Wall Through Cell Bending Using Lab-on-Chip Technology

8.1 LOC for measuring elastic modulus of pollen tube cell wall

Addition to the interesting potential of microfluidic environment in characterizing the static and dynamic response of pollen tube to global and local chemical treatments (explained in chapters 4-7), the microfludic platform is able to study the biomechanics of pollen tube and provide *ex vivo* environment for studying invasive life style of pollen tube. This chapter presents a Bending LOC (BLOC) for measuring the elastic modulus of pollen tube cell wall which is not measurable using conventional methods. This work has been published in *Lab on a chip* journal, DOI: 10.1039/c3lc00012e.

Abstract

Biomechanical and mathematical modeling of plant developmental processes requires quantitative information about the structural and mechanical properties of living cells, tissues and cellular components. A crucial mechanical property of plant cells is the mechanical stiffness or Young's modulus of its cell wall. Measuring this property in situ at single cell wall level is technically challenging. Here, a bending test is implemented in a chip, called Bending-Lab-on-chip (BLOC), to quantify this biomechanical property for a widely investigated cellular model system, the pollen tube. Pollen along with culture medium is introduced into a microfluidic chip and the growing pollen tube is exposed to a bending force created through fluid loading. The flexural rigidity of the pollen tube and the Young's modulus of the cell wall are estimated through finite element modeling of the

observed fluid-structure interaction. An average value of 350 MPa was experimentally estimated for the Young's modulus in longitudinal direction of the cell wall of Camellia pollen tubes. This value is in agreement with the result of an independent method based on cellular shrinkage after plasmolysis and with the mechanical properties of in vitro reconstituted cellulose-callose material.

8.2 Introduction

Plant cells are surrounded by a stiff extracellular matrix, the cell wall. This structural feature consists mostly of polysaccharides and is crucially important both for plant development and for the mechanical behavior of plant tissues under external loading. Modeling mechanical aspects of plant cell functioning therefore requires quantitative information on the mechanical properties of this structure. Plant cell walls are formed in two stages. The primary cell wall is the only layer surrounding young undifferentiated cells and parenchymatic cells. Its mechanical properties determine when and how plant cells grow, a process that is driven by the internal turgor pressure but controlled in space and time by the cell wall (Geitmann *et al.*, 2009c). The secondary cell wall is formed in certain cell types during the final steps of differentiation and it rigidifies the wall significantly. The mechanical properties of both the primary and secondary plant cell walls have traditionally been measured using tensile tests such as instron measurements for which macroscopic pieces of tissue are used (Cosgrove, 1993). Mechanical measurements on individual, living plant cells are technically more challenging, due to the small size of the objects (Geitmann, 2006b, c). One of the techniques used is based on the pressure probe, an invasive method that requires injecting a microscopic needle into the cell (Tomos *et al.*, 1999). By

increasing the internal pressure through injection of oil and measuring the resulting increase in cell size, the volumetric Young's modulus of the cell wall can be determined. A less invasive technique, cell compression, has been used to assess the fracture force necessary to rupture the cell wall (Wang *et al.*, 2006). However, both of these techniques assume that the cell wall mechanical properties are distributed relatively uniformly around the measured cell. They are unsuitable for cells with non-uniform distribution of mechanical properties since the weakest region within the cellular envelope would dominate the overall behavior. Subcellular resolution of cell wall mechanical characterization has been achieved with micro-indentation and atomic force microscopy. These have been employed to with the aim to assess the mechanical properties of living plant (Routier-Kierzkowska *et al.*, 2012) and fungal (Zhao *et al.*, 2005) cell walls. Local compression or penetration forces are applied on a material and can serve to assess the Young's modulus, based on the assumption that the material is isotropic and homogeneous. However, the plant cell wall is not a homogenous material, considering its complex composition of multiple types of polysaccharides, various types of molecular linkages and highly anisotropic mechanical behavior (Baskin, 2005; Cosgrove, 2005; Geitmann, 2010b). Therefore, the local stiffness value obtained by an invasive or compression based technique such as atomic force microscopy does not necessarily correspond to the overall tensile behavior of the cell wall material, the crucial property that determines the relationship between the cell wall and the turgor pressure. To obtain information about the tensile strength of the cell wall, the method of choice, therefore, needs to be the application of a tensile stress. This is not trivial when a single cell is to be measured. Excision of the wall of a single plant cell has been accomplished for such tensile testing(Wei *et al.*, 2006), but

was only feasible due to the enormous size of the test cell in question, a Chara algae (diameter approximately 1 mm).

Tip growing cells such as fungal hyphae, root hairs and pollen tubes (Fig 8.1) are much smaller in diameter than Chara algae but display significant subcellular variations in biochemical composition of the cell wall in the growing region of the cell (Deacon, 1997; Geitmann and Steer, 2006b) that are reflected in spatial differences in mechanical cell wall behavior (Geitmann *et al.*, 2004; Zerzour *et al.*, 2009b). Among these cell types, the pollen tube is the best investigated in terms of the spatial distribution of cell wall components (Chebli *et al.*, 2012) and the mechanical principles governing the growth process (Fayant *et al.*, 2010b; Kroeger *et al.*, 2011b). The pollen tube is a cylindrical protuberance formed from the pollen grain, the male gametophyte in the flowering plants, upon contact with a receptive pistil, and it has the function to deliver the sperm cells to the ovule for fertilization.

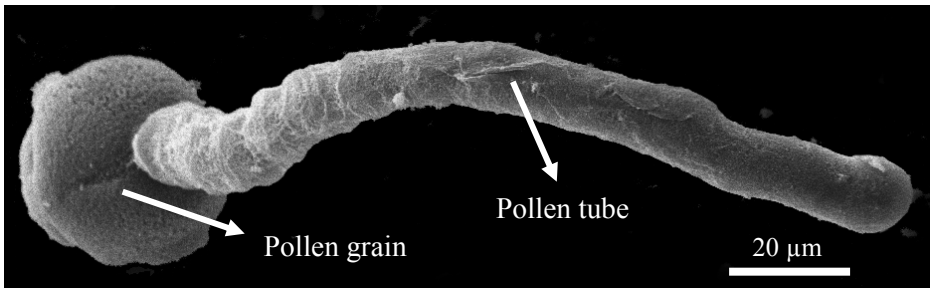

Figure 8.1: Scanning electron micrograph of a pollen tube emerging from a Camellia pollen grain.

Modeling based on finite element analysis predicts that pollen tubes have a relatively soft cell wall at the apex, whereas the wall forming the large cylindrical portion of the cell is expected to be more rigid (Fayant *et al.*, 2010c). Pressure based methods (Tomos and

Leigh, 1999) may therefore not allow to determine the mechanical properties of the cylindrical region of the cell wall since the apical region might yield and rupture before the cylindrical region is sufficiently stretched for its deformation to be measurable. Comparative studies using micro-indentation have allowed to monitor temporal changes to the cell wall in space and time (Geitmann and Parre, 2004; Zerzour *et al.*, 2009b), but this technique was not suitable to determine absolute values of the mechanical properties of the tube wall, since the geometry of the cell-indenter interface critically influences the measured values (Bolduc *et al.*, 2006). Recently, Vogler et al (Vogler *et al.*, 2012) used cellular force microscopy (CFM), a local compression technique similar to micro-indentation and atomic force microscopy, to quantify the local apparent stiffness of the pollen tube and to estimate the Young's modulus of the cell wall through numerical analysis. This method provided a first experimental estimation for the Young's modulus of the pollen tube cell wall. However, given that in this method the turgor pressure significantly influences the measured values for apparent cellular stiffness, the deduced values for the Young's modulus and tensile properties of the cell wall strongly depend on a number of assumptions such as cell wall thickness, fully compressible cell wall material and frictionless contact between pollen tube and CFM tip, thus introducing several potential sources for imprecision. The pollen tube has become an important cellular model system (Cheung and Wu, 2008), whose growth behavior has been the subject of numerous modeling attempts (Kroeger and Geitmann, 2011b; Kroeger *et al.*, 2012a). Hitherto, those models that include the mechanical properties as a parameter, used values obtained from in vitro reconstituted plant cell wall material (Fayant *et al.*, 2010c), for example those for pectin or cellulose (Edge *et al.*, 2000; Endress *et al.*, 1996). Given that living cell walls

comprise a complex network of several types of polymers the composition and stoichiometry of which vary between cell types and plant species, relying on information obtained from in vitro reconstituted, individual cell wall components is unsatisfactory at best. Therefore, the quantitative determination of the mechanical properties of the pollen tube cell wall represents a fundamental piece of information required for future biomechanical modeling of this cell type in particular, and it represents a proof of concept for other walled cells of cylindrical shape. Furthermore, a quantitative experimental assay will allow phenotyping of mutants and assessing the effect of pharmacological and enzymatic treatments in more reliable manner.

In this chapter, we present a Lab-on-chip (LOC) approach to quantitatively determine the Young's modulus of the Camellia pollen tube cell wall based on a whole cell bending test. For this purpose we used an implementation of the TipChip, a microfluidic based platform recently developed for the analysis of tip growing cells (Agudelo *et al.*, 2012c). Similar to other Bio-MEMS devices that are used for diagnostic use, drug development and biosensor assays (Cheung and Renaud, 2006b; Giouroudi *et al.*, 2008a; Nuxoll and Siegel, 2009b), the closed microenvironment allows for cellular analysis (Tatic-Lucic, 2007) within the microfluidic environment in order to characterize the cellular response to the external signals.(Grossmann *et al.*, 2011b; Takayama *et al.*, 2001) The particular adaptation of the TipChip consists in the fact that spherical cell bodies such as pollen grains are injected into the LOC, positioned in front of narrow microchannels by fluid flow and that only after positioning the actual cellular protuberance to be studied, the pollen tube, is formed. In the present set-up the pollen tube is first guided to grow through a short microchannel and

subsequently into a larger bending test chamber where it is exposed to a bending force applied by fluid flow orientated perpendicular to the tube. Based on the observed flexural rigidity of the cell, the Young's modulus of the cell wall in longitudinal direction is estimated using finite element analysis of the experimental geometry.

8.3 Materials and methods

8.3.1 LOC design

The Bending-Lab-On-Chip (BLOC) employs fluid loading on a trapped and elongated pollen tube with the aim to apply a bending load. The overall design consists of a main chamber to deliver and trap a single pollen grain, a growth microchannel through which the growing tube is guided into the bending test chamber where it is exposed to the fluid loading (Fig. 8.2,A). The main chamber consists of an inlet to introduce the pollen grain suspension, the entry of a single microchannel at which a pollen grain is to be trapped, and an outlet to remove any excess accumulation of pollen grains. Positioning of the pollen grain is achieved by injection of the pollen suspension into the pollen inlet by a syringe pump and by hydrodynamic force that transports one or two pollen grains into the entrance of the growth microchannel. The growth microchannel is fed by an additional channel, the control channel, that allows to position the pollen tube against the opposite side wall of the growth microchannel. The test chamber includes an inlet and outlet for introducing fluid flow in a direction perpendicular to the elongating pollen. This design ensures the application of nearly uniform fluid loading on the pollen tube with the aim to cause bending (Figs. 2,B,C).

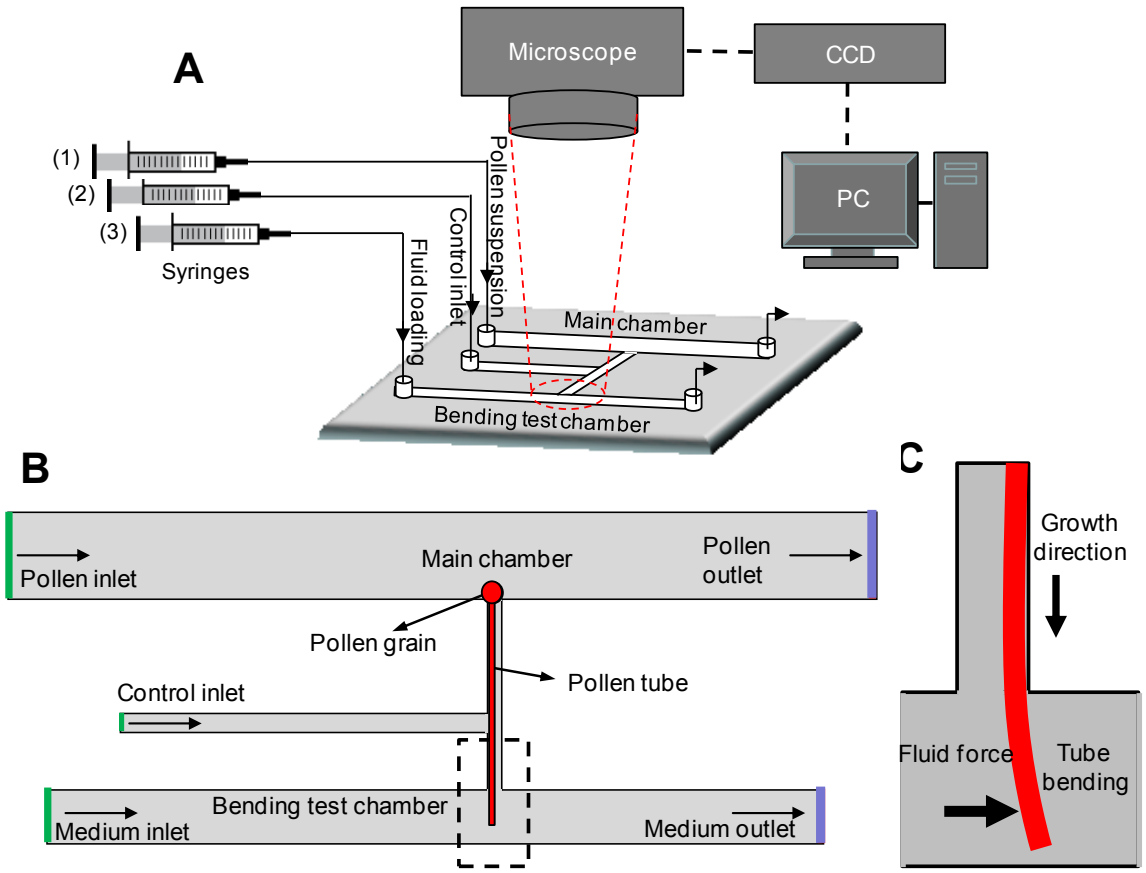

Figure 8.2: BLOC design, **A)** Schematic design of BLOC set-up with three inlets and two outlets for bending test on the pollen tube. **B)** Details of the BLOC microfluidic network. The design consists of the main chamber to introduce the pollen grain suspension, a growth microchannel into which the elongating tube is guided, a control inlet to position the pollen tube against the opposite side wall and the bending test chamber for the application of flow induced bending force. **C)** Close up view of pollen tube bending under fluid loading within the bending test chamber.

The dimensions of the different components of the microfluidic network were chosen to fit the dimensions of pollen grains and tubes from *Camellia japonica*. The microchannel was set to be 30 µm wide to accommodate the pollen tube (typical diameter: 12-19 µm) and to prevent the grain (typical diameter 60 µm) from entering. The depth of the entire network was 80 µm to enable pollen grains to move freely without stacking vertically. The width of the testing chamber was set to 300 µm. The pollen tube was allowed to grow along the

growth microchannel and then to enter and grow into the test chamber. The bending tests were executed when the length of pollen tube portion reaching into the bending test chamber was at least 150 μm.

8.3.2 LOC fabrication

The fabrication follows conventional procedures and starts with the fabrication of a mold on SU8 negative photoresist (MicroChem Corp.) using standard photolithographic technique. To reach the thickness of 80 μm, SU-8 2035 is spin coated on silicon wafer. The SU-8 is baked for 3 min at 65ºC and for 7 min at 95ºC on a hotplate. After soft-baking, the resist is cooled down at room temperature and exposed to UV light using a photo mask for 30s. Post-exposure bake step is then carried out by baking the resist for 3 min at 65ºC and for 6 min at 95ºC in order to cross-link the SU-8. The SU-8 layer is then developed to obtain the SU-8 mold. The microfluidic device is then made by soft lithography of Polydimethylsiloxane (PDMS) compound on SU8 mold. The cured PDMS layer is peeled off from the mold and bonded to a glass cover slip to seal the microfluidic network. Fig 8.3 shows the design architecture of the fabricated device. It was noticed repeatedly that the pollen grain and tube is pushed backward when the elongating tube encounters a mechanical obstacle or when the fluid flow is applied in the direction opposite to the growth direction. This made straight growth microchannels unsuitable for the bending test. Hence, a kink had to be introduced into the growth microchannel to immobilize the tube and to prevent any backward movement potentially induced due to the fluid pressure in the control channel or in the bending test chamber (Figs. 8.3B,C).

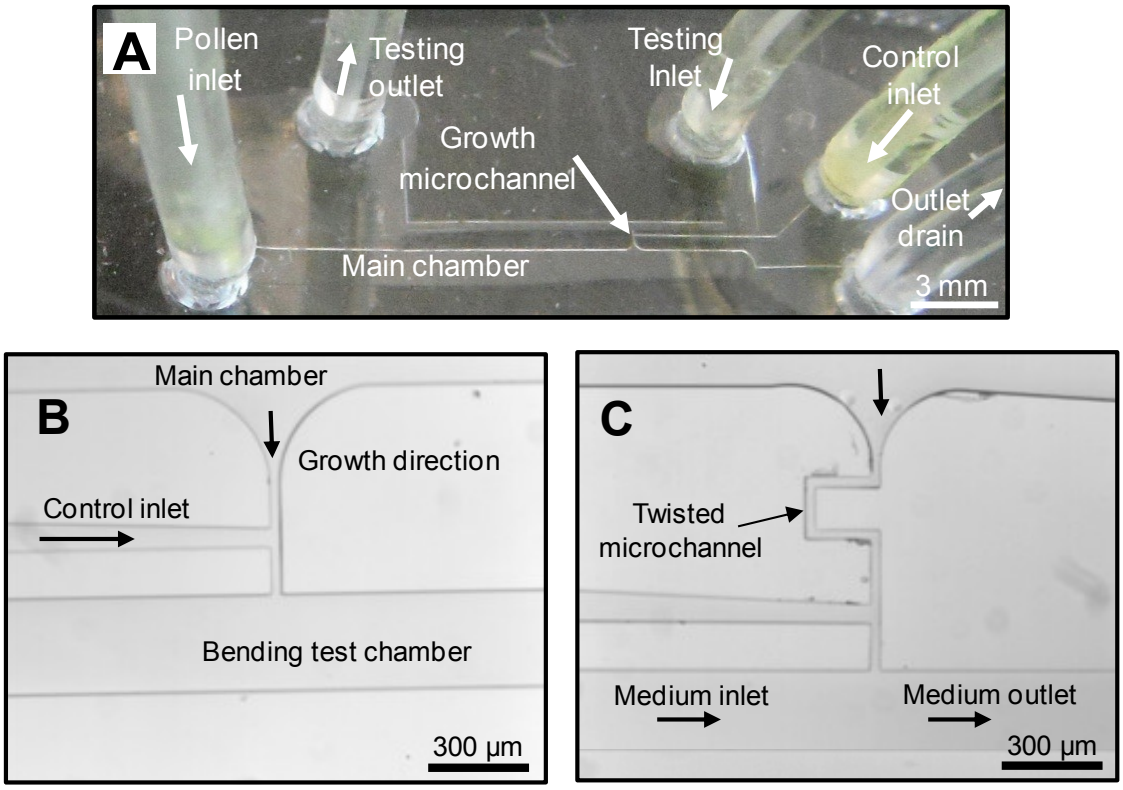

Figure 8.3: Design architecture of fabricated device, A) Fabricated BLOC, B) Close up view of microfluidic network. A straight growth microchannel connects the main chamber to the bending test chamber. C) A kink was introduced into the growth microchannel to prevent any backward movement of pollen by the flow occurring in the control channel or test chamber.

8.3.3 Pollen collection and germination

Camellia japonica pollen collected from a plant in the Montreal Botanical Garden was dehydrated on anhydrous silica gel overnight and stored in gelatin capsules at -20°C. Before use, the pollen was rehydrated in a humid chamber at room temperature for at least 30 min. The pollen was then suspended in growth medium containing 2.54 mM $Ca(NO_3)_2 \cdot 4H_2O$, 1.62 mM H_3BO_3, 1 mM KNO_3, 0.8 mM $MgSO_4 \cdot 7H_2O$ and 8% sucrose (w/v) (Bou Daher and Geitmann, 2011d) and a drop of the suspension is placed on a microscope slide to monitor the beginning of germination. When the pollen started

germinating (approximately 30 minutes after contact with the growth medium) the suspension was introduced into the microdevice.

8.3.4 Optical microscopy

Micrographs of pollen tube bending under fluid force were taken with a 20X objective, 0.4 NA, and an inverted optical microscope Nikon Eclipse 80i equipped with Infinity 1 camera. Micrographs of pollen tube bursting were taken with a 40X objective, 0.65 NA.

8.4 Results

8.4.1 Bending of the pollen tube through fluid loading

To perform the bending test, a suspension of germinated *Camellia* pollen grains in growth medium was injected into the main chamber of the LOC using a syringe pump. The elongation of the growing tube was monitored microscopically until it had grown through the microchannel into the bending test chamber with at least 150 μm of tube length protruding into the test chamber (Fig 8.4B). In the particular LOC used for this bending test, three different types of inlets were connected to motor controlled syringes to enable controlled fluid flow (Fig 8.4A). Syringe 1 and inlet 1 enabled positioning of the pollen grains in the main chamber. Fluid flow through this inlet and through the outlet of the main chamber was blocked once a pollen grain was positioned at the entrance of growth microchannel. Inlet 2 supplied by syringe 2 fed the control microchannel and enabled fluid flow to mechanically position the pollen tube against the opposite wall of the microchannel. The fluid from inlet 2 was collected from the outlet of the bending test chamber. Once the pollen tube was positioned against the microchannel sidewall, the flow through the control channel was stopped. Subsequently, syringe 3 and inlet 3 were used to

supply the fluid flow used to exert a bending load on the portion of the pollen tube protruding into this chamber (Fig. 8.4A,B). The fluid from inlets 3 was collected through the outlet of the bending test chamber.

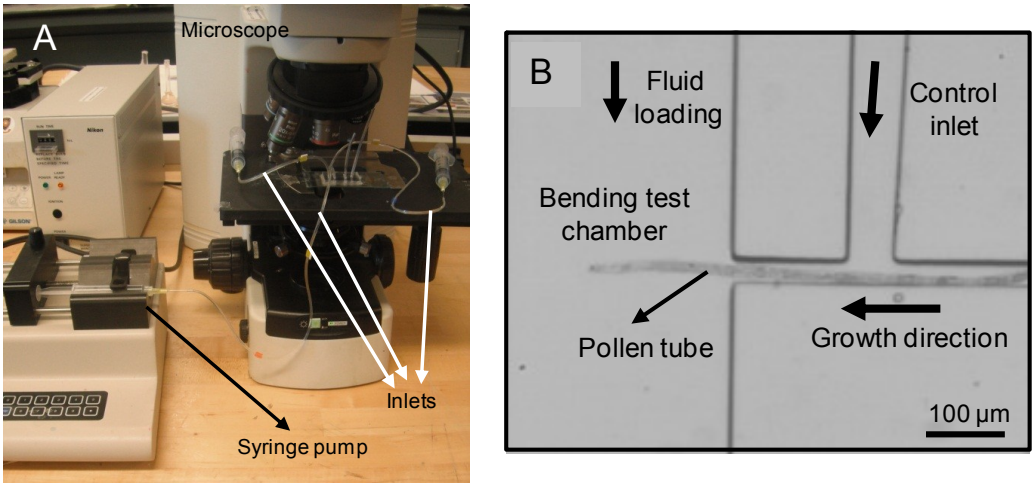

Figure 8.4: Bending test on pollen tube. A) Experimental setup for bending test, B) Growth of pollen tube along the growth microchannel toward the bending test chamber. Fluid flow through the control inlet pushes the pollen tube to the sidewall.

In order to perform a bending test, fluid flow through inlet 3 was initiated with varying inlet flow velocities and the resulting deflection of pollen tube at an equilibrium position was recorded by optical microscopy (Fig. 8.5). Upon suspending this flow, the pollen tube returned to the original shape.

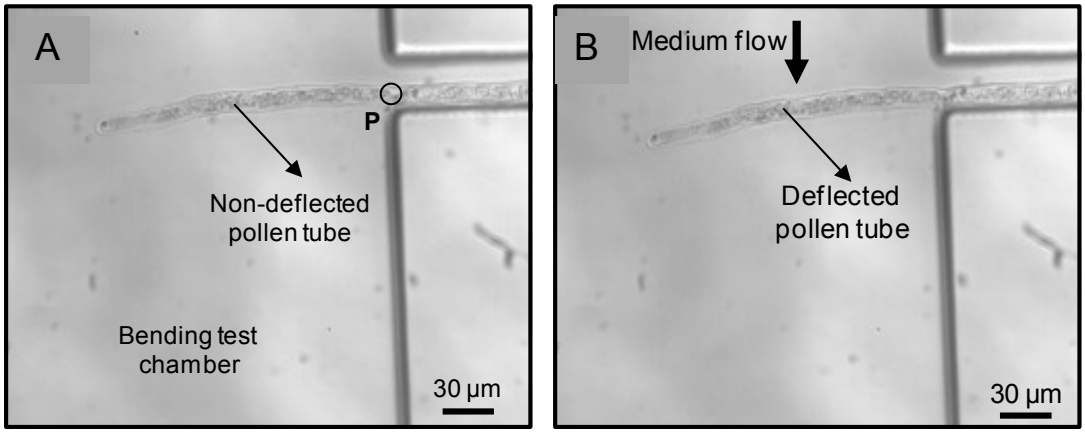

Figure 8.5: A) The non-deflected position of pollen tube within the bending test chamber. B) The deflected pollen tube under flow loading for inlet flow velocity of 30 mm/s.

Three different flow velocities through the test chamber were tested: 20, 30 and 40 mm/s. Since despite the microchannel kink and positioning against the microchannel side wall, the portion of pollen tube protruding into the test chamber was not fully supported at the exit point P of the microchannel (Fig. 8.5,A), the induced deflection of the pollen tube included both bending and rotation terms. Based on the free body diagram of this portion, the net rotational stiffness, K_R, includes the rotation term resulting from the separation of this portion from the distal portion of the tube located within the growth microchannel and the moment created by friction force. For lower fluid velocities, this was taken into account in the analysis. Higher fluid velocities were not used for calculation, since the pollen tube rotation around pivot point P became too large to quantify the bending component of the motion.

8.4.2 Determination of bending and rotation

In order to be able to estimate the material properties of the pollen tube cell wall from the bending experiment, only the deflection of the cell due to bending has to be considered. Since the observed fluid flow driven deflection of the pollen tube is the result of a

combination of rotation and bending, we modeled the experimental geometry to differentiate between the two movements (Fig 8.6A). K_T is the translational stiffness, K_R is the rotational stiffness, L is the length of the pollen tube suspended within the testing chamber and q is the flow-induced distributed force on the pollen tube. As the pollen tube portion located within the growth microchannel is supported by the channel sidewall, the translational stiffness (K_T) in this portion of the tube is approximated to infinity (Fig 8.6A). This means that the translational displacement of the pollen tube at pivot point P is close to zero and the tip deflection is a function of rotational and bending stiffness. Since the flow through the control channel toward the outlet of bending test chamber was stopped before performing the bending test, the pollen tube on protrusion portion was not affected by the force from the flow through the control channel . To extract the bending component from the combination of bending-rotation movement, the superposition principle was employed as shown in Fig 8.6,B. Based on the total deflection of pollen tube's tip (δ_T) and the rotational deflection (δ_θ) from image analysis, the pure bending deflection (δ_B) is obtained by subtraction (Fig 8.6, B).

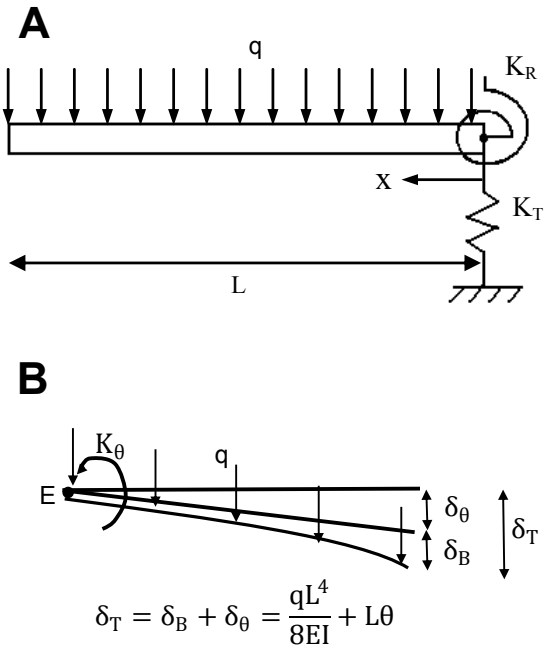

Figure 8.6: A) Schematic of the model for the combined bending and rotation of pollen tube subjected to fluid loading. B) Superposition principle for combined bending-rotation of pollen tube under flow testing.

The amount of rotation and, in consequence, the deflection due to rotation (δ_θ) was determined by tracing a line through key points E, F and G in the images of both the undeflected and the deflected tube (Fig 8.7). The difference between the total deflection and deflection due to rotation was estimated for three different medium flow velocities (Table 8.1). Finite element analysis was then used to solve the fluid structure interaction and to determine the Young's modulus of pollen tube cell wall subjected to pure bending fluid force.

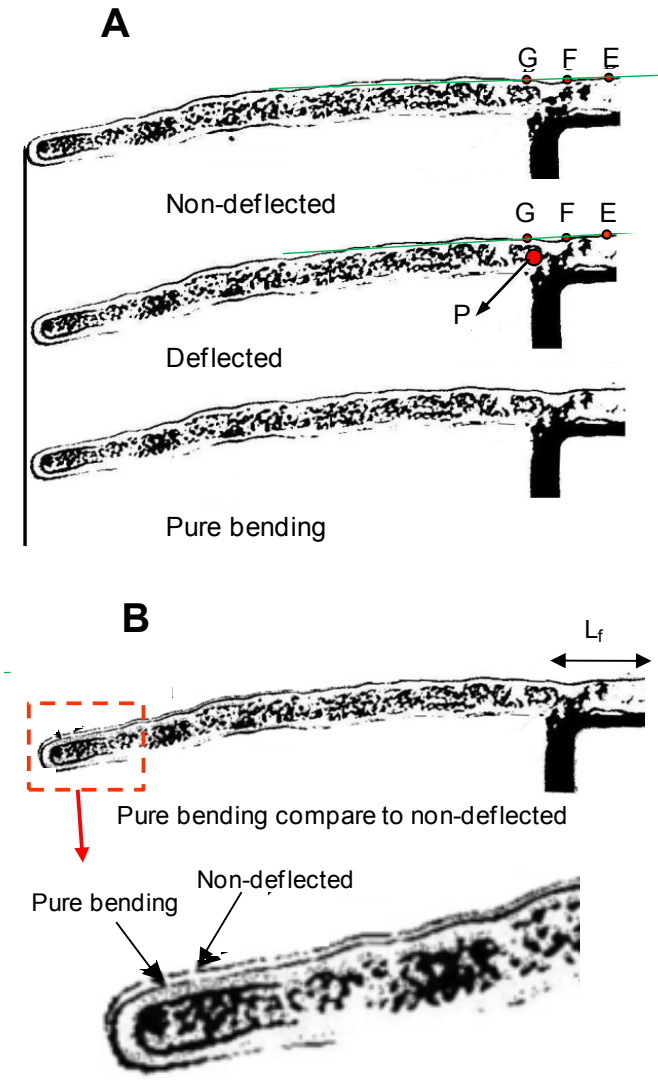

Figure 8.7: A) Image processing used to extract the pure bending component from the combined movement resulting from rotation and bending. The rotational deflection ($\boldsymbol{\delta_\theta}$) was determined by tracing a line through key points E, F and G in the images. B) The comparison of pure bending and non-deflected pollen tube shows the pure bending ($\boldsymbol{\delta_B}$) of pollen tube under fluid loading

Table 8.1 Experimental results of total pollen tube's tip deflection ($\boldsymbol{\delta_T}$), the rotational deflection ($\boldsymbol{\delta_\theta}$) and the pure bending deflection ($\boldsymbol{\delta_B}$) for different flow velocities

Fluid velocity (mm/s)	Total tip deflection ($\boldsymbol{\delta_T}$) (μm)	Rotational deflection ($\boldsymbol{\delta_\theta}$) (μm)	Pure bending deflection ($\boldsymbol{\delta_B = \delta_T - \delta_\theta}$) (μm)
20	8.1	7.2	0.9
30	10.8	9.3	1.5
40	14.7	12.6	2.1

8.4.3 Modeling 3D fluid flow for calculation of bending force

The bending deflection (δ_B), was used to model the interaction between pollen tube and fluid flow using finite element methods. For this purpose, only the test chamber with one inlet, one outlet and the suspended pollen tube subjected to fluid flow were considered, whereas the remainder of the microfluidic network was neglected (Fig 8.8,A). For simplification, the flow analysis was first solved to establish the velocity field and pressure gradient in the vicinity of the pollen tube. The flow-induced bending force, the sum of flow induced viscous drag force and pressure gradient over the pollen tube, were then extracted and applied to the thin-walled, pressurized cylindrical pollen tube to estimate the pollen tube deflection.

For the numerical analysis of the fluid domain, the pollen tube was modeled as a rigid rod, which means it has no deflection under fluid flow. The pollen tube was suspended within the test chamber (300 µm width, 80 µm height). The length and average diameter of the pollen tube were set to be 190 µm and 13.7 µm, respectively. The fluid properties were based on water with a density of 1000 kg/m^3 and dynamic viscosity of 0.001 Pa.s. As the distribution chamber outlet was blocked during the bending test, backward flow along the microchannel from the test chamber towards the distribution chamber was neglected. Microscopic observation showed that pollen tubes were typically positioned about 20 µm above the bottom surface of the test chamber. The flow was governed by Navier-Stokes and continuity equations. As boundary condition, the fluid velocities listed in Table 8.1 were used for inlet fluid velocity. The pressure at the outlet was set to atmospheric pressure. For all other boundaries, no-slip conditions were defined. COMSOL multiphysics

3.5 software was employed to solve the fluid domain governing equations. The element type of Lagrange Quadratic was chosen to mesh the design. The number of mesh elements for this simulation is 15480 with 84350 degrees of freedom. The results of the fluid analysis were calculated for the three inlet fluid velocities. Fig 8.8B illustrates the flow field for the inlet velocity of 30 mm/s.

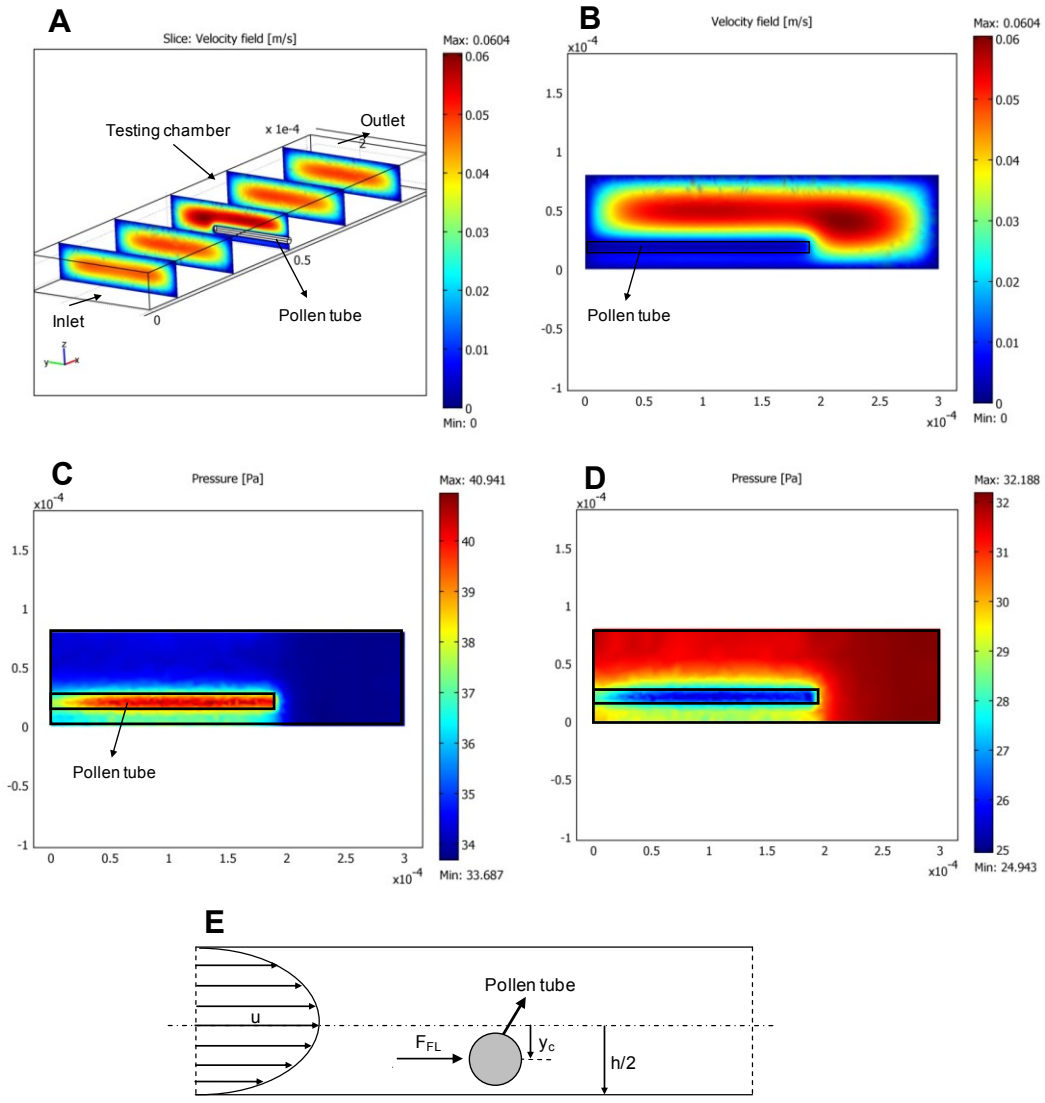

Figure 8.8: Estimation of the pressure gradient and velocity field within bending test chamber by 3D fluid flow analysis, **A)** Velocity field at different locations within the bending test chamber, **B)** Velocity field at the cross section of 1 µm prior to the contact with the pollen tube, **C)** Pressure distribution before the contact with the pollen tube, **D)** Pressure distribution after the contact with the pollen tube. **E)** Side view of the test chamber

The flow-induced bending force (F_{FL}) acting on the pollen tube consists of two components, the viscous drag force and the pressure component which can be determined by employing the drag coefficient(Janson *et al.*, 2004; Lien *et al.*, 2007) (Fig 8.8). Based on the drag coefficient, the viscous drag force per unit area (F_D) is obtained by equation (8.1).

$$F_D = \frac{1}{2}\rho C_D U^2 \tag{8-1}$$

where C_D is the drag coefficient, ρ is the fluid density and U is the fluid velocity. The flow pattern around a cylinder depends on the Reynolds number. For very low Reynolds number (Re <0.5), the viscous drag is dominant and the Stoke's law is valid(Kundu, 1990) to obtain the C_D as C_D =24/Re, where Re=Ud/ν and ν=μ/ρ is the dynamic viscosity of the fluid and d is the diameter of tube. Due to non-slip boundary conditions at the chamber sidewall, the velocity profile follows the parabolic equation (Fig. 8.8E). Since the pollen tube axis is not at the vertical center of the chamber (h/2), the fluid velocity corresponding to the center axis of pollen tube is considered as U within equations (8.1).

The results of Fig 8.8,C,D indicate that the pressure difference along the pollen tube length is negligible. This means that the pressure component of the flow-induced force (F_{FL}) can be modeled as an evenly distributed force on the boundaries of the pollen tube. The total bending force on the pollen tube is obtained by adding the pressure loading and the viscous drag force.

8.4.4 Reverse engineering of the Young's modulus of the cell wall

For 3D structural analysis, the pollen tube was modeled as a long, isotropic thin-walled cylindrical tube (Fig 8.9A). The geometry of pollen tube was extracted from microscopic data. The thickness of the cell wall of the *Camellia* pollen tube was set to be 250 nm based on the estimate from brightfield micrographs taken with a 60X objective (NA 1.4) and transmission electron micrographs.(Hasegawa *et al.*, 1996; Nakamura *et al.*, 1982) The Poisson ratio was set to 0.3 (Bolduc *et al.*, 2006). Fixed boundary conditions were set for the fixed end of pollen tube. Using COMSOL Multyphysics 3.5 software, the flow-induced bending force (F_{FL}= F_D) was then applied to the cylindrical structure representing the pollen tube and used to extract the Young's modulus of the pollen tube cell wall in longitudinal direction using iterative fitting (Fig. 8.9B, Table 8.2). The element type of Lagrange Quadratic was chosen to mesh the pollen tube. The number of mesh elements for this simulation is 89756 elements with 1340987 degrees of freedom. The sensitivity of the results to the number of mesh elements was evaluated considering 5% criterion error. Identical values for the compression and tension elastic moduli of pollen tube cell wall in longitudinal direction were assumed. The average of the estimated values based on measurements taken at different fluid velocities was approximately E=350 MPa.

Table 8.2 Estimation of Young's modulus for different medium inlet velocity

Inlet velocity (mm/s)	Pollen tube deflection (μm)	Estimated E (MPa)
20	0.9	340
30	1.5	315
40	2.4	390
		Average = 350

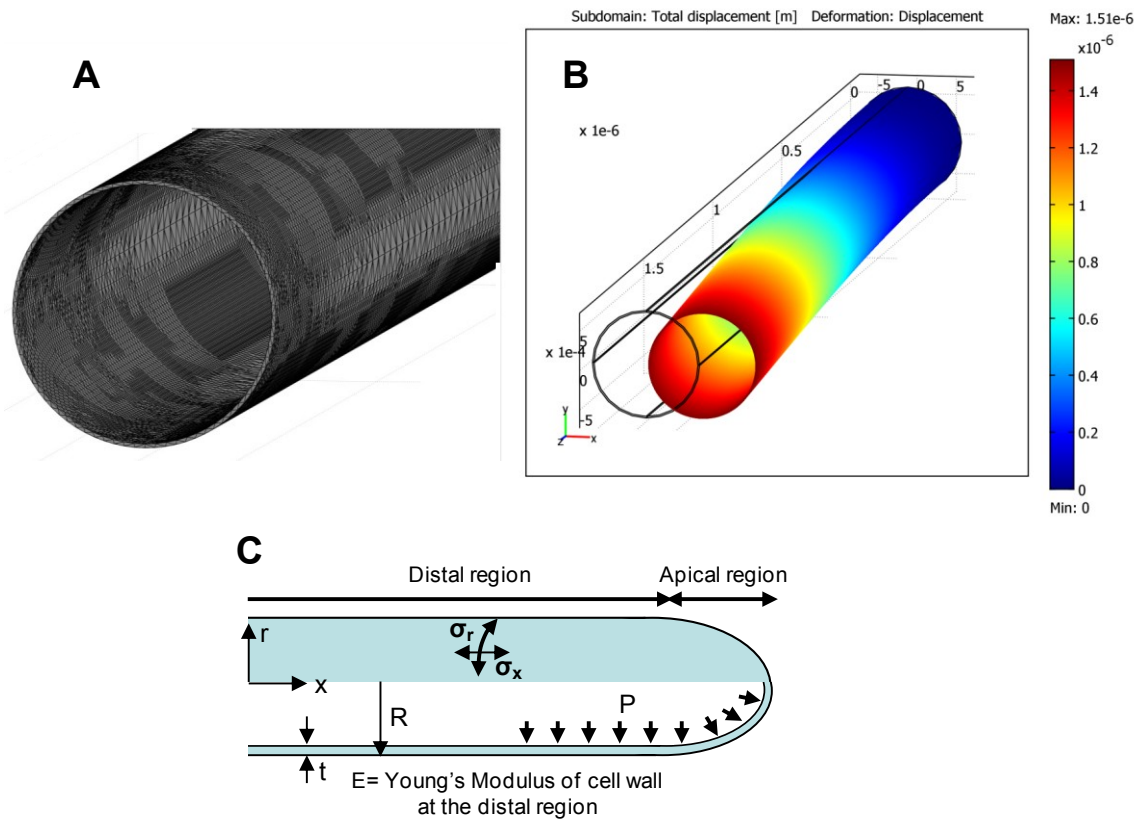

Figure 8.9: Numerical analysis of pollen tube deflection under fluid loading with the velocity of 30 mm/s, **A)** Close up of the 3D meshing of the pollen tube modeled as long cylindrical, hollow tube, **B)** Deflected pollen tube under fluid loading with the velocity of 30 mm/s. Color coding shows the displacement in µm from the original shape. **C)** Longitudinal (σ_x) and circumferential (σ_r) tensile stresses in pollen tube cell wall due to internal turgor pressure (P)

The pollen tube is a turgid cell with an internal turgor pressure P that supplies the driving force for elongation, but also ensures the erectile stability of the tube (Fig 8.9,C). This pressure causes longitudinal (σ_x) and circumferential (σ_r) tensile stresses in the tube cell wall (Fig 8.9,C). Our first calculation above did not take the internal pressure into consideration. To determine the contribution of the potential erectile effect of the turgor pressure on the estimated Young's modulus, the pressure was applied as distributed force on the internal surface of the tube. The result of the finite element analysis does not show a

significant effect of the 0.4 MPa turgor pressure on the estimated modulus. Next, the effect of the presence of the incompressible aqueous cytoplasm within the pollen tube was modeled as a solid with small resistance to shear and elongation. A Young's modulus of 1 Pa and a Poisson's ratio of 0.49 were used for the cytoplasm core. The numerical results show that at the small deflections simulated here, the presence of this liquid core changes the Young's modulus by less than 1%.

Based on microscopic measurements, we had assumed a cell wall thickness (t) of 250 nm for *Camellia* pollen tubes. To assess the possible error associated with the inaccuracy of the microscopic measurement of cell wall thickness, the effect of different cell wall thicknesses on the Young's modulus of the cell wall was estimated by iterative fitting. In these simulations, the pollen tube was subjected to 20 mm/s fluid loading. The numerical results show that for a wall thickness of 200 nm the Young's modulus would be 420 MPa whereas for a wall thickness of 300 nm it would be 280 MPa. This indicates that while knowing the exact wall thickness of the tested tube would be ideal for the calculation, the values of the Young's modulus remain within the same order of magnitude within a biologically relevant range of wall thickness values.

8.4.5 Assessment of Young's modulus from cell wall relaxation

To corroborate the value for the Young's modulus of the pollen tube cell wall obtained by the bending test, we employed a second experimental test. Upon bursting, and hence removal of the internal turgor pressure (P), the longitudinal (σ_x) and circumferential (σ_r) stresses on the tube cell wall are removed and the pollen tube shrinks in size, both

longitudinally and in girth (Fig 8.9,C). Pollen tube bursting can be induced experimentally or it occasionally occurs without obvious external trigger. We exploited such events to determine the length and girth of pollen tubes before and after bursting. In one case, the diameter of a *Camellia* pollen tube (d) was reduced from 15 µm before bursting to 14.55 µm after bursting. Assuming a turgor pressure of 0.4 MPa (Benkert *et al.*, 1997) and using $\Delta d=2PR^2/tE$, this yields E= 400 MPa for the Young's modulus in transverse direction (Fig 8.9,C). Considering that the length of the tube (L) was reduced from 370 µm to 362.7 µm and using longitudinal strain equation of $\Delta L=P(RL)/2Et$, E= 305 MPa is estimated for the Young's modulus in longitudinal direction.

8.5 Discussion

The primary plant cell wall is an intriguing material that has both elastic and plastic properties both of which can be modified by the cell to regulate plant developmental processes (Taiz, 1984). The cell wall has been compared to a composite material, although this analogy has its limitations. However, it is crucial to note that the material properties of the cell wall have the potential to be anisotropic in-plane, a characteristic that determines cellular geometry resulting from morphogenetic growth processes. Most values for the Young's modulus of primary plant cell wall material stem either from studies of *in vitro* reconstituted wall material (Chanliaud *et al.*, 2002) or bulk measurements of multicellular tissue samples. Published values for the Young's modulus vary from 30–110 MPa for the cell wall of the inner pericarp tissue of tomato and fungal hyphae (Wang *et al.*, 2006; Zhao *et al.*) to 3 GPa for the cell walls of potato tuber parenchyma tissue cells (Hiller *et al.*, 1996). A single cell study on *Chara corallina* algae yielded 300-400 MPa (Wei *et al.*,

2007). The accuracy of the estimated value depends on the precision of the measuring instrument, the assumptions for unknown parameters, and the power of modeling used to calculate these values (Dintwa *et al.*, 2011).

The estimated value of the Young's modulus reported here for the cylindrical cell wall of the *Camellia* pollen tube is comparable with the value of 120-250 MPa obtained for *in vitro* reconstituted cell wall material with similar molecular composition (Chanliaud *et al.*, 2002). More importantly, the mechanical model used here to extract the Young's modulus values from the bending experiments is relatively simple and straightforward thus reducing the influence of unknown or difficult to determine parameters. This distinguishes our method from measurements based on micro-penetration (Hiller *et al.*, 1996), compression (Blewett *et al.*, 2000),(Wang *et al.*, 2006) and micro-indentation (Zhao *et al.*) which necessitate modeling the complicated interaction between cell and indenter, requiring assumptions such as perfectly vertical loading and frictionless contact between cell and indenter, and where the turgor pressure critically influences the measured apparent stiffness values. Our calculations show that for a long rigid tube subjected to a small bending angle, the effect of turgor pressure on the calculated Young's modulus is negligible. The bending test thus allows for the quantification of the overall tensile properties of the cell wall, but on the other hand, it does not allow to measure subcellular variations such as the mechanical properties of the cell wall at the growing apex although these could be calculated based on prior modeling (Fayant *et al.*, 2010a). Our method is therefore complementary to those developed in the past.

The Young's modulus we established for *Camellia* pollen tubes is in the same order of magnitude but significantly higher than that measured by Vogler et al (Vogler *et al.*, 2012) for lily pollen tubes. Whether this difference is due to the use of different plant species, or whether this reflects the different measuring methods is unclear. However, the value determined in our bending test corresponds extremely well to the value determined in the conceptually completely different shrinkage test done on the same cell type (350 MPa in the bending test, 305 MPa for the longitudinal Young's modulus in the shrinkage test). Intriguingly, the shrinkage test also allowed us to calculate the transverse Young's modulus which was higher than the longitudinal Young's modulus with 400 MPa. This apparent anisotropy is consistent with a putatively necessary higher stiffness that is needed to counteract the higher tensile stress in circumferential direction in a tubular cell.(Geitmann and Steer, 2006a) However, it is unclear how this anisotropy can be explained structurally since in pollen tubes the cell wall components known to bear the main tensile stress, cellulose microfibrils, are known to be oriented helically with relatively low pitch, or even parallel to the long axis (Aouar *et al.*, 2010; Chebli *et al.*, 2012). Whether or not the other cell wall components, namely pectin or callose, contribute to any anisotropy therefore warrants further research (Parre *et al.*, 2005b; Parre and Geitmann, 2005c). In this context it is interesting to note that xyluglucans seem to play a role in determining the tube diameter and hence may influence the material properties in circumferential direction by crosslinking cellulose microfibrils (Chebli *et al.*, 2012).

The experimentally determined values for the Young's modulus of the pollen tube cell wall enable us to inform mechanical models of these cells (Fayant *et al.*, 2010c) and thus will

contribute to our understanding of cellular morphogenesis and plant developmental processes in much more accurate manner. Similarly, the effect of mutations or enzymatic treatments on cell wall structure and thus on the mechanical behavior of this cellular component can be assessed in quantitative fashion and by assessing overall cell wall properties. Our method is therefore complementary to previously used tests that are based on the application of highly localized deformations.

8.6 Summary and conclusions

In this paper, a novel experimental approach is presented to estimate the Young's modulus of the cell wall of *Camellia* pollen tubes. The deflection of the pollen tube is measured under flow-induced bending allowing for straightforward calculation of the Young's modulus of the cell wall material. This method can easily be adapted to pollen tubes of other plant species, to other tip growing cells (fungal hyphae, root hairs), but also to abiotic objects. The testing platform can be modified to perform sequential bending tests on different length portions of an individual tip growing cell and the effects of enzymes, inhibitors or mutation induced changes to the cell wall structure can be quantified in highly reproducible manner making the present BLOC platform an important tool for cell biology.

Chapter 9

Quantification of Cellular Penetrative Forces Using Lab-on-Chip Technology

9.1 Mechanical interaction of pollen tube and microgaps

In this chapter, the pollen tube response to the mechanical signals is explored through characterizing the interaction of pollen tube and micromechanical gap. The results help in understanding the pollen tube growth through different tissues toward the ovule and the tube bursting once it reaches the ovule. It also helps to understand the interplay of the turgor pressure and cell wall mechanical properties in regulating the growth. The content of this chapter has been published in *Proceedings of National Academy of Science (PNAS), Doi:10.1073/pnas.1221677110* with my contribution as the first author..

Abstract

Tip growing cells have the unique property to invade living tissues and abiotic growth matrices. To do so, they exert significant penetrative forces. In plant and fungal cells, these forces are generated by the hydrostatic turgor pressure. Using the TipChip, a microfluidic device developed for tip growing cells, we tested the ability to exert penetrative forces generated in pollen tubes, the fastest growing plant cells. The tubes were guided to grow through microscopic gaps made of elastic polydimethylsiloxane (PDMS) material. Based on the deformation of the gaps, the wedge force exerted by the elongating tubes was determined using finite element methods. The data revealed that increasing mechanical impedance was met by the pollen tubes through modulation of the cell wall compliance and thus a change in the force acting on the obstacle. Tubes that successfully passed a

narrow gap frequently burst raising questions about the sperm discharge mechanism in the flowering plants.

9.2 Introduction

Tip growing cells such as neurons, fungal hyphae, root hairs and pollen tubes have the remarkable ability to follow external guidance cues and to penetrate surrounding living tissues or abiotic matrices. The purpose of this invasive growth activity depends on the cell type and ranges from exploring the environment with the goal to procure nutrients and water (fungi, root hairs) to the establishment of contact between remote locations in the organism (neurons) and the delivery of gametes (pollen tubes). The common challenge encountered by tip growing cells is the necessity to overcome the mechanical impedance of the tissue or matrix to be penetrated. Two complementary strategies are generally employed, typically in combination: the cell produces enzymes or other agents to soften or dissolve the mechanical obstacle in its path, and/or the cell uses mechanical force to penetrate or displace the substrate. Whereas in animal cells the force required for a cell to migrate and invade is generated by the cytoskeleton either by way of motor proteins (Ishijima *et al.*, 1991) or by polymerization of the cytoskeletal filaments proper (Cojoc *et al.*, 2007; Theriot, 2000), in plant and fungal cells any pushing force is generated by the internal turgor pressure. This difference is consistent with the fundamentally different mechanics of the growth process in walled cells. Fungal hyphae and plant cells are surrounded by a polysaccharidic cell wall and all morphogenetic processes necessitate a mechanical deformation of this stiff extracellular matrix. The driving force for this process is supplied by the turgor pressure (Schopfer, 2006) and only if the cell's own wall is pliable

enough to yield to the turgor pressure can force be exerted onto the surrounding substrate. In tip growing cells, the turgor pressure has been determined to be between 0.4 and 0.8 MPa for fungal hyphae (Howard and Valent, 1996; Lew, 2005) and 0.1 to 0.4 MPa for pollen tubes (Benkert *et al.*, 1997). Although the cytoskeleton plays an important role in plant and fungal cell morphogenesis by regulating where and when cell wall components are deposited (Smith *et al.*, 2005), cytoskeletal polymerization activity is not directly involved in the force generation required for cellular growth or invasive activities (Money, 1997).

Because of the predominantly invasive life style of fungi and oomycetes, and the direct correlation between the efficiency of this behavior and pathogenicity, the mechanism of invasive growth in these organisms has been studied in detail (Bastmeyer *et al.*, 2002; Bechinger *et al.*, 1999; Money, 1997; Money, 2004a; Money, 2007b). Already more than a century ago, the invasive force of fungal hyphae has been measured using a gold membrane as mechanical resistance (Miyoshi, 1895), and more recently a strain gauge (Money, 2001), an optical wave guide (Bechinger *et al.*, 1999; Geitmann, 2006a), and optical tweezers (Wright *et al.*, 2005) have been employed for this purpose. The invasive ability of tip growing cells in plants on the other hand remains largely unexplored. Pollen tubes have been investigated using different concentrations of an agarose-stiffened growth matrix (Gossot and Geitmann, 2007), but no quantitative values for invasive force generation by this or other tip growing plant cells have been reported hitherto. Our goal was to address this lack of knowledge for the pollen tube, the fastest growing cell in the plant body, whose invasive life style is the fundamental underpinning of sexual reproduction in flowering plants.

The pollen tube is a tubular protrusion formed by the pollen grain upon landing on a receptive stigma. Its function is the delivery of the male gametes from the pollen grain (male gametophyte) to the female gametophyte located in the ovules of the flower. The pollen tube is, therefore, the crucial link between the sexual partners during the reproduction process in higher plants and its successful elongation growth is pivotal for fertilization and seed set. The distance the pollen tube has to cover is species-dependent and can be several tens of centimeters. Given that speed is a direct competitive selection factor for fertilization success, pollen tube growth rates are rather impressive with up to 1 cm/h (Taylor *et al.*, 1997; Williams, 2008). Albeit with somewhat reduced growth rates, pollen tube growth can easily be triggered in an *in vitro* set-up and the resulting cellular shape and morphogenesis are virtually identical to the *in situ* situation (Bou Daher *et al.*, 2008).

In order to find its path to the ovule, the pollen tube has to invade a series of tissues composing the pistil of the receptive flower (Palanivelu and Tsukamoto, 2011b). Starting from the stigmatic tissue on which it lands, it has to subsequently penetrate through the transmitting tissue, a cellular mass located within the central canal of the style that connects the stigma with the ovary (Erbar, 2003). Upon reaching the ovary, the pollen tube passes onto the internal surface of the placenta. It follows guidance cues emitted by the female gametophyte to embark on the funiculus, a stalk attaching the ovule to the placenta, and then targets the micropyle, an opening in the teguments enveloping the ovule (Fig 9.1).

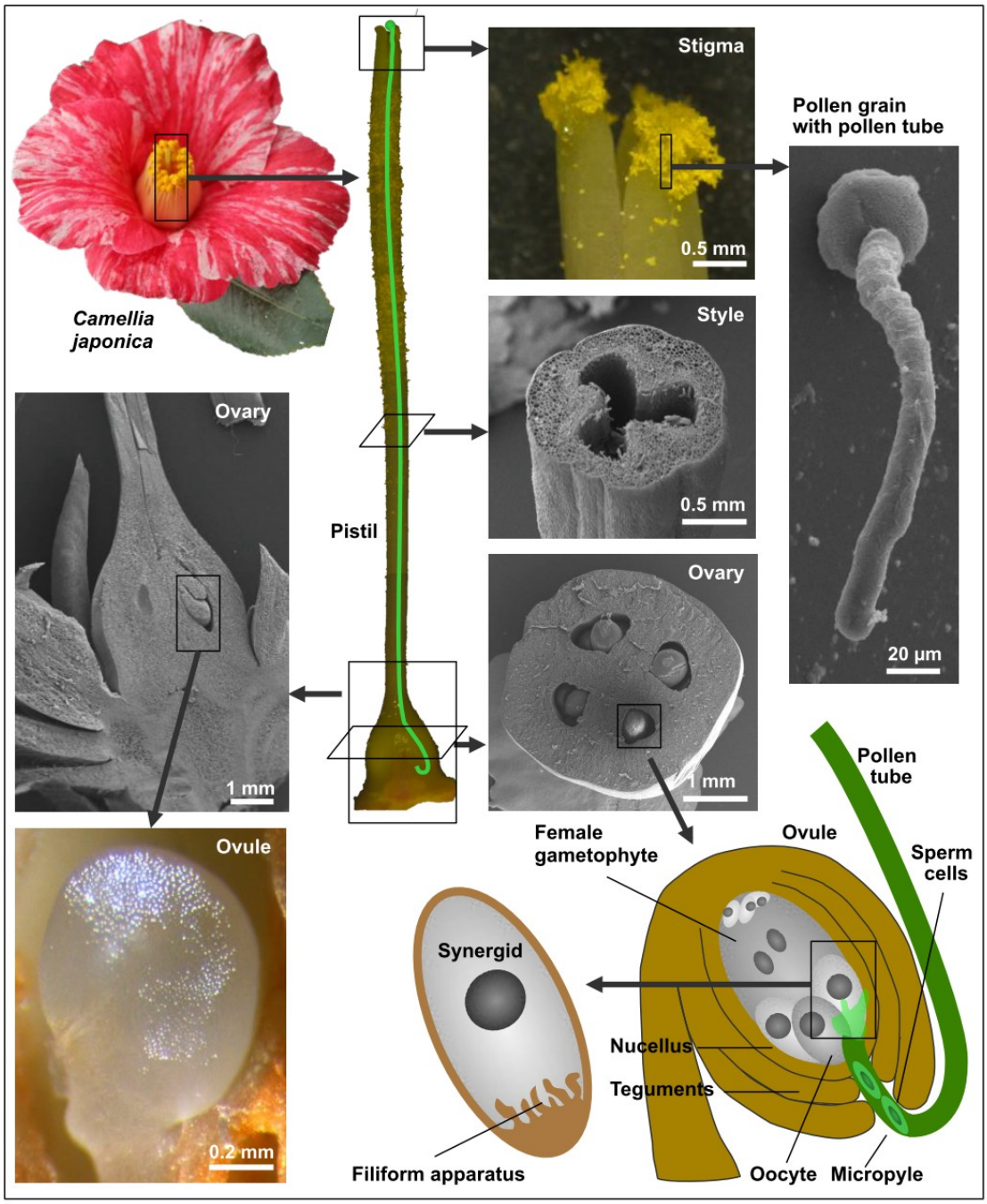

Figure 9.1: Pathway of pollen tube within *Camellia* pistil. The pistil of Camellia flower has a length of approximately 30 mm. The pollen grain (green sphere) lands on stigma, and tube invades the style to reach the ovary. In the Camellia pistil the style is hollow and does not pose a mechanical obstacle. Mechanical impedance to pollen tube elongation is present at the transition region between style and ovary, and at the entrance to the ovule in form of the micropylar opening, the nucellus and the filiform apparatus of the synergids.

Upon invading the micropyle, the pollen tube has to cross the nucellus, a tissue layer surrounding the female gametophyte, and then enter in contact with the synergids, two cells located adjacent to the egg cell. Here, the tube penetrates the filiform apparatus of one of the synergids and bursts open at its apex and releases the two sperm cells, one of which moves towards the egg cell, and fertilizes it to yield the zygote and future embryo (Berger *et al.*, 2008). The other sperm cell fuses with the diploid central cell of the female gametophyte to form an accessory zygote that subsequently develops into the endosperm, a tissue that nourishes the growing embryo during its development.

As the pollen tube grows, the most mechanically challenging situations are likely to be the entry through the cuticle covering the stigmatic papillae (if present), the passage through the transmitting tissue, the entry into the micropyle, and the penetration of the synergids. Depending on the species, the transmitting tissue can either be a lining surrounding a hollow canal, leaving ample, mucous filled space for the tube to elongate in. In many species, however, this canal is completely filled with the transmitting tissue and the tube has to invade the apoplastic space between the cells composing this tissue (Erbar, 2003). Transmission electron microscopy has shown that the space between the cells is typically narrower than what would be required for the tube to pass unhindered (Lennon *et al.*, 1998; Uwate *et al.*, 1980). Depending on the plant species, pollen tube invasion is facilitated by digestive enzymes that soften the apoplast and that are secreted either by the pollen tube (Raghavan, 1997) or by the pistillar cells themselves (Gasser *et al.*, 1993) or the transmitting tissue is triggered to undergo programmed cell death (Wang *et al.*, 1996). However, neither of these processes is likely to completely liquefy the matrix to be

invaded. Therefore, it is reasonable to assume that the pollen tube exerts an invasive force. From a mechanical point of view, the process of elongation of the pollen tube when forcing through the apoplast is similar to that of a balloon catheter used for angioplasty - the widening of a narrow blood vessel to prevent heart infarct.

To quantitatively assess the invasive ability of the pollen tube, we adapted a previously developed microfluidic platform, the TipChip (Agudelo *et al.*, in press-a; Agudelo *et al.*, in press-b; Agudelo *et al.*, 2012e). In this device, pollen tubes are guided to elongate through narrow microchannels specifically designed to accommodate testing devices such as mechanical obstacles, along its path. Although technically possible, we did not opt for a conventional strain gauge in the present setup, since a perpendicularly placed force sensor is known to underestimate the invasive force of tip growing cells because of a cellular shape change upon orthogonal contact of the elongating cell with the flat surface of the strain gauge (Money, 2007b). Even more importantly, rather than presenting flat, perpendicular obstacles, the apoplast of the transmissing tissue consists of narrow gaps. Therefore, we designed the microchannels with a series of narrow gaps through which the pollen tubes had to squeeze in order to continue their elongation. This geometry more accurately represents the microstructure of the *in vivo* growth environment within the stylar tissue and the physical constraints in the path of pollen tube elongation (Fig 9.1). The deformation of the sidewalls forming the microscopic gaps, together with the physical properties of the PDMS (polydimethylsiloxane) material used, allowed us to determine the wedge force that is exerted by the penetrating pollen tube in the direction normal to the

contact surface with the microgap sidewall. Different gap sizes were employed to test the pollen tube behavior and its limitations in terms of gap navigation.

9.3 Design of microfluidic device and quantification of pollen tube behavior in microgap features

In order to challenge elongating pollen tubes with a precisely calibrated microstructured feature resembling the mechanical obstacles of the pistillar tissue, a modular LOC device developed earlier, the TipChip (Agudelo *et al.*, 2012b) was adapted to expose pollen tubes of *Camellia japonica* to microscopic gaps. The microfluidic network of the TipChip consists of a distribution chamber into which pollen grains are injected and serially arranged microchannels along which the pollen tubes grow (Fig 9.2). The entire network has a depth of 80 µm to allow the pollen grains (diameter 60 µm) to move freely but to prevent their stacking in z-direction. Laminar flow within the distribution chamber transports the pollen grains to the entrances of the microchannels where the grains are trapped. Excess pollen grains are evacuated through an outlet at the far end of the distribution chamber.

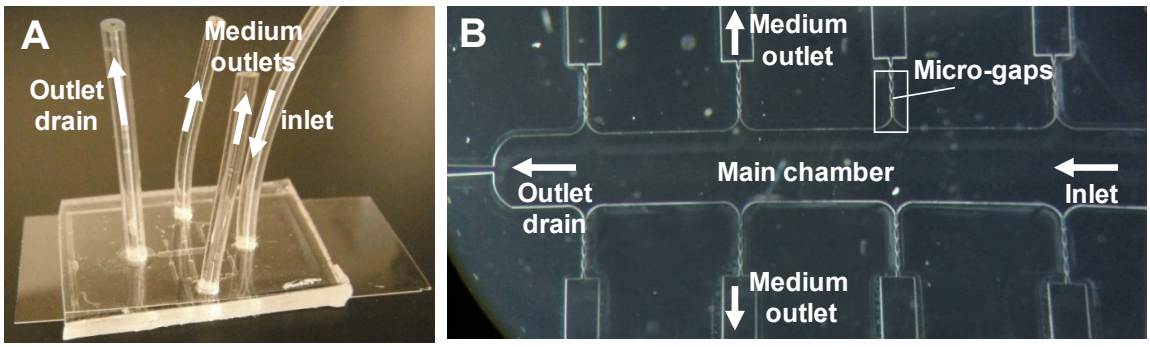

Figure 9.2: Experimental setup for exposure of pollen tubes to microgaps (a) Lab-on-chip device illustrating arrangements of inlet and outlets, (b) Micrograph showing the geometry of the microfluidic network.

Upon germination, the elongating pollen tubes are guided through the microchannel (width 50 µm) and can thus be exposed to mechanical obstacles. These obstacles are positioned at least 100 µm from the microchannel entrance to ensure normal and unimpeded germination of the grain and initial tube growth. In the present setup, the microchannels were designed to feature four narrow gaps alternating with normal microchannel width of 50 µm (Fig 9.3). These micro-gaps were shaped as vertical slits with tapered sidewalls leaving a limited width (W) at the smallest end section. W was set to be slightly below the size of the average *Camellia* pollen tube diameter (D_1) for the first gap and increasingly smaller for the three subsequent gaps. Each subsequent gap was set to be 2 µm narrower than the previous. The two designs used here started either at a gap size of W = 17 µm or 16 µm ending with W = 11 µm or 10 µm, respectively, for the fourth gap.

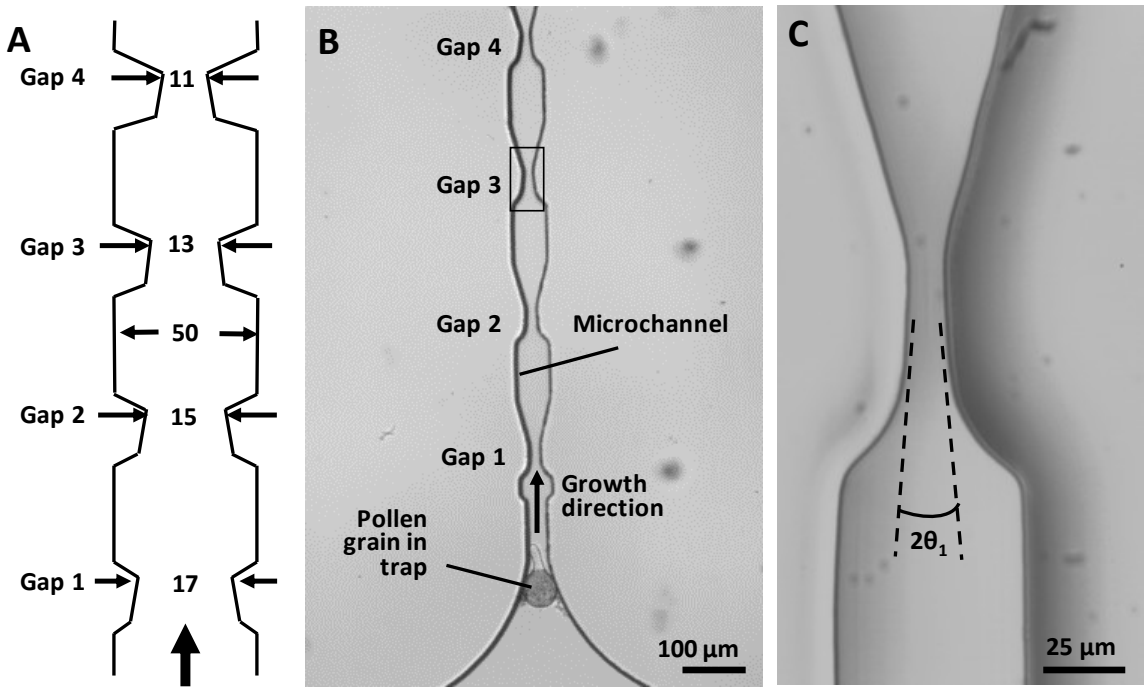

Figure 9.3: (a) Dimensions of the microchannel with repeated narrow regions (microgaps). Numbers are in µm; the drawing does not reflect the aspect ratio. (b) Brightfield micrograph of the geometry of a microchannel comprising the channel entrance with trapped pollen grain and four subsequent gaps, (c) Detail of a microgap indicated in (D) showing opening angle θ

A pollen tube growing toward a micro-gap hit the sidewall at the start point S (Fig 9.4,a). To continue growing, the tube was forced to either apply an extrusive force on the sidewalls and deform these or to form a narrower tube (constriction in y direction). The micro-gaps had limited lengths in x-direction (50 µm) and the pollen tubes left the micro-gap at end point E to return into the standard microchannel width with 50 µm (Fig 9.3a,b). The interaction between the pollen tube and the sidewalls resulted either in the deformation of the sidewalls or in a reduction in pollen tube diameter to D_2 (Fig 9.4,b) or in a combination of both. θ_1 was the angle between the growth direction and the sidewall before deformation. Depending upon the response of pollen tube, the angle between the growth direction and the sidewall after interaction (θ_2) could vary between θ_1 (undeflected

sidewall, pollen tube shape adapted to gap shape) and 0 (completely deflected sidewall, no reduction of the pollen tube diameter).

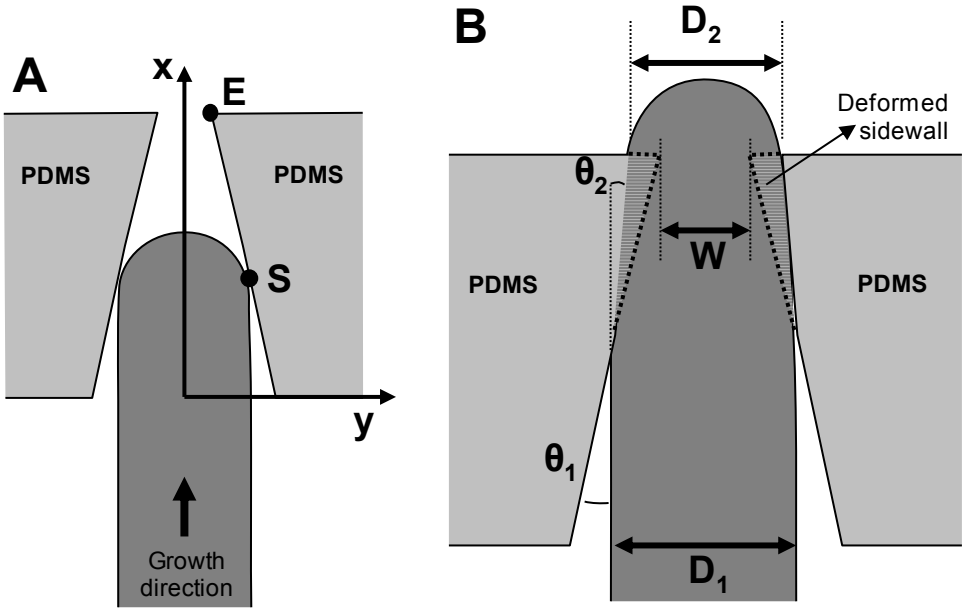

Figure 9.4: Simplified schematic view of interaction between elongating pollen tube and micro-gap, (A) The pollen tube is in contact with both tapered side walls forming the micro-gap at point S. (B) The passing pollen tube deforms the PDMS side walls of the gap to change their angles from θ_1 to θ_2. After passage of the gap, the original width of the pollen tube D_1 can be remporarily reduced to D_2.

The tapered shape of the micro-gap ensured that the pollen tube did not change growth direction to avoid the obstacle, a phenomenon that is commonly observed with obstacles presented perpendicular to the growth direction (Gossot and Geitmann, 2007). The interaction between pollen tube and micro-gap was quantified by determining the change in the pollen tube diameter and the deflection of the PDMS sidewall forming the gap.

9.4 Pollen tubes navigate through micro-gaps by exerting an extrusive force and adapting cell shape

The unimpeded growth rate of Camellia pollen tubes along the microchannels varied between 4 and 11 μm/min. The diameter of the unchallenged pollen tubes ranged from 13 to 21 μm, and depending on the individual diameter, the first and/or second micro-gap did not pose a mechanical obstacle for the respective tube. Four different types of behavior were observed upon the encounter of the pollen tubes with narrower gaps: a) The pollen tube passed through the gap without being deformed visibly, but by deforming the PDMS side walls (n=20) (Fig 9.5,A). b) The pollen tube passed through the gap by changing cell shape (n=5). The reduction of the tube diameter observed microscopically could be either a true reduction in the diameter of the circular cross-section or a transition from round to oval. The apparent reduction in diameter was temporary and upon emerging into a wide portion of the microchannel it typically returned to the original cell diameter (Fig 9.5,B) or became significantly wider than the original tube (Fig 9.5,C). This widening was temporary and the tube eventually returned to its original diameter. c) The pollen tube passed the gap and upon entering the wider portion of the channel it burst (n=8) (Fig 9.5,D). d) The pollen tube stalled in the gap (n=5) (Fig 9.5,E). The fact that individual pollen tubes behaved differently during gap passage demonstrates that the material properties of the PDMS used here were appropriate to assess the mechanical force generation of Camellia pollen tubes. If all tubes had passed the gaps without effect on tube shape, this would have been indicative of the PDMS material being too soft to represent an obstacle. If the gap walls would never be deformed by the passing tubes, the PDMS material would have been too hard. Both situations would have prevented the calculation of the wedge force.

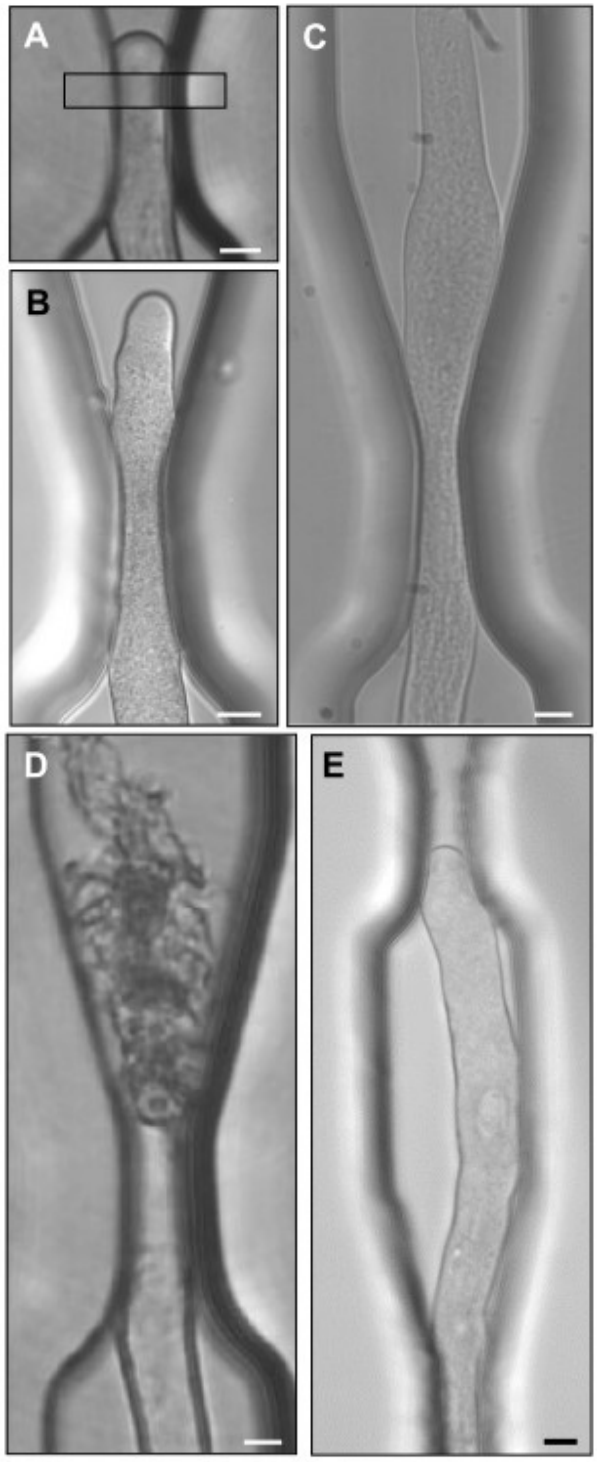

Figure 9.5: Different types of pollen tube behavior during passage through micro-gap, (A) The pollen tube deflects the side walls almost completely to maintain its diameter. (B) The pollen tube becomes narrower in y-direction to pass the gap, (C) Following passage of the gap the pollen tube bursts, (D) The pollen tube stalls and is unable to pass through the gap. The buckling indicates that elongation proceded as long as possible. Scale: 5 µm

To determine whether these different types of behavior could be correlated with a particular ratio between pollen tube diameter and gap size, these parameters were plotted (Fig 9.6). The plot clearly indicates that at a ratio of pollen tube diameter/gap size of 1.20 or below, the pollen tube was able to pass without lasting effect on its shape or growth rate. At a ratio between 1.20 and 1.33 the pollen tube passed, but it either burst after emerging from the gap or its diameter was temporarily reduced. A ratio above 1.33 prevented the pollen tube from passing and caused it to stall.

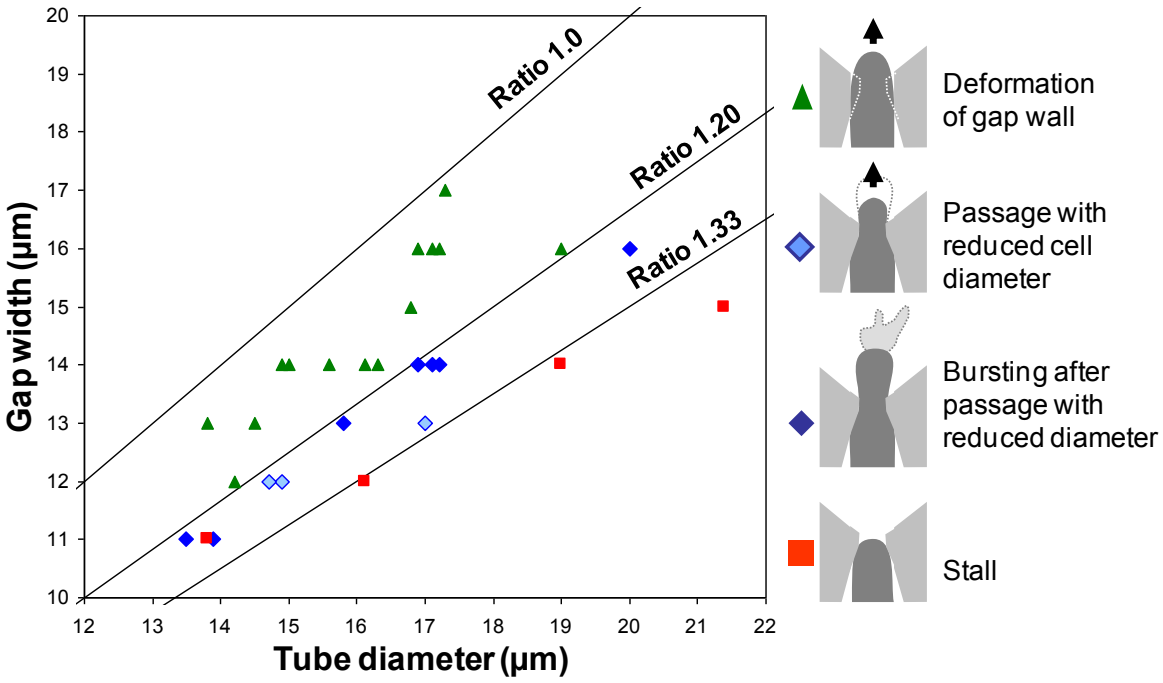

Figure 9.6: Effect of the ratio between pollen tube diameter and gap width on pollen tube behavior. Between ratio 1.0 and 1.20, the pollen tubes deform the gap to pass almost without narrowing their diameter (green triangle). Below this ratio the pollen tube diameter is reduced (blue diamond) and frequently the tubes burst upon returning to the original diameter following gap passage (solid blue diamonds). At a ratio around 1.33 and below the tubes stall and are not able to pass the gap (red square).

The pollen tubes that successfully navigated the gap, generally displayed a reduced growth rate while passing through the narrow portion (Fig. 9.7). The growth rate sped up again after emerging from the gap, but within the critical ratio range of 1.20 to 1.33, this frequently led to bursting (Fig 9.6,9.7).

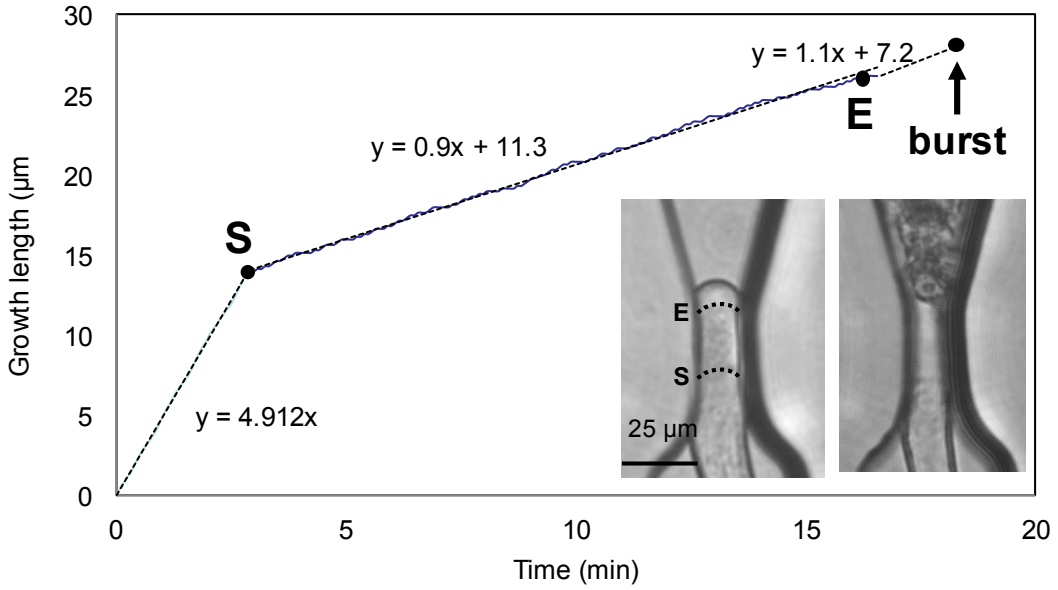

Figure 9.7: Change growth rate during microgap passage. Upon encountering the narrow region of the gap at point S, the tube slows down considerable. After exiting the narrow region at point E it starts growing faster but bursts soon after.

9.5 Male germ unit

The male germ unit of the pollen tube consists of the vegetative nucleus and the two sperm cells surrounded by a double membrane (Fig 9.8). These structures are physically connected to each other (McCue *et al.*, 2011) and move forward in the elongating tube guided by the microtubule cytoskeleton of the vegetative cell (Åström *et al.*, 1995). Our observations showed that in *Camellia* pollen tubes the vegetative nucleus is the closer to the tip than the sperm cells, with a distance of approximately 60 to 80 µm from the apex, whereas the sperm cells were located immediately adjacent in distal direction with their

nuclei at approximately 120 µm and 155 µm away from the tip. During normal growth, these distances were maintained very stably.

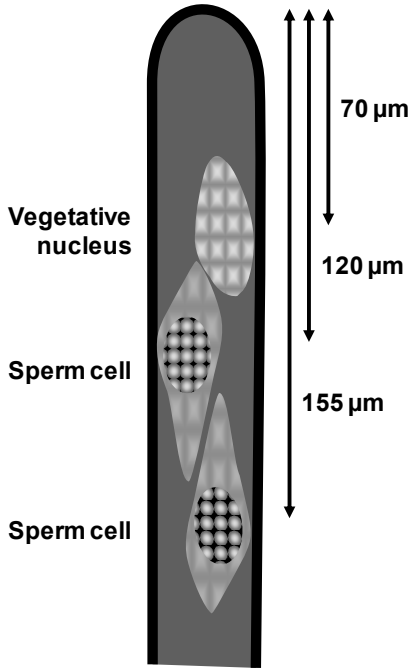

Figure 9.8: Passage of the male germ unit through a micro-gap, Schematic representation of the male germ unit consisting of vegetative nucleus and sperm cells with typical distances from the tip of the pollen tube. Objects are not to scale.

During passage through a narrow gap, the vegetative nucleus occasionally had difficulties passing the narrow passage after the pollen tube tip had successfully grown through (Fig. 9.9). The nucleus was able to turn or twist to pass the gap, but this could entail a delay in forward movement compared to the speed of the growing tip. In these cases, once having cleared the gap, the vegetative nucleus then usually sped up its forward movement to regain its normal distance from the tip. Importantly, when pollen tube bursting was induced by passage through a narrow gap, the male germ unit could be stuck behind the gap instead of being ejected (Fig. 9.9).

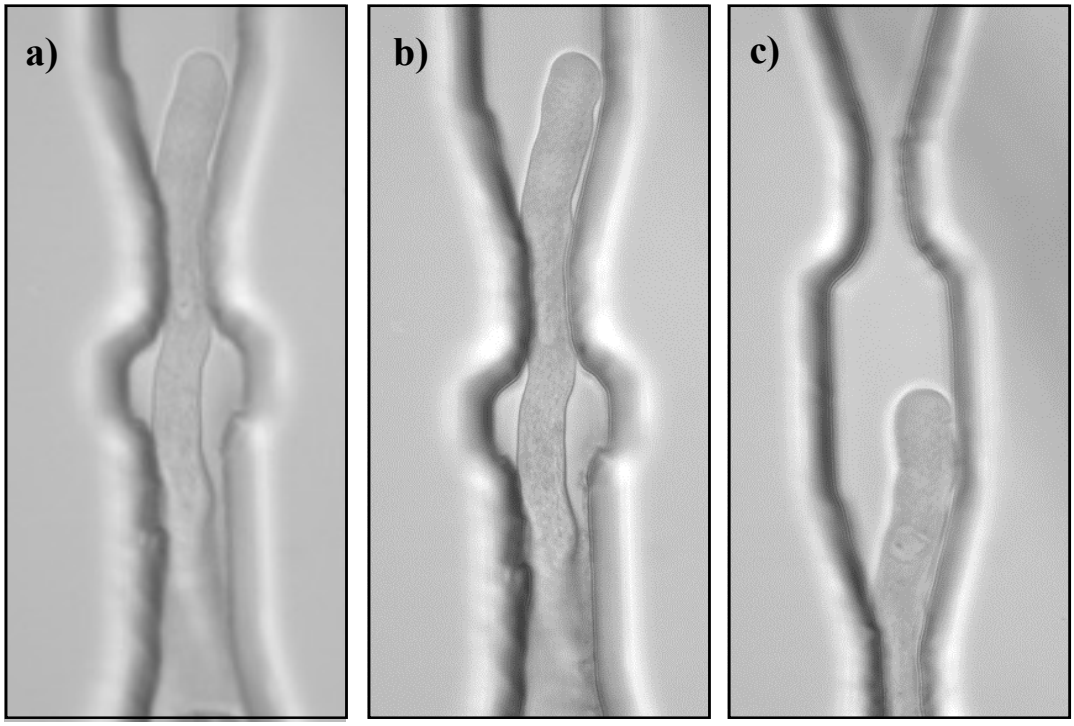

Figure 9.9: Passage of the male germ unit through a micro-gap, Brightfield micrographs of pollen tube passing a gap. The vegetative nucleus wiggles to pass the gap.

9.6 Finite element simulation of interaction between pollen tube and sidewalls

While tubes with a size ratio of 1.2 or higher coped with the slit-shaped micro-gap by changing their shape, those with ratios between 1.0 and 1.2 were able to penetrate the gap without significant changes to their shape, deforming the tapered PDMS side walls instead (Fig 9.10,A). This demonstrates that pollen tubes are able to exert a wedge force in the lateral direction that ensures maintenance of the cell shape against forces exerted by the surrounding pistillar tissue. In order to quantify this wedge force, we modeled the interaction between pollen tube and micro-gap using finite element analysis.

First, the actual contact area between the pollen tube and the micro-gap during growth was established. This was based on the geometry observed when pollen tubes passed a gap

without detectable change in tube diameter. It was assumed that the maximum contact area is achieved when the hemisphere shaped tip has passed the gap and the cylindrical tubular portion is in contact with the gap wall. The tube was therefore represented as a cylinder with a constant diameter of 17 µm (Fig 9.10,B). The micro-gap is modeled as a three dimensional structure with tapered sidewalls with a starting width of 20 µm that narrows down to 14 µm (Fig. 9.10). The intersection of the cylindrical tube and the tapered sidewall of the micro-gap is determined using a CAD design software (AutoCad 2007). Projection of the contact surface on the sidewall plane (area labeled as CA in Fig. 9.10A,B) when the dome has completely passed through micro-gap is shown in Fig. 9.10,B.

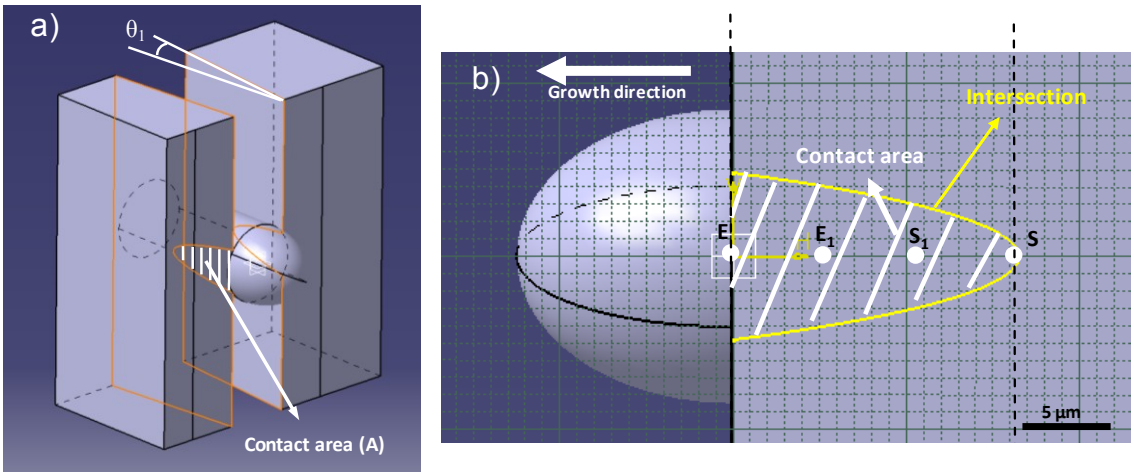

Figure 9.10: Finite element model for the simulation of force exertion by the pollen tube on the side walls of the micro-gap, (a) 3D representation indicating the contact surface between pollen tube and micro-gap when pollen tube is in full contact with the sidewall, (b) Position of four reference points on the contact area starting with point S upon initial contact and ending with point E, the exit of the gap. Points S_1 and E_1 are two sample points equally spaced between S and E.

In order to model the effect of the lateral force exerted by the pollen tube on the PDMS sidewall, a constant pressure is applied on the contact area (Fig. 9.11). During pollen tube growth into the narrow region of the gap, the contact zone increases from zero to the

maximum value CA_{max} at which the PDMS deformation satisfies the deflection required for passing the tube fully through the micro-gap. Based on the Young's modulus of PDMS material (Armani *et al.*, 1999) and the measured sidewall deformation required to permit pollen tube passage, the normal pressure exerted on the sidewall and the resulting normal force are calculated. The induced normal force, or wedge force (F) changes from zero at initial contact to a maximum value of F_{max} corresponding to the maximum contact area CA_{max} when the tip leaves the gap at point E.

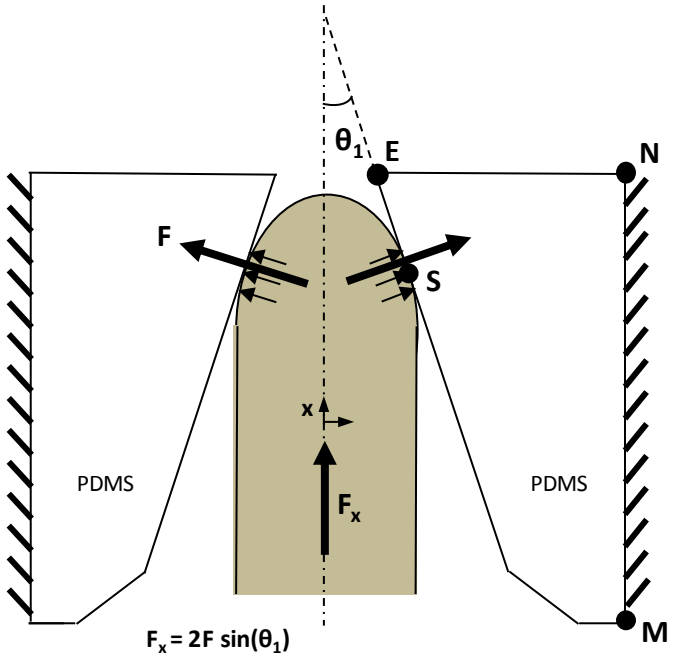

Figure 9.11: Top view of the simulated geometry indicating the orientation of the force vectors

Stress strain relations are used to extract the wedge force from the interaction between the pollen tube and the sidewalls. Assuming small deflections, Navier's equation for static analysis is obtained as follows:

$$\mathbf{L^T cLu + F = 0} \tag{9-1}$$

where **c** is matrix of material constants, **F** is the volume force extracted from the applied normal pressure P to the contact surface, **u** is the vector of deformations, **L** is the differential operator given by (Liu, 2003):

$$L=\begin{bmatrix} \frac{\partial}{\partial x} & 0 & 0 \\ 0 & \frac{\partial}{\partial y} & 0 \\ 0 & 0 & \frac{\partial}{\partial z} \\ 0 & \frac{\partial}{\partial z} & \frac{\partial}{\partial y} \\ \frac{\partial}{\partial z} & 0 & \frac{\partial}{\partial x} \\ \frac{\partial}{\partial y} & \frac{\partial}{\partial x} & 0 \end{bmatrix} \tag{9-2}$$

To solve the governing Navier's equation for the presented interaction model, finite element analysis is implemented using COMSOL Multiphysics 3.5 software. The element type of Lagrange Quadratic was chosen to mesh the design. The number of mesh elements for this simulation is 105367 with 458796 degrees of freedom. The sensitivity of the results to the number of mesh elements was evaluated considering 5% criterion error. As the boundary condition for FEM analysis, the micro-gap along the MN line is the fixed support (Fig. 9.11). The normal pressure P is applied to the contact zone. A Young's modulus of E=1 MPa and a Poisson's ratio of ν=0.4 are chosen for the PDMS material (Armani *et al.*, 1999). In order to determine the pressure that satisfies the required deflection allowing pollen tube passage, the deflection of the PDMS micro-gap at point E is estimated for various normal pressures P (Fig. 9.12).

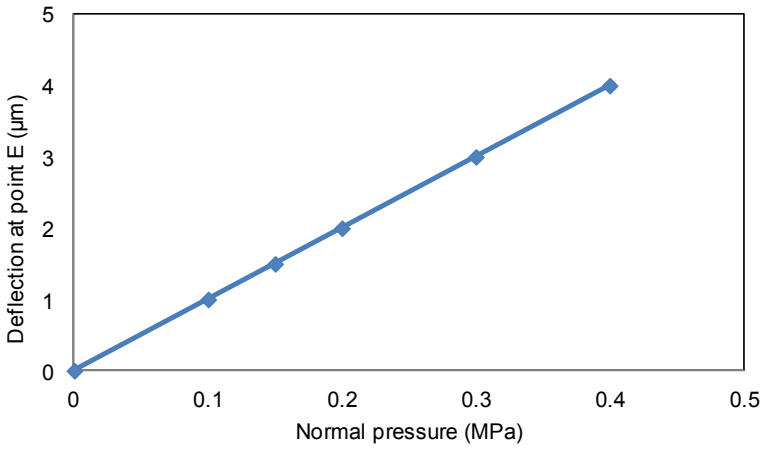

Figure 9.12: Effect of varying turgor pressure on side wall Top view of the simulated geometry indicating the orientation of the force vectors deflection at point E as simulated by the FE model The simulations show that a deflection of 1.5 µm at point E (equal to the experimentally observed deflection to $\theta_2 = 0$) requires a constant pressure of 0.15 MPa (Fig. 9.13).

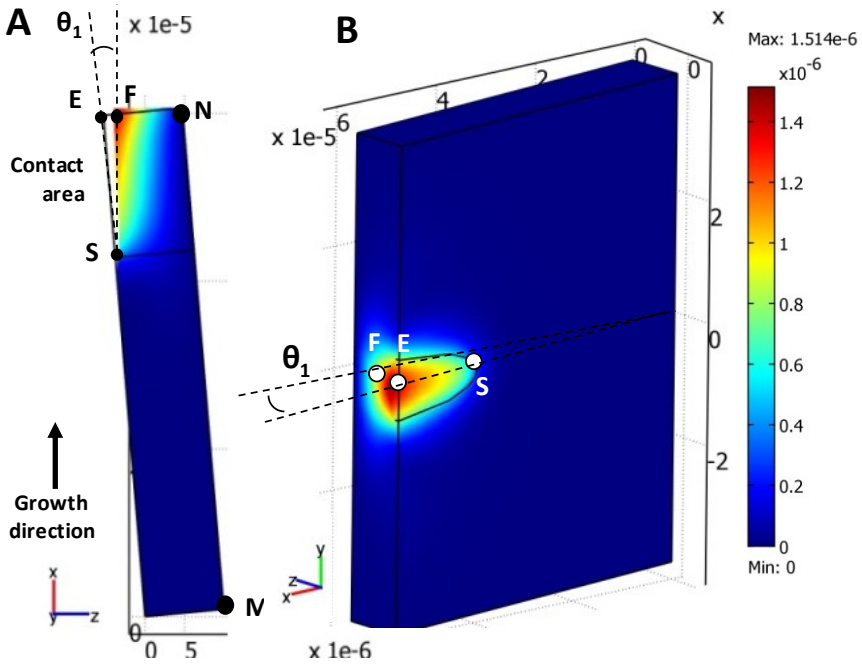

Figure 9.13: Top view (E) and 3D view (F) of side wall deflection at F= 0.15 MPa

Based on the estimated pressure, wedge force F is extracted. At the moment of maximum contact, when the tube reached the narrowest region of the gap, the total contact area

between tube and gap wall is 98 μm^2. At this point F is predicted to be 14.7 μN. (Fig. 9.11). The simulations show that prior to the moment of maximal contact, the wedge pressure P increases almost linearly due to the linearly narrowing gap toward the end, while the wedge force F increases non-linearly as the wedge pressure linearly and the contact area nonlinearly increases (Fig. 9.14).

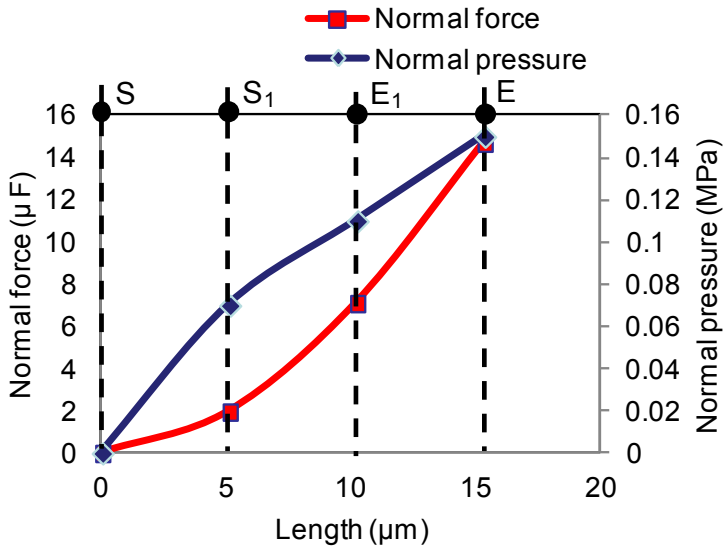

Figure 9.14: Normal force F and normal pressure required for side wall deformation during pollen tube passage through the gap

In addition, based on the wedge force and the deflection of the wall, the corresponding total energy required to deflect the micro-gap with a contact area of CA can be calculated using the following Equation (8-3) (Beer *et al.*, 1974).

$$U = \int \delta \boldsymbol{\varepsilon}^T \boldsymbol{\sigma} dV \qquad (9\text{-}3)$$

where U is the energy and dV is the volume element. Similarly to the wedge force, the total predicted energy required to let the pollen tube overcome the resistance of one sidewall during gap passage increases in non-linear manner (Fig. 9.15).

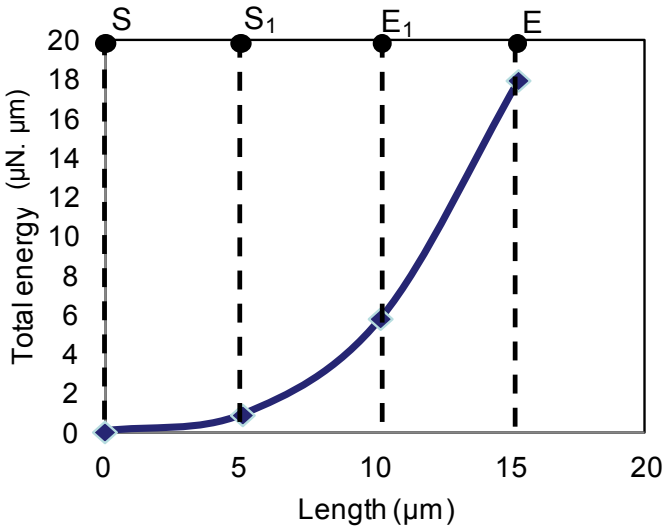

Figure 9.15: Total energy required for side wall deflection during pollen tube passage through gap

9.7 Discussion and conclusions

Tip growing cells such as neurons, fungal hyphae, root hairs and pollen tubes, have the formidable task to invade surrounding tissues or other substrates. The purpose of this invasive activity differs between the cell types, but the common challenge for all of these cells is the necessity to navigate mechanical obstacles and exert force to displace and invade the surrounding matrix. In the case of the pollen tube, this invasive behavior serves to deliver the gametes to their destination, and therefore, unlike the other tip growing cell types, the pollen tube has the function of a catheter-like delivery system. This requires not only invasive force, but also the protection of the contents that is to be transported, the male germ unit. It is crucial that the pollen tube remains tubular, since a kink or collapse in the cylindrical tube shape would prevent the passage of the sperm cells. This requires the

exertion of pressure perpendicular the growth direction. Therefore, rather than comparing the invading pollen tube to a solid object such as a needle, the mechanical analog of a pollen tube is a balloon catheter that is conventionally used to widen blocked arteries during angioplasty. To assess the behavior of the pollen tube when faced with an obstacle we presented elongating tubes with a structural feature that resembles those it encounters *in planta* - the apoplast and narrow intercellular spaces of the transmitting tissue. Our observations demonstrate that the tube does not avoid a narrow opening but proceeds by invading it. An elastic opening causing moderate size constraint was completely deformed during the passage, but narrower slits caused a change in pollen tube shape. If this constriction was too narrow, the passage of the germ cells was indeed jeopardized and, if not blocked, was at least temporarily slowed down. In this context it is intriguing to note that the tubular diameter of the pollen tube seems to be hardwired into the pollen tubes of a particular species, illustrated by the fact that tube diameter varies significantly between species (with 5 µm in Arabidopsis and 17 µm in Camellia) but only insignificantly within a given species. The return of the *Camellia* pollen tube to its previous diameter after gap passage indicates the endogenous control of cell shape that ensures the successful transport of the male germ unit without it getting stuck. The precise mechanism controlling pollen tube diameter is subject to numerous biological and modeling approaches (Fayant *et al.*, 2010b) (Kroeger and Geitmann, 2012b), but how species-specific differences can be explained warrants further research.

The observed bursting events after micro-gap passage open an intriguing avenue to a possible mechanism for sperm cell release. The two immotile sperm cells carried by the

pollen tube are released by bursting once the pollen tube enters the female gametophyte. Several agents involved in inter-gametophyte signaling and attraction of pollen tubes have been recently identified (Amien *et al.*, 2010). However, the physiological mechanisms leading to pollen tube burst and thus sperm discharge remain elusive. Based on our observations one could propose that simple mechanical signal, an opening that is narrower than the tube diameter, could represent a trigger mechanism. However, several of our findings speak against this hypothesis. The range in size ratios that seems to be conducive to bursting is very narrow - between 1.20 and 1.33. At ratios lower than 1.20, the tube simply grows through the gap and beyond without bursting, and at ratios higher than 1.33 the tube stalls. Given the variability of pollen tube diameter within a single pollen batch, a particular gap size in the micropyle would only allow successful delivery of sperm cells by a subset of pollen tubes that have the correct diameter relative to the gap size. Since there is no obvious interest for an ovule to practice exclusion based on pollen tube size, this method does therefore not seem to be biologically relevant and the search for chemical or proteic triggers remains an urgent topic (Amien *et al.*, 2010). Secondly, even if the tube bursts following the successful passage of a narrow gap with the appropriate size ratio, the male germ unit does not necessarily pass the narrow gap and might not leave the tube, as shown in Fig. 9.16. This further confirms that a mechanical constraint is unlikely to be involved in sperm discharge in plants.

c 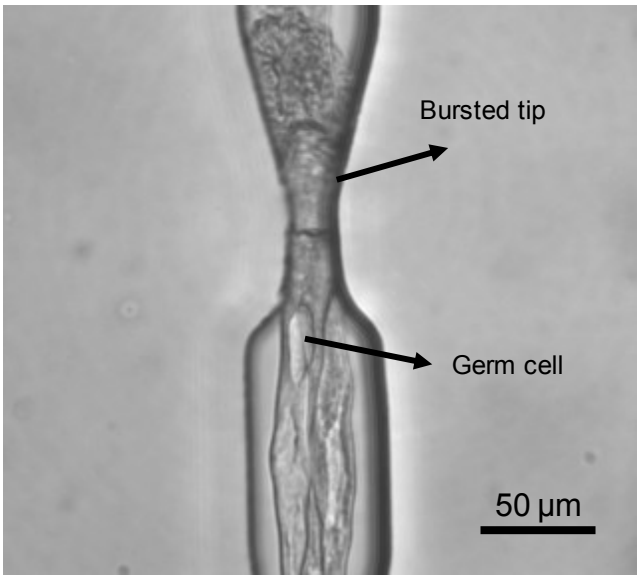

Figure 9.16: The gamete cell does not pass the narrow gap even when the tube burst following the successful passage of the gap

The precisely defined geometry and known mechanical properties of the material used for the micro-gaps in the microfluidic device allowed us to calculate the wedge force of the pollen tubes using finite element methods. We determined that a maximum pressure of 0.15 MPa is exerted on the gap walls at point E, when the tube has reached the narrowest point of the gap. The turgor pressure of *Camellia* pollen tubes is not known, but in lily pollen tubes an average turgor pressure of 0.2 MPa has been determined (Benkert *et al.*, 1997). Our estimated wedge pressure is thus in the same order of magnitude but clearly below this value. In this context, it is important to point out that while the hydrostatic turgor pressure provides an upper limit to the force exerted by the pollen tube, the force transmitted to the outside of the cell is generally far below this value. In fungal hyphae the invasive force typically amounts to only 10% of the turgor pressure (Money, 2004b). The reason for this is the fact that none of the hydrostatic turgor pressure in the cell is exerted against the external growth matrix unless the wall relaxes and has some freedom to expand.

Only some environmental conditions this fraction was found to increase up to 54% in fungal hyphae (Money, 2004b).

During elongation growth the cell wall material at the pollen tube apex yields constantly, but in controlled manner to the turgor that serves as a driving force for its stretching (Rojas *et al.*, 2011). It is thought that tip growing cells are able to modulate their invasive force by changing the compliance of the cell wall, but experimental evidence for this has been elusive. Intriguingly, a detailed analysis of the behavior of the *Camellia* pollen tube during gap passage provides evidence for this notion. The FE simulations showed that during the interaction between advancing pollen tube tip and gap walls, the total energy required to overcome the sidewall resistance increases nonlinearly with the contact area. Assuming constant potential energy of the pollen tube for the growth, a gradual decrease of growth rate would be expected as increasingly more energy is dissipated during passage through the narrowing gap. However, the time course plots of the growth rate did not indicate a significant drop in the growth rate between the initial contact with the gap walls and the narrowest part (Fig. 9.7). This observation suggests that the pollen tube is able adapt to the continuously increasing mechanical impedance. In principle, this could occur either by increasing the turgor or reducing the tensile resistance in the cell wall. Based on our data we are unable to distinguish between the two alternatives, although the latter would be more in line with widely accepted principles of pollen tube functioning and growth regulation (Winship *et al.*, 2010; Winship *et al.*, 2011a). The notion that during gap passage the equilibrium between cell wall compliance and turgor changes is further confirmed by the finding that tubes emerging from a very narrow gap have the tendency to

burst when emerging into the wider part of the channel. This behavior is akin to bursting of hyphae that are exposed to a temperature shock. This failure was purported to occur as a result of a sudden change in the relationship between cell wall properties and turgor pressure (Money, 2007a).

Chapter 10

Conclusions and suggestions for future work

10.1 Conclusions

Biomechanical aspects of pollen tube growth includes 1) the role of turgor pressure as driving force, 2) the role of cytoplasm in providing raw materials for generation of new cell wall and 3) the contribution of ionic fluxes in adjusting mechanical properties of cell wall and morphogenesis. As the overall regulatory mechanism of pollen tube growth is controlled by a combinatory effects of these elements, the research to study the effect of any of these parameters on growth regulation and their interplay relation is highly valuable.

The questions in this context are: 1) Is the turgor pressure constant and the dynamic oscillation of tip growth is only due to oscillation of mechanical properties of cell wall, 2) Does turgor pressure alter locally at the tip or vary globally within the cell, 3) What would be the interplay of turgor pressure and cell wall mechanical properties to regulate the dynamic growth and its self similarity, 4) How the water and nutrient are absorbed into the cell either through the cell wall at the tip or distal region, 5) How ionic influxes change the mechanical properties of cell wall and alter the growth rate and growth direction, 6) Which one of chemical agents in culture medium regulates the mechanical properties of cell wall, and 7) How would be the growth of pollen tube in absence of intracellular flux at the tip and only due to its cytoplasmic contents.

Despite extensive biological experiments on characterizing biomechanics of pollen tube to find out the role of these elements and to answer above questions, there are still many technical challenges to detect the influence of these agents. Response to any of these questions will assist to clarify one aspect of complicated growth mechanism of pollen tube. The technical challenges in the context of cell biomechanics of pollen tube and limitations of current technology are as following.

1) How to quantify the turgor pressure and its variation within pollen tube at both distal and tip regions: Answering this question will help to find out the contribution of pressure on dynamic oscillatory growth of pollen tube and to know whether the turgor pressure is a prerequisite for the growth. Pressure probes are still the only direct method to measure the pressure within the cell. It has been able to detect turgor pressure within several species of pollen tubes and fungal hyphae, though no detectable turgor pressure was reported for some species of growing tubes either due to lack of pressure or because of the limit in sensitivity of probe. The indirect methods estimate turgor pressure through quantification of cell growth force at the tip, micro-indentation of cell wall at different region and modeling the manipulation. These two different methods have been able to estimate turgor pressure, but they lack the ability to detect the oscillation in turgor pressure because these methods do indirect detection of turgor pressure through manipulating cell wall which need a modeling step further to correlate the measured force at the tip and turgor pressure. Since the true mechanical properties of cell wall and its gradient are not still quantified, the correlation of growth force and turgor pressure need extensive modeling steps. In the case of micro-indentation, the geometry of indenter is involved in modeling which prevent

simple detection in oscillation of turgor pressure due to addition of several unknown parameters to the model.

2) What are the mechanical properties of cell wall at either distal or apical region and how they can be quantified: The mechanical properties of cell wall include elastic modulus of cell wall, the degree of visco-elasticity or visco-plasticity, stress relaxation limit, stiffness, the degree of anisotropy and gradient of mechanical properties from distal region to the apical region. The techniques with the ability of measuring any of these parameters will have contribution in our understanding from the role of cell wall in the growth mechanism. Since the cell wall is involved in oscillatory dynamic growth of pollen tube, it is important to know how the oscillation in mechanical properties of cell wall is correlated with the oscillation of growth rate and oscillation in turgor pressure. Micro-indentation has been used to measure the stiffness and elastic modulus of cell wall at both distal and apical region, however it was not successful to measure the variation of cell wall mechanical properties during the growth. Moreover, the measured values are extracted from local micro-manipulation of the cell wall and may not reflect the real quantity of fully composite and anisotropic cell wall of pollen tube. Development of techniques to quantify the level of anisotropy in mechanical properties of cell wall with the ability to measure a more realistic value for elastic modulus of cell wall instead of local values is beneficial.

3) Modeling is an effective tool to correlate turgor pressure and cell wall mechanical properties in order to find out the interplay of these two major parameters in regulating the oscillatory dynamic of growth and biomechanics of cell wall: Although both theoretical

and experimental models have been exploited to do this correlation, they all lack sufficient and accurate experimental data for the turgor pressure, mechanical properties of cell wall and their variation. The models have based a series of assumptions without validation by experimental results. The techniques with the capability of quantifying the biomechanical parameters of pollen tube growth will also benefit the modeling aspects.

4) The role of ionic influx in regulation of tip growth is the other major question in context of cell biomechanics: Endocytosis is believed to be involved in change of mechanical properties of cell wall and effective on oscillatory dynamic of growth. Although the variation of ions flux and its gradient along the tube can be detected at the location of cell wall using ion probes, the role of these ions in cell morphogenesis, control of mechanical properties of cell wall and eventually on regulating growth direction is still under question. To approach this target, the lack of local chemical treatment of cell wall has been always a limitation. The global treatment of cell wall is not able to locally change the properties of cell wall, so it is not able to give more information about the role of ionic flux in cell wall mechanical properties and growth direction in biomechanical context. The development of new methods with the ability of local treatment at the tip will enable the local change of ionic flux at one side of the tip and in consequence change the mechanical properties of cell wall at that side. This will result in the change of cell morphogenesis and cell wall reorientation which is a valuable piece of information in characterizing biomechanics of pollen tube.

Knowing the questions in context with the pollen tube biomechanics and the limitations of current detection techniques, we believe that microdevice and microfluidic environment is an effective platform to serve biology of tip growing plant cells. Hence, our main objective in this thesis was to develop different microfluidic platforms in order to target several of previous questions and to argue about the role of turgor pressure, cell wall mechanical properties of cell wall and ionic flux on biomechanics of pollen tube.

Prior targeting these questions, we developed a microfluidic platform to overcome the general challenges of trapping individual pollen tube in order to chemically or mechanically stimulate the cell. In addition, since there was no control on the presence of identical growth environment for pollen tubes growing in open assays, the results were not simply comparable. The lack of these two requirements has led to even contradictory results about behavior of pollen tube growth. In first step, we developed a flexible microfluidic platform, TipChip, which meets the two above requirements of single cell trapping and identical growth condition for a series of pollen tubes. The main components of this microfluidic chip included the microfluidic network for cell manipulation and trapping, growth microchannels for trapping individual pollen grains and growing one pollen tube along them. The configuration of the microfluidic network was developed in a way that allows simultaneous observation and chemical or mechanical manipulation of multiple pollen tubes.

Since the biologists believe that the major regulation of growth occurs at the tip through interaction of internal turgor pressure, cell wall and ionic flux at the tip, it would be

valuable to have an ex-vivo environment with the possibility of growing pollen tube in the air. The enhanced versions of TipChip were used to locally treat the pollen tube at the tip or the distal region of cell wall. This has overcome the limitation of open assays to stimulate distal region of pollen tube without any influence on the tip. The pollen tube was able to elongate within the air while the distal region of pollen tube was in contact with the culture medium similar to in-vivo growth of pollen tube in air when it was approaching the micropyle. We detected the increase of growth rate of pollen tube when it entered the air and the drop of growth rate once the tube penetrated from the air trap to the culture medium. Within the air trap, pollen tube tip is not in contact with the culture medium meaning absence of any intracellular ionic flux at the tip. Hence, this platform argues about the questions that to what extent the water uptake occurs at either the distal or apical regions and how ionic flux such as calcium flux at the tip is essential for the growth. To know whether the pollen tube is able to absorb water through its distal region and not only through its tip, we changed the sucrose concentration of medium around the distal region of pollen tube. Interestingly, pollen tubes responded to the change of sucrose concentration through change of their growth rate. Under low concentration of sucrose (4%), pollen tubes growing in air burst in a minute showing that the turgor pressure has increased through water uptake at distal region. However, when we changed the Ca^{+2} in the medium, no detectable change of growth rate was detected even in case of zero calcium concentration of the medium. This helps to verify the hypothesize that there might be internal source of Ca^{+2} ions within the cell wall or cytoplasm as there is no external source of Ca^{+2} ions when the tip was growing in the air. Similar experiments can be done to study how important are the flux of other ions on the growth behavior.

TipChip also assisted to argue on the question of how ionic flux change the cell wall morphogenesis and mechanical properties of cell wall. The prerequisite for this understanding is to develop a technique with the capability of local treatment of cell wall. TipChip platform provided this environment to locally stimulate the tip in order to study the effect of ionic flux on cell morphogenesis and particularly the electrotropism. For local chemical treatment, a laminar flow based microfluidic device was developed that allows for continuous administration of two different solutions with a movable interface that allows to dynamically target the moving tip. Calcium as known to orient pollen tube growth was used as a test substance. We could develop microfluidic chip to locally introduce two different Ca^{+2} ion concentrations (2.54 mM and 5.08 mM) toward the tip. Continuous flow prevents the build-up of cell-generated and overlaying gradients that render the situation complex. Interestingly, the tube turned to the concentration that had previously been established to be optimal for pollen tube growth, rather than to the higher concentration of the ion. This illustrates that rather than growing towards a source of high calcium, the tube will search for an optimum calcium concentration. Furthermore, rather than turning 90º towards the preferred solution, the tube turned forming an obtuse angle (deviation of approximately 20º from the original growth direction), but the turn was repeated after a lag time. This turning angle was identical to the angle measured in the same species (*Camellia*) following a very different type of directional trigger - an electrical field (Bou Daher *et al.*, 2011b). Pollen tubes of other species were shown to perform much more dramatic turns as illustrated in a variety of experimental set-ups (Higashiyama *et al.*, 2008; Prado *et al.*, 2004). However, these dramatic turns were typically preceded by a

temporary arrest of pollen tube growth. Inversely, turns with angles up to 90º can also be achieved in the absence of directional trigger, but by temporarily arresting growth (Zerzour *et al.*, 2009b). The microfluidic set-up was suitable and will be extremely useful for a variety of conceptually very different experimental strategies: 1) Testing attractants for tip growth or agents causing repulsion, 2) Establishing sensitivity thresholds and 3) Local administration of specific agents interfering with cellular functioning, all to study the biomechanics of cell wall.

Tip growing cells is thought to be able to modulate their invasive force by changing the compliance of the cell wall, but experimental evidence for this has been elusive. The detailed analysis of the behavior of the pollen tube during gap passage provided evidence for this thought. In this regard, we devised microgap structures to provide mechanical stimulation to the growing pollen tube and we used FE analysis to study this interaction. The FE simulations showed that during the interaction between advancing pollen tube tip and gap walls, the total energy required to overcome the sidewall resistance increases nonlinearly with the contact area. Assuming constant energy of the pollen tube for the growth, a gradual decrease of growth rate would be expected as increasingly more energy is dissipated during passage through the narrowing gap. Since the time course plots of the growth rate did not indicate a significant drop in the growth rate between the initial contact with the gap walls and the narrowest part, it suggests that the pollen tube is able to adapt to the continuously increasing mechanical impedance. This could occur either by increasing the turgor or reducing the tensile resistance in the cell wall showing the interplay roles of these two parameters in regulating growth in response to external cues. We are still unable

to distinguish between the two alternatives, although the later would be more in line with widely accepted principles of pollen tube functioning and growth regulation (Winship *et al.*, 2010; Winship *et al.*, 2011a). The notion that during gap passage the equilibrium between cell wall compliance and turgor changes is further confirmed by the finding that tubes emerging from a very narrow gap have the tendency to burst when emerging into the wider part of the channel.

The other method to study the interplay of turgor pressure and cell wall mechanical properties is to exploit the power of modeling, though it needs better estimation of cell wall mechanical properties. Here in this thesis, in order to quantify the mechanical properties of cell wall not through local manipulation of cell wall, but through bending test on growing pollen tube, we developed BLOC chip. The deflection of the pollen tube is measured under flow-induced bending allowing for straightforward calculation of the Young's modulus of the cell wall material. We quantified the value of 350 MPa for the Young's modulus of pollen tube cell wall at distal region. This technique lacks the deficiency of local manipulations and gives us a more realistic value of mechanical properties of cell wall. Although this bending technique is not able to measure the Young's modulus of cell wall at the tip, it will be a significant number which can be used for modeling the gradient of elastic modulus from the distal region to the apical region. This quantity can also be used to calibrate the micro-indentation technique in order to measure the oscillation of cell wall mechanical properties at the tip.

Technical challenges exist for the study of dynamic oscillation of growth. To know how the turgor pressure or ionic flux can change the dynamic pattern of growth rate, we should be able to change the growth environment and meanwhile we need to accurately take images of the growing tip in order to measure the growth force. The change of culture medium around pollen tube in open assays will move pollen grains and complicate the imaging from tube growth. Hence, there has been high demand to position the grain at a position which has not been accessible using conventional techniques. TipChip enabled us to trap individual pollen grains at the entrance of a microchannel. Since the pollen is positioned, we can stably change the medium and measure the growth rate while it elongates in a confined environment of a microchannel within a size of slightly bigger than tube diameter.

Unlike earlier dynamic analyses of pollen tube growth, we were able to detect secondary oscillation frequencies with higher frequency values superimposed on the previously reported primary frequency. Our findings illustrate that even in the apparent absence of low frequency oscillations - a phenomenon that is typical for young pollen tubes - there always are secondary peak frequencies indicating that pollen tube growth is constantly under dynamic motion. Our finding that slight changes in the growth environment change both frequencies offers a promising avenue for the investigation of the feedback mechanisms governing cellular growth. In addition, the accurate study of dynamic growth of pollen tube was used to distinguish the effect of toxic (growth inhibitive) or growth inhibitors on the dynamic growth. The variation of both lower and higher mode dynamic oscillation of cell growth rate under different toxic Al concentrations was complementarily

detected as dynamic cell response. Although pollen tube responded to the growth promoting agents such as sucrose in the form of shift on oscillation frequencies of growth rate, in case of toxic agent, the peak frequencies were disrupted without any shift on frequencies. This criterion was used to distinguish the presence of toxic chemical agents in the culture medium.

In meeting defined objectives, the thesis was successful in designing, fabricating and testing microfluidic platforms for studying biology of tip growing plant cell under chemical and mechanical interaction. The platforms provided *ex-vivo* environment for answering questions regarding the invasive behavior of pollen tube growth through different growth tissues and to study different aspects of biomechanics of pollen tube.

10.2 Scope for further research and development

Several interesting and important results have been obtained from the present thesis. Diverse microfluidic platforms were employed which provided wide variety of studies for characterizing biology of pollen tube. Based on the present work, several potential researches have been identified for further development. The following list is not exhaustive, but it contains proposals for research that could improve the present design.

- *TipChip, a microfluidic platform for various tip growing cells:* The presented MEMS-based platform for pollen tube research represents a novel and extremely powerful tool which can be used for multiple applications in research on other tip growing cells such as fungal hyphae, root hairs and filamentous yeast. Its modular design allows for the

incorporation of various features and can be equipped with different integrated sensors. The design is compatible with multilayer PDMS fabrication technique which will facilitate integrating electrodes or microcantilevers for biosensors. The thesis provided sufficient experimental evidences for a proof of concept and it can provide solutions to numerous biological problems for other tip growing cells. The design of the TipChip allowed high resolution and fluorescence imaging and was conceived to allow parallel observation of multiple cells making it suitable for large scale approaches such as phenotyping.

- *Detecting agents involved in pollen tube reorientation*: The modified version of TipChip proposed for local chemical treatment of the pollen tube's tip is suitable and will be extremely useful for testing other attractants for pollen tube growth or agents causing repulsion. Moreover, it can be used to apply specific agents interfering with cellular functioning such as ion channel blockers, inhibitors of cytoskeletal polymerization or enzymes modulating the mechanical properties of the cell wall. It can easily be adapted to be used for other cell types displaying target regions that move due to growth or crawling.

- *Characterizing the interplay of turgor pressure and cell wall mechanical properties:* The growth of pollen tube's tip within air trap was successfully tested to study local treatment of pollen tube at the distal region. This air trap-based microfluidic platform can be used for other growth regulators or inhibitors to identify more accurately the role of tip fluxes in regulating the growth.

- *Detecting higher modes of oscillatory growth as new window to detect higher mode oscillation of underlying cellular processes*: In the present work, the secondary oscillation

peak frequency in the growth rate was successfully detected. Hence, it is expected to observe the corresponding secondary peak frequencies in the dynamics of underlying cellular processes (Zerzour *et al.*, 2009a). Detecting these will pose a challenge to the measuring techniques required such as the vibrating probe (for ion flux) and the sensitivity of fluorescent markers (for ion concentrations and motion of cytoplasmic structures such as vesicles and organelles), but future implementations of our microfluidic device will be used to meet these challenges. A detailed analysis of secondary oscillation frequencies may contribute to solving outstanding questions in this field such as the controversy around the fundamental underpinnings of the change in growth rate. Oscillations in turgor pressure were suggested as the cause of the oscillatory changes in growth rate, but these were not confirmed experimentally either by pressure probe or micro-indentation. However, there might be oscillations in turgor pressure with an amplitude below the resolution of measuring technique and more detailed analyses are warranted. On the other hand, the presence of a complicated oscillation pattern with primary and secondary frequencies is probably easier to explain with variations in the material properties of the cell wall as postulated earlier. The material properties are influenced by subtle changes in the ion flux pattern and exocytosis rate, but more research is warranted to clarify this issue. The analyses of secondary frequencies offer a promising avenue to do so.

Whole cell toxicity sensing: The effect of toxic Al substance on pollen tube growth was concentration-dependent so that the time of bursting and degree of oscillation disruption were correlated to the substance concentration. The toxicity testing of other toxic materials such as various heavy metals and mercury using current technique within microfluidic

platform would be interested to know whether the response is concentration-dependent or not related.

- *Detecting anisotropy of mechanical properties of cell wall using BLOC chip:* The experimentally determined values for the Young's modulus of the pollen tube cell wall in present work enabled us to support mechanical models of these cells and thus will contribute to our understanding of cellular morphogenesis and plant developmental processes in much more accurate manner. This method can easily be adapted to pollen tubes of other plant species, to other tip growing cells (fungal hyphae, root hairs). Regarding anisotropy of cell wall, it is unclear how this anisotropy can be explained structurally, since in pollen tubes, the cell wall components are known to bear the main tensile stress, while cellulose microfibrils, are known to be oriented helically with relatively low pitch, or even parallel to the long axis (Aouar *et al.*, 2010; Chebli *et al.*, 2012). Whether or not the other cell wall components, namely, pectin or callose, contribute to any anisotropy therefore warrants further research (Parre and Geitmann, 2005b, c). In this context it is interesting to note that xyluglucans seem to play a role in determining the tube diameter and hence may influence the material properties in circumferential direction by crosslinking cellulose microfibrils (Chebli *et al.*, 2012). The testing platform can be modified to perform sequential bending tests on different length portions of an individual tip growing cell and the effects of enzymes, inhibitors or mutation induced changes to the cell wall structure can be quantified in highly reproducible manner making the present BLOC platform an important tool for cell biology.

10.3 Contributions of the present work

From the current thesis, the following articles have been published.

10.3.1 Journal papers

[1] **A. Sanati Nezhad**, M. Naghavi, M. Packirisamy, R. Bhat, A. Geitmann, "*Quantification of cellular penetrative forces using Lab-on-chip technology and reverse engineering"*, Porc. Natl. Acad. Sci., 2013, vol: 110, pp: 8093-8098, 2013.

[2] C. G. Agudelo*, **A. Sanati Nezhad***, M. Ghanbari*, M. Naghavi, M. Packirisamy, A. Geitmann, "*TipChip - a modular, MEMS (micro-electro-mechanical systems) based platform for the investigation of tip growing cells*", The plant J, vol: 73, pp:1057-1068, 2013. [***equal contributions**].

[3] **A. Sanati Nezhad**, M. Naghavi, M. Packirisamy, R. Bhat, A. Geitmann, "*Quantitative determination of the biomechanical properties of the pollen tube cell wall using Lab-on-chip technology*", Lab on Chip, 2013, vol: 13, pp: 2599-2608, 2013.

[4] **A. Sanati Nezhad**, M. Packirisamy, R. Bhat, A. Geitmann, "*Characterization of oscillatory growth dynamics of Camellia pollen tubes within microfluidic environment*", J Biomed. Eng, IEEE. Trans., 2013 [In press].

[5] **A. Sanati Nezhad**, Mahmood Ghanbari, Carlos Agudelo, Muthukumaran Packirisamy, Rama B. Bhat, Anja Geitmann, "*PDMS microcantilever-based flow sensor integration for lab-on-chip*", IEEE sensors J, vol. 13, pp: 601-609, 2012.

[6] C. G. Agudelo, **A. Sanati Nezhad**, M. Ghanbari, M. Packirisamy, A. Geitmann, "*A Microfluidic Platform for the Investigation of Elongation Growth in Pollen Tubes*", J. Micromechanics and Microengineering, vol. 22, 115009, 2012.

[7] **A. Sanati Nezhad**, M. Ghanbari, C. G. Agudelo, M. Naghavi, M. Packirisamy, R. B. Bhat, A. Geitmann, "*Flow assisted entrapment of pollen grains in a microfluidic platform for in-vitro study of plant cell growth*", 2012 [Minor Revision under J. Biomedical Microdevices].

[8] **A. Sanati Nezhad**, M. Packirisamy, A. Geitmann, "*Aiming at a moving target - Using microfluidics to locally administer drugs to the growing end of a pollen tube*", 2013 [Submitted to J Nature Communications].

[9] **A. Sanati Nezhad**, Mahsa Naghavi, M Packirisamy, R. Bhat, A. Geitmann, "*Lab-on-chip for local treatment of pollen tube at distal region to determine the contribution of pollen tube apex on* regulating the growth", 2013 [To be submitted to Nature Communication].

[10] **A. Sanati Nezhad,** M. Packirisamy, R. Bhat, A. Geitmann, "*ToxChip: whole-cell sensing of toxic substances using plant cells within microfluidic environment*", 2013 [To be submitted to Lab on Chip].

[11] M. Ghanbari, **A. Sanati Nezhad**, C.G. Agudelo, M. Naghavi, M. Packirisamy, A. Geitmann, "*Flow-assisted localized growth of pollen tubes for a LOC",* 2013 [Submitted to J of Bioscience and Bioengineering].

10.3.2 Conferences and presentations

[1] **A. Sanati Nezhad**, M. Packirisamy, R.B. Bhat, A. Geitmann, "*Self mechanical anchoring of pollen tube within microfluidic environment and the applications*", ICETE-13, India, May 15-16, 2013.

[2] **A. Sanati Nezhad**, M. Packirisamy, R.B. Bhat, "*Buckling approach on pollen tube for measuring growth force*", Advanced in Microfluidics & Nanofluidics, Indiana, USA, May 25-26, 2013.

[3] **A. Sanati Nezhad**, M. Packirisamy, R.B. Bhat, "*Measuring growth force of pollen tube using vertical microcantilever*", 10th Intenational Workshop on Nanomechanical Sensing, Stanford University, USA, May 1-3, 2013.

[4] **A. Sanati Nezhad**, M. Naghavi, M. Packirisamy, R. Bhat, A. Geitmann , "*Quantification of Force Generation during Invasive Cellular Growth using Microfluidics and Reverse Engineering*", Annual Meeting of the Biophysical Society, Philadelphia, USA, February 2-6, 2013.

[5] C. Agudelo, **A. Sanati Nezhad**, M. Ghanbari, M. Naghavi, M. Packirisamy, A. Geitmann "*Combining live cell imaging and MEMS (microelectromechanical systems) technology*", Annual Meeting of Microscopical Society of Canada, University of Victoria, British Columbia, Canada, June 19-21, 2013.

[6] **A. Sanati Nezhad**, M. Ghanbari, C. Agudelo, M. Packirisamy, R.B. Bhat, "*A new PDMS microcantilever with integrated waveguide for biosensing application*", Photonic North 2012, Montreal, Canada.

[7] **A. Sanati Nezhad**, M. Ghanbari, M. Packirisamy, R. B. Bha*t "Simulation of detecting PDMS microcantilever deflection using Integrated Optical fibers",* Photonic North 2011, Ottawa, Proc. SPIE vol:8007, 80071R ,Canada.

[8] M. Ghanbari, M. Packirisamy, **A. Sanati Nezhad**, "*Finite Element Modeling of Novel MEMS Based Pressure/flow Sensor with Optical readout"* Photonic North 2011, Ottawa, Canada.

[9] **A. Sanati Nezhad**, I. Stiharu, M. Packirisamy, R. B. Bhat, "*Modelling of Adhesive Forces in Nanotweezer*", 6th Int. Conf. on MEMS NANO, and Smart Systems, ICMENS 2010, China.

A few more papers are in pipeline and will be submitted for publication soon.

References:

Agudelo C, Packirisamy M, Geitmann A. in press, a. Lab-on-a-Chip for studying growing pollen tubes. In: Žárský V, Cvrčková F, eds. *Plant Cell Morphogenesis: Methods and Protocols*: Springer.

Agudelo C, Sanati A, Ghanbari M, Packirisamy M, Geitmann A. 2012a. A microfluidic platform for the investigation of elongation growth in pollen tubes. *Journal of Micromechanics and Microengineering* 22, 115009.

Agudelo C, Sanati Nezhad A, Ghanbari M, Naghavi M, Packirisamy M, Bhat R, Geitmann A. 2013. TipChip - a modular, MEMS (micro-electro-mechanical systems) based platform for experimentation and phenotyping of tip growing cells. The Plant J 73, 1057-1068.

Ahmed D, Mao X, Shi J, Juluri BK, Huang TJ. 2009. A millisecond micromixer via single-bubble-based acoustic streaming. *Lab Chip* 9, 2738-2741.

Amien S, Kliwer I, Márton ML, Debener T, Geiger D, Becker D, Dresselhaus T. 2010. Defensin-like ZmES4 mediates pollen tube burst in maize via opening of the potassium channel KZM1. *PLoS Biology* 8, e1000388.

Andersson H, Van den Berg A. 2003. Microfluidic devices for cellomics: a review. *Sensors and Actuators B: Chemical* 92, 315-325.

Aouar L, Chebli Y, Geitmann A. 2010. Morphogenesis of complex plant cell shapes: the mechanical role of crystalline cellulose in growing pollen tubes. *Sexual Plant Reproduction* 23, 15-27.

Armani D, Liu C, Aluru N. 1999. Re-configurable fluid circuits by PDMS elastomer micromachining. IEEE, 222-227.

Åström H, Sorri O, Raudaskoski M. 1995. Role of microtubules in the movement of the vegetative nucleus and generative cell in tobacco pollen tubes. *Sexual Plant Reproduction* 8, 61-69.

Barile F, Dierickx P, Kristen U. 1994. In vitro cytotoxicity testing for prediction of acute human toxicity. *Cell Biology and Toxicology* 10, 155-162.

Bartnicki-Garcia S, Bracker CE, Gierz G, López-Franco R, Lu H. 2000. Mapping the growth of fungal hyphae: orthogonal cell wall expansion during tip growth and the role of turgor. *Biophysical Journal* 79, 2382-2390.

Baskin T. 2005. Anisotropic expansion of the plant cell wall. *Annual Review of Cell and Developmental Biology* 21, 203-222.

Bastmeyer M, Deising HB, Bechinger C. 2002. Force exertion in fungal infection. *Annu Rev Biophys Biomol Struct* 31, 321-342.

Bechinger C, Giebel K-F, Schnell M, Leiderer P, Deising HB, Bastmeyer M. 1999. Optical measurements of invasive forces exerted by appressoria of a plant pathogenic fungus. *Science* 285, 1896-1899.

Beer FP, Johnston Jr ER. 1974. Mechanics of Materials, 1981. McGraw-Hill, New York.

Benkert R, Obermeyer G, Bentrup FW. 1997. The turgor pressure of growing lily pollen tubes. *Protoplasma* 198, 1-8.

Bentley A, Atkinson A, Jezek J, Rawson D. 2001. Whole cell biosensors—electrochemical and optical approaches to ecotoxicity testing. *Toxicology In Vitro* 15, 469-475.

Berger F, Hamamura Y, Ingouff M, Higashiyama T. 2008. Double fertilization - caught in the act. *Trends in Plant Science* 13, 437-443.

Betz T, Lim D, Käs JA. 2006. Neuronal growth: a bistable stochastic process. *Physical Review letters* 96, 98103.

Bhanushali M, Bagale V, Shirode A, Joshi Y, Kadam V. 2011. An in-vitro toxicity testing-a reliable alternative to toxicity testing by reduction, replacement and refinement of animals. *International Journal of Advances in Pharmaceutical Sciences* 1.

Bhogal N, Grindon C, Combes R, Balls M. 2005. Toxicity testing: creating a revolution based on new technologies. *TRENDS in Biotechnology* 23, 299-307.

Blamey FPC. 2001. The role of the root cell wall in aluminum toxicity. Plant Nutrient Acquisition: New Perspectives, 201-226

Blewett J, Burrows K, Thomas C. 2000. A micromanipulation method to measure the mechanical properties of single tomato suspension cells. *Biotechnology Letters* 22, 1877-1883.

Bolduc JF, Lewis LJ, Aubin CÉ, Geitmann A. 2006. Finite-element analysis of geometrical factors in micro-indentation of pollen tubes. *Biomechanics and Modeling in Mechanobiology* 5, 227-236.

Bou Daher F, Chebli Y, Geitmann A. 2008. Optimization of conditions for germination of cold-stored *Arabidopsis thaliana* pollen. *Plant Cell Reports* 28, 347–357.

Bou Daher F, Geitmann A. 2011. Actin is involved in pollen tube tropism through redefining the spatial targeting of secretory vesicles. *Traffic* 12, 1537–1551

Bove J, Vaillancourt B, Kroeger J, Hepler PK, Wiseman PW, Geitmann A. 2008a. Magnitude and direction of vesicle dynamics in growing pollen tubes using spatiotemporal image correlation spectroscopy (STICS). *Plant Physiology* 147, 1646-1658.

Bove J, Vaillancourt B, Kroeger J, Hepler PK, Wiseman PW, Geitmann A. 2008b. Magnitude and direction of vesicle dynamics in growing pollen tubes using spatiotemporal image correlation spectroscopy and fluorescence recovery after photobleaching. *Plant Physiology* 147, 1646-1658.

Bradke F, Dotti CG. 1999. The role of local actin instability in axon formation. *Science* 283, 1931-1934.

Bragheri F, Ferrara L, Bellini N, Vishnubhatla KC, Minzioni P, Ramponi R, Osellame R, Cristiani I. 2010. Optofluidic chip for single cell trapping and stretching fabricated by a femtosecond laser. *Journal of Biophotonics* 3, 234-243.

Braschler T, Johann R, Heule M, Metref L, Renaud P. 2005. Gentle cell trapping and release on a microfluidic chip by in situ alginate hydrogel formation. *Lab Chip* 5, 553-559.

Breslauer DN, Lee PJ, Lee LP. 2006. Microfluidics-based systems biology. *Mol. BioSyst.* 2, 97-112.

Burgarella S, Merlo S, Dell'Anna B, Zarola G, Bianchessi M. 2010. A modular micro-fluidic platform for cells handling by dielectrophoresis. *Microelectronic Engineering* 87, 2124-2133.

Carpita NC, Gibeaut DM. 1993. Structural models of primary cell walls in flowering plants: consistency of molecular structure with the physical properties of the walls during growth. *The Plant Journal* 3, 1-30.

Catroux P, Rougier A, Dossou K, Cottin M. 1993. The silicon microphysiometer for testing ocular toxicity in vitro. *Toxicology in vitro* 7, 465-469.

Chanliaud E, Burrows KM, Jeronimidis G, Gidley MJ. 2002. Mechanical properties of primary plant cell wall analogues. *Planta* 215, 989-996.

Chebli Y, Geitmann A. 2007. Mechanical principles governing pollen tube growth. *Funct Plant Sci Biotechnol* 1, 232-245.

Chebli Y, Kaneda M, Zerzour R, Geitmann A. 2012. The Cell Wall of the Arabidopsis Pollen Tube—Spatial Distribution, Recycling, and Network Formation of Polysaccharides. *Plant Physiology* 160, 1940-1955.

Chebli Y, Kroeger J, Geitmann A. 2013. Transport logistics in pollen tubes. *Molecular Plant*. 10.1093/mp/sst073.

Cheung AY, Wu H. 2008. Structural and signaling networks for the polar cell growth machinery in pollen tubes. *Annu. Rev. Plant Biol.* 59, 547-572.

Cheung K, Renaud P. 2006. BioMEMS for medicine: On-chip cell characterization and implantable microelectrodes. *Solid State Electronics* 50, 551-557.

Cojoc D, Difato F, Ferrari E, Shahapure R, Laishram J, Massimo Righi M, Di Fabrizio E, Torre V. 2007. Properties of the force exerted by filopodia and lamellipodia and the involvement of cytoskeletal components. *PLoS One* 2, e1072.

Cosgrove DJ. 1993. Wall extensibility: its nature, measurement and relationship to plant cell growth. *New Phytologist* 124, 1-23.

Cosgrove DJ. 2005. Growth of the plant cell wall. *Nature Reviews - Molecular Cell Biology* 6, 850-861.

Crutchfield J, Farmer D, Packard N, Shaw R, Jones G, Donnelly R. 1980. Power spectral analysis of a dynamical system. *Physics Letters A* 76, 1-4.

Davis DJ, Burlak C, Money NP. 2000. Osmotic pressure of fungal compatible osmolytes. *Mycological Research* 104, 800-804.

Deacon J. 1997. *Modern Mycology*. Oxford: Blackwell Science.

Desprat N, Richert A, Simeon J, Asnacios A. 2005. Creep function of a single living cell. *Biophysical journal* 88, 2224-2233.

Diao J, Young L, Kim S, Fogarty EA, Heilman SM, Zhou P, Shuler ML, Wu M, DeLisa MP. 2006. A three-channel microfluidic device for generating static linear gradients and its application to the quantitative analysis of bacterial chemotaxis. *Lab on a Chip* 6, 381-388.

Dinesh J. 2009. Modelling and Simulation of a Single Particle in Laminar Flow Regime of a Newtonian Liquid. *Proceedings of the COMSOL Conference, Bangalore*.

Dintwa E, Jancsók P, Mebatsion H, Verlinden B, Verboven P, Wang C, Thomas C, Tijskens E, Ramon H, Nicolaï B. 2011. A finite element model for mechanical deformation of single tomato suspension cells. *Journal of Food Engineering* 103, 265-272.

Dittrich PS, Manz A. 2006. Lab-on-a-chip: microfluidics in drug discovery. *Nature Reviews Drug Discovery* 5, 210-218.

Donahue BS, Abercrombie R. 1987. Free diffusion coefficient of ionic calcium in cytoplasm. *Cell Calcium* 8, 437-448.

Dumais J, Shaw SL, Steele CR, Long SR, Ray PM. 2006. An anisotropic-viscoplastic model of plant cell morphogenesis by tip growth. *International Journal of Developmental Biology* 50, 209-222.

Edge S, Steele DF, Chen A, Tobyn MJ, Staniforth JN. 2000. The mechanical properties of compacts of microcrystalline cellulose and silicified microcrystalline cellulose. *International journal of Pharmaceutics* 200, 67-72.

Endress HU, Döschl-Volle C, Dengler K. 1996. Rheological methods to characterize pectins in solutions and gels. *Progress in Biotechnology* 14, 407-423.

Erbar C. 2003. Pollen tube transmitting tissue: Role of comptetition of male gametophytes. *International Journal of Plant Science* 164, S265-S277.

Falconnet D, Csucs G, Michelle Grandin H, Textor M. 2006. Surface engineering approaches to micropattern surfaces for cell-based assays. *Biomaterials* 27, 3044-3063.

Fayant P, Girlanda O, Chebli Y, Aubin C-É, Villemure I, Geitmann A. 2010. Finite element model of polar growth in pollen tubes. *The Plant Cell* 22, 2579-2593.

Feijó J, Malhó R, Obermeyer G. 1995a. Ion dynamics and its possible role during in vitro pollen germination and tube growth. *Protoplasma* 187, 155-167.

Feijó JA, Malhó R, Pais MS. 1995b. Electrical currents, ion channels and ion pumps during germination and growth of pollen tubes. *Protoplasma* 187, 155-167.

Feijo JA, Sainhas J, Holdaway-Clarke T, Cordeiro MS, Kunkel JG, Hepler PK. 2001. Cellular oscillations and the regulation of growth: the pollen tube paradigm. *BioEssays* 23, 86-94.

Feijó JA, Sainhas J, Holdaway-Clarke TL, Cordeiro MS, Kunkel JG, Hepler PK. 2001. Cellular oscillations and the regulation of growth: the pollen tube paradigm. *BioEssays* 23, 86-94.

Felekis D, Muntwyler S, Vogler H, Beyeler F, Grossniklaus U, Nelson B. 2011. Quantifying growth mechanics of living, growing plant cells *in situ* using microrobotics. *Micro Nano Letters* 6, 311-316.

Flanagan LA, Rhee SW, Schwartz PH, Lee AP, Monuki ES, Jeon NL. 2005. Human neural stem cell growth and differentiation in a gradient-generating microfluidic device. *Lab on a Chip* 5, 401-406.

Franklin-Tong VE. 1999. Signaling and the modulation of pollen tube growth. *The Plant Cell* 11, 727-738.

Galdberger AL, David R. 1990. Chaos and fractals in human physiology [J]. *Scientific American* 262, 42-49.

Gasser CS, Robinson-Beers K. 1993. Pistil development. *Plant Cell* 5, 1231-1239.

Geitmann A. 1999. The rheological properties of the pollen tube cell wall.

Geitmann A. 2001. Functions and evolutionary origin of hyphal turgor pressure. *Cell biology of plant and fungal tip growth* 328, 161.

Geitmann A. 2006. Experimental approaches used to quantify physical parameters at cellular and subcellular levels. *American Journal of Botany* 93, 1380-1390.

Geitmann A. 2006. Plant and fungal cytomechanics: quantifying and modeling cellular architecture. *Canadian Journal of Botany* 84, 581-593.

Geitmann A. 2010a. How to shape a cylinder: pollen tube as a model system for the generation of complex cellular geometry. *Sexual Plant Reproduction* 23, 63-71.

Geitmann A. 2010b. Mechanical modeling and structural analysis of the primary plant cell wall. *Current Opinion in Plant Biology* 13, 693–699

Geitmann A, Cresti M. 1998. Ca< sup> 2+</sup> channels control the rapid expansions in pulsating growth of< i> Petunia hybrida</i> pollen tubes. *Journal of Plant Physiology* 152, 439-447.

Geitmann A, Cresti M, Heath IB. 2001. *Cell biology of plant and fungal tip growth*. Amsterdam: IOS Press.

Geitmann A, Dumais J. 2009a. Not-so-tip-growth. *Plant Signaling & Behavior* 4, 136.

Geitmann A, Emons AMC. 2000. The cytoskeleton in plant and fungal cell tip growth. *Journal of Microscopy* 198, 218-245.

Geitmann A, Li YQ, Cresti M. 1996. The role of the cytoskeleton and dictyosome activity in the pulsatory growth of Nicotiana tabacum and Petunia hybrida pollen tubes. *Botanica Acta* 109, 102-109.

Geitmann A, McConnaughey W, Lang-Pauluzzi I, Franklin-Tong VE, Emons AMC. 2004. Cytomechanical properties of *Papaver* pollen tubes are altered after self-incompatibility challenge. *Biophysical Journal* 86, 3314-3323.

Geitmann A, Ortega JKE. 2009c. Mechanics and modeling of plant cell growth. *Trends in Plant Science* 14, 467-478.

Geitmann A, Palanivelu R. 2007a. Fertilization requires communication: signal generation and perception during pollen tube guidance. *Floriculture and Ornamental Biotechnology* 1, 77-89.

Geitmann A, Parre E. 2004. The local cytomechanical properties of growing pollen tubes correspond to the axial distribution of structural cellular elements. *Sexual Plant Reproduction* 17, 9-16.

Geitmann A, Steer M. 2006a. The architecture and properties of the pollen tube cell wall. *The Pollen Tube*, 177-200.

Geitmann A, Steer MW. 2006b. The architecture and properties of the pollen tube cell wall. In: Malhó R, ed. *The pollen tube: a cellular and molecular perspective, Plant Cell Monographs*, Vol. 3. Berlin Heidelberg: Springer Verlag, 177-200.

Giouroudi I, Kosel J, Scheffer C. 2008a. BioMEMS in Diagnostics: A Review and Recent Developments. *Recent Patents on Engineering* 2, 114-121.

Gossot O, Geitmann A. 2007. Pollen tube growth - Coping with mechanical obstacles involves the cytoskeleton. *Planta* 226, 405-416.

Green PB. 1968. Growth physics in Nitella: a method for continuous in vivo analysis of extensibility based on a micro-manometer technique for turgor pressure. *Plant Physiology* 43, 1169.

Greene N. 2002. Computer systems for the prediction of toxicity: an update. *Advanced Drug Delivery Reviews* 54, 417-431.

Grossmann G, Guo W-J, Ehrhardt D, Frommer W, Sit R, Quake S, Meier M. 2011a. The RootChip: An integrated microfluidic chip for plant science. *Plant Cell* 23, 1-7.

Haessler U, Kalinin Y, Swartz MA, Wu M. 2009. An agarose-based microfluidic platform with a gradient buffer for 3D chemotaxis studies. *Biomedical Microdevices* 11, 827-835.

Hamill OP, Marty A, Neher E, Sakmann B, Sigworth F. 1981. Improved patch-clamp techniques for high-resolution current recording from cells and cell-free membrane patches. *Pflügers Archiv European Journal of Physiology* 391, 85-100.

Harold FM, Harold RL, Money NP. 1995. What forces drive cell wall expansion? *Canadian Journal of Botany* 73, 379-383.

Hasegawa Y, Nakamura S, Nakamura N. 1996. Immunocytochemical localization of callose in the germinated pollen of Camellia japonica. *Protoplasma* 194, 133-139.

Heath IB, Steinberg G. 1999. Mechanisms of hyphal tip growth: tube dwelling amebae revisited. *Fungal Genetics and Biology* 28, 79-93.

Hepler PK, Vidali L, Cheung AY. 2001. Polarized cell growth in higher plants. *Annual Review of Cell and Developmental Biology* 17, 159-187.

Higashiyama T, Hamamura Y. 2008. Gametophytic pollen tube guidance. *Sexual Plant Reproduction* 21, 17-26.

Hiller S, Bruce D, Jeronimidis G. 1996. A micro-penetration technique for mechanical testing of plant cell walls. *Journal of Texture Studies* 27, 559-587.

Holdaway-Clarke TL, Feijó JA, Hackett GR, Kunkel JG, Hepler PK. 1997. Pollen tube growth and the intracellular cytosolic calcium gradient oscillate in phase while extracellular calcium influx is delayed. *The Plant Cell* 9, 1999-2010.

Holdaway-Clarke TL, Hepler PK. 2003. Control of pollen tube growth: role of ion gradients and fluxes. *New Phytologist* 159, 539-563.

Honys D, Twell D. 2003. Comparative analysis of the *Arabidopsis* pollen transcriptome. *Plant Physiology* 132, 640-652.

Honys D, Twell D. 2004. Transcriptome analysis of haploid male gametophyte development in *Arabidopsis*. *Genome Biology* 5, R85.

Howard RJ, Valent B. 1996. Breaking and entering: host penetration by the fungal rice blast pathogen Magnaporthe grisea. *Annual Reviews in Microbiology* 50, 491-512.

Hughes MP, Morgan H. 1998. Dielectrophoretic trapping of single sub-micrometre scale bioparticles. *Journal of Physics D: Applied Physics* 31, 2205.

Hüsken D, Steudle E, Zimmermann U. 1978. Pressure probe technique for measuring water relations of cells in higher plants. *Plant Physiology* 61, 158.

Ishijima A, Doi T, Sakurada K, Yanagida T. 1991. Subpiconewton force fluctuations of actomyosin *in vitro*. *Nature* 352, 301-306.

Janson ME, Dogterom M. 2004. A bending mode analysis for growing microtubules: evidence for a velocity-dependent rigidity. *Biophysical Journal* 87, 2723-2736.

Jin Y, Kannan S, Wu M, Zhao JX. 2007. Toxicity of luminescent silica nanoparticles to living cells. *Chemical Research in Toxicology* 20, 1126-1133.

Johnson MA, Preuss D. 2002. Plotting a course: multiple signals guide pollen tubes to their targets. *Developmental Cell* 2, 273-281.

Kamholz AE, Yager P. 2001. Theoretical analysis of molecular diffusion in pressure-driven laminar flow in microfluidic channels. *Biophysical Journal* 80, 155-160.

Kanea RS, Takayamaa S, Ostuni E, Ingberb DE, Whitesides GM. 2007. Patterning proteins and cells using soft lithography. *The Biomaterials Silver Jubilee Compendium: The Best Papers Published in Biomaterials, 1980-2004*, 161.

Kendrick M, McIntyre D, Ostroverkhova O. 2009. Wavelength dependence of optical tweezer trapping forces on dye-doped polystyrene microspheres. *JOSA B* 26, 2189-2198.

Knight JB, Vishwanath A, Brody JP, Austin RH. 1998. Hydrodynamic focusing on a silicon chip: mixing nanoliters in microseconds. *Physical Review Letters* 80, 3863-3866.

Kobel S, Valero A, Latt J, Renaud P, Lutolf M. 2010. Optimization of microfluidic single cell trapping for long-term on-chip culture. *Lab Chip* 10, 857-863.

Krichevsky A, Kozlovsky SV, Tian GW, Chen MH, Zaltsman A, Citovsky V. 2007. How pollen tubes grow. *Developmental Biology* 303, 405-420.

KRISTEN U, BISCHOFF N, LISBOA S, SCHIRMER E, WITT S, QUADER H. 2002. Morphology of cell injury: an approach to the EDIT programme by the use of tobacco pollen tubes. *ATLA. Alternatives to Laboratory Animals* 30, 323-329.

Kristen U, Friedrich RE. 2006. Toxicity screening of mouthwashes in the pollen tube growth test: safety assessment of recommended dilutions. *Brazilian Dental Journal* 17, 58.

Kristen U, Kappler R. 1995. The pollen tube growth test. *Methods in Molecular Biology[METHODS MOL. BIOL.]. 1995.*

Kroeger J, Geitmann A. 2011. Modeling pollen tube growth: Feeling the pressure to deliver testifiable predictions. *Plant signaling & behavior* 6.

Kroeger J, Geitmann A. 2011b. Pollen tube growth: getting a grip on cell biology through modeling. *Mechanics Research Communications*.

Kroeger J, Geitmann A. 2012. The pollen tube paradigm revisited. *Current Opinion in Plant Biology*. 15, 618–624.

Kroeger JH, Daher FB, Grant M, Geitmann A. 2009. Microfilament orientation constrains vesicle flow and spatial distribution in growing pollen tubes. *Biophysical Journal* 97, 1822-1831.

Kroeger JH, Geitmann A, Grant M. 2008. Model for calcium dependent oscillatory growth in pollen tubes. *Journal of Theoretical Biology* 253, 363-374.

Kühtreiber WM, Jaffe LF. 1990. Detection of extracellular calcium gradients with a calcium-specific vibrating electrode. *The Journal of cell biology* 110, 1565-1573.

Kundu P. 1990. *Fluid Mechanics*. San Diego Academic Press.

Lee P, Helman N, Lim W, Hung P. 2008a. A microfluidic system for dynamic yeast cell imaging. *Biotechniques* 44, 91-95.

Lee SW, Kang JY, Lee IH, Ryu SS, Kwak SM, Shin KS, Kim C, Jung HI, Kim TS. 2008b. Single-cell assay on CD-like lab chip using centrifugal massive single-cell trap. *Sensors and Actuators A: Physical* 143, 64-69.

Lennon KA, Roy S, Hepler PK, Lord EM. 1998. The structure of the transmitting tissue of Arabidopsis thaliana (L.) and the path of pollen tube growth. *Sexual Plant Reproduction* 11, 49-59.

Lew RR. 2005. Mass flow and pressure-driven hyphal extension in Neurospora crassa. *Microbiology* 151, 2685-2692.

Lien V, Vollmer F. 2007. Microfluidic flow rate detection based on integrated optical fiber cantilever. *Lab Chip* 7, 1352-1356.

Lin F, Nguyen CMC, Wang SJ, Saadi W, Gross SP, Jeon NL. 2005. Neutrophil migration in opposing chemoattractant gradients using microfluidic chemotaxis devices. *Annals of Biomedical Engineering* 33, 475-482.

Lin F, Saadi W, Rhee SW, Wang SJ, Mittal S, Jeon NL. 2004. Generation of dynamic temporal and spatial concentration gradients using microfluidic devices. *Lab Chip* 4, 164-167.

Lin YC, Jen CM, Huang MY, Wu CY, Lin XZ. 2001. Electroporation microchips for continuous gene transfection. *Sensors and Actuators B: Chemical* 79, 137-143.

Lindstedt S, Calder III W. 1981. Body size, physiological time, and longevity of homeothermic animals. *Quarterly Review of Biology*, 1-16.

Liu GR. 2003. *Mesh free methods: moving beyond the finite element method*: CRC Press.

Lopez-Franco R, Bartnicki-Garcia S, Bracker CE. 1994. Pulsed growth of fungal hyphal tips. *Proceedings of the National Academy of Sciences* 91, 12228-12232.

Lucchetta EM, Lee JH, Fu LA, Patel NH, Ismagilov RF. 2005. Dynamics of Drosophila embryonic patterning network perturbed in space and time using microfluidics. *Nature* 434, 1134-1138.

Ma B, Ruwet V, Corieri P, Theunissen R, Riethmuller M, Darquenne C. 2009. CFD simulation and experimental validation of fluid flow and particle transport in a model of alveolated airways. *Journal of Aerosol Science* 40, 403-414.

Magrez A, Kasas S, Salicio V, Pasquier N, Seo JW, Celio M, Catsicas S, Schwaller B, Forró L. 2006. Cellular toxicity of carbon-based nanomaterials. *Nano Letters* 6, 1121-1125.

Malhó R. 1998. Role of 1, 4, 5-inositol triphosphate-induced Ca^{2+} release in pollen tube orientation. *Sexual Plant Reproduction* 11, 231-235.

Malhó R. 2006. *The pollen tube: a cellular and molecular perspective*. Berlin Heidelberg: Springer Verlag.

Malhó R, Castanho-Coelho P, Pierson ES, Derksen J. 2005. Endocytosis and membrane recycling in pollen tubes. In: Šamaj J, Baluška F, Menzel D, eds. *Plant Endocytosis*. Germany: Springer-Verlag, 277-292.

Malhó R, Feijó J, Pais M. 1992. Effect of electrical fields and external ionic currents on pollen-tube orientation. *Sexual Plant Reproduction* 5, 57-63.

Malho R, Read ND, Pais MS, Trewavas AJ. 1994. Role of cytosolic free calcium in the reorientation of pollen ube growth. *The Plant Journal* 5, 331-341.

Malho R, Trewavas AJ. 1996. Localized apical increases of cytosolic free calcium control pollen tube orientation. *The Plant Cell* 8, 1935-1949.

McCue AD, Cresti M, Feijó JA, Slotkin RK. 2011. Cytoplasmic connection of sperm cells to the pollen vegetative cell nucleus: potential roles of the male germ unit revisited. *Journal of Experimental Botany* 62, 1621-1631.

McKenna ST, Kunkel JG, Bosch M, Rounds CM, Vidali L, Winship LJ, Hepler PK. 2009. Exocytosis precedes and predicts the increase in growth in oscillating pollen tubes. *The Plant Cell Online* 21, 3026-3040.

Melling A. 1997. Tracer particles and seeding for particle image velocimetry. *Measurement Science and Technology* 8, 1406.

Mengying Zhang JW, Limu Wang, Kang Xiao and Weijia Wen. 2010. A simple method for fabricating multi-layer PDMS structures for 3D microfluidic chips. *Lab Chip* 10, 1199–1203.

Messerli M, Robinson KR. 1997. Tip localized Ca^{2+} pulses are coincident with peak pulsatile growth rates in pollen tubes of *Lilium longiflorum*. *Journal of Cell Science* 110, 1269-1278.

Messerli M, Robinson KR. 1998. Cytoplasmic acidification and current influx follow growth pulses of *Lilium longiflorum* pollen tubes. *Plant Journal* 16, 87-91.

Messerli MA, Créton R, Jaffe LF, Robinson KR. 2000a. Periodic increases in elongation rate precede increases in cytosolic Ca^{2+} during pollen tube growth. *Developmental Biology* 222, 84-98.

Messerli MA, Créton R, Jaffe LF, Robinson KR. 2000b. Periodic increases in elongation rate precede increases in cytosolic Ca< sup> 2+</sup> during pollen tube growth. *Developmental Biology* 222, 84-98.

Messerli MA, Danuser G, Robinson KR. 1999. Pulsatile influxes of H+, K+ and Ca2+ lag growth pulses of Lilium longiflorum pollen tubes. *Journal of Cell Science* 112, 1497-1509.

Messerli MA, Robinson KR. 2003. Ionic and osmotic disruption of the lily pollen tube oscillator: testing proposed models. *Planta* 217, 147-157.

Michard E, Dias P, Feijó JA. 2008. Tobacco pollen tubes as cellular models for ion dynamics: improved spatial and temporal resolution of extracellular flux and free cytosolic concentration of

calcium and protons using pHluorin and YC3. 1 CaMeleon. *Sexual Plant Reproduction* 21, 169-181.

Miyoshi M. 1895. Die Durchbohrung von Membranen durch Pilzfäden. *Jahrb. Wissensch. Bot.* 28, 269-289.

Money N. 2007a. Biomechanics of invasive hyphal growth. *Biology of the Fungal Cell*, 237-249.

Money NP. 1997. Wishful thinking of turgor revisited: The mechanics of fungal growth. *Fungal Genetics and Biology* 21, 173- 187.

Money NP. 2001. Biomechanics of invasive hyphal growth. In: Howard RJ, Gow NAR, eds. *The Mycota: Biology of the Fungal Cell*, Vol. 8. New York, New York, USA: Springer, 3-17.

Money NP. 2004a. The fungal dining habit: a biomechanical perspective. *Mycologist* 18, 71-76.

Money NP. 2007b. Biomechanics of invasive hyphal growth. In: Howard RJ, Gow NAR, eds. *Biology of the Fungal Cell*. Berlin Heidelberg: Springer-Verlag, 237-249.

Money NP, Davis CM, Ravishankar JP. 2004. Biomechanical evidence for convergent evolution of the invasive growth process among fungi and oomycete water molds. *Fungal Genetics and Biology* 41, 872-876.

Mrksich M, Chen CS, Xia Y, Dike LE, Ingber DE, Whitesides GM. 1996. Controlling cell attachment on contoured surfaces with self-assembled monolayers of alkanethiolates on gold. *Proceedings of the National Academy of Sciences* 93, 10775.

Nakamura S, Miki-Hirosige H, Iwanami Y. 1982. Ultrastructural study of Camellia japonica pollen treated with myrmicacin, an ant-origin inhibitor. *American Journal of Botany*, 538-545.

Nuxoll E, Siegel R. 2009a. BioMEMS devices for drug delivery. *IEEE Engineering in Medicine and Biology Magazine* 28, 31-39.

Nuxoll E, Siegel R. 2009b. BioMEMS devices for drug delivery. *Engineering in Medicine and Biology Magazine, IEEE* 28, 31-39.

Nye M. 2006. Progress Toward Replacing Animals in Toxicity Testing for Cosmetics.

Palanivelu R, Johnson MA. 2011a. Functional genomics of pollen tube-pistil interactions in *Arabidopsis*. *Biochemical Society Transactions* 38, 593–597.

Palanivelu R, Preuss D. 2000. Pollen tube targetting and axon guidance: Parallels in tip growth mechanisms. *Trends in Cell Biology* 10, 517- 524.

Palanivelu R, Tsukamoto T. 2011b. Pathfinding in angiosperm reproduction: pollen tube guidance by pistils ensures successful double fertilization. *WIREs Developmental Biology* 1, 96-113.

Panovko YG, Gubanova II. 1973. Stability and oscillation of elastic systems: Modern concepts, paradoxes and errors.

Paoletti E. 1992. Effects of acidity and detergent on in vitro pollen germination and tube growth in forest tree species. *Tree Physiology* 10, 357-366.

Parre E, Geitmann A. 2005a. More than a leak sealant - the physical properties of callose in pollen tubes. *Plant Physiology* 137, 274-286.

Parre E, Geitmann A. 2005c. Pectin and the role of the physical properties of the cell wall in pollen tube growth of Solanum chacoense. *Planta* 220, 582-592.

Parton R, Fischer-Parton S, Watahiki M, Trewavas A. 2001. Dynamics of the apical vesicle accumulation and the rate of growth are related in individual pollen tubes. *Journal of Cell Science* 114, 2685-2695.

Parton RM, Fischer-Parton S, Trewavas AJ, Watahiki MK. 2003. Pollen tubes exhibit regular periodic membrane trafficking events in the absence of apical extension. *Journal of Cell Science* 116, 2707-2719.

Picton J, Steer M. 1983a. Evidence for the role of Ca 2+ ions in tip extension in pollen tubes. *Protoplasma* 115, 11-17.

Picton JM, Steer MW. 1983b. Membrane recycling and the control of secretory activity in pollen tubes. *Journal of Cell Science* 63, 303-310.

Pierson E, Li Y, Zhang H, Willemse M, Linskens H, Cresti M. 1995. pulsatory growth of pollen tubes-investigation of a possible relationship with the periodic distribution of cell-wall components. 44, 121-128.

Pierson E, Miller D, Callaham D, Van Aken J, Hackett G, Hepler P. 1996. Tip-localized calcium entry fluctuates during pollen tube growth. *Developmental Biology* 174, 160-173.

Pierson ES, Miller DD, Callaham DA, Shipley AM, Rivers BA, Cresti M, Hepler PK. 1994. Pollen tube growth is coupled to the extracellular calcium ion flux and the intracellular calcium gradient: effect of BAPTA-type buffers and hypertonic media. *The Plant Cell* 6, 1815-1828.

Pina C, Pinto F, Feijó JA, Becker JD. 2005. Gene family analysis of the *Arabidopsis* pollen transcriptome reveals biological implications for cell growth, division control, an gene expression regulation. *Plant Physiology* 138, 744-756.

Piñeros M, Tester M. 1997. Calcium channels in higher plant cells: selectivity, regulation and pharmacology. *Journal of Experimental Botany* 48, 551.

Plyushch TA, Willemse M, Franssen-Verheijen M, Reinders M. 1995. Structural aspects of in vitro pollen tube growth and micropylar penetration inGasteria verrucosa (Mill.) H. Duval andLilium longiflorum Thunb. *Protoplasma* 187, 13-21.

Prado AM, Porterfield DM, Feijo JA. 2004. Nitric oxide is involved in growth regulation and re-orientation of pollen tubes. *Development* 131, 2707-2714.

Qureshi A, Bulich A, Isenberg D. 1998. Microtox toxicity test systems–where they stand today. *Microscale Testing in Aquatic Toxicology: Advances, Techniques, and Practice, PG Wells, K. Lee, and C. Blaise, Eds., CRC Press, Boca Raton, FL*, 185-199.

Raghavan V. 1997. *Molecular Embryology of Flowering Plants*. Cambridge, UK: Cambridge University Press.

Rezanejad F. 2009. Air pollution effects on structure, proteins and flavonoids in pollen grains of Thuja orientalis L.(Cupressaceae). *Grana* 48, 205-213.

Rojas E, Hotton S, Dumais J. 2011. Chemically mediated mechanical expansion of the pollen tube cell wall. *Biophysical Journal* 101, 1844–1853.

Routier-Kierzkowska A-L, Weber A, Kochova P, Felekis D, Nelson B, Kühlemeier C, Smith R. 2012. Cellular force microscopy for in vivo measurements of plant tissue mechanics. *Plant Physiology* 158, 1514–1522.

Sakmann B, Patlak J, Neher E. 1980. Single acetylcholine-activated channels show burst-kinetics in presence of desensitizing concentrations of agonist. *Nature* 286, 71-73.

Sanati Nezhad A, Agudelo C, Ghanbari M, Packirisamy M, Bhat R, Geitmann A. 2013a. PDMS microcantilever-based flow sensor integration for lab-on-a-chip. *IEEE sensors.* 13, 601-609.

Sanati Nezhad A, Ghanbari M, Agudelo CG, Naghavi M, Packirisamy M, Bhat RB, Geitmann A. 2013b. Flow assisted entrapment of pollen grains in a microfluidic platform for in-vitro study of plant cell growth. *Biomedical Microdevices [Minor Revision]*.

Sanati Nezhad A, Naghavi M, Packirisamy M, Bhat R, Geitmann A. 2013c. Quantification of the Young's modulus of the primary plant cell wall using Bending-Lab-On-Chip (BLOC). *Lab Chip*. 13, 2599-2608.

Sanati Nezhad A, Packirisamy M, Bhat RB, Geitmann A. 2013d. In vitro study of oscillatory growth dynamics of *Camellia* pollen tubes in microfluidic environment. *Biomedical Engineering, IEEE Transaction*, [In Press].

Sanati Nezhad A, Packirisamy M, Bhat RB, Geitmann A. 2013e. Quantification of cellular penetrative forces using Lab-on-a-Chip technology and finite element modeling. *Proceedings of the National Academy of Sciences.* 110, pp: 8093-8098.

Sawano A, Takayama S, Matsuda M, Miyawaki A. 2002. Lateral propagation of EGF signaling after local stimulation is dependent on receptor density. *Developmental Cell* 3, 245-257.

Sawidis T. 2008. Effect of cadmium on pollen germination and tube growth in Lilium longiflorum and Nicotiana tabacum. *Protoplasma* 233, 95-106.

Sawidis T, Reiss HD. 1995. Effects of heavy metals on pollen tube growth and ultrastructure. *Protoplasma* 185, 113-122.

Schopfer P. 2006. Biomechanics of plant growth. *American Journal of Botany* 93, 1415-1425.

Seo J, Ionescu-Zanetti C, Diamond J, Lal R, Lee LP. 2004. Integrated multiple patch-clamp array chip via lateral cell trapping junctions. *Applied Physics Letters* 84, 1973.

Shanker AK, Cervantes C, Loza-Tavera H, Avudainayagam S. 2005. Chromium toxicity in plants. *Environment International* 31, 739-753.

Sheng X, Zhang S, Jiang L, Li K, Gao Y, Li X. 2012. Lead Stress Disrupts the Cytoskeleton Organization and Cell Wall Construction During Picea wilsonii Pollen Germination and Tube Growth. *Biological Trace Element Research*, 1-8.

Smith LG, Oppenheimer DG. 2005. Spatial control of cell expansion by the plant cytoskeleton. *Annual Review of Cell and Developmental Biology* 21, 271-295.

Speranza A, Ferri P, Battistelli M, Falcieri E, Crinelli R, Scoccianti V. 2007. Both trivalent and hexavalent chromium strongly alter in vitro germination and ultrastructure of kiwifruit pollen. *Chemosphere* 66, 1165-1174.

Spetzler D, York J, Dobbin C, Martin J, Ishmukhametov R, Day L, Yu J, Kang H, Porter K, Hornung T. 2007. Recent developments of bio-molecular motors as on-chip devices using single molecule techniques. *Lab on a Chip* 7, 1633-1643.

Stammati AP, Silano V, Zucco F. 1981. Toxicology investigations with cell culture systems. *Toxicology* 20, 91-153.

Strube K, Janke D, Kappler R, Kristen U. 1991. Toxicity of some herbicides to< i> in vitro</i> growing tobacco pollen tubes (the pollen test). *Environmental and Experimental Botany* 31, 217-222.

Sung JH, Shuler ML. 2009. Prevention of air bubble formation in a microfluidic perfusion cell culture system using a microscale bubble trap. *Biomedical Microdevices* 11, 731-738.

Taiz L. 1984. Plant cell expansion: regulation of cell wall mechanical properties. *Annual Review of Plant Physiology* 35, 585-657.

Takayama S, Ostuni E, LeDuc P, Naruse K, Ingber DE, Whitesides GM. 2001. Subcellular positioning of small molecules. *Nature* 411, 1016.

Takayama S, Ostuni E, LeDuc P, Naruse K, Ingber DE, Whitesides GM. 2003. Selective chemical treatment of cellular microdomains using multiple laminar streams. *Chemistry & Biology* 10, 123-130.

Takeuchi H, Higashiyama T. 2011. Attraction of tip-growing pollen tubes by the female gametophyte. *Current Opinion in Plant Biology*.

Tan W, Desai TA. 2003. Microfluidic patterning of cells in extracellular matrix biopolymers: effects of channel size, cell type, and matrix composition on pattern integrity. *Tissue Engineering* 9, 255-267.

Tan WH, Takeuchi S. 2007. A trap-and-release integrated microfluidic system for dynamic microarray applications. *Proceedings of the National Academy of Sciences* 104, 1146.

Tatic-Lucic S. 2007. Applications of BioMEMS in Cell-Related Research. IEEE, 1-1.

Taylor LP, Hepler PK. 1997. Pollen germination and tube growth. *Annual Review of Plant Physiology and Plant Molecular Biology* 48, 461-491.

Terry SC, Jerman JH, Angell JB. 1979. A gas chromatographic air analyzer fabricated on a silicon wafer. *Electron Devices, IEEE Transactions* 26, 1880-1886.

Theriot JA. 2000. The polymerization motor. *Traffic* 1, 19-28.

Thiébaud P, Lauer L, Knoll W, Offenhäusser A. 2002. PDMS device for patterned application of microfluids to neuronal cells arranged by microcontact printing. *Biosensors and Bioelectronics* 17, 87-93.

Tomos A. 1988. Cellular water relations of plants. *Water Sci. Rev* 3, 186-277.

Tomos AD, Leigh RA. 1999. The pressure probe: a versatile tool in plant cell physiology. *Annual review of plant biology* 50, 447-472.

Tong ZQ, Balzer EM, Dallas MR, Hung WC, Stebe KJ, Konstantopoulos K. 2012. Chemotaxis of cell populations through confined spaces at single-cell resolution. *PLoS One* 7, e29211.

Tovar AR, Patel MV, Lee AP. 2011. Lateral air cavities for microfluidic pumping with the use of acoustic energy. *Microfluidics and Nanofluidics* 10, 1269-1278.

Uwate WJ, Lin J, Ryugo K, Stallman V. 1980. Cellular components of the midstylar transmitting tissue of *Prunus avium*. *Canadian Journal of Botany* 60, 98-104.

Vogler H, Draeger C, Weber A, Felekis D, Eichenberger C, Routier-Kierzkowska AL, Boisson-Dernier A, Ringli C, Nelson BJ, Smith RS. 2012. The pollen tube: a soft shell with a hard core. *The Plant Journal*.

Waliszewski P, Konarski J. 2001a. Tissue as a self-organizing system with fractal dynamics. *Advances in Space Research* 28, 545-548.

Waliszewski Pa, Molski M, Konarski J. 2001b. On the relationship between fractal geometry of space and time in which a system of interacting cells exists and dynamics of gene expression. *Acta Biochimica Polonica* 48, 209-220.

Wang F, Wang H, Wang J, Wang HY, Rummel PL, Garimella SV, Lu C. 2008. Microfluidic delivery of small molecules into mammalian cells based on hydrodynamic focusing. *Biotechnology and Bioengineering* 100, 150-158.

Wang H, Wu H-M, Cheung A. 1996. Pollination induces mRNA poly(A) tail-shortening and cell deterioration in flower transmitting tissue. *Plant Journal* 9, 715-727.

Wang L, Hukin D, Pritchard J, Thomas C. 2006. Comparison of plant cell turgor pressure measurement by pressure probe and micromanipulation. *Biotechnology Letters* 28, 1147-1150.

Waring JF, Ciurlionis R, Jolly RA, Heindel M, Ulrich RG. 2001. Microarray analysis of hepatotoxins in vitro reveals a correlation between gene expression profiles and mechanisms of toxicity. *Toxicology Letters* 120, 359-368.

Wei C, Lintilhac LS, Lintilhac PM. 2006. Loss of stability, pH, and the anisotropic extensibility of *Chara* cell walls. *Planta* 223, 1058-1067.

Wei C, Lintilhac PM. 2007. Loss of stability: a new look at the physics of cell wall behavior during plant cell growth. *Plant Physiology* 145, 763-772.

West GB, Woodruff WH, Brown JH. 2002. Allometric scaling of metabolic rate from molecules and mitochondria to cells and mammals. *Proceedings of the National Academy of Sciences of the United States of America* 99, 2473-2478.

Wheeler AJ, Ganji AR. 1996. *Introduction to engineering experimentation*: Prentice Hall Englewood Cliffs, NJ.

Wheeler AR, Throndset WR, Whelan RJ, Leach AM, Zare RN, Liao YH, Farrell K, Manger ID, Daridon A. 2003. Microfluidic device for single-cell analysis. *Analytical Chemistry* 75, 3581-3586.

Williams J. 2008. Novelties of the flowering plant pollen tube underlie diversification of a key life history stage. *Proceedings of the National Academy of Sciences of the United States of America* 105, 11259–11263.

Wilsen KL, Hepler PK. 2007. Sperm delivery in flowering plants: the control of pollen tube growth. *Bioscience* 57, 835-844.

Winship LJ, Obermeyer G, Geitmann A, Hepler PK. 2010. Under pressure, cell walls set the pace. *Trends in Plant Science* 15, 363-369.

Winship LJ, Obermeyer G, Geitmann A, Hepler PK. 2011. Pollen tubes and the physical world. *Trends in Plant Science* 16, 353-355

Wright G, Arlt J, Poon W, Read N. 2005. Measuring fungal growth forces with optical tweezers. *Proc SPIE* 5930, F1–F7.

Xiong ZT, Peng YH. 2001. Response of pollen germination and tube growth to cadmium with special reference to low concentration exposure. *Ecotoxicology and Environmental Safety* 48, 51-55.

Yang M, Li CW, Yang J. 2002. Cell docking and on-chip monitoring of cellular reactions with a controlled concentration gradient on a microfluidic device. *Analytical Chemistry* 74, 3991-4001.

Yasuda K. 2000. Non-destructive, non-contact handling method for biomaterials in micro-chamber by ultrasound. *Sensors and Actuators B: Chemical* 64, 128-135.

Yetisen A, Jiang L, Cooper J, Qin Y, Palanivelu R, Zohar Y. 2011a. A microsystem-based assay for studying pollen tube guidance in plant reproduction. *Journal of Micromechanics and Microengineering* 21, e054018.

Zerzour R, Kroeger J, Geitmann A. 2009. Polar growth in pollen tubes is associated with spatially confined dynamic changes in cell mechanical properties. *Developmental Biology* 334, 437-446.

Zhang W, Rengel Z, Kuo J, Yan G. 1999. Aluminium effects on pollen germination and tube growth of Chamelaucium uncinatum. A comparison with other Ca^{2+} antagonists. *Annals of Botany* 84, 559-564.

Zhao L, Schaefer D, Xu H, Modi SJ, LaCourse WR, Marten MR. 2005. Elastic properties of the cell wall of *Aspergillus nidulans* studied with atomic force microscopy. *Biotechnology Progress* 21, 292-299.

Ziaie B, Baldi A, Lei M, Gu Y, Siegel RA. 2004. Hard and soft micromachining for BioMEMS: review of techniques and examples of applications in microfluidics and drug delivery. *Advanced Drug Delivery Reviews* 56, 145-172.

Zonia L. 2010. Spatial and temporal integration of signalling networks regulating pollen tube growth. *Journal of Experimental Botany* 61, 1939-1957.

Zonia L, Feijó JA. 2003. State and spectral properties of chloride oscillations in pollen. *Biophysical Journal* 84, 1387-1398.

Zonia L, Müller M, Munnik T. 2006. Hydrodynamics and cell volume oscillations in the pollen tube apical region are integral components of the biomechanics of Nicotiana tabacum pollen tube growth. *Cell Biochemistry and Biophysics* 46, 209-232.

Zonia L, Munnik T. 2011. Understanding pollen tube growth: the hydrodynamic model versus the cell wall model. *Trends in Plant Science*.

Zou H, Mellon S, Syms R, Tanner K. 2006. 2-dimensional MEMS dielectrophoresis device for osteoblast cell stimulation. *Biomedical Microdevices* 8, 353–359.